UNIVERSITY OF SOUTHAMPTON

FACULTY OF ENGINEERING, SCIENCE & MATHEMATICS

School of Engineering Sciences

Reduction of Downhole Friction by Electrochemical Methods

by

Mohd Nur Fitri Ismail

Thesis for the degree of Doctor of Philosophy

November 2010

UNIVERSITY OF SOUTHAMPTON

ABSTRACT

FACULTY OF ENGINEERING, SCIENCE AND MATHEMATICS
SCHOOL OF ENGINEERING SCIENCES

Doctor of Philosophy

REDUCTION OF DOWNHOLE FRICTION BY ELECTROCHEMICAL METHODS

By Mohd Nur Fitri Ismail

High torque and drag is one of the major problems encountered by the downhole drilling companies and is exacerbated when directional drilling techniques are used. Thus, reducing friction is key to reducing the requirements of drilling equipment and is one of the most researched areas by the oil and gas companies.

This study investigated an electrochemical method to control friction for AISI 4340 steel/AISI 4340 steel, and AISI 4340 steel/sandstone sliding contacts lubricated by baseline solutions and the downhole drilling muds. The tribometer used was a pin-on-disc, modified to incorporate a three-eectrode electrochemical cell allowing potential control of the rotating disc. The overpotential† used was in the range of ±1 V, whilst the load and speed were kept constant at 50 N and 0.03 m s^{-1} respectively (to replicate downhole conditions). Lubrication involved the addition of electroactive friction modifier additives to allow electrochemical friction control.

Initial experiments using pure electrochemical methods established the the behaviour of steel samples immersed in all the test solutions/lubricants. Evidence of additive adsorption was seen via the limiting current response in the potentiodynamic polarisation test, especially at anodic overpotentials with additive containing lubricants such as octanoate.

For the baseline solutions, without the additive, friction for steel/steel was found to be independent of applied potential. Evidence of abrasion and adhesion were also seen using a Scanning Electron Microscope (SEM). However, incorporation of octanoate additive resulted in a decrease in friction at anodic overpotentials, up to 66%, due to the formation of iron octanoate tribofilm. Furthermore, abrasion, adhesion and sample wear rates were also reduced. In the bentonite drilling mud, friction levels were generally higher than the baseline solutions, due to the presense of two-body abrasion induced by entrained particles. Incorporation of octanoate also produced dependence of friction on potential in the mud, in which friction was reduced at anodic overpotentials, reaching levels as low as the octanoate solution (baseline with additive). Abrasion and adhesion was also reduced. The polymer drilling mud showed inherent lubricity, but friction was even lower at anodic overpotentials with the incorporation of octanoate additive (62% reduction cf. no additive).

Alternative types of additives were tested and showed different effects on friction, depending on the hydrocarbon chain lengths and polar charge. Butyrate (C_4) resulted in less friction reduction cf. octanoate (C_8), whilst oleate (C_{18}) showed more reduction. CTAB, however, showed reduction at cathodic overpotentials owing to its positive charge.

For the steel/sandstone contact, no dependence of friction on overpotential was seen, using the bentonite mud only. However, the octanoate additive resulted in lower friction at anodic overpotentials. Two contact arrangements were employed, *i.e.*, (i) steel pin/sandstone disc, and (ii) sandstone disc/steel pin, both resulting in similar friction behaviour.

X-ray Photoelectron Spectroscopy (XPS) of worn surfaces of steel suggested the formation of a weak octanoate tribofilm at cathodic overpotentials, probably due to the loosely-packed adsorption. However, a robust tribofilm was formed at anodic overpotentials, due to the development of a relatively close-packed adsorption layer. The low friction contacts at anodic overpotentials correlate with low values of current density, which supports the formation of a tribofilm, passivating the surface.

†Overpotential is the difference between applied potential and the open circuit potential (OCP)

Table of Contents

List of Figures

Chapter 2

Chapter 3

Chapter 4

Chapter 7

Chapter 8

Chapter 9

List of Tables

Chapter 2

Chapter 3

Chapter 4

Chapter 5

Chapter 6

Chapter 7

Chapter 8

DECLARATION OF AUTHORSHIP

I, Mohd Nur Fitri Ismail declare that the thesis entitled Reduction of Downhole Friction by Electrochemical Methods and the work presented in the thesis are both my own, and have been generated by me as the result of my own original research. I confirm that:

- this work was done wholly or mainly while in candidature for a research degree at this University;
- where any part of this thesis has previously been submitted for a degree or any other qualification at this University or any other institution, this has been clearly stated;
- where I have consulted the published work of others, this is always clearly attributed;
- where I have quoted from the work of others, the source is always given. With the exception of such quotations, this thesis is entirely my own work;
- I have acknowledged all main sources of help;
- where the thesis is based on work done by myself jointly with others, I have made clear exactly what was done by others and what I have contributed myself;
- parts of this work have been published as: (please see next page)

Signed: ……..

Date: 20th January 2011

Publications

The published work related to different parts of this work is listed below:

- Surface Potential Effects on Friction and Abrasion of Sliding Contacts Lubricated by Aqueous Solutions
  MNF Ismail, TJ Harvey, JA Wharton, RJK Wood, A Humphreys
  Wear, 267, 2009, pp 1978-1986

- Surface Potential Effects on Friction and Abrasion of Sliding Contacts Lubricated by Bentonite and Polymer Based Solutions
  M Ismail, R Wood, A Humphreys, J Wharton, T Harvey
  Conference Proceedings of the World Tribology Congress (WTC) Japan, 2009

- Electrochemical Control of Friction Lubricated by Aqueous Solutions
  MNF Ismail, TJ Harvey, JA Wharton, RJK Wood, A Humphreys
  Conference Proceedings of the Mission of Tribology (MoT), 2009

- Electrochemical Friction Control Using Downhole Drilling Lubricants
  MNF. Ismail, RJK. Wood, A Humphreys, JA Wharton, TJ Harvey
  Conference Proceedings of the Society of Tribologists and Lubrication Engineers (STLE) Annual Meeting, 2010

- Controlling the Friction of a Steel/Sandstone Contact by Varying the Surface Potential
  MNF Ismail, T. Harvey, JA Wharton, RJK Wood, A Humphreys
  Conference Proceedings of UK-China Summer School 2010

Acknowledgements

In the name of Allah the most gracious and merciful. May peace and blessings be upon Muhammad, His messenger.

First of all, I would like to express my gratitude to the supervisory board consisting of Prof. Robert Wood, Dr. Julian Wharton and Dr. Alan Humphreys, as well as Dr. Terry Harvey who was my project advisor. To this point, contemplating on my last three years' experience, I am very grateful that I was given the opportunity, and most importantly, the trust, to undertake the responsibility of this project. It is beyond the slightest doubt that I am a new and improved person than who I was, just before I embarked onto this project. It has always been a 'roller coaster' emotion, operating a PhD project, as many would agree, but it were with the constant enthusiasm and intellectual engagement of the supervisors and advisor, amalgamated with my hard work, plus many hours of careful thinking and planning, that made it all possible (of course with God's will). As any successful project in the world, be it in art, social, engineering, etc., there were numerous people who had provided some sort of benefit, directly or otherwise, thus, I would like to acknowledge them here, but I am sure that I will miss a few (so, please accept my advanced apologies).

This project would not have been as it is now, without the regular steerage and funding from Schlumberger. The Mechanical and Materials research group at Schlumberger-Doll Research (USA), to which I am directly involved with, had given precious support in various ways. Hitoshi is greatly appreciated for continuing the progression of this project. Louise, at Schlumberger Cambridge (UK) provided valuable information regarding the formulations of mud. Mike from MI-Swaco kindly provided the additives used for mixing the polymer mud. Dave at Cardiff University is appreciated for his help in conducting the XPS measurements.

Part of my priceless experience is to witness the expansion of my research group from a subset of the Materials Research Group into an independant national Centre for Advanced Tribology at Southampton (nCATS). There was just too many who I have involved with in productive discussions, including previous students who shared my office - Mandar, Sun Dan, Mark, Xioguang, Prasanna, Jenny, Azlan, Nick, Ram, Lily and Keisuke, who were there especially during my first year which was the most challenging. Current nCATS students – Shiva, Stephane (lunch mates), Martin, Stefano, Rich, Jonee, Chao, etc. Members of staff also supported my work, who were – Steve (technician who fabricated the samples and rig modifications), Sue, Jurgita, Mike, Dave and all the post-docs and lecturers. Furthermore, other University staffs include – Gwyneth, Materials group secretary, and John, the rock cutting technician at SOES.

Lastly, and by no means the least, my gratitude go to my family and friends, whom, without them, would have left my life dull and undecorated. My mother Kamariah, father, Ismail, parents in-law, Fatimah and Raini, Along, and all my siblings. Also, thank you Wanee, "buah hatiku," for complimenting me in every possible way, such as being by my side at all times especially whenever my experiments went horribly wrong, and allowing me to feed on her hard earned money during the course of writing this thesis (my funding ran out 3 months ago). Of course, I have to mention all my friends in general, who were here and made my experience in Southampton joyful and exciting, and the friends in Malaysia who I have neglected for years.

Thank you ALL...

1 Introduction

1.1 Project Background

Downhole refers to the bore during petroleum exploration, which could be either drilled from the sea bed or from the Earth's surface. Recent advances in drilling technology have allowed new milestones to be achieved, such as with the drilling and completion of wells which are longer than 10 km. A few of the main technical hurdles to the success of this well were reducing torque and drag (which is a tribological problem), controlling fluid circulation and maintaining directional control [1]. Oil exploration has evolved from a just vertical boring towards directional drilling that enables drilling in a complicated pathway. Therefore, to meet the new millenium's demand for energy, oil exploration has to be efficient and has the technological capability to reach deeper reservoirs.

Tribology with respect to oilwell drilling industry relates to the sliding conditions either during the actual drilling itself or in the tools. During oilwell drilling there is a substantial friction in between the earth formation (rock) and the drill string (steel). Furthermore, steel pipe casing will be installed in a drilled bore to support it but also means that there is a potential for steel/steel sliding (casing/drill string). Complex drilling techniques such as directional drilling imposes high friction of the sliding contacts especially at the curvatures. Therefore, low friction is desired in horizontal and highly deviated wellbores where the friction forces limit the passage of tools along the wellbore [2].

1.2 Objectives of the Project

The aim of this project was to develop a novel technique to allow friction and wear reduction, by integrating mechanical and electrochemical methods, in a simulated downhole drilling conditions.

The main objectives of this project are listed below:

- To design a tribometer which incorporates a three electrode electrochemical cell to allow study in the area of tribochemistry
- To assess the concept of reducing the friction by applying potentials. This includes the contacts between steel/steel and steel/sandstone which are simulating the drilling conditions. A reduction in friction by 10% was envisaged.
- To experiment with different friction modifying additives to aid the understanding of the friction reduction concept.
- To characterise the adsorption of the additive, and use this method to aid the analysis of the friction and wear results.
- To relate between the electrochemical test results in beaker with the recorded results during the sliding tests. This would increase the understanding of the mechanism of the additives in producing a tribofilm which is useful for low friction and wear.

1.3 Thesis Structure

Chapter 2 – Literature Review

The previous work published is discussed focusing on the relevant fundamental aspects of this study such as in the areas of tribology, electrochemistry and particularly the effect of potential (or current) on friction and wear. The fundamental understanding of the drilling mud and its composition is also focused.

Chapter 3 – Methodology

This chapter presents the overall experimental methodology employed in this study and the preparation steps taken prior to the tests, in-test and post-test analyses. Furthermore, the modification implemented in the existing pin-on-disc rig is also presented.

Chapter 4 – Steel / Steel Contacts in Baseline Solution

This chapter is the core analysis of this project, which consists of the experiments conducted in the modified pin-on-disc tribometer in the steel/steel contact. Some fundamental

tribochemical understandings were established in this chapter which inspired a lot of other work conducted.

Chapter 5 – Steel / Steel Contacts in Drilling Mud

This chapter extends the fundamental work presented in Chapter 4 by conducting the tests in the drilling mud, simulating the actual drilling processes.

Chapter 6 – XPS Analysis of the Adsorbed Octanoate Additives

Chapter 6 reports on the analysis of the X-ray Photoelectron Spectroscopy (XPS) data of he scans made on the discs. This established some evidence of the adsorption of the octanoate additive to influence friction and wear.

Chapter 7 – Steel/sandstone Contacts

Chapter 7 includes the discussions on the steel/sandstone contacts, simulating the sliding condition found during open-hole drilling (uncased). These tests are for exploring the reproducibility of the concept previously found in the steel/steel contacts (Chapter 4).

Chapter 8 – Investigation of Electrochemical Performance of the Additives

Discusses the results of the electrochemical tests conducted in beaker in comparison to the tests done in the modified setup. Discussions about the reproducibility of the electrochemical results in the rig are made to assess the feasibility and reliability of the modified rig.

Chapter 9 – Summary of the Mechanism of Contacts

This chapter includes the summary of all the mechanism of contacts found under the different test conditions employed.

Chapter 10 – Conclusions

Some concluding remarks related to the results presented in this project are reported.

Chapter 11 – Future Work

The possible directions in which this study will be focusing on in the future are briefly discussed in this chapter.

Chapter 12 - References

This chapter lists the references relevant to this project.

2 Literature Review

2.1 Introduction

This chapter will present the review of the literature relevant to this project. Essentially, a general introduction to the process of oil well drilling will be presented first, which will identify the need for reducing friction and wear in that condition. Furthermore, the fundamentals related to the subject of tribology will be discussed which are important to establish the basic understanding related to the concepts of this project.

In addition, the review includes literature on tribochemistry, which is a subtopic in tribology aiming at assessing the relationship between surface chemical reactions and mechanical performance. Since the majority of the experimental work in this study involved the incorporation of friction modifying additives which adsorb onto the contacting surfaces, a review on the characteristics of these molecules will also be discussed.

2.2 Introduction to drilling

2.2.1 Typical drilling processes

2.2.1.1 Geophysical and Geographical Survey

Typically, a drilling company, such as Schlumberger, will conduct geophysical surveys to locate and gain as much information as possible regarding an oil or gas reservoir. This is done through transmitting waves into the earth (seismic) and recording the reflected in which will be analysed by a computer. Figure 2.1 shows the typical vehicles used to carry out the seismic data acquisition processes. The data can be used to locate the reservoirs along with other geographical information and can be viewed in 2D and 3D. This method is advantageous because it offers a non-destructive evaluation of the subsurface. This process is relatively cheap and allows a strong foundation for the company to rely on for the decision making to drill for oil.

(a) (b)

Figure 2.1. The seismic data recording can be done by (a) marine and (b) land vehicles, depending on the location of the reservoirs [2].

2.2.1.2 Drilling

Once the seismic analysis has been established, a well can be drilled to explore the reservoir. This provides more insight into the quality of the reservoir as it allows chemical and physical analyses. It is a relatively expensive process, thus can only be done after rigorous preparation procedures. Geological tests can also be conducted on the cut formation and are usually recorded in a log to aid further analysis.

Drilling involves constructing a rig, such as shown in Figure 2.2, at a suitable location which is often chosen for its favourable geographical and geological conditions. In the construction and operation of the oil rig, an array of materials are used, from steel for the drill string and casing, to drilling mud components, bearing in mind that the distance of a drilled well can reach thousands of metres.

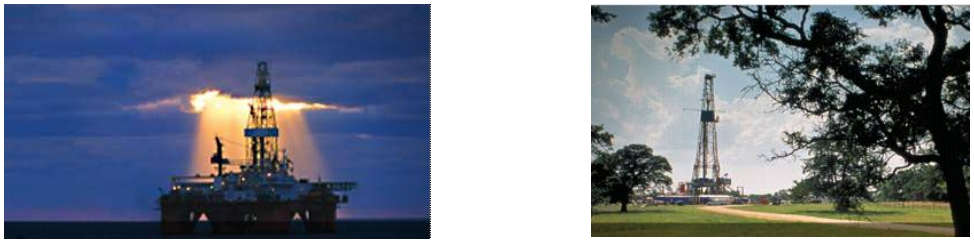

(a) (b)

Figure 2.2 A type of drilling rig (a) offshore, and (b) onshore [2].

The typical oil rig setup is schematically shown in Figure 2.3. A swivel is responsible for holding the weight of the drill string, apart from allowing rotational motion of the whole assembly. In situations where downhole motors are not used, the whole assembly needs to be rotated, which is made possible by the kelly and rotary table. During operation, the rotary table will spin the kelly, which is attached to the drill string, thus making the whole assembly to rotate. At the bottom end of the drill assembly, the drill collar is installed, which is a heavy tube to provide weight to the bit. Finally, the drill bit finishes off the assembly which is where the rock cutting action is made.

A drilling mud is pumped into the well to impart various characteristics, such as lubrication, fluid loss prevention, cooling the bit, stabilise the pressure etc. The mud is pumped through the kelly hose and into the kelly, in which it will travel along the drill string, exiting at the nozzle located at the drill bit. The mud will then be circulated to the surface and passes through a shaker, which filters the debris, especially cut formation. A mud pit serves as a reservoir for the filtered mud which is ready for reuse. The drilling mud composition and hydrodynamic parameters are amongst the most important parts to be engineered and controlled to make the drilling processes are as efficient and cost effective as possible (more details will be presented in Subsection 2.2.4).

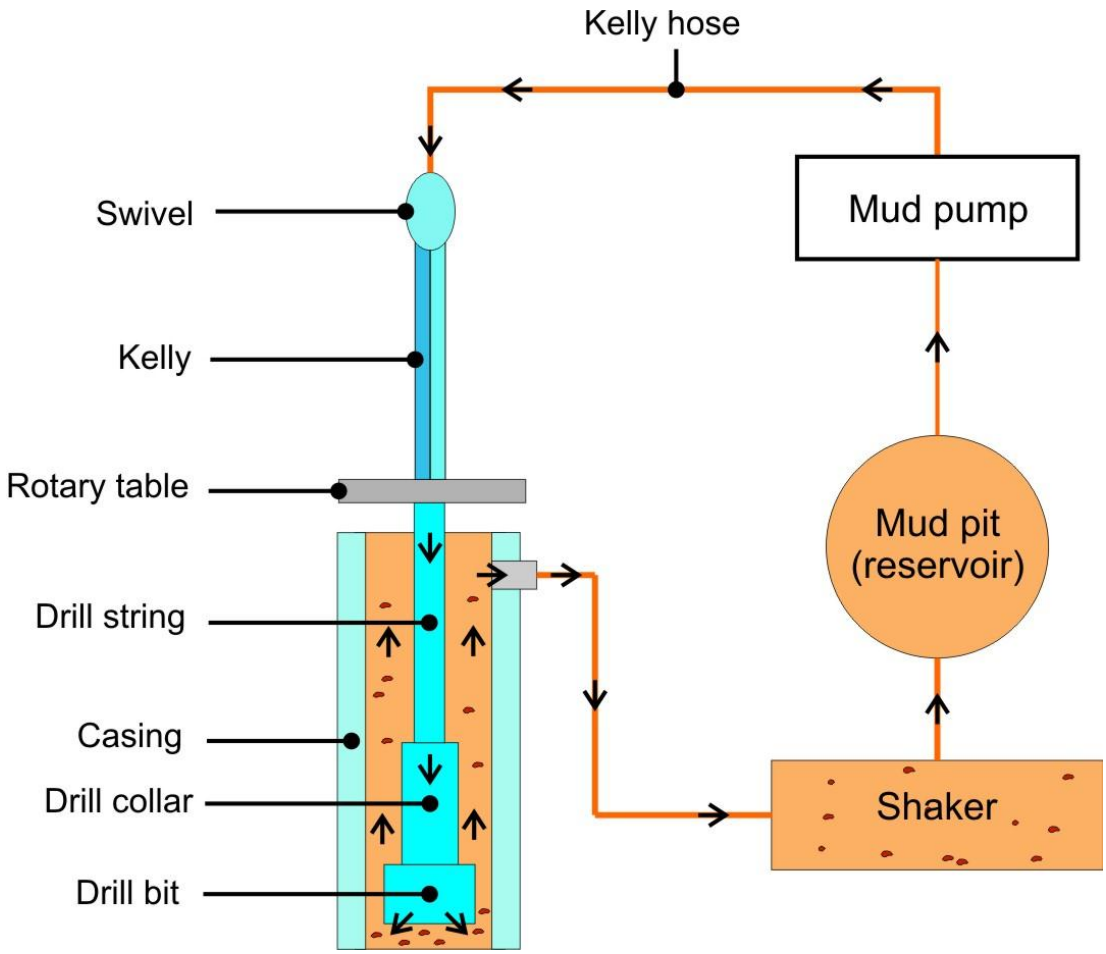

Figure 2.3. Schematic of a typical system found on an oil drilling rig. Arrows are showing the circulation of the drilling mud.

Once the well has reached a certain depth, steel casing will be installed (see Figure 2.3 previously). The casing is a large diameter pipe, which is not part of the actual drilling process, but is important to prevent situations such as formation damage and fluid loss, to name a few.. Typically, the space between the casing the well is filled with cement which seals the gap, avoiding unwanted flow of reservoir fluid on the outer side of the casing. This process is usually known as the Cementing phase [2-4]. Afterwards, the Completion follows, which accounts for the processes taken to prepare the well for oil and gas recovery. It involves installing the necessary equipments and perforating the casing. Finally, the Production phase involves the steps aiming at recovering the reserves, as much as possible and at the highest rates [5].

2.2.2 Materials Subjected to Sliding Contacts during Downhole Drilling

Downhole drilling uses numerous different materials which are in contact. Figure 2.4 shows examples of the two contact types which typically occur – steel/steel and steel/rock, which are one of the causes of high friction during drilling [6, 7]. The steel/steel contact occurs

when the drillstring slides on the casing of the well. However, steel/rock contact occurs between the drillstring and formation (well), where the casing has not been installed. The casing and drillstring steels are typically made of low alloy steel, normally AISI 4340, due to the low cost but reasonable mechanical and chemical properties. Therefore, this project involved simulating these two contact types in the laboratory, which will be presented in detail in the next Chapter 3.

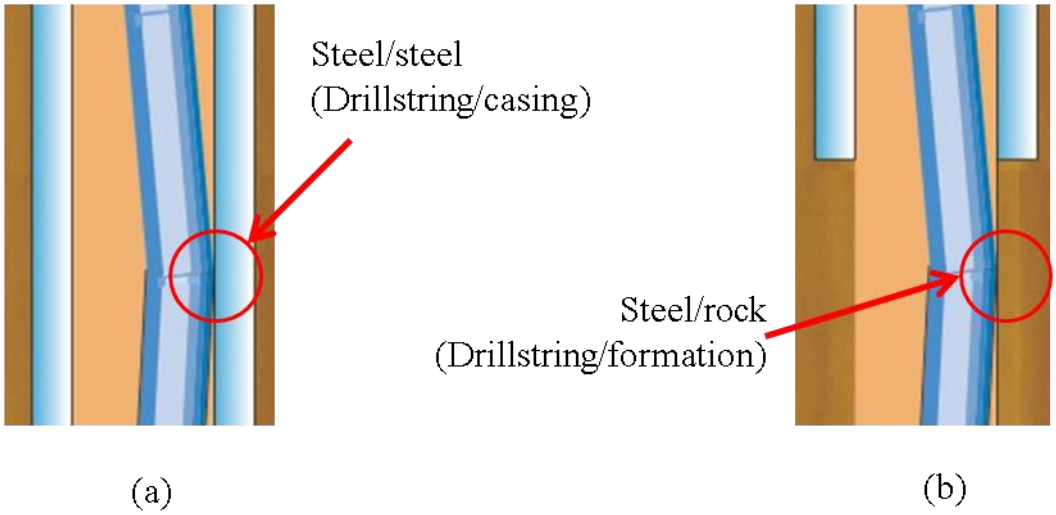

Figure 2.4. Schematic of the steel/steel and steel/rock contacts occurred during drilling.

The formation type differs from one geographical area to another, and also varies with the depth into the earth. The complication increases when these different rocks have different mechanical, physical and compositional properties such as hardness and porosity. For example, Ersoy and Waller [8] studied the wear of drill bits in a simulated laboratory equipment. They performed extensive investigation on the wear mechanism of the bits and factors influencing the wear rates. For example, they claimed that the properties of the rocks have great influence on the levels of wear. Table 2-1 lists some of the properties of the rocks which were examined. They reported that, for limestone, the grains were made of soft calcite particles and were bonded weakly in the rock matrix, thus resulted in low drill bit wear (see Figure 2.5). Furthermore, they reported that the wear rate increased in proportion to the content of the harder silica particles, *i.e.*, being the highest with sandstone. Apart from this, they also reported that the type of drill bit used (such as polycrystalline diamond compact (PDC) or impregnated diamond core), the speed of rotation, and weight on bit (WOB, which is the normal weight applied on the drill bit) will also give different wear rates and mechanisms. For instance, in PDC bits, the cutters are harder than any of the abrasives encountered during drilling, but the binder (matrix) is susceptible to wear and will result in cutter loss. Therefore, the complexity of the tribological systems encountered during drilling requires a sound engineering judgement to maintain optimum operation.

Rock type	Silica content / %	UCS / MPa	BTS / MPa	Young's Modulus / GPa	Mohs Hardness
Limestone	0	28.1	2.86	9.74	2.85
Sandstone	91.22	37.45	3.21	9.85	6.44
Siltstone	81.62	90.54	7.49	17.70	5.51
Granite	72.38	106.15	8.60	19.78	5.74
Diorite	51.57	375.2	30.26	37.38	5.95

Table 2-1. A few properties of different rocks adapted from [8]. UCS is the ultimate compressive strength, and BTS is the Brazillian tensile strength (a standard testing method used for characterising the tensile strength of rock materials).

The wear rates of the three types of bits, sliding aginst all the rocks listed in Table 2-1, are shown in Figure 2.5. The lowest wear rate was found in all bit types, by using the limestone counterface. However, sandstone gave relatively higher wear rate values cf. limestone, with the exception of the impregnated bit which gave the highest value amongst all the test samples. Siltstone gave a similar trend to sandstone, in which the wear rate was increasing from pin, hybrid to impregnated. To the contrary, both granite and diorite showed an inverse trend, *i.e.*, the wear rates decrease from pin to impregnated. Therefore, these results suggest that wear of the bit during downhole drilling operations will vary from one well to another, depending on the geological characteristics. However, the understanding of the wear behaviour of the bit (obtained from laboratory tests) would probably allow the operator to anticipate the levels of wear, hence aid in the planning of bit replacement prior to catastrophic failure.

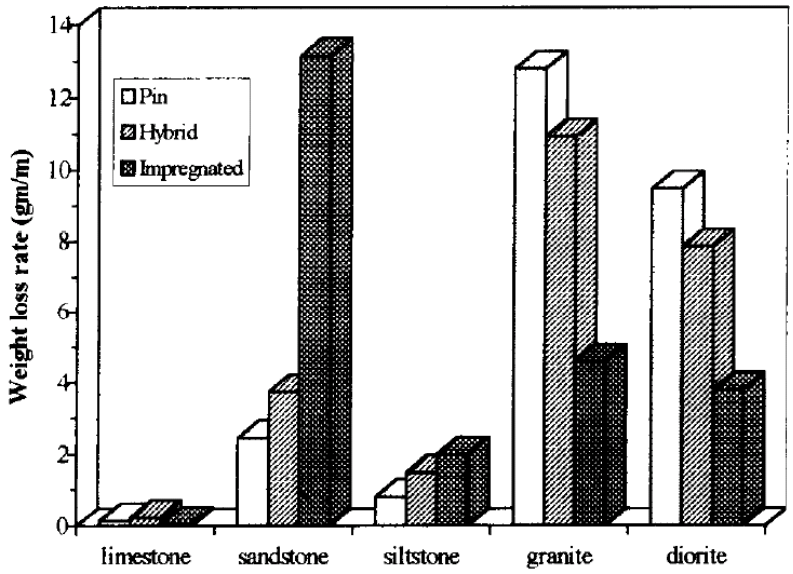

Figure 2.5. The rate of weight loss (wear rate) after drilling the different rock types, by using three bits: PDC (pin), impregnated diamond core (impregnated) and hybrid.

2.2.3 Tribological Problems Related to the Drilling Process

Typically, the tribological problems encountered during oil well drilling are enormous and encompass the phenomena such as erosion, corrosion, abrasion and excessive friction. However, this project is concerned with the sliding contacts in that environment, particularly in the methods that could be used to reduce the friction and wear. Therefore, this subsection (Subsection 2.2.3) will give a brief introduction to the origins of high friction and component wear.

2.2.3.1 Torque and Drag

2.2.3.1.1 Origin of Torque and Drag and the Importance to mitigate it

One of the most vital problems that limit the efficiency of drilling is when excessive torque is needed to turn the drillstring and bit, which would require the turntable to exert more force. The other hurdle is the sliding force required to move the assembly up or down the hole which is widely known in industry as drag. These two are usually quoted together as the problem of 'torque and drag' and can be caused by several factors namely tight hole conditions, keyseats, differential sticking, cuttings buildup and the sliding friction (between steel-steel and steel-rock). Johancsik *et al.* [9] built a mathematical model of directional drilling and compared it with that of the field measurements. They installed an instrument at the joint between the Kelly and drillstring to monitor the vertical forces during drilling (effectively a strain gauge). In addition, a torque meter was also installed at the rotary table which allowed the tangential forces to be monitored. These two setups enabled the calculation of drag and torque respectively. The field test was conducted in three wells with different well path trajectory and mud compositions. However, most of the wellbore were cased at least by 70% along the path (therefore predominantly steel/steel contact). They reported that the sliding friction is the main cause of the excessive torque and drag, and that the typical coefficient of friction using a water based mud is between 0.25 and 0.40.

Excessive torque and drag can cause many negative effects such as slow drilling rates. In most cases, a problem called differential sticking could occur, which is the greatest problem encountered by the oil and gas contractors worldwide [10]. The problem arises when the pressure of the drilling mud is greater than the formation pressure, and when the rotation is stopped, which caused a mud cake to form due to the dehydrated mud. A stuck drill string may interrupt the drilling process for weeks and can sometimes lead to abandonment of the well. These are obviously costly for the drilling companies not only that they have to pay extra labour hours, also to replace tools more often. Millions of dollars are spent in research and development to improve the drilling mud and the method of drilling to overcome these problems [2].

The mechanism of differential sticking is schematically shown in Figure 2.6. During drilling, the high pressure from the drilling mud, or at high angle deviations, cause the drillstring to slide against the filter cake. This filter cake formation is typical of the drilling mud, which is beneficial in sealing the pores of the formation, preventing fluid loss or invasion. During motion, a thin film of drilling mud will develop, which will separate the drillstring and filter cake (Figure 2.6 (a)). However, when rotation stops, or due to excessive mud pressure (pressure of mud higher than formation), the drillstring will bear against the formation, which produces high friction (Figure 2.6 (b)). Furthermore, after a while, thicker mud cake will be produced due to agglomeration of the bentonite clay particles (constituent of the mud), which will increase the area of contact, therefore increasing the 'sticking'. As a result, it is almost impossible for the rotation to restart without difficulty [10, 11].

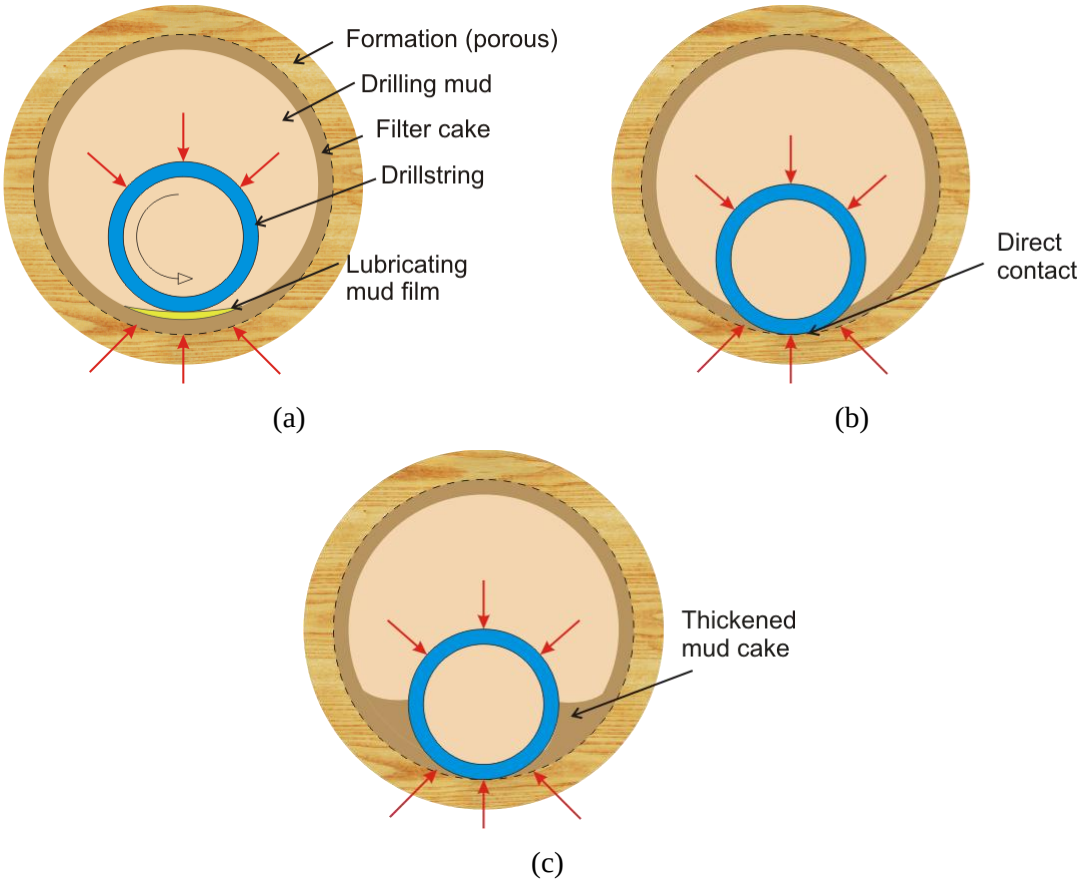

Figure 2.6. A schematic of the cross-sectional view of the drilling process showing (a) a lubricated sliding during motion, (b) a direct contact between drilstring and formation at stationary, and (c) a production of mud cake after stationary for some time. Red arrows indicate the pressure due to drilling mud and formation. Adapted from [10, 11].

A current drilling method, called 'directional drilling' allows drilling highly complex pathways so that difficult areas can be avoided. This is beneficial such as to prevent the well path encountering areas of excessive torque and drag, such as the region of low formation pressures. Furthermore, it permits the drilling company to exploit difficult to reach oil reservoirs. However, additional problems will arise such as the higher cost of drilling and the need for more complex methods to prevent borehole collapse, as well as the increasingly significant torque and drag especially when the drill string bears against the side of the hole (casing) at numerous points along the path, such as shown by Figure 2.7 (representing one contact only) [12].

Therefore, it is clear that overcoming the torque and drag problem would offer great advantages to the oil and gas drilling industry in extracting the buried petroleum. Especially, labour and operational costs could be reduced, such as by the increase in tool lifetime, and the reduced power needed to operate the drill assembly. Therefore, it is envisaged that deeper wells could be drilled, allowing the exploitation of the difficult to reach reservoirs.

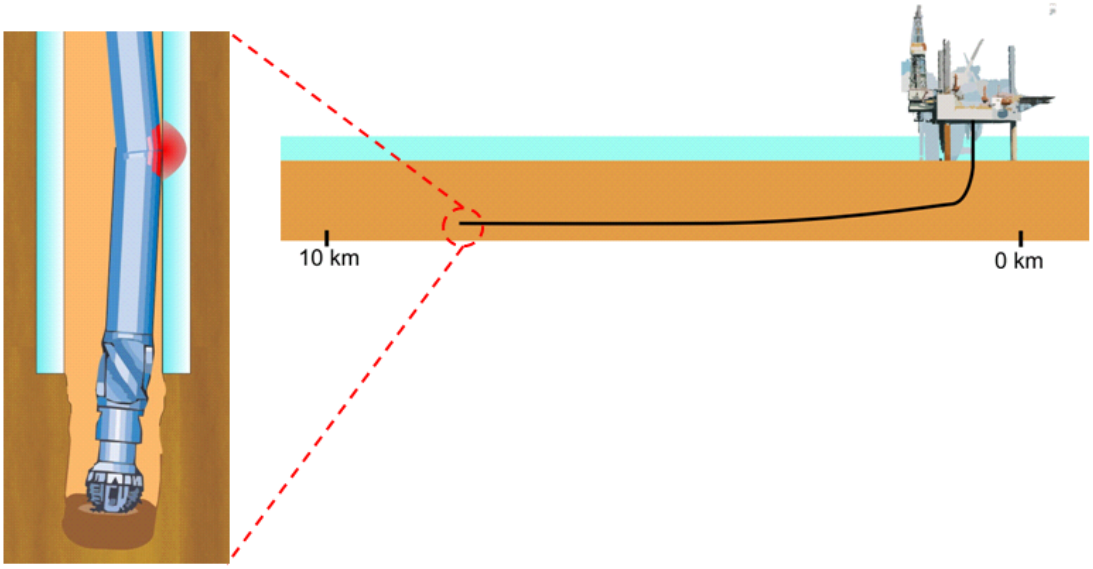

Figure 2.7. Schematic of directional drilling highlighting the area that produces the high torque and drag. The high friction contact such as shown could occur at numerous points along the well path.

2.2.3.1.2 Conventional Methods to Reduce Torque and Drag

Since reducing the torque and drag is crucial in efficient drilling, the drilling companies have been using various techniques to achieve this goal, such as [6, 7, 9, 12]:

i. Ensuring timely hole cleaning operation is made between drilling operations. Methods such as back reaming for cleaning the wellbore has been shown to reduce the torque when drilling restarts [7].

ii. Designing the optimum well path profile, particularly in the details of the curve of the path that is best for reducing friction between the drillstring and wellbore.

iii. Using an improved drilling mud formulation such as by including lubricating additives. Specialist engineers are usually given the responsibility to formulate the best mud for specific wells and work closely with research teams to develop new additives which are superior in performance.

2.2.3.2 Component wear

Component wear is also one of the biggest problems faced by the drilling industry apart from the high torque and drag. As discussed previously, it is reported that the wear of the drill bits is influenced by factors such as the properties of the rock being drilled, among others [8].

Thakare [13] employed a micro-abrasion rig, and a modified ASTM G65 tribometer to assess the wear of sprayed and sintered tungsten carbide (WC)-hardmetals (material widely used in the oilfield industry) exposed to silica sand slurry, simulating the conditions of

downhole drilling, *i.e.*, the cut formation. It was reported that the micro and macro abrasion (relating to the sizes of grooves) obtained from the used drill components, were successfully replicated in the laboratory experiments. Furthermore, it was concluded that the wear mechanisms were related to the size of the abrasives in the slurry. Particularly, the WC-10Co-4Cr coating underwent delamination due to subsurface cracking, which increased with abrasive size. In addition, the sintered WC-5.7Co-0.3Cr underwent carbide grain cracking, also increased with abrasive size. The effect of corrosion was also tested, such as the formation of a localised corrosion around the carbide grains.

Other workers such as Reyes and Neville [14] studied the degradation of the drill tool components from the erosion and corrosion perspective. They claimed that the erosion damage is most profound at the nozzle on the drill bit, in which the drilling mud exits with high velocity, pressure, as well as temperature. Damage could be done to the drill bit inserts (cutters) by removal, due to the weakening of the joints or binder, which in some cases caused a complete drilling failure at less than 300 m of well depth (see example in Figure 2.8). In their investigation, they employed the impingement of a liquid slurry (500 mg L^{-1} sand in 3.5% NaCl solution) onto three different downhole materials, namely cobalt-based alloy, nickel-based composite coating with tungsten carbide, and tungsten carbide copper-based solid cermet; at 45º, 60º, 75 º and 90 º angles. Their results show that the materials degrade by different mechanisms owing to the microstructures. Furthermore, the damage is a complex combination of mechanical and electrochemical processes and interactions, which varied with impact angles.

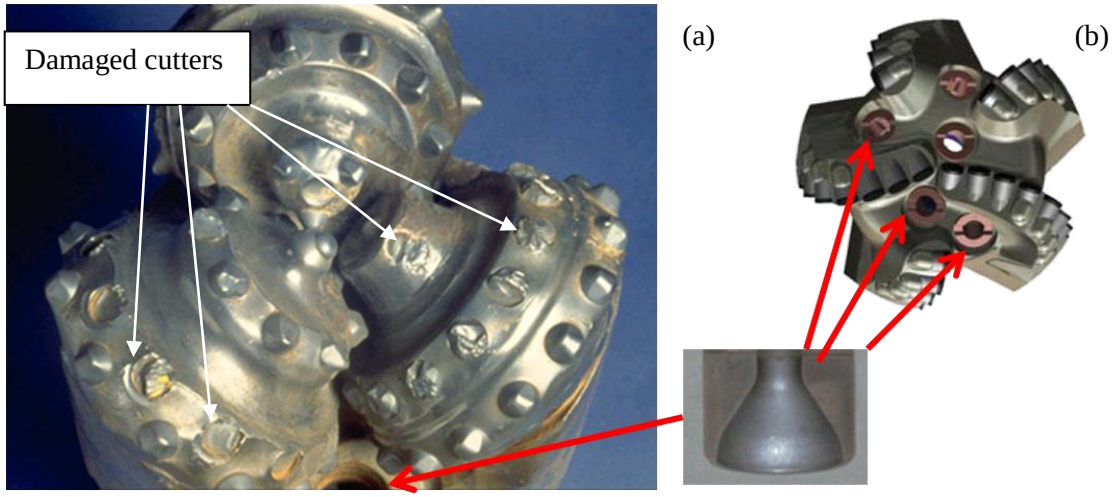

Figure 2.8. Examples of two types of drilling bits: (a) a worn roller cone with damaged cutters, and (b) polycrystalline diamond compact (PDC). A cross sectional side view of the nozzle in which the mud exits in high velocity is shown on bottom right. Adapted from [15, 16].

Generally, there are numerous other published work related to understanding and reducing the tribological problems during downhole drilling. Many of these are especially published in dedicated journals such as by the Society of Petroleum Engineers (SPE), which receives contributions from various oilfield companies, dating from decades ago. In addition to this, there are also contributions from research institutes (including the abovementioned), such as by Truhan *et al.* [17, 18] who tested the wear behaviour of various cladding materials for downhole use, exposed to simulated drilling mud. Therefore, the work mentioned here are just to provide an overall discussion of the complex behaviour of drill tool wear.

In summary, erosive wear could be found due to the presence of the sand particles from rock cuttings in the drilling mud, in combination with the harsh conditions such as high temperature and pressure. Conversely, abrasive wear can be caused by the sliding action between the drillstring or drill collar with the side wall, which can be cased or uncased, and can be exacerbated by the presence of cuttings or sand which can increase abrasion levels [13, 17, 18]. Furthermore, corrosion coexists, and is a complex and unwanted occurrence which aids the material degradation.

2.2.4 The Drilling Mud/Fluid

This subsection (Subsection 2.2.4) will present the functions and compositions of the drilling mud used in the drilling process as described previously. The main components of the drilling mud, such as the base fluid are discussed, along with other important constituents such as the friction modifying additives. However, only subject areas relevant to this project will be reviewed, since the engineering behind the formulation of the drilling mud is a major discussion of its own.

2.2.4.1 The Types of Mud Typically Used

Historically, the purpose of drilling mud was to remove cuttings from the borehole. Nowadays the function of the drilling mud are expanded to include [12]:

- Carry away cuttings from beneath the drill bit and to transport them up the drill-casing annulus.
- Cool and clean the drill bit.
- Reduce friction between the drilling string and the sides of the hole.
- Maintain the stability of uncased sections of the borehole.
- Prevent the inflow of fluids from permeable rocks penetrated
- Form a thin, low-permeability filter cake which seals pores and other openings in the geological formations penetrated by drill bit.

- Assist in the collection and interpretation of information available from drill cuttings, cores, and electrical logs.
- To drive the drill bit and directional systems.

The drilling mud is usually classified by its principal constituent *i.e.* gas, water- or oil-based. Some components are added to modify the rheology of the mud (such as bentonite particles or polymers) so that an optimal performance can be achieved during drilling. Additionally, solids are often used to increase the density of the mud (such as inert barite particles) to stabilise the bore formation pressure [12].

A gas-based fluid is used to remove drill cuttings by a high velocity stream of air or natural gas. It is good at reducing the damage to productive zones and provides a faster drilling rate. Foaming agents are required to avoid minor inflows of formation water. However, formations that have high water content will limit the use of gas-based fluids.

Oil based muds can cause problems due to their non environmental-friendly nature both in operation and disposal, thus only 5 to 10% of wells drilled use these. Whereas water-based drilling muds are generally recognised as being more environmental-friendly, and are widely used [5]. Unfortunately the utilisation of a water based mud results in higher friction than the oil based counterpart. Therefore, improving the lubricity of the water based mud offers great advantages to the drilling industry in particular to minimise the problems of excessive torque and drag [12].

Often the best formulation is unique to a particular well because of the many factors that govern the production of an effective and efficient drilling. A drilling mud engineer would have to consider several factors (apart from the discussed) when deciding the appropriate ingredients such as filter cake formation, corrosion, rock mechanics, formation chemistry, logistics and economics [19].

2.2.4.2 Comparing and Contrasting the Water and Oil Based Mud

A brief comparison of the water and oil based mud, focusing on the functions needed for downhole conditions are shown in Table 2-2 below. There are trade offs between using water and oil based muds, although, new types of mud are being developed to have both the good qualities of water and oil based muds, which are synthetic chemicals such as esters, ethers, polyalphaolefins, glycols, etc [5].

Required Functions	Water based mud	Oil based mud
Lubricity	Less lubricious and highly dependant upon the additive to impart low friction	Naturally low in friction
Corrosion	High corrosion unless incorporating a corrosion inhibitor	Low corrosion
Temperature stability	Relatively low	High
Cost	Low	High
Environmental impact	Low	High when spilled in the sea
Shale stability	Additives such as K^+ and Ca^{++} salts can only slow water migration	Able to stop water migration to shale by osmotic pressure, thus preventing swelling
Handling	Does not require complex machinery, except for mixing and filtering (cleaning)	Requires extra equipment to carefully collect and store, especially with diesel oil (toxic when used)

Table 2-2. A few different functions of the water and oil based mud in comparison [5, 12].

2.2.4.3 Friction Reducing Additives for Water Based Mud

As mentioned, reducing torque drag has been an industrial priority in many years. This is done by adding, in relatively small amounts (typically 1 to 3 wt% concentrations), lubricating agents into the drilling mud [20, 21]. These additives are called "lubricants" in the oil industry, and laboratory tests showed that friction reduction can be obtained significantly, in some cases by up to 70% cf. the case without the lubricants [20].

Mondshine [11] has reported the effect of various additives on the coefficient of friction of water based muds. The test procedure consisted of a steel test block simulating the bore wall which was loaded against a test ring by a torque arm (this is effectively a block-on-ring setup, which will be discussed in Section 2.3.2). The rotational speed was 60 rpm and the contact stress used was 5 MPa, which were claimed to represent field conditions. The tests included two types of mud – (A) 15 g bentonite in 350 ml water, and (B) 15 g bentonite, 60 g shale, 3 g chrome lignosulphate, 0.5 caustic soda in 350 ml water. The results are summarised in Table 2-3. Generally, it showed that only fatty acid, sulfurised fatty acid, and a blend of triglycerides and alcohols effectively reduced the coefficient of friction in all muds (see highlighted rows in Table 2-3).

Additive name	Concen-tration / kg m^{-3}	Coefficient of friction		
		Water	Mud A	Mud B
No additive	0	0.36	0.44	0.23
Diesel oil	0.29	0.23	0.38	0.23
Asphalt	22.8	0.36	0.38	0.23
Asphalt + Diesel oil	22.8 + 0.29	0.23	0.38	0.23
Graphite	22.8	0.36	0.40	0.23
Graphite + Diesel oil	22.8 + 0.29	0.23	0.40	0.23
Sulfurised fatty acid	*11.4*	*0.17*	*0.12*	*0.17*
Fatty acid	*11.4*	*0.07*	*0.14*	*0.17*
Alcohol	5.7	0.16	0.40	0.23
Sulfonated asphalt	22.8	0.25	0.30	0.25
Sulfonated asphalt + diesel oil	22.8 + 0.29	0.07	0.06	0.17
Blend of modified triglycerides and alcohols	*11.4*	*0.07*	*0.06*	*0.17*

Table 2-3. Effect of various water additives on the coefficient of friction of water and two fresh water muds. The highlighted rows are the additives with most reduction effect. Table adapted from [11].

The three highlighted rows from Table 2-3 were used to calculate the percentage of reduction in friction, with respect to the condition of no additive, and are shown in Table 2-4. Generally, the most reduction in friction was given by the blend of modified triglycerides and alcohols, which were 81% and 86%, in water and mud A respectively. In water, the fatty acid gave higher reduction (at 81%) cf. the sulfurised fatty acid (at 53%). However, the case was the opposite in mud A, in which the sulfurised fatty acid gave a higher reduction at 73% cf. fatty acid at 68%. All additive gave only small percentage of reduction in mud B, at 26%.

Additive name	Amount of reduction in friction with respect to no additive / %		
	Water	Mud A	Mud B
Sulfurised fatty acid	53	73	26
Fatty acid	81	68	26
Blend of modified triglycerides and alcohols	81	86	26

Table 2-4. Reduction of friction of the three additives with respect to the condition where no additive was present. Information adapted from previous Table 2-2. The values of coefficient of friction at no additive were given in column 2 in Table 2-2.

Therefore, the results shown in both Table 2-3 and Table 2-4 reflect the different levels of friction that could be obtained by just changing the additive type and the base fluid (mud), obtained from laboratory tests. These results were in agreement with field measurements which gave coefficient of friction values in the range of 0.25 and 0.40 (no additive was used)

[9]. Nevertheless, the best option for the formulation of a drilling mud is with the minimum cost, practical and environment friendly, which is the responsibility of the mud engineer. For example, recently, more research has been done into using esters and vegetable oils as the lubricant additive [20].

2.2.4.4 Viscosity Enhancer for Water Based Drilling Mud

This subsection (Subsection 2.2.4.4) will present the review of the additives used for the purpose of increasing the viscosity of water, which will produce the drilling mud. Mainly, the two types of additives are the bentonite particles and polymer, in which the chemical and physical properties in both cases will be presented.

2.2.4.4.1 Physical Properties of the Drilling Mud for Cuttings Transport

The drilling muds are non-newtonian fluids, in which the viscosity changes with shear rate. It falls under the thixotropic type fluid which thins (reduce in viscosity) over time at elevated shear rates. The action of shearing at constant rate distorts the structure of the bentonite particle arrangement, but it can be recovered when stopped. On the other hand, disorientation or deformation of the molecular network conforming to the direction of shear is seen in polymer based mud [22]. Understanding of this behaviour is important since the change of viscosity means that the cuttings carrying capacity of the drilling mud has also changed [23].

A graph of the thixotropic behaviour of the drilling muds is shown in Figure 2.9. Viscosity is defined as the ratio of the shear stress to the shear rate, therefore the reduction in viscosity is seen at higher shear rates. The yield point is an extrapolated stress at zero shear rate (from lab tests), which is widely used in the drilling industry to quantify the cuttings carrying capacity of the drilling mud in static conditions.

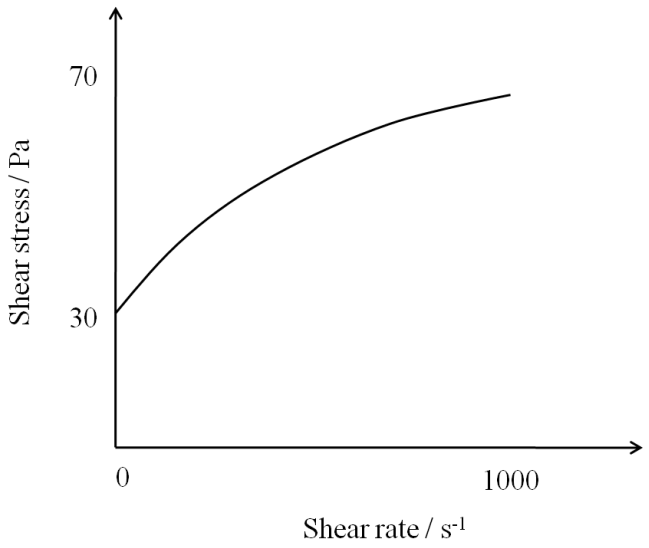

Figure 2.9. Thixotropic behaviour (shear thinning) of the drilling muds [23].

As discussed previously, the drilling mud is pumped through the drill string and at high shear rates. After exiting at the drill bit's nozzle, the velocity will reduce immediately. Therefore, at the annulus, the shear rate is considerably low and the viscosity is sufficient to provide cuttings transport ability. Other factors such as salt content, temperature and surfactant also play important role in the physical behaviour of the drilling mud [22-24].

2.2.4.4.2 The Chemistry of Bentonite Drilling Mud

Bentonite particles are obtained from crushed clay, which are found from weathered volcanic ash. The particles consist of a plate-like microstructure of octahedral aluminium or magnesium hydroxides, sandwiched between tetrahedral silica layers, and are called as unit layers as shown in Figure 2.10 [25].

The unit layer is charged, which make the molecules interact with each other and the environment. This is due to the base surface of the unit layer which consists of a fixed negative charge; and a pH dependant charge at the edges. Zhao *et. al* [26] confirmed using the Atomic Force Microscope (AFM) that the base surface charge do not change with pH, unlike the edges.

The permanent negative charge on the basal surface are produced by the substitution of Fe^{3+} or Al^{3+} for Si^{4+}; or, Mg^{2+} or Fe^{2+} for Al^{3+} ions in the octahedral sheet. These substitutions create charge deficiencies therefore producing the net negative charge [25]. On the other hand, the edges of the platelets can be positively or negatively charged due to the discontinuity of the molecular structure at the edges which exposes the Si^{4+}, Mg^{3+}, Al^{3+} or Fe^{3+} ions [27, 28]. At low pH (acidic), the abundance of H^{+} ions can react with the exposed ions at the edges producing positive charges. Conversely, at high pH (alkaline), OH^{-} ions

can react to produce negative charges. The transition pH at which the edges crosses between net positive and net negative charge is called the Point of Zero Charge (PZC). Previous work determined the pzc of bentonite to be around pH 6.5 [26, 27].

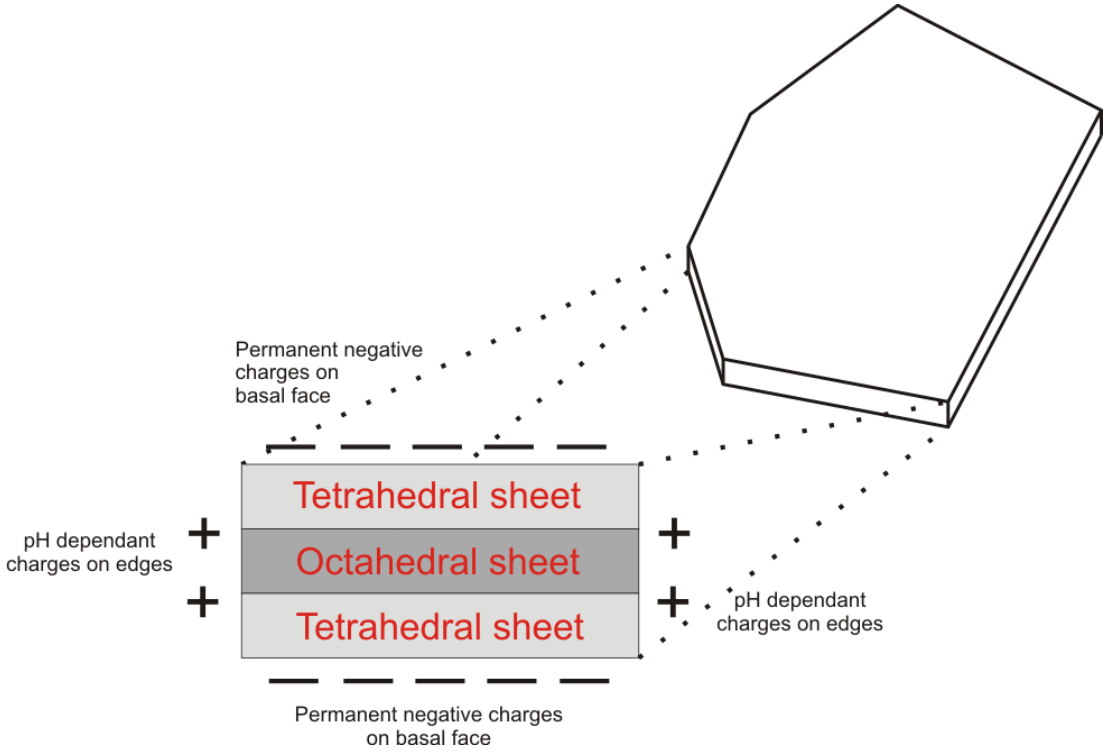

Figure 2.10. Two dimensional schematic of the unit layer structure of bentonite. The tetrahedral sheets consist of silicon and oxygen atoms while the octahedral sheet consists of magnesium and aluminium atoms.

The effect of the negatively charge basal surface is the adsorption of cations, such as Ca^{2+} or Na^{+}. When immersed in water, these adsorbed cations can exchange with cations of another species in the water, thus known as the exchangeable cations. These exchangeable cations are important in determining the swelling of the bentonite particles which are exploited in industrial applications to increase the viscosity of fluid, water pollutant removal and cosmetic products. Sodium ions are only weakly bonded to the surface and can easily diffuse away, which do not create a competition for water adsorption, thus the bentonite can swell easily [12].

The effect of having the different combinations of charges on the basal and edge is variation in the orientation of these unit layers when dispersed in water. This can have a substantial effect on the physical properties of the bulk fluid. Table 2-5 briefly shows the different types of particle orientation. The flocculated particles are commonly referred as the cardhouse structure and are responsible for the continuous gel property. Aggregation can be obtained by adding cationic surfactant in the mud to reduce the exposed negative charge on the basal surface. The pH of the drilling mud is always kept at alkaline values (around 8 or 9), so that the edges are negatively charged and results in a dispersed particle orientation (not

aggregated). Ultimately, these orientations are important because they affect the physical properties of the bulk mixture. For instance, a non-aggregated or dispersed orientation would provide high gel strength, which would be able to provide the viscosity enhancing effect needed during drilling.

Basal charge	Edge charge	Orientation	Schematic	Physical effect
Negative	Positive	Edge-to-face	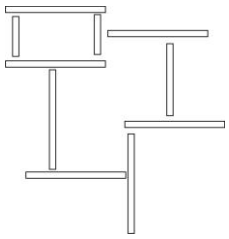	Flocculation – continuous gel structure
Weak Negative	Negative	Face-to-face	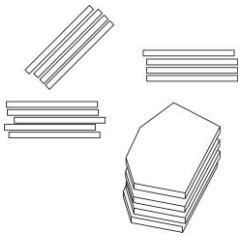	Aggregation – decrease in gel strength
Negative	Weak positive	Edge-to-edge	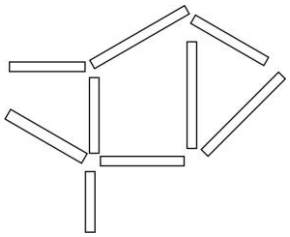	Flocculation – continuous gel structure

Table 2-5. Types of particle arrangement/orientation in a bentonite mud which affects the physical behaviour. The dispersed orientation found during the negative basal and negative edge charges are not included.

2.2.4.4.3 Polymer as an Alternative to Clay in Water Based Mud

The purpose of using the clay particles is to mainly provide a viscosity enhancing effect in the mud. However, in terms of lubricity, substituting polymer for clay would result in a significant reduction of friction [29]. Although, the use of polymers are not limited to imparting lubricity, but includes other important functions such as fluid loss control agent. For example, Caenn and Chillingar *et. al* [5] reviewed the types of polymers which are used to add to the drilling mud. They reported that the types of polymers used are either natural (*e.g.* starch), modified natural (*e.g.* carboxymethylcellulose (CMC)), or synthetic (*e.g.* polyacrylates). In addition, the advantage of some of the polymers is when the use of clay particles is not practical, such as in high salt content waters. In such conditions the clay particles will be unstable, but starch, for example, would be able to provide filtration control.

However, the utilisation of polymers are limited due to the environment temperature, because of the susceptibility of the molecules for decomposition [30].

Polymers consist of the repeated number of unit cells, called monomer, which are linked together either in straight or branched chains forming macromolecules. Therefore, the orientation of these molecules could provide viscosity enhancing effects, such as found in the CMC, where the coiled molecules could stretch linearly when added to water (thus increasing viscosity) [30]. The petroleum industry utilises both type of polymers which are solid-state and in solutions for various applications beyond the drilling mud formulation [4].

2.3 Fundamentals of Tribology

The word tribology was first coined in 1966 by a UK government committee, although friction wear and lubrication had been studied prior to that. Tribology was defined as 'the science and technology of interacting surfaces in a state of relative motion and the practices thereto' [31, 32]. This section (Section 2.3) will review the fundamentals of tribology related to the basic understanding of friction, wear, boundary lubrication and the mechanics of a point contact. These are important to establish the understanding of the experimental work undertaken in this project, apart from aiding the analysing of the test results, which will be presented later in this thesis.

2.3.1 Friction and Wear

Friction is defined as "the resistance encountered by one body in moving over another when subjected to applied normal load" (see Figure 2.11) [31]. The friction force, *F*, is the force which opposes the sliding motion, and the ratio of *F* to the normal load, *W*, *i.e.*, *F/W*, *is* defined as the *coefficient of friction, μ*. There are three important laws that govern the friction force. The first is that the friction force is proportional to load. This law agrees with Bowden and Tabor's theories in which the increased real area of contact (owing to increased load) results in higher adhesive forces between the surfaces thus increasing friction. Second, the law states that friction is independent of apparent area of contact. This is true since the critical property is the real area of contact which cannot be measured easily. The third law states that friction is independent of sliding velocity, but inapplicable in some conditions such as when the material is subjected to thermal deformation due to the frictional heating, or stick-slip conditions. The second and third laws depend on the condition of the contact such as the presence of lubricant (*e.g.* water or oil) and the type of lubrication, *e.g.* hydrodynamic, elasto-hydrodynamic or boundary lubrication [33].

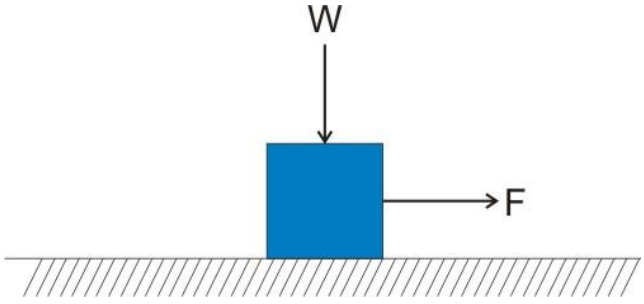

Figure 2.11. Schematic of a body sliding on a plane.

Wear is defined as the progressive damage, involving material loss, which occurs on the surface of a component as a result of relative motion to the adjacent working parts. Various phenomena that cause wear are such as adhesion, abrasion, and delamination. A simple theoretical analysis of abrasive wear was due to Holm and Archard. The model assumes that

the contact can only occur at the asperities and that the true area of contact will be equal to the sum of the individual asperity contacts (will be discussed in detail in Subsection 2.3.3). The Archard wear equation is given by,

$$Q = K\frac{W}{H} \qquad \textbf{eqn. 2.1}$$

which asserts that the general wear, Q is proportional to the ratio of the normal load to the hardness of the softer material. K is a constant of proportionality usually known as the wear coefficient, it is dimensionless and less than unity. A rather more useful quantity is the ratio K/H which is known as the dimensional wear coefficient or specific wear rate in $m^2\ N^{-1}$ [31, 32].

Abrasive wear is defined as wear in which hard asperities on one body or discrete particles, moving across a softer body under some load, penetrate and remove material from the surface of the softer body, leaving a groove [34]. A wide approach to classifying abrasive wear is by dividing into two basic modes known as two-body abrasion and three-body rolling, as schematically shown in Figure 2.12 [34]. The result of a two-body abrasion mechanism is a grooved surface while a three-body rolling would be an indented surface.

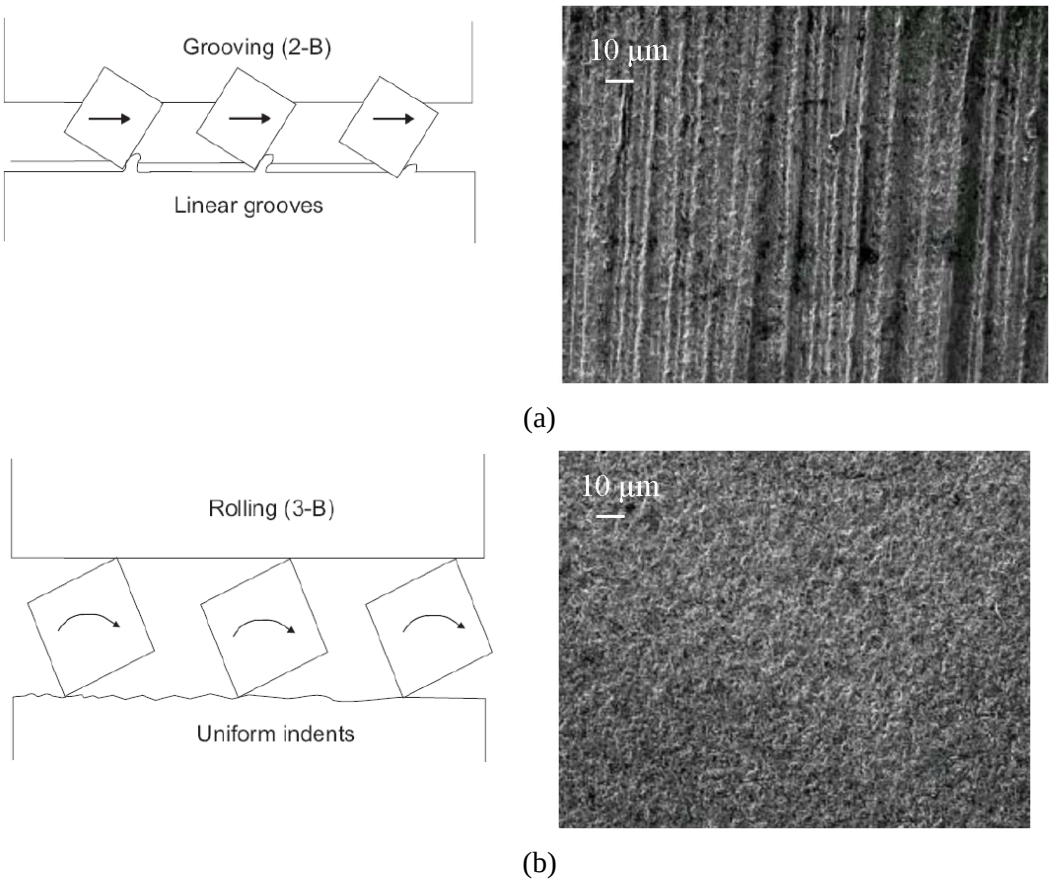

Figure 2.12. Schematic (left) and a Scanning Electron Microscopy (SEM) example (right) of (a) the two-body abrasion (grooving), and (b) three-body rolling. Adapted from [13, 31].

Furthermore, debris can form as a result of the ploughing and can be ejected to the environment or remain in the contact. The debris itself can also undergo other processes such as work hardening or corrosion thus can significantly affect the friction and/or the extent of wear of the sliding surfaces [35]. It is also likely that the sliding can produce debris at the asperity contacts and transfer the debris onto the other surface, such as shown in Figure 2.13 [31, 36].

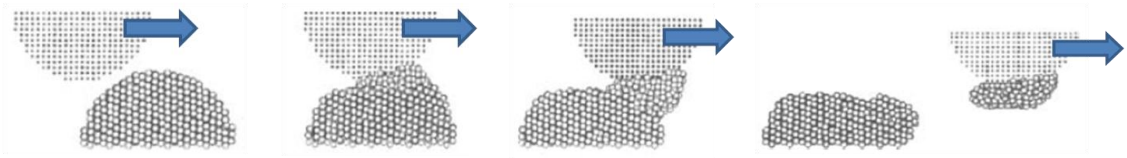

Figure 2.13. Simulation of a material transfer during asperity contact at (a) just before contact, (b) the surfaces adhering to each other, (c) plastic deformation of the softer surface, and, (d) detachment and transfer of debris. Adapted from [36].

2.3.2 Lubrication

2.3.2.1 Different Types of Lubrication Regimes

Reviewing the types of lubrication regimes could be done by virtue of the classic work by Richard Stribeck in 1902 (Stribeck curve), as shown in Figure 2.14 [37]. The test was conducted using a bearing rig setup, but could be used to explain the regimes of lubrication clearly. The graph shows a relationship between coefficient of friction and the product of $\eta U/W$ (Somerfield equation), where η is the bulk viscosity of the lubricant fluid, U is the sliding velocity and W is the normal load.

Generally, in the hydrodynamic regime, the sliding surfaces could be separated by the lubricating film, which could be wedged into the contact. This lubrication type could develop in conforming geometries such as found in journal bearings. Note that this regime does not give the lowest friction, due to the presence of drag forces from the fluid especially at higher velocities [38]. In the elastohydrodynamic (EHL) regime, the effective separation of the surfaces is lower and results in some contact between the surface asperities. This lubrication type is found in contact geometries that are non-conformal, such as between a sphere and a plane, where the pressure is higher than for hydrodynamic lubrication.

In the boundary lubrication regime, the lubrication film does not exist, which is found in contacts of high pressure and low sliding speed. Furthermore, this contact could develop when aqueous solutions are used as the lubricant instead of oil. Therefore, the lubrication of this type involves the adsorption of molecules on the surfaces to separate the bare contact between asperities. This regime gives the highest friction and wear [31, 39]. The boundary lubrication phenomena will be discussed further in the next subsection (2.3.2.2).

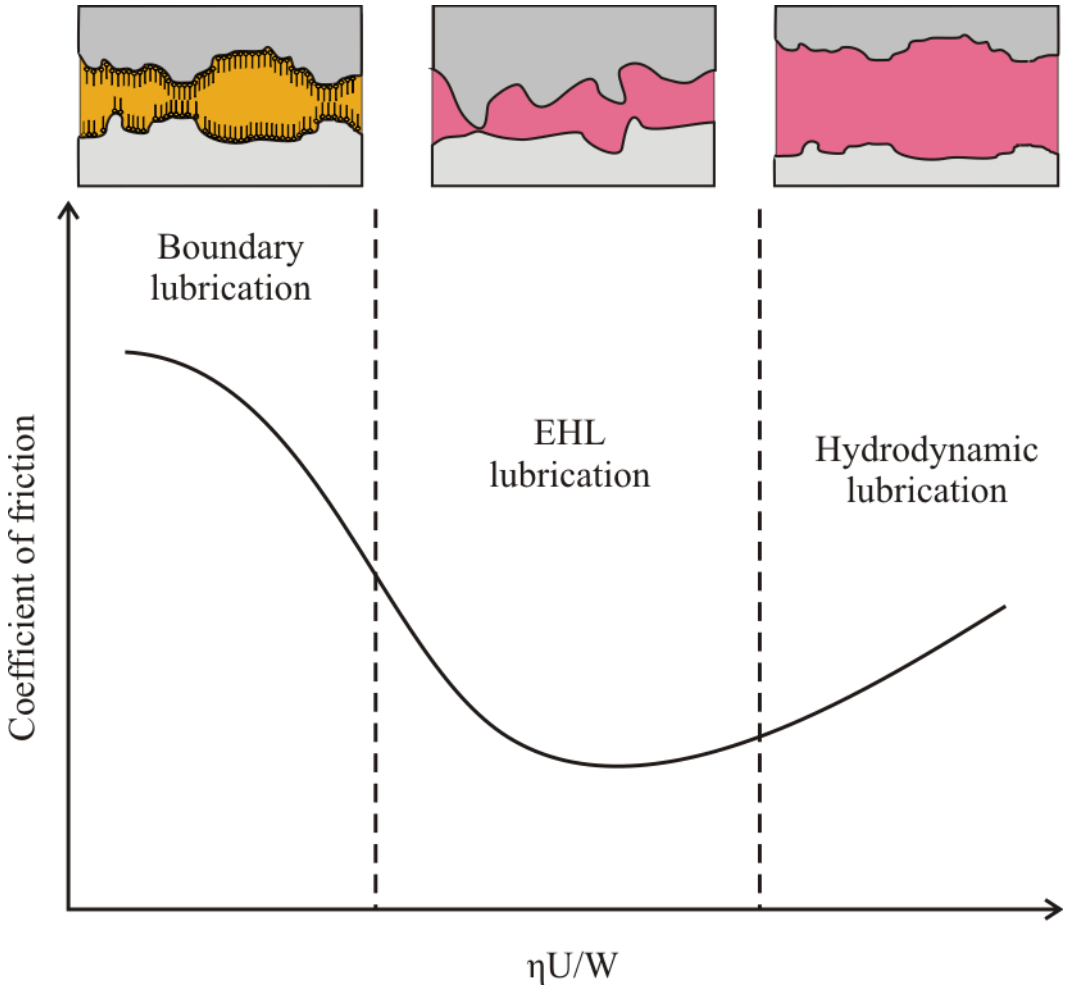

Figure 2.14. The Stribeck curve consisting of coefficient of friction *vs.* Somerfield equation (ηU/W). Adapted from [31]. Note that the Somerfield number is equivalent to the ratio of the height of separation between the surfaces to the roughness of the surfaces.

2.3.2.2 Boundary Lubrication

According to the friction model by Bowden and Tabor, friction can be modelled as being a sum of adhesion force between the two contacting metals and the deformation force needed to plough the asperities [40]. The relationship of the coefficient of friction due to adhesion is shown by,

$$\mu_{adh} = \frac{s}{H} \qquad \textbf{eqn. 2.2}$$

where s is the shear strength of the softer material and H is the indentation hardness of the same material. Hence, the presence of a low shear strength film between the contacting surfaces will reduce friction and wear of the contact. This is the mechanism of boundary lubrication.

Within this range of operation, the bulk properties of the fluid such as its density and viscosity, are of relatively low importance, while its chemical and composition, as well as that of the underlying metals or substrates become increasingly significant [31, 32, 41, 42].

Since 1915, small proportions of fatty acid additives have been used in refined mineral oils to provide lubrication. Such additives are still used today to impart friction reducing along with wear reducing properties to lubricants and fuels [42]. It is well-known that additives with polar groups adhere strongly to the metal surface and the separation between the hydrocarbon tails provide the mechanism for friction reduction both in aqueous and non-aqueous media (see Figure 2.15). In addition, longer hydrocarbon chains are reported to provide better reduction in friction [40, 43, 44]. The molecular weight represents the length of the hydrocarbon tail of the molecules and it was shown that as it was increased, coefficient of friction can be reduced significantly. Gellman and Spencer [39] judiciously reviewed on the relationship between surface chemistry and tribology. It was reported that the phenomena of boundary lubrication exists at the most extreme tribological conditions, which made it important, and is an area of less understood until recently. For example, there has been dispute over the development of either a monolayer or multilayer adsorption on the contacting surfaces to impart lubrication, which is now believed to be a combination of both. However, the real implications of each individual condition (*i.e.*, mono- or multilayer) are still unclear and are an active research subject. Some published work related to the chemistry of these additives will be discussed further in Section 2.5.

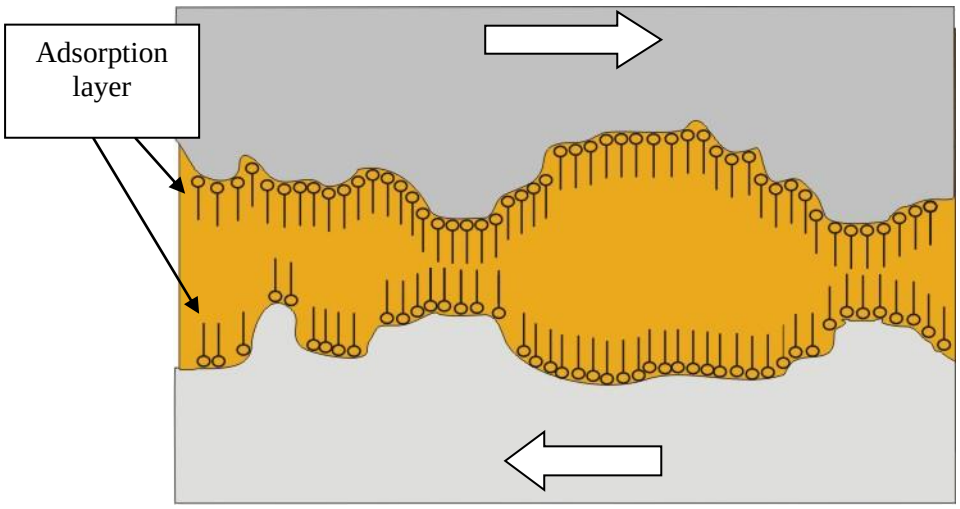

Figure 2.15. Schematic of surface separation by the boundary layer mechanism.

2.3.3 Contact Mechanics

2.3.3.1 Hertzian Contact Stress

The first analysis of the stresses at the contact of two elastic solids was reported by Hertz in 1882 [45]. The model stated that when a sphere is pressed against a flat surface, contact will occur over a circular area of radius *a*, see Figure 2.16 [31].

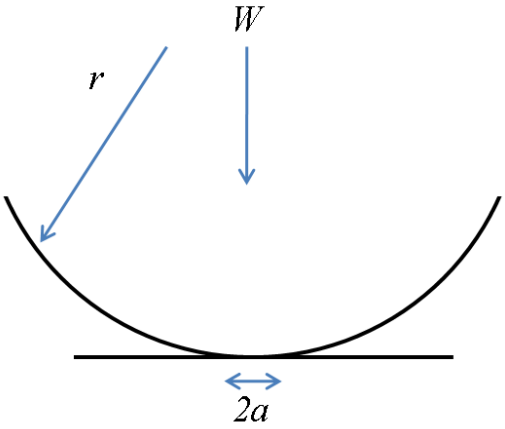

Figure 2.16. Elastic deformation of a sphere of radius *r*, pressed against a plane surface under a load *W*. The radius of the contact circle is *a* [31].

Therefore, the area of the contact in m^2 is given by [31],

$$\pi a^2 \approx 0.83\pi \left(\frac{Wr}{E}\right)^{\frac{2}{3}} \qquad \textbf{eqn. 2.3}$$

where E is the elastic modulus which depends on Young's moduli, E_1 and E_2 and on the Poisson's ratio, ν_1 and ν_2 for the materials of the sphere and plane by,

$$\frac{1}{E} = \frac{(1-\nu_1^2)}{E_1} + \frac{(1-\nu_2^2)}{E_2} \qquad \textbf{eqn. 2.4}$$

Therefore, the contact pressure in N m^{-2} between a sphere and a flat plane could be calculated by dividing the normal load by the area of contact (given by eqn. 2.3). However, the value is useful only before sliding commences, due to the plastic deformation and material removal occurring during tribological tests.

2.3.3.2 Theory of Contact Area

The Hertz model shown in Figure 2.16 previously, represented the theoretical approach towards deriving an equation for the nominal contact area between a sphere and a flat plane. However, Archard in 1957 [46] generally described that the real contact between two surfaces occurs on the micro scale, by the concept of 'protruberances on protruberances on protuberances,' which defined the idea of surface roughness in qualitative terms (see Figure 2.17). Bowden and Tabor used the term 'asperities' to describe the real contact points.

These two theories appreciated that even polished surfaces are not 'ideally' flat and have been used widely to ascribe the fundamentals of friction and wear of sliding materials [47]. Bowden and Tabor's theory was based on the Hertzian contact stress calculation in which they claimed that the area of the asperities already in contact will increase with applied load. This relates to the friction and wear of sliding materials because the increased real contact area gives rise to the levels of adhesion and deformation at the micro scale. A better roughness contact model was given by Greenwood and Williamson [48] which included the effects of plastic deformation of the asperities and applied statistical approach towards understanding the distribution of the peaks. The combination of all these theories have led to a fundamental understanding of tribology, and is constantly being developed and redefined [47].

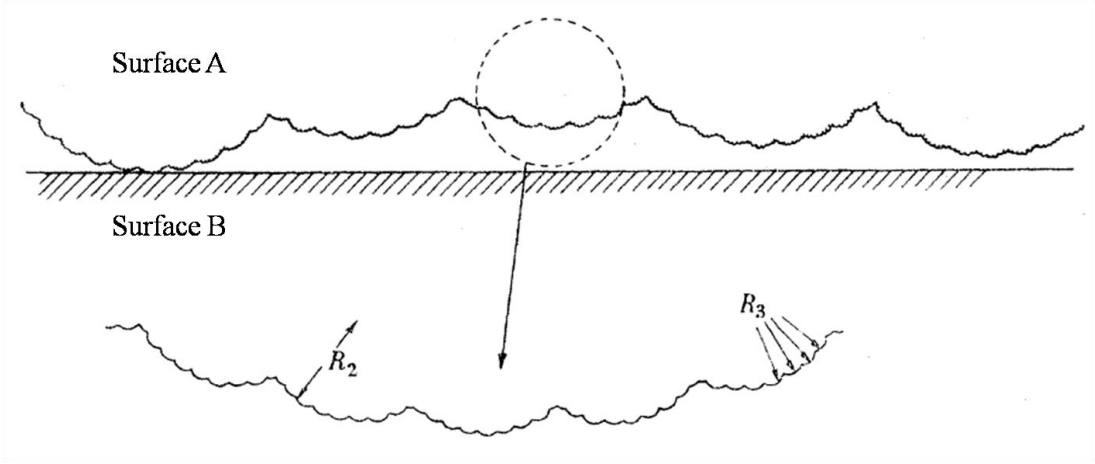

Figure 2.17. Schematic of the Archard's theory of surface roughness adapted from [46].

2.3.4 Friction and Wear Testing Methods in Tribology

According to Gee and Neale [49] there are numerous reasons for performing friction and wear tests. One of them is to characterise the materials performance and determine how different materials or variations in their structure can affect friction and wear. Another reason is to obtain a greater understanding of the underlying mechanisms. These two types of studies are normally carried out in the laboratory with relatively simple test set-ups and methodologies. Other testing approaches such as field tests or machinery bench tests may often result in greater cost and complexity whilst reducing experimental controllability and flexibility.

It is important that the experimental design and conditions should be appropriate and relevant to the real life conditions seen in service, although it is not easy due to experimental constraints. Thus, it is desirable to simplify the conditions so that greater experimental control is obtained leading to a better understanding of the test results [49]. Typical test machines for uniaxial sliding contacts are illustrated in Figure 2.18. This current study will

employ the pin-on-disc test configuration with an additional control of the electric potential of the disc. Details of the test method will be discussed further in Chapter 3.

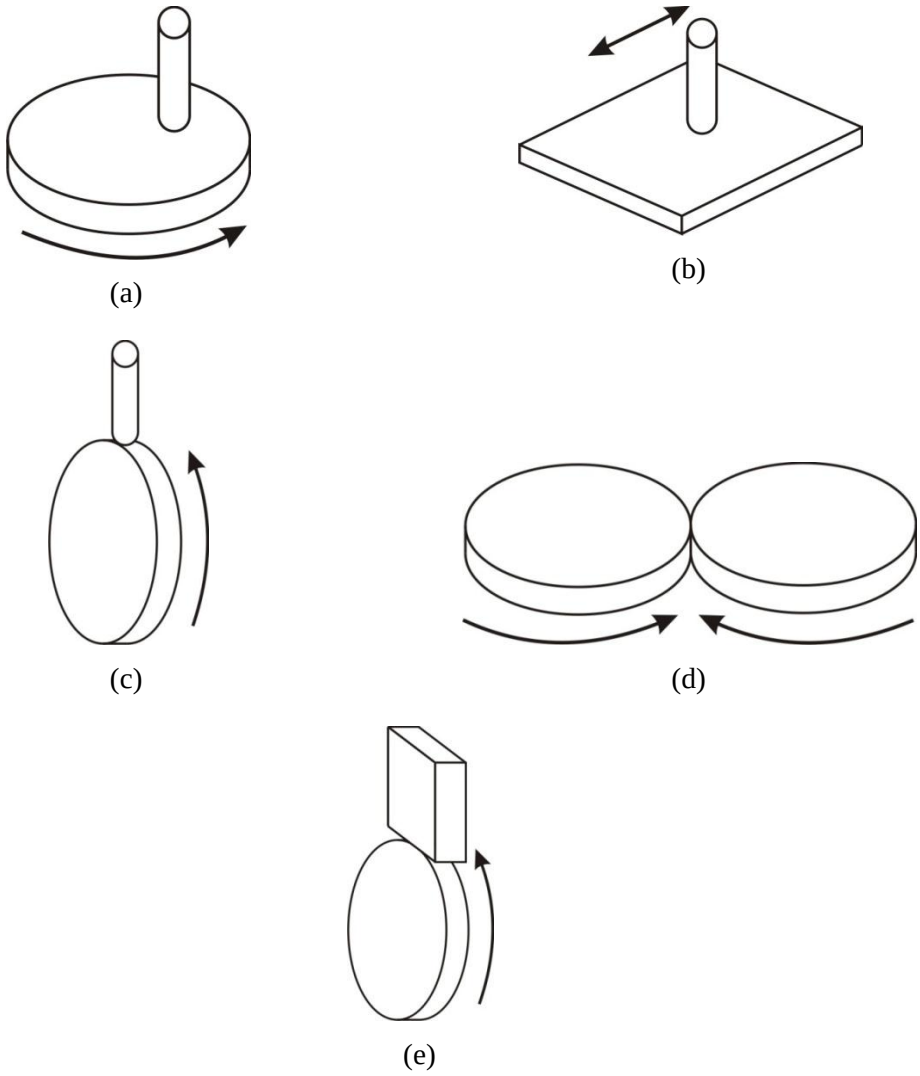

Figure 2.18. Schematic of different test configurations. Pin-on-disc (a); pin-on-flat (b); pin-on-ring (c); ring-on-ring (d), and; block-on-ring (e).

2.4 Corrosion and Triboelectrochemistry

This section will introduce the fundamental electrochemical processes of corrosion. Therefore, the discussions on the basics of tribology as presented previously could be amalgamated with the electrochemical explanations, to introduce the area of triboelectrochemistry.

2.4.1 Corrosion

2.4.1.1 Corrosion of Metals

Corrosion means the dissolution/oxidation of a material under the electrochemical action of the surrounding environment at the surface [50]. Since aqueous corrosion is an electrochemical process, it requires both cathodic (reduction) and anodic (oxidation) processes occurring at the same time, *i.e.*, electron-consuming and electron-producing respectively. An anode and cathode couple can be found by electrically connecting two dissimilar metals, or alternatively, they can exist within the same surface of a material such as shown in Figure 2.19. An electrolyte is important to complete the corrosion process, by carrying the charged ions.

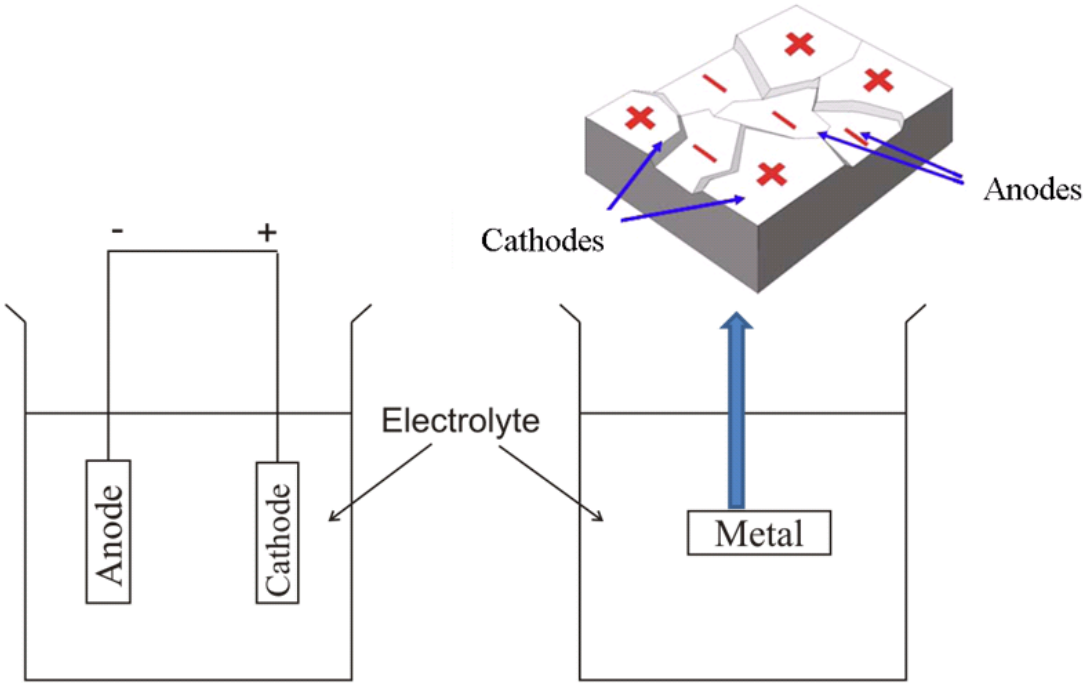

Figure 2.19. Schematic of a galvanic couple of dissimilar metals electrically connected by an external wire (left), and existing within the same surface of a metal or alloy (right).

Most metals, with the exception of the inert metals such as gold, are unstable at room temperature when in contact with oxygen at atmospheric partial pressures and thermodynamically tend to form oxide films on the surface, which is a corrosion process

[51]. Therefore, if zinc is immersed in conducting water, a spontaneous electrochemical reaction will occur at the interface of the metal/solution especially in the presence of dissolved oxygen. The water will act as the electrolyte in the system. The anodic reaction of metal (M) is usually expressed by the simplified equation [52]:

$$\mathrm{M} \rightleftharpoons \mathrm{M}^{z+} + ze^{-} \qquad \textbf{eqn. 2.5}$$

where *z* is commonly 1, 2, or 3 (related to the valency of the metal). Thus for zinc, the anodic reaction is $\mathrm{Zn} \rightleftharpoons \mathrm{Zn}^{2+} + 2e^{-}$, and could be coupled with these few types of cathodic reactions (depending on environmental conditions):

$$\mathrm{O_2} + ze^{-} \rightleftharpoons \frac{z}{2}\mathrm{O}^{2-} \qquad \textbf{eqn. 2.6}$$

$$\mathrm{O_2} + 2\mathrm{H_2O} + 4e^{-} \rightleftharpoons 4\mathrm{OH}^{-} \qquad \textbf{eqn. 2.7}$$

$$2\mathrm{H}^{+} + 2e^{-} \rightleftharpoons \mathrm{H_2} \qquad \textbf{eqn. 2.8}$$

$$\mathrm{O_2} + 4\mathrm{H}^{+} + 4e^{-} \rightleftharpoons 2\mathrm{H_2O} \qquad \textbf{eqn. 2.9}$$

The explanations of each cathodic reaction (eqn. 2.6 to eqn. 2.9) when coupled with the Zn anodic reaction is summarised in Table 2-6 below.

Cathodic Reaction	Schematic	Comments
eqn. 2.6	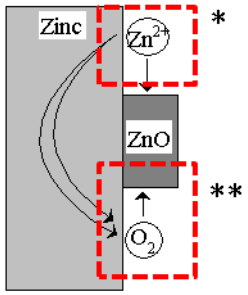	Represents conditions of high temperature and dry corrosion
eqn. 2.7	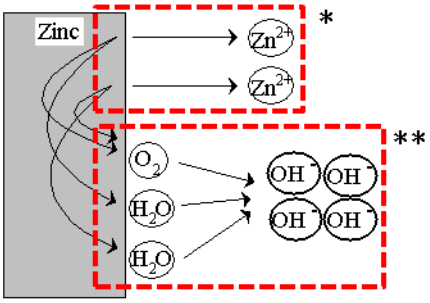	Predominant in neutral and alkaline conditions
eqn. 2.8	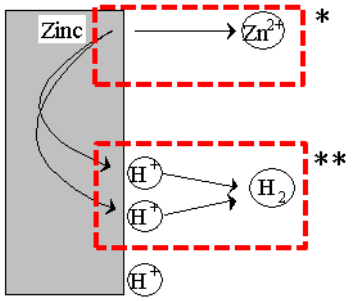	Predominant in acidic conditions
eqn. 2.9	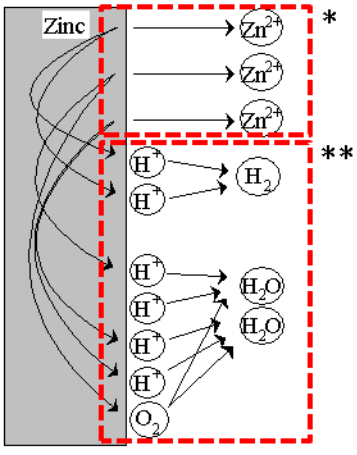	Predominant in acidic condtions with presence of dissolved oxygen

Table 2-6. List of the possible cathodic reactions coupled with the anodic reaction, with schematics representing the processes and comments for each condition. * Anodic reactions. ** Cathodic reactions. After Harvey [53].

2.4.1.2 Passivation of Steels as a Means of Corrosion Protection

Corrosion can be suppressed by disrupting the redox process. This can be done by having a protective layer on the surface which acts as a physical barrier for the steel surface from the environment, thus preventing chemical or electrochemical reactions. For instance, stainless

steels have at least 12% chromium content which produces a thin chromium oxide film that is relatively adherent, uniform and strong (which is called passive layer), see Figure 2.20 [54]. Alternatively, coatings can be applied to produce similar protection.

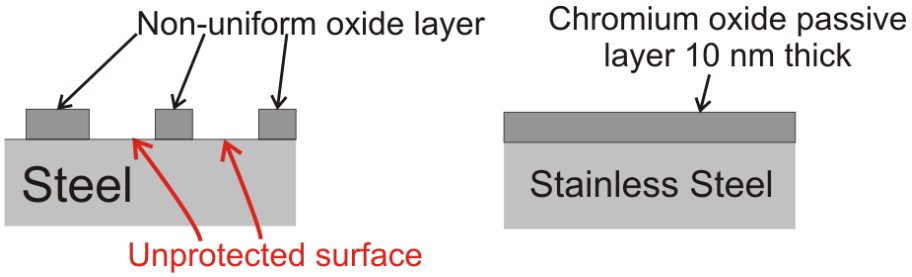

Figure 2.20. Schematic of the oxide layer formed on a steel surface (left) showing a non-uniform layer and stainless steel (right) showing a uniform and robust passive layer.

The oxide layer formed on steel are not uniform and are also porous (incomplete), thus are not suitable for corrosion protection. A useful method to prevent corrosion is using inhibitors which adsorb onto the steel surface and inhibit either the electrochemical reactions. Generally, the mechanism of action of these inhibitors could be described in four ways, that are (i) formation of a physical barrier, (ii) decrease in the reactivity of the metal, (iii) modifications to the electrical double layer, and (iv) participation of the inhibitors in the partial reactions [53].

2.4.1.3 Pourbaix Diagram for Iron

Pourbaix in 1945 investigated the behaviour of various pure metals immersed in electrolytes of different pH, whilst varying the applied potential [55]. Figure 2.21 shows an example of the Pourbaix diagram (or potential-pH diagram) of iron at 25 °C. The diagram allows the construction of a map of the thermodynamic possibilities of the iron surface. However, the disadvantage is that there is no indication of the kinetics of the reaction.

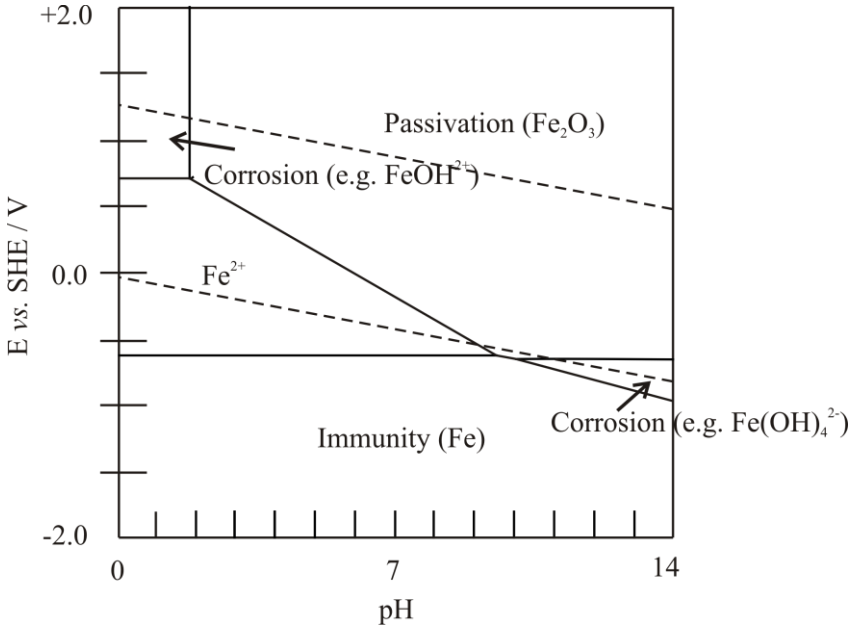

Figure 2.21. Pourbaix diagram for iron showing the different surface chemical states at various applied potential (*E*) with respect to the ambient pH at 25 °C. Adapted from [55, 56].

An example of the use of Porbaix diagram in tribology has been demonstrated by Stack and Jana [56] who modelled the erosion-corrosion behaviour of pure metals, namely Fe, Ni, Al and Cu. Their model was based on experimental data (using erosion rig), consisting of a normal impact angle (90 °C), and by utilising a 300 g L^{-1} concentration of quartz particles in water (at three pH values of 5, 7 and 9). The velocity was between 0.1 and 100 m s^{-1}, whilst the applied potential between –1.0 to 0.2 V *vs.* SCE. They constructed a few maps relating the wear mechanisms of the metals to the experiment parameters, primarily by using the ratio of the total rate of metal wastage due to corrosion (K_c), to total rate of metal wastage due to erosion (K_e), *i.e.* K_c/K_e. An example of the wear mechanism map of Fe for pH 9, constructed in the velocity-applied potential graph is shown in Figure 2.22. The graph shows that at cathodic potentials, the wear mechanism is pure corrosion due to the absence of corrosion reactions (immunity zone in the Pourbaix diagram). However, the effect of corrosion, *i.e.*, dissolution and passivation, become increasingly prevalent at anodic overpotentials. Furthermore, the variation of particle velocity also affected the wear mechanisms at anodic, owing to its consequence on the passivation film. More discussions on the inter-relationship between tribology and electrochemistry will be discussed later in this chapter.

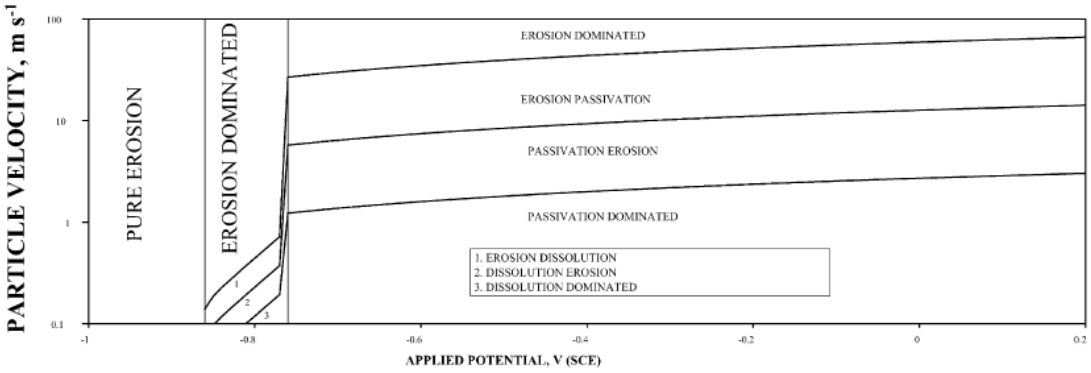

Figure 2.22. An example of a velocity-applied potential map for Fe for pH 9. After [56].

2.4.1.4 Corrosion in the Oil and Gas Industry

The US government produced a report which claimed that the total cost of corrosion in 1998 was $276 billion, which was 3.1% of the GDP. Corrosion due to hydrocarbon exploration and production industry only was estimated at $1.4 billion [57].

Oil and gas industry's corrosion manifests itself in several forms, among which is the widely known CO_2 corrosion (sweet corrosion). In sweet corrosion, the dissolved CO_2 reacts with the steel surface to form scale ($FeCO_3$), which is uniform on the steel surface [58]. On the contrary, Abelev *et al.* [59] claimed that sour corrosion (H_2S corrosion) prevails when the concentration of H_2S is above 5 ppm. They reported that the sulphur reacts to form a complete passive layer below this concentration, whilst thick and porous layer formed above this concentration. However, Ren *et al.* [58] studied the effects of sour corrosion at elevated temperatures (100 °C) and found that the presence of H_2S increased the general corrosion rate even at low concentration. In simple terms, one of the proposed mechanisms of sour corrosion is shown below [59]:

$$Fe + H_2S + H_2O \rightleftharpoons FeSH^- + H_3O^+ \quad \text{eqn. 2.10}$$

$$FeSH^- \rightleftharpoons Fe(SH) + e^- \quad \text{eqn. 2.11}$$

The complex interaction between the Fe, H_2S and H_2O system produces an adsorbed species $FeSH^-$ as shown in eqn. 2.10, which then forms a corrosion product on steel as shown in eqn. 2.11. In summary, the type of corrosion product on the steel surface differs with pH. This will then affect the levels corrosion, or a complete layer can be obtained which reduces the overall corrosion rate (passivation) [59].

In addition, presence of chloride ions could also cause the increase in corrosion. This is due to the ions interacting with the passive films on the metals (especially on iron which is widely studied), which could result in film breakdown [57]. This type of corrosion is predominant in offshore structures.

2.4.2 Definition of Triboelectrochemistry

Tribocorrosion (also called triboelectrochemistry) can be defined as an irreversible transformation of a material resulting from simultaneous physico-chemical and mechanical surface interactions occurring in a tribological contact [60]. The interaction between mechanical wear processes and electrochemical and/or chemical corrosion processes which leads to a material loss rate can be quantified such as [35]:

Tribocorrosion = *mechanical* wear process + *electrochemical* (and/or *chemical*) response **eqn. 2.12**

Therefore in a tribocorrosion study, the total damage in a sliding contact under wear-corrosion, T is given by

$$T = Q_m + C + S + A \quad \textbf{eqn. 2.13}$$

where Q_m is the mass loss due to wear due to purely mechanical processes, C is the solids free flow corrosion rate, *i.e.*, wear due to pure corrosion, S is the synergistic or wear due to corrosion, and A is the additive or corrosion due to wear.

The study of tribocorrosion can be done using a tribotester incorporating an electrochemical cell. For instance, in a reciprocating rig, the plate can be the electrode in which its potential is being controlled while a pin will be sliding against it [61]. This would allow features such as the relationship between mechanical, chemical, synergy and additive wear to be assessed, such as by implementing eqn. 2.13. Section 2.4.3 will review the concept of the electrochemical cell and how it can be incorporated into a tribotester.

The drill components are subject to impingement of high-velocity fluid and with the presence of hard particles such as the cuttings or from the drilling mud contituents, will result in erosion [62]. In some cases, the abrasion due to the fine particles can cause delamination of the WC-Co hard coatings that are meant to protect the components [13]. In both cases, the severity of wear can also be increased with the combination of corrosion.

2.4.3 Electrochemical Cell for Triboelectrochemistry Testing

2.4.3.1 Open Circuit Potential (OCP)

A metal will become charged when immersed in an electrolyte. The value of the potential at which this occurs is called the free corrosion potential and the symbol used is E_{corr} or open circuit potential (OCP). At equilibrium, this potential is constant. For materials such as titanium or stainless steels, the passive layer on the surface produces a stable OCP reading. A typical laboratory experiment to measure the OCP employs an electrical connection between

the material of interest, which is referred to as the working electrode (WE), and an electrode with a stable potential to offer as a reference point, commonly referred to as the reference electrode (RE).

2.4.3.2 The Three Electrode Cell

The three electrode cell is the standard laboratory apparatus for the quantitative investigation of the corrosion properties of materials (see Figure 2.23) [52]. This cell has been used widely in the triboelectrochemical field to study the effect of potential on wear and friction of alloys and steels in aqueous and non aqueous media. A counter electrode (CE) is the third electrode, which carries the current created in the circuit and is usually inert so that it does not affect the behaviour of the working electrode. Typical materials used for counter electrode are graphite (carbon) and platinum. The other requirement for the counter electrode is to have a large surface area relative to the working electrode so that it is not limiting the current flow. A 100-fold increase in the surface area of an electrode can be achieved by coating it with a thin layer of platinum [63], which also allows a cheaper alternative to using a pure platinum electrode. The reference electrode (RE) has a high input impedance, so that negligible current can be drawn through the reference electrode [64]. A commonly used reference electrode is the silver/silver chloride (Ag/AgCl) electrode, where a silver wire is immersed in a AgCl solution (saturated with KCL) and is connected to the outer electrolyte via a porous frit. A typical three-electrode cell can be incorporated into a tribotester by having all the three electrodes immersed in the test solution, as shown in Figure 2.24. In this example, the potential of the plate is controlled while the counterface is rubbing on it during a test, with an example of a graph showing the effect of sliding on the current response (right of Figure 2.24).

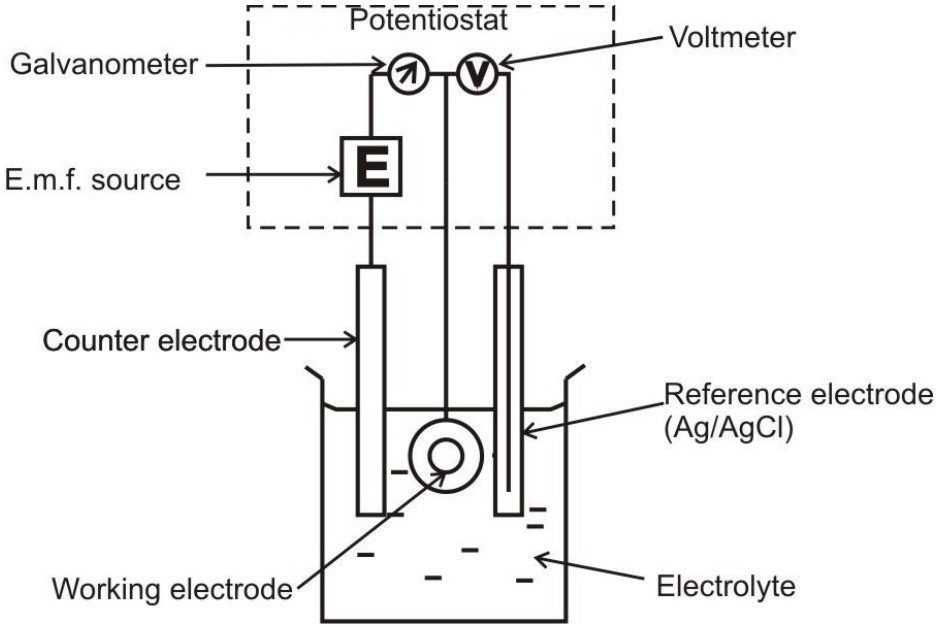

Figure 2.23. Schematic of a three electrode cell.

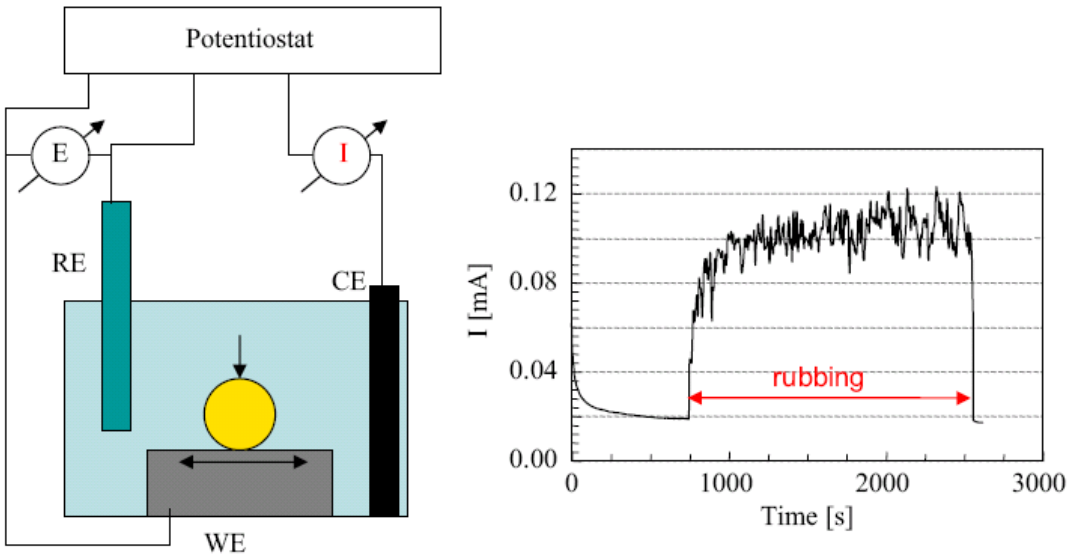

Figure 2.24. Schematic view of a tribocorrosion experimental set-up. After Mischler [61].

2.4.3.3 Polarisation

By using a three electrode cell, it is possible to apply a potential to the working electrode above or below the OCP. This potential application, *E*, alters the electrode potential from the OCP and is known as polarisation [52].

The mathematical deviation of *E* from the OCP is given the term '**overpotential**,' E_η, as shown by this equation [65]

$$E_\eta = E - E_{corr} \qquad \textbf{eqn. 2.14}$$

Applying an overpotential results in a net flow of current, *I*, between the counter electrode and working electrode. Since current is related to the amount of charge flow per unit time which is dependent on the area of the electrode, it is convenient to use the term current density, *i*, in $A.cm^{-2}$ to represent current activity.

A potentiodynamic polarisation test involves sweeping the potential of a metal (working electrode) usually from a cathodic to anodic potentials. The result is often plotted as potential against log current density, as shown in Figure 2.25 [13, 52]. At the start of potential, the current density is high, indicating a high cathodic reaction such as given by eqn. 2.7. As the potential increases, the cathodic reaction will gradually reduce down to a minimum value, at which the corrosion potential, E_{corr}, is obtained (theoretically equivalent to OCP). Above the E_{corr}, the current density gradually increases again, indicating the predominance of anodic reaction (such as metal dissolution). However, the current density will decrease dramatically at the passivation potential, E_p, which is typical of passive alloys such as stainless steels. This is due to the production of the passive layer on the surface which is not a good conductor (semiconductor), therefore impeding current flow. Alternatively, this is also useful for indicating the process of adsorption of corrosion inhibitors [66]. The current density will increase very rapidly at the tranpassive potential, E_b, due to the breakdown of the passive film, such as due to pitting corrosion.

The Tafel extrapolation lines could be fitted to the test result, which are useful for getting the values of the Tafel Constants, *i.e.*, β_a and β_c, for the anodic and cathodic reactions respectively. These values are usually in mV $decade^{-1}$, used for devising a general equation to describe the overall corrosion process, which is not detailed here. The intersection of the lines gives the current density value at equilibrium potential, i_{corr} [52]. An example of the practical use was shown by Larabi *et al.* [67] who tested the efficiency of corrosion inhibitor (2-mercapto-1-methylimidazole) on copper in hydrochloric acid, and reported that the i_{corr} value decreased with inhibitor concentration, indicating higher efficiency (better corrosion protection).

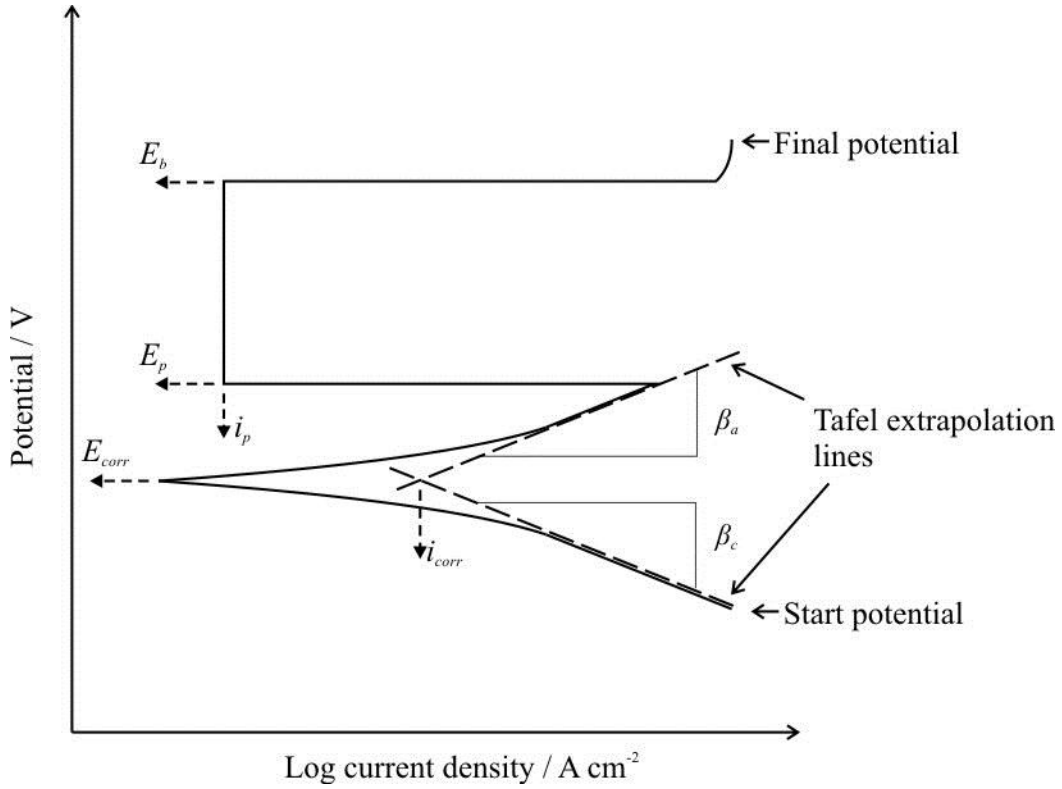

Figure 2.25. Graph of potential / V *vs.* log current density / A cm^{-2} plot showing the important information that could be obtained [13, 52].

2.4.3.4 Alternative Types of Triboelectrochemical Cell Setup

The triboelectrochemical cell described so far employed the use of a three electrode cell to generate potential application. However, Mischler [61] reviewed the three types of electrochemical techniques that could used to apply a potential to a sample, or working electrode, in a triboelectrochemical test.

The second cell type simply employs the reference electrode and working electrode only *i.e.*, omitting the counter electrode (see Figure 2.26 (a)). The counterface slides against the working electrode whilst the potential is being recorded. This test cell employs the OCP test setup, which was discussed previously in Subsection 2.4.3.1. This setup is also used in this project. However, the disadvantage of this setup is that there is no way of controlling the potential of the working ectrode, due to the absence of the counter electrode.

The third type is to couple similar metals (see Figure 2.26 (b)). Initially, both WE and CE have similar OCP values. During sliding, the removal of the passive layer on the WE will cause a change in the OCP value. This will create a galvanic couple with the CE (unworn sample) and causes current to flow. However, this method is not used in this project.

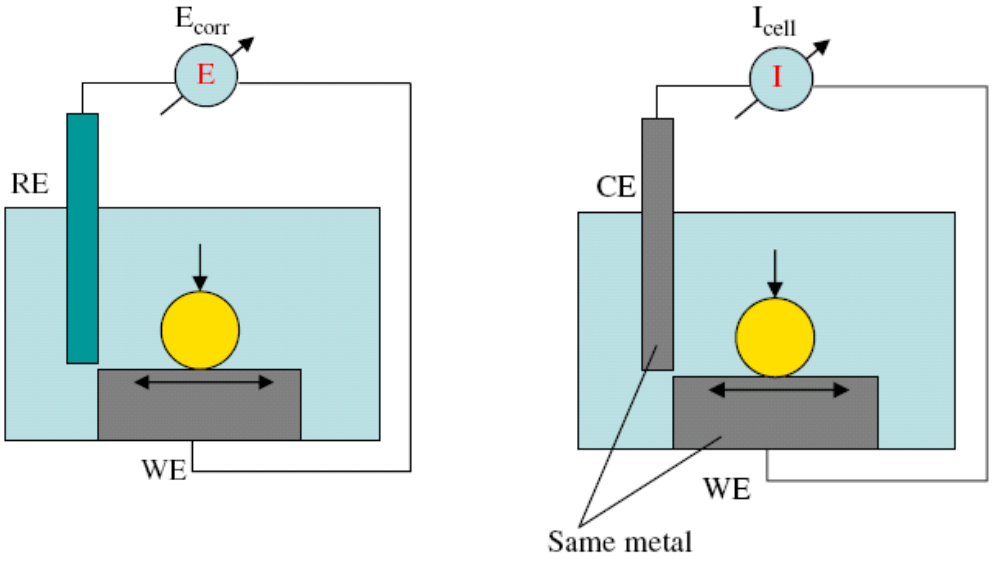

(a) (b)

Figure 2.26. The alternative methods of potential application using (a) OCP test setup, and (b) the same metal for both the counter electrode (CE) and working electrode (WE).

2.5 Adsorption of Charged Molecules to Influence Tribological Performance

2.5.1 Adsorption of Molecules on Solid Surfaces

2.5.1.1 Basic Concept

Adsorption is defined as the enrichment of one or more components in an interfacial layer [68]. It is the term used to describe the process whereby a molecule (adsorbate) forms a bond to the surface (adsorbent). It must also be distinguished from absorption, which refers to molecules entering the bulk of the substrate [69]. Adsorption is a process that occurs at the interface of gas/solid and liquid/solid.

An immersion of a metal in an aqueous electrolyte will result in the production of a double layer, which is a non-homogeneous distribution of adsorbed ions. Whereas, the diffusion layer is the distribution of the molecules away from it, as schematically shown in Figure 2.27 [52, 70]. Within the double layer, opposite charged molecules could either be electrostatic attracted which would drive the adsorption process. Alternatively, charge transfer (electron) between the adsorbed molecules and the electrode could take place. These are known as physisorption and chemisorptions respectively and will be discussed in the next Subsection 2.5.1.2.

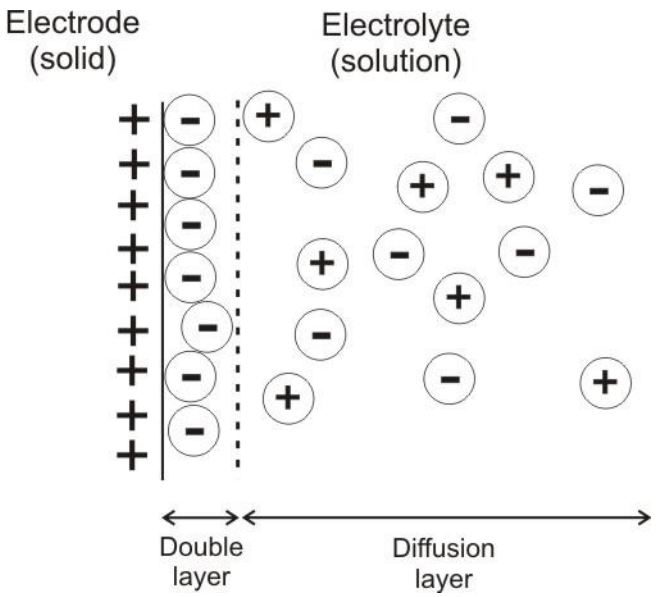

Figure 2.27. Schematics of the double layer and diffusion layer.

Adsorption of surfactants on solids in contact with aqueous solutions is important for controlling a variety of interfacial processes such as detergency, cleansing action of personal care products, flocculation and dispersion, enhanced oil recovery, mineral flotation and other solid separations [71]. From the tribological point of view, adsorption and reaction on sliding surfaces enhances the lubrication effect which leads to the current understanding and active research of friction modifiers such as oleic acid, and anti-wear additives such as zinc dialkyl dithiophosphate (ZnDDP) [31, 72, 73].

2.5.1.2 Types of Adsorption Processes – Chemisorption and Physisorption

The adsorption on a solid surface may involve only physical interactions due to van der Waals forces, or there may be a chemical interaction with the formation of chemical bonds between the adsorbent and adsorbate. These two processes are referred to as physical adsorption (physisorption) and chemical adsorption (chemisorption), respectively [70].

Chemical adsorption is characterised by chemical specifity as the chemical reaction between the adsorbate molecules and groups on the substrate is highly specific. On the other hand, physisorption is a general one and occurs in any solid/fluid system, which is also reversible by simply reducing the pressure (usually without raising the temperature). Whereas, the desorption of chemisorbed molecule is usually very difficult as it requires the breaking of chemical bonds [68, 70].

2.5.1.3 The Effects of Adsorption on Steel

i. Corrosion Inhibitors

There are various types of corrosion inhibitors and they are selected depending on the field of application. One of the ways to assess the action of the corrosion inhibitors is by testing a steel immersed in a solution containing the diluted inhibitor, and conducting a potentiodynamic polarisation experiment. Therefore the results could be plotted in the potential / V *vs. log i* / A cm^{-2} graph (detailed discussed presented previously in Subsection 2.4.3.3).

A corrosion inhibitor which reduces the anodic reaction would yield a higher E_{corr} cf. the test with the absence of inhibitor (or lower concentration). Conversely, a reduced cathodic reaction due to the inhibitor will cause a reduction in the E_{corr} value. In a mixed type inhibitor, there might be no change in the E_{corr}, but the value of i_{corr} will show a reduction [54, 67]. A summary of the actions of these inhibitors is given in Table 2-7.

Inhibition Type	Change in E_{corr}	Change in i_{corr}
Anodic	Increase	Reduction
Cathodic	Decrease	Reduction
Mixed	Possibly unchanged	Reduction

Table 2-7. The list of corrosion inhibition types and the effects which could be detected by the potentiodynamic polarisation test methods.

ii. Friction Modifiers

In addition, the adsorbed molecules help to reduce friction by reducing direct steel/steel contact, as discussed previously in Section 2.3.2. Thus, some effective corrosion inhibitors can also act as friction modifiers. Fatty acids such as octanoic acid or octadecanoic acid are used for their friction modifying properties. The fatty acid molecules adsorb and react with the bare metal to produce metal carboxylates or metal "soap". The low shear strength of the opposing vertically arranged hydrocarbon chains gives a low friction contact [42, 74]. The fatty acid used in the drilling mud consist of molecules which work in the same way (detailed previously in Section 2.2.3).

iii. Anti Wear and Extreme Pressure Additives

Anti wear and extreme pressure additives react with steel to form a low shear strength film on the surface, which function by producing a sacrificial wear protection film, *i.e.*, forming films that are relatively easy to be removed by mechanical actions [31, 75]. The effectiveness of this film formation requires a few factors which are (i) high temperature

conditions such as around 200 ºC to promote thermochemical reactions, which is the most important process, (ii) high contact pressures to promote polimerisation, (iii) formation of metal-organic complexes, and (iv) presence of metal catalysis where relevant [75].

Cao *et al.* [76] synthesised a few types of fatty acids having more than 10 carbons in the hydrocarbon chain, with sulphur, to produce anti wear additives which were low in toxicity and skin irritation. They reported that the natural fatty acid only resulted in friction reduction, but when synthesized, resulted in the combined action of friction and wear reduction, *i.e.*, acting as anti wear and extreme pressure additives, apart from friction modifiers. It was reported that the sulphur imparts the characteristic of anti wear and extreme pressure to the molecules.

Therefore, adsorption and tribochemical reactions are the core of the production of this film, and must be aided by high temperature, pressure and shear of the film, which is why they are commonly used in engines and gears [72, 77].

2.5.2 The Arrangement of the Adsorbed Molecules

Gellman and Spencer [39] extensively reviewed the published work on boundary lubrication, from the first proposed theory of monolayer adsorption in 1925, to the recent work on determining either a monolayer or multilayer formation. However, the following review in this project will focus on some of the essential work relating to the arrangement of the molecules when adsorbed onto surfaces.

Brandon *et al.* [4] used a reciprocating self mated mild steel, in a pin on plate contact mode, lubricated by 60 mM of sodium octanoate solution. They reported a 50% reduction in friction when anodic potentials were applied, owing to the adsorption of these additives. Furthermore, they postulated that the film consisted of a multilayer arrangement.

However, Duffy *et al.* [74] extended the work, by employing a reciprocating iron sphere on flat mild steel samples, lubricated by aqueous octanoate and oleate solutions. Surface vibrational spectroscopy was used to analyse the structure of adsorbed octanoate molecules on iron, subjected to anodic potential application. They concluded that a monolayer adsorption of iron octanoate is enough to provide friction reduction (see Figure 2.28) as opposed to a multilayer structure postulated by Brandon *et al.* [4]. Furthermore, the octanoate molecules were reported to form islands that have an isotropic (disordered) arrangement.

Later, Zhu *et al.* [78] used a reciprocating pin on flat (iron/iron) lubricated by aqueous octanoate solutions. They investigated the octanoate film using Fourier Transform Infrared

Spectroscopy (FTIR) and confirmed the chemisorbed iron (II) octanoate on the iron surface at anodic potentials, and therefore explains the tenacity of the layers from being removed. This is a positive effect, in which the layers will not easily fail at high contact pressures and can prevent direct steel/steel contact.

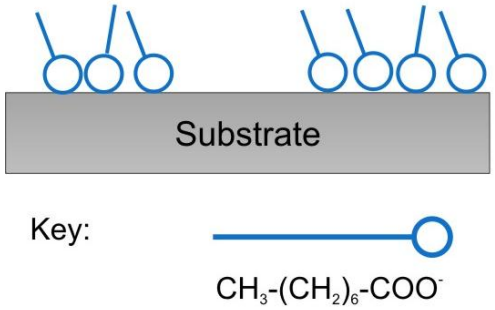

Figure 2.28. Simple schematic of the monolayer adsorption film of iron (II) octanoate on a steel surface (substrate).

Furthermore, Duffy *et al.* [74] studied iron/mild steel sliding contacts in a solution of 10 mM potassium oleate. The oleate molecule contains more carbon atoms (*i.e.*, longer chain) and a double bond in the hydrocarbon chain c.f. the octanoate molecule. They form bilayer adsorption films which are important for the reduction of friction and wear. The value of coefficient of friction was also relatively low, at 0.09, cf. the octanoate test solution at 0.25. The lower friction was due to the formation of more ordered molecular arrangement, promoted by strong hydrocarbon chain-chain interactions between the molecules. These interactions are plausible for the longer hydrocarbon chains, *i.e.*, typically with more than ten CH_2 groups. The resulting attraction is relatively strong cf. the shorter molecules, and is even comparable to the covalent bonds between the molecules and the steel substrate (the chemisorption bond). For example, for alkene molecules, the Van der Waals energy for a CH_2 group in a close packed arrangement is around 7 kJ mol^{-1}. Therefore this results in a total energy of 126 kJ mol^{-1} in a C_{18} alkene, which is comparable to that of the covalent bond of around 100 – 300 kJ mol^{-1} [79]. Furthermore, Duffy *et al.* [74] added that the bilayer structures are less likely to form in the sodium octanoate solution due to the shorter hydrocarbon chains of the molecules (see Figure 2.29 (a)) [74].

Duffy *et al.* [74] further reported that the bilayer (as shown in Figure 2.29 (b)) composed of a lower layer of oleate molecules that are tenaciously bound through their carboxylate groups (chemisorbed), and an upper layer in which the molecules are physisorbed through hydrophobic interactions with the lower layer. The formation of this bilayer plays some role in stabilising the lubricating film, particularly in promoting the formation of the closely packed layer covalently bound to the substrate. They concluded that the mechanism of monolayer or bilayer is not well understood so far. However, they suggested that when the contact area is small or at low sliding speeds, the upper layer will not be stable enough to be

present in the contact, hence is being squeezed out. However, when the contact area is high or at high sliding speeds, the upper layer can be entrapped in the contact and provide further separation of the sliding surfaces.

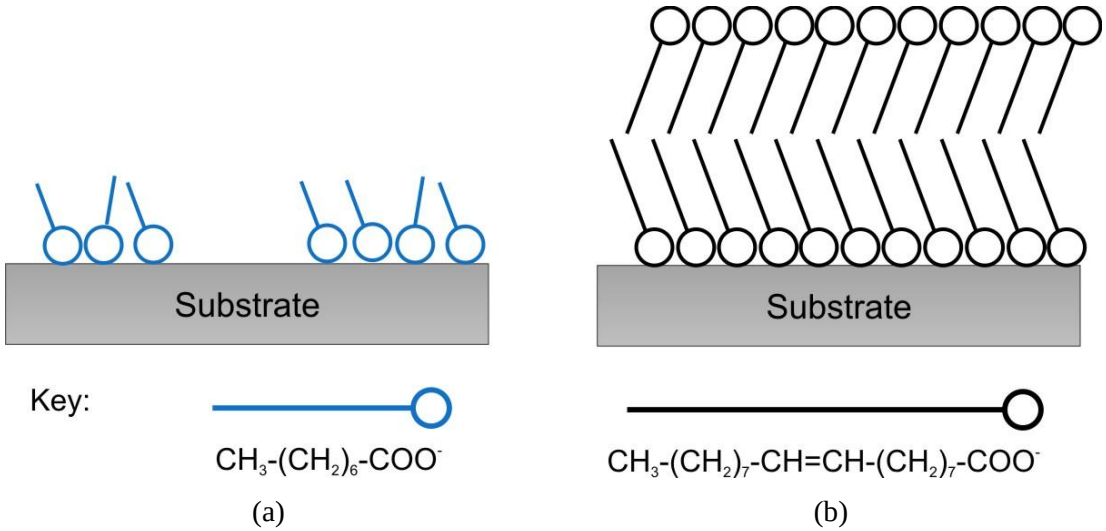

Figure 2.29. Schematic of the structure of the adsorption film of octanoate (a), and; oleate (b) molecules adapted and modified from Duffy *et al.* [74]. The octanoate form islands of disordered and monolayered film while the oleate molecules form an ordered and bilayered film.

2.5.3 General Requirements for a Good Boundary Lubricating Film

Lee *et al.* [80] deposited three types of alkenethiols self assembled monolayers (SAM) on gold at 1 mM, namely, (i) alkanethiolssheptadecanethiol, (ii) 2,2-dipentadecyl-1,3-propanedithiol, and (iii) 2-pentadecyl-1,3-propanedithiol (see Figure 2.30). The molecular packing densities decrease in the order of (i) > (ii) >> (iii). They studied the frictional response of each case using an Atomic Force Microscope (AFM). It was found that the levels of friction, either during the increasing or decreasing load regimes showed a good correlation with the packing density (opposite order), *i.e.*, (iii) >> (ii) > (i), (see Figure 2.31). Therefore, this shows that a close-packed (and ordered) assembly would result in a better friction reduction. The sliding on the loosely packed layers dissipates more energy through molecular deformations which contributes to the rise of friction.

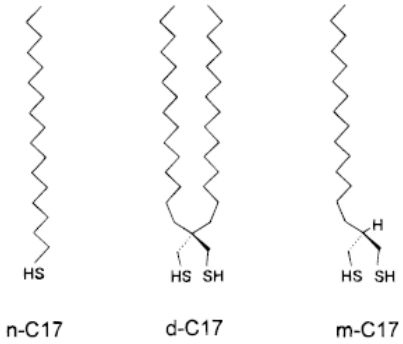

Figure 2.30. Molecular structure of the three types of alkenethiols: (i) alkanethiolssheptadecanethiol (left), (ii) 2,2-dipentadecyl-1,3-propanedithiol (middle), and (iii) 2-pentadecyl-1,3-propanedithiol (right). Adapted from [80].

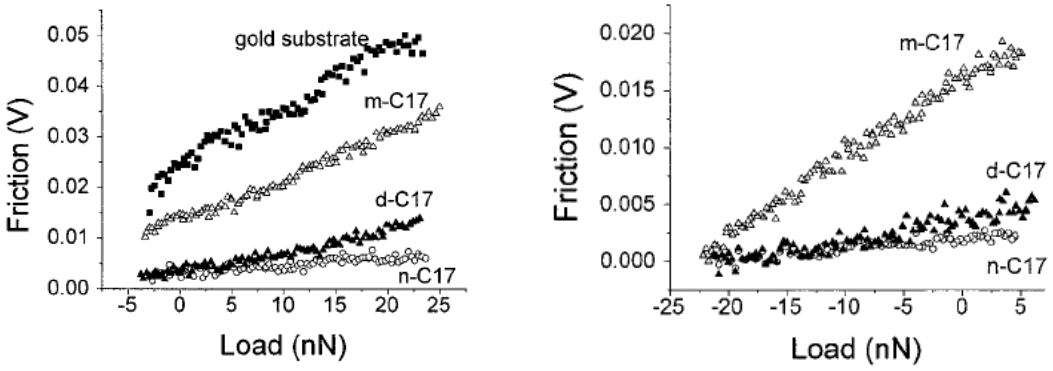

(a) (b)

Figure 2.31. Result of the AFM showing representative friction-load regime during (a) increasing load, and (b) decreasing load [80].

Berg and Klenerman [81] pressed a bronze sphere coated with 200 nm gold on a flat sapphire prism. The sphere was exposed to alkanethiol additives, namely octadecanethiol (ODT) and octanethiol (OT), *i.e.*, C_{18} and C_8 respectively, in methanol solution. Furthermore, they used vibrational spectroscopy to monitor the mechanically compressed monolayers. The result of the sum frequencies (SF) showed that the peaks shift to lower frequency and became weaker when contact pressure was increased (see top of Figure 2.32). This was attributed to the rearrangement of the terminal methyl groups (lost in orientational bias). The SF also showed that the molecules remained straight in compression (see bottom of Figure 2.32). Upon relieve of the contact stress (unloading), the peaks reappear indicating the molecules attained similar arrangement to initial. Furthermore, the behaviours were similar between ODT and OT, which suggested similar mechanism, irrespective of molecular weight. They extended their work by boiling the ODT sample at 65 ºC for 90 s, to introduce some defects. The result is a loosely packed layer, in which the SF showed less reversible peak behaviours, therefore indicating that the film disorder more easily. This might suggest that even the long chain molecules will fail to provide reduction in friction if the film is not properly packed.

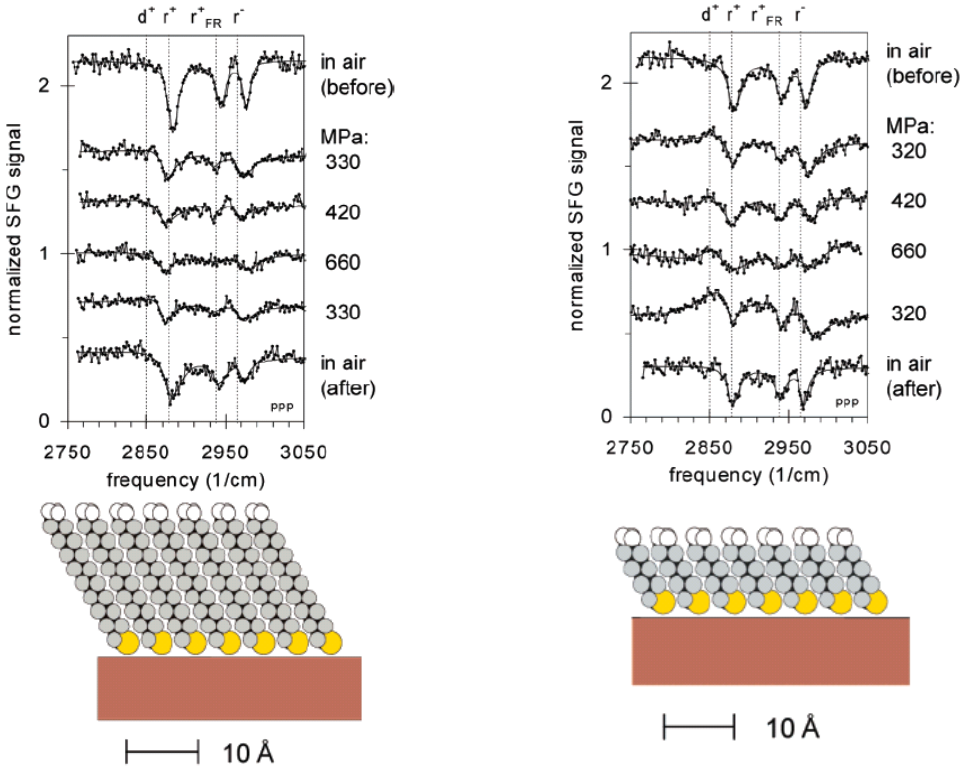

(a) (b)

Figure 2.32. The results of the sum frequency showing the effect of compression on the ODT (left) and OT (right). The corresponding schematic of the molecular arrangements are shown on the bottom [81].

Sahoo and Biswas [82] used pin on disc setup on the macro- and nano-scale, in addition to a lateral force microscopy. They deposited two types of fatty acid additives, namely saturated stearic acid (SA) and unsaturated linoleic acid (LA), onto EN31 steel grade samples (see Figure 2.33). The additives were dispersed in hexadecane (5% v/v), and the contact pressures were varied from 10 MPa to 2.5 GPa. They reported that LA could give the lowest friction when given sufficient time for the molecules to disentangle and conform parallel to the steel surface (see Figure 2.34). It was also suggested from X-ray Photoelectron Spectroscopy (XPS) measurements, that when the hydrocarbon chain of unsaturated fatty acids (LA) are tilted and pressed in a contact, the double bond region allows coupling with the steel to produce a better lubricating film. Therefore, this explains the slightly higher friction by the saturated fatty acids (SA).

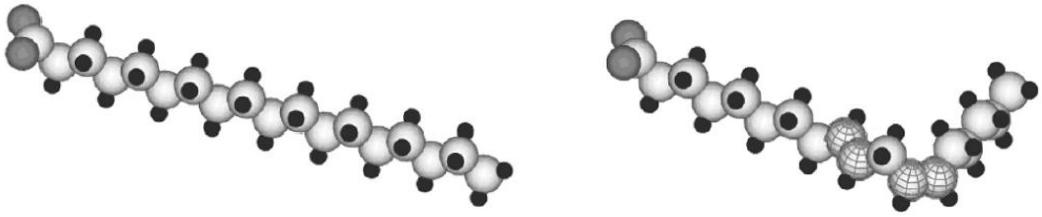

Figure 2.33. Molecular structure of the SA (left) and LA (right). Key: carbon atoms are white, hydrogen are black, oxygen are grey, and the meshed spheres in LA denote the double bonds [82].

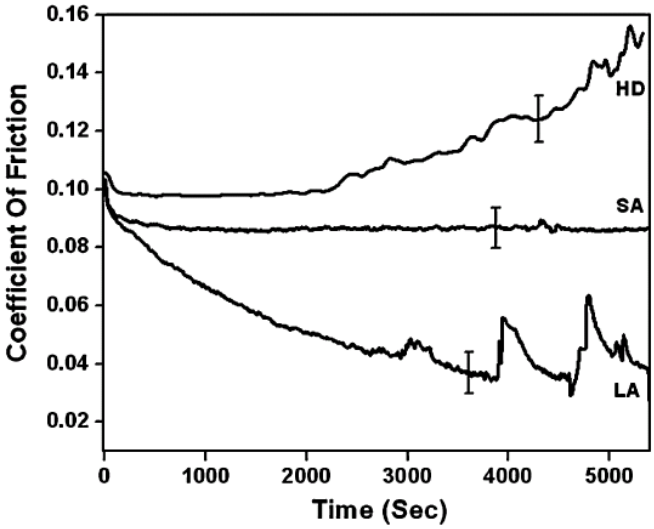

Figure 2.34. Graph of coefficient of friction *vs.* time / s for the macro-scale pin-on-disc test, employing 60 N normal load (mean Hertzian contact pressure of 10 MPa), 0.35 m.s^{-1} sliding velocity. Error bars are standard deviation from 5 tests. HD is hexadecane [82].

Adhvaryu *et. al* [77] used a rotating ball (52100 steel) on disc (1018 steel) tribometer to study the lubrication of cottonseed, canola, olive, and meadowfoam oil dispersed in hexadecane. These were chosen due to being environmental friendly, and could be an alternative for industrial applications replacing mineral oils. They tested the effects of oil concentrations on friction. Generally, they found that the results were similar among the oils, in which at low concentrations, the friction were high, and rapidly decreased at higher additive concentrations, see example in Figure 2.35. This is due to the adsorption of the additives which become more complete, *i.e.*, covering more areas at higher concentrations. Furthermore, they used the experimental results as shown in Figure 2.35 to calculate the free adsorption energy (ΔG_{ads}) of each oil, using the equation,

$$\Delta G_{ads} = -RT \ln\left(\frac{\theta}{(1-\theta)C_s}\right) \qquad \textbf{eqn. 2.15}$$

where R is the universal gas constant, T is the absolute temperature, C_s is the concentration of solute in solvent, and θ is obtained from the graph. Therefore, they reported that stronger adsorption (lower ΔG_{ads} value) were found at the conditions of (i) higher degree of molecule functionality (quantity of charged groups in a molecule), (ii) low number of double bonds in the molecule (lowest is olive oil), (iii) higher content of oleic acid in the oil (highest in olive oil acid).

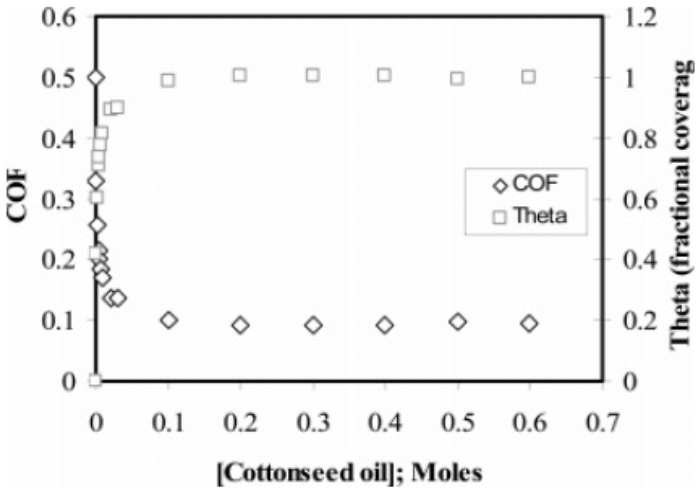

Figure 2.35. The trend of friction with respect to the concentration of additive (cottonseed oil) and the relationship with the additive fractional coverage [77].

2.6 Controlling Potential to Influence Friction in Aqueous Environments

2.6.1 Early Understanding

The first work that combines electrochemical methods with tribological studies was done by Edison (1877) during his invention of the telephone in which he controlled friction by passing a current to an electrode [83, 84]. Clark [85, 86] used a method relatively similar to Edison, that is by suspending a metal wire around a rotating Perspex cylinder in different solutions, see Figure 2.36. He concluded that by using a tungsten wire, adsorption of hydroxyl ions was responsible for friction reduction but this was ruled out later [87]. Furthermore he conducted tests in clay slurry solutions and found a parabolic dependence of friction with potential. Finer suspended particles gave a better friction dependence on potential and it was claimed that the orientation of the clay particles on the surface was responsible for the friction change.

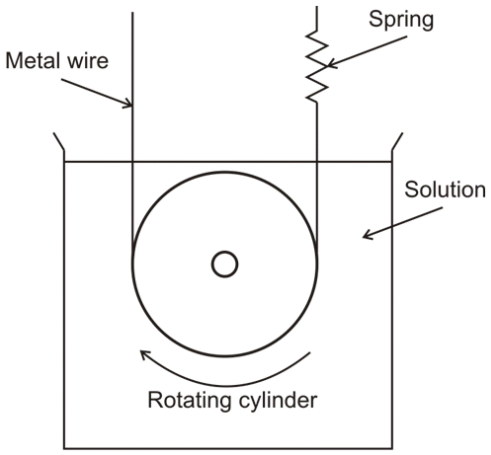

Figure 2.36. Schematic of Clark's experiment apparatus [85, 86].

In 1961, Staicopolus [88] designed a revolving-cup friction-measuring apparatus in which the adsorption/desorption of ionic species on the solid surface was investigated as a function of applied potential, see Figure 2.37. The apparatus consisted of a pendulum which was provided with a spherical fulcrum. It rests in a conical cavity of the test electrode which was filled with the test solution. The conical surface constitutes the metal/solution interface. It was found that the adsorption/desorption behaviour of the CrO_4^{2-} was responsible for the change in friction [84].

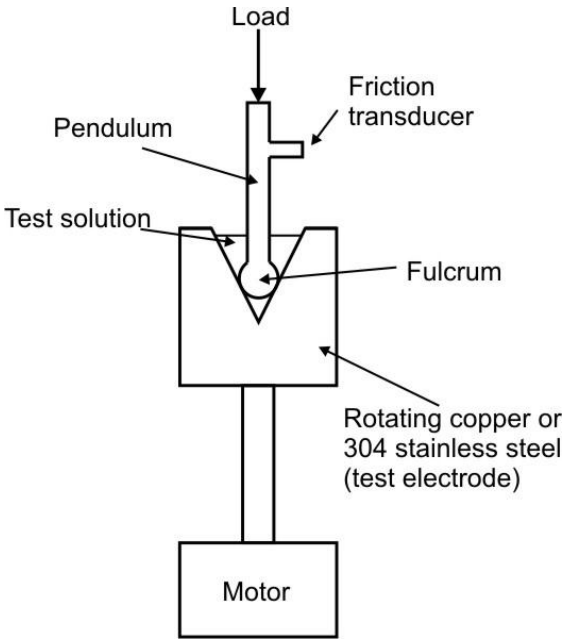

Figure 2.37. Simplified schematic of friction apparatus by Staicopolus [88].

Bockris and Argade [89] derived a quantitative expression for the dependence of coefficient of friction upon potential on the basis that the electrostatic repulsion between two contacting solids is responsible for the decrease in friction, see Figure 2.38. The model was based on the theory that ions adsorbed at the double layer interface on both surfaces will repel against

each other when the surfaces are brought together. They derived an equation for the coefficient of friction,

$$\mu = \frac{\sigma_T A_o}{\omega + \left(\frac{2\pi}{\epsilon}\right) q_\epsilon^2 (A - A_o)} \qquad \textbf{eqn. 2.16}$$

where A is the total are of contact (nominal), A_o is the non contact area, q_ϵ is the charge on the solution side of the double layer, σ_T is the shear stress, ω is the weight of the counterface, ϵ is the dielectric constant. This theory was subsequently revised by Bockris *et al.* [90] with a new assumption that the repulsion is regarded as the interaction approximately as that between two Guoy layers, instead of the double layer. However, Later work by Kelsall *et al.* [87] using high friction reciprocating machine found that the theory of the dependence of friction by electrostatic repulsion can only be accounted for at low pressure contacts. In their experiments, the effect of electrostatic repulsion to reduce friction was found to rapidly diminish as the contact pressure was increased from 2.3 MPa to 7.8 MPa.

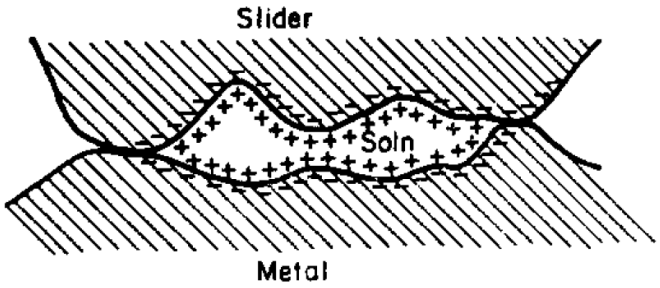

Figure 2.38. Schematic of the double layer repulsion from [89].

Meng *et al.* [91] modelled the effect of the variation in friction with applied external voltage (potential). Three types of contacts were used in a ball-on-disc arrangement: Si_3N_4 ball/steel disc, Si_3N_4 ball/brass disc and SiO_2/steel disc, with 1wt% zinc stearate used as the lubricant. Voltages of magnitudes 2.5, 5, and 10 V were applied at 600 s which were switched off at 1200 s, during the sliding. It was reported that the friction increased with application of voltage, and subsequently drop at the point that the voltage was switched off, can be modelled as a parabolic response.

2.6.2 Recent Experimental Investigations

In 1992 Brandon *et al.* [92] studied the effects of potential on the static friction of steel contacts lubricated by 1 wt.% octanoic acid (pH 9.2) in a iron/steel contact. The experiments consisted of a steel rider on an iron wire (which is electrically controlled). The static coefficient of friction was determined by tilting the apparatus until the rider slid along the wire, within the stationary solution, see Figure 2.39. The angle that the rider starts to slide was recorded and the coefficient of friction taken as the tangent of the angle. It was found that the static coefficient of friction between mild steel and iron was reduced by more than

50% (from 0.52 to 0.25) on changing the electrode potential from -400 to 300 mV *vs*. SHE. This was due to adsorption of the octanoate molecules at anodic (positive) potentials.

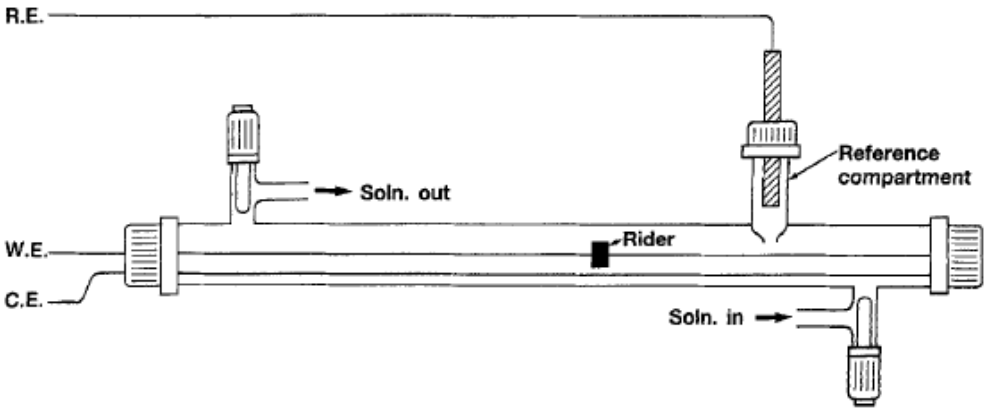

Figure 2.39. Schematic of the tilt cell [92].

Brandon *et al.* [93, 94] also studied the effects of potential upon dynamic friction and wear in 1 wt.% octanoic acid (pH 9.2) and bentonite based drilling mud. The materials used were mild steel self mated pairs, with a few experiment runs using steel/sandstone and mild steel/high speed steel contacts. A TE 77 reciprocating pin-on-plate machine was used in their study. A reduction of friction of 50% was reported for a metal/metal contact in the octanoic acid solution when an anodic potential was applied, see Figure 2.40. The trends showed a strong dependence of friction with potential that when a positive (or anodic) potential was applied, adsorption of the octanoate species was effective and produced a low friction adsorption film. Figure 2.41 and Figure 2.42 show the variation of the wear of the mating samples with potential adapted from [93]. It was also reported that at OCP, adhesive wear was seen when loads higher than 20 N was applied, whilst at application of 600 mV potential *vs.* SHE, adhesive wear can be suppressed even when the load was increased up to 160 N. They claimed that partial film breakdown was seen starting at 80 N (at OCP).

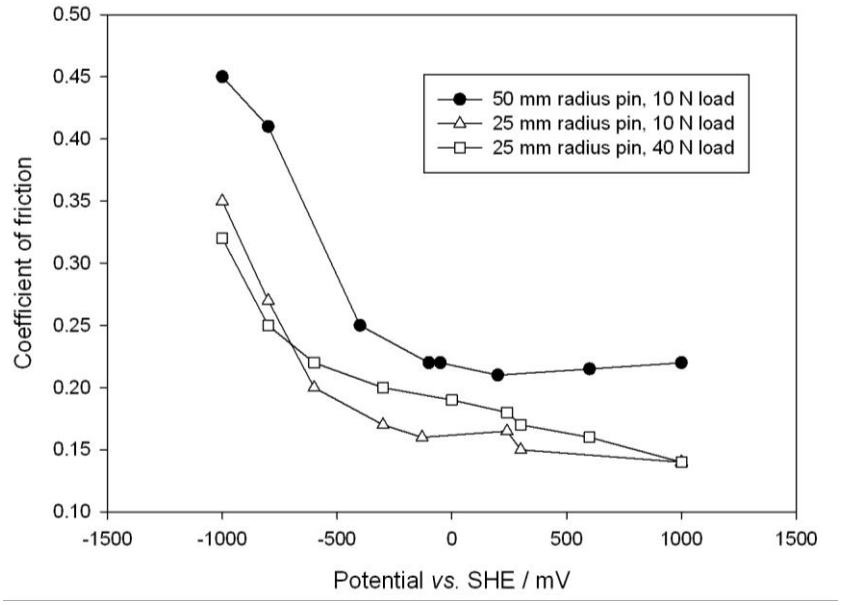

Figure 2.40. Variation of average dynamic coefficient of friction with potential vs. the Standard Hydrogen Electrode (SHE) adapted from [93].

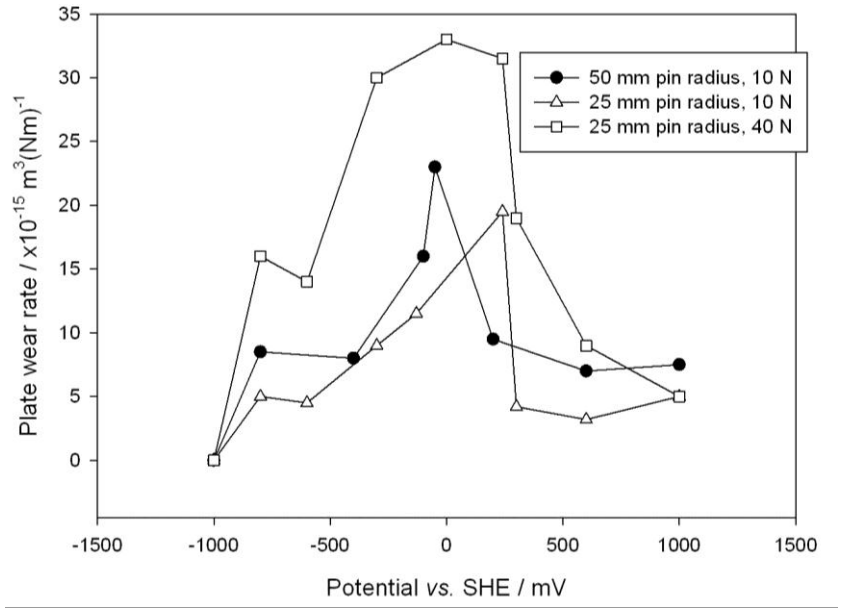

Figure 2.41. Plate wear rate plotted against potential in 1 wt.% octanoic acid pH 9.2, at different pin radius and normal load [93].

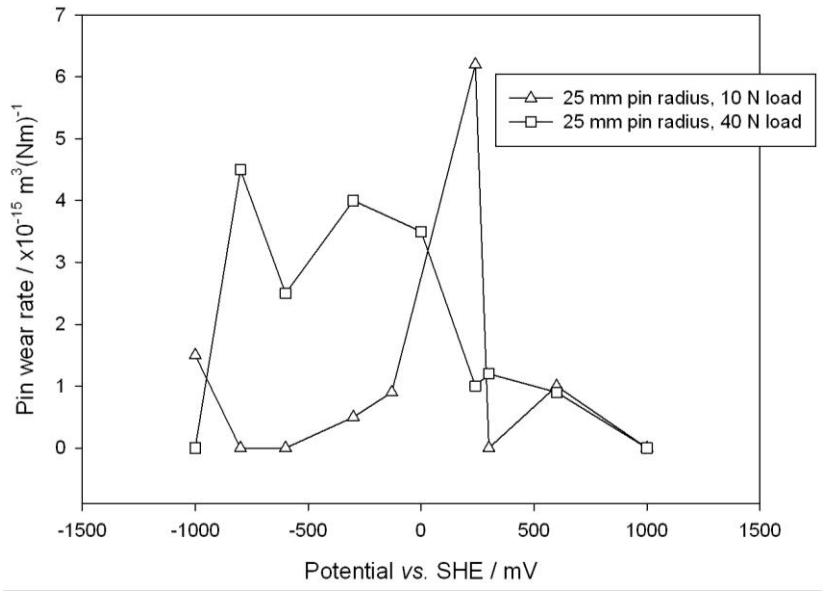

Figure 2.42. Wear rate plotted against potential in 1 wt.% octanoic acid pH 9.2 [93].

Zhu *et al.* [95] studied 0.02 M Na_2SO_4 + 0.001 M octanoic acid pH 9, by applying -1.1 V (cathodic) and +0.4 V (anodic) *vs.* SCE potentials. Atomic force microscopy (AFM) was used to measure the spatial distribution of friction, on the surface of iron electrodes under controlled potential. The μ friction at anodic potential was much lower and the surface smoother than the former as shown by AFM imaging, see Figure 2.43. Fourier Transform Infrared Spectroscopy (FTIR) surface analysis indicated the formation of iron octanoate at the low friction anodic potential. Scanning Tunnelling Microscope (STM) was also used to observe the iron octanoate film formation, which revealed the thickening and spreading of the layer across the iron surface with time, as shown in Figure 2.44.

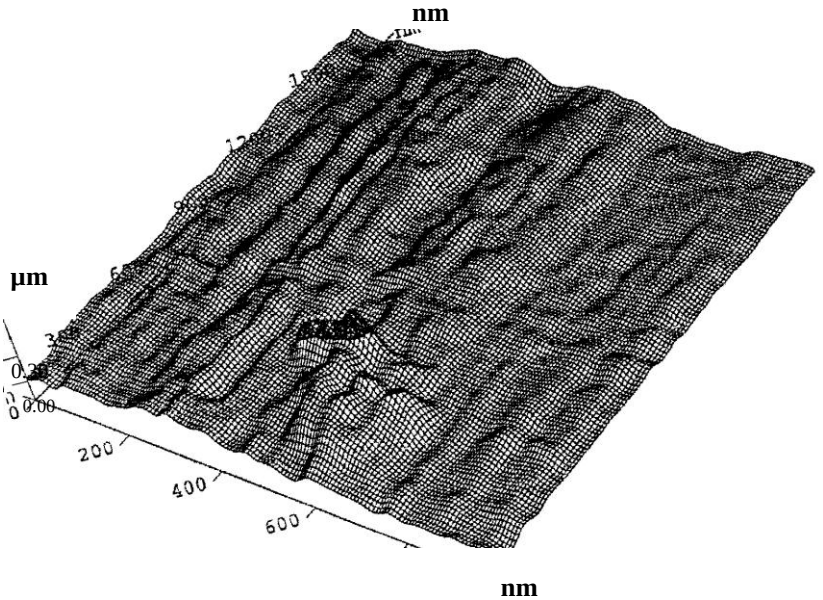

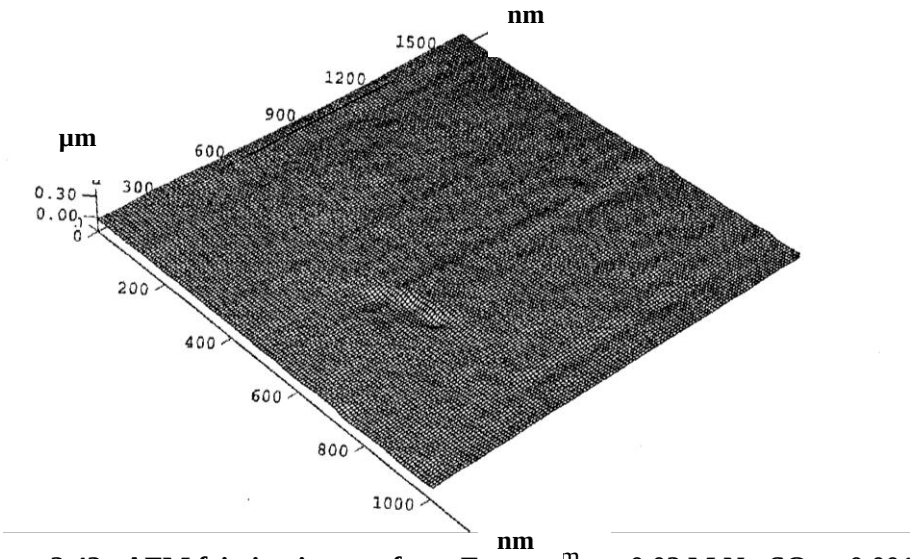

Figure 2.43. AFM friction images from F[illegible]n 0.02 M Na_2SO_4 + 0.001 M octanoate pH 9: (a) at –1.0 V *vs.* SCE; (b) at +0.4 V *vs.* SCE from [95].

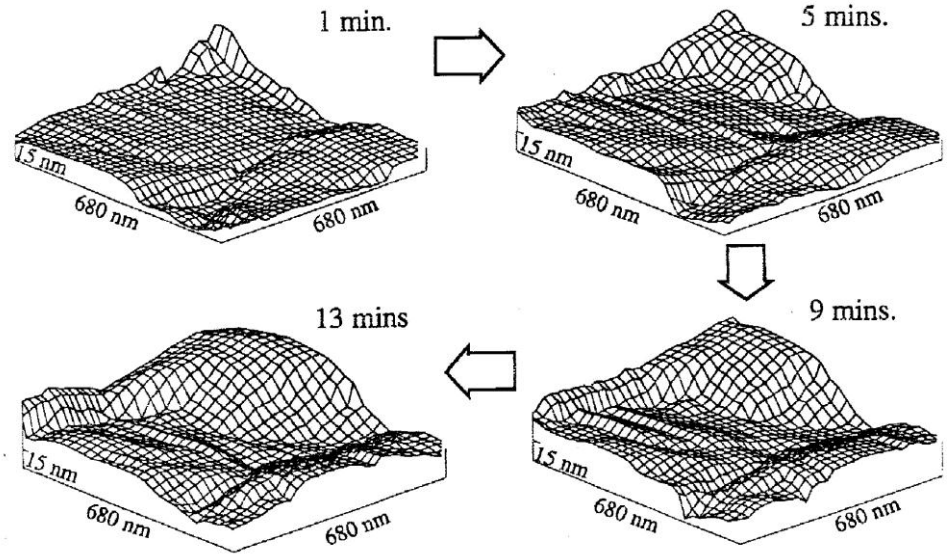

Figure 2.44. Time resolved STM images from Fe surface at +0.3 V *vs.* SCE in 0.1 M Na_2SO_4 + 0.001 M octanoate pH 9 from [95].

Meng *et al.* [96] studied the control of friction of metal/ceramic contacts in aqueous solutions using a ball-on-plate reciprocating friction machine with an electrochemical method. The plate specimen consisted of a copper material partitioned into two sections by an insulating material, while the ball was Si_3N_4. The lubricant was sodium laurylsulfonate solution + 0.01 M sodium sulphate (to increase conductivity), set at a temperature of 22 °C. During the experiment, only one partition had an applied potential, while the other was left isolated. The wear track extended from one partition to another laterally. The aim was to study if the friction can be controlled locally. Their results confirmed that the local friction can be manipulated to some extent by controlling the potential, owing to the removal or generation of a lubricating film (adsorbed film of laurysulfonic acid). By applying a cathodic potential, the oxide film was stripped off the copper surface, resulting in high

friction due to direct metal/ceramic contact (μ > 0.15). Whereas, when no potential was applied, low friction was obtained which was reported to be due to the presence of oxidation and adsorbed film (μ ≈ 0.07).

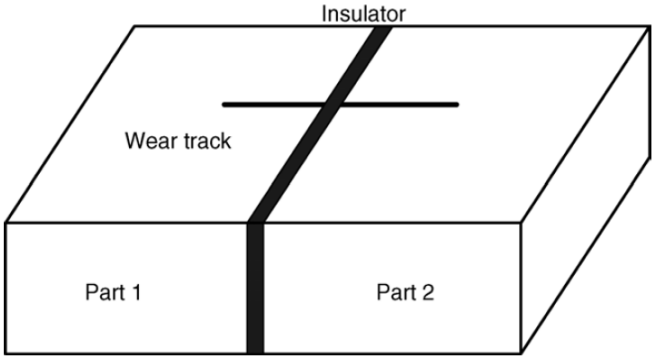

Figure 2.45. Schematic of the copper specimen with two parts [96].

2.6.3 Active Switching for Dynamic Friction Control

Jiang *et al.* [97] studied the sliding pair of zirconia and AISI 304 stainless steel in a ball on disc contact mode. The solutions used were aqueous sodium dodecyl sulphate at 0.1, 0.5 and 1 mM concentrations. While the zirconia balls were rotating, the potential of the disc was varied between values negative and positive to the OCP, which produced high (μ = 0.45) and low (μ = 0.10) friction respectively. It was also reported that the response of these transition from low to high and vice versa followed the behaviour of the applied potential closely *i.e.*, either a square or sinusoidal wave (see Figure 2.46).

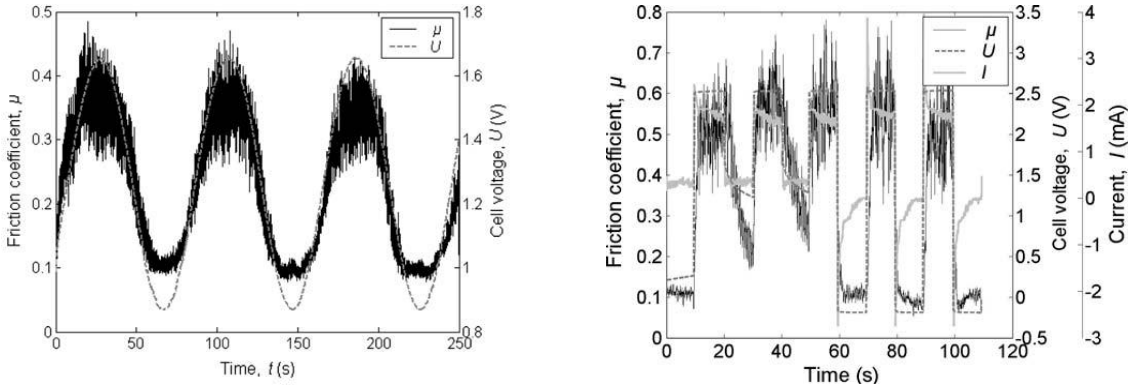

(a) (b)

Figure 2.46. Response of friction on the variation of the cell voltage (potential) in a (a) sinusoidal and (b) square wave modes [98]. *μ* is coefficient of friction which is the response of the variation in the cell voltage, *U*. *I* is the response of current in the sinusoidal wave mode.

Su *et al.* [99] devised an apparatus comprising a tungsten carbide pressed against a rotating copper cylinder in the presence of various commercial emulsion lubricants (composition details not provided). The copper cylinder was rotated at 1750 rpm and its potential was varied using a potentiostat, see Figure 2.47. X-ray Photoelectron Spectroscopy (XPS)

analysis confirmed the reaction of copper and the fatty acid additive (a hydrocarbon compound) when anodic potentials were applied, which also produced a low friction adsorbed film. It was also found that potential-independent friction could be modified by adding a specific polar substance to the lubricant to make it potential-dependant. They also applied the technique of reducing friction by potential control into industrial wire drawing and reported that by applying a potential of 1.5 V *vs*. Standard Calomel Electrode (SCE) the friction force needed to draw a copper wire lubricated with a commercial emulsion lubricant was reduced by 45% (see Figure 2.48). An SEM study of the drawn wire showed that the surface was smoother when it was drawn with potential control, see Figure 2.49.

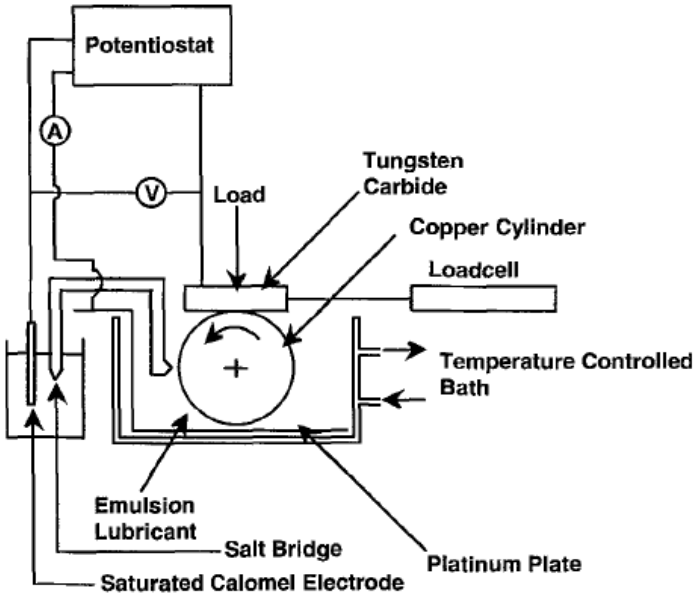

Figure 2.47. Schematic of the laboratory friction test [99].

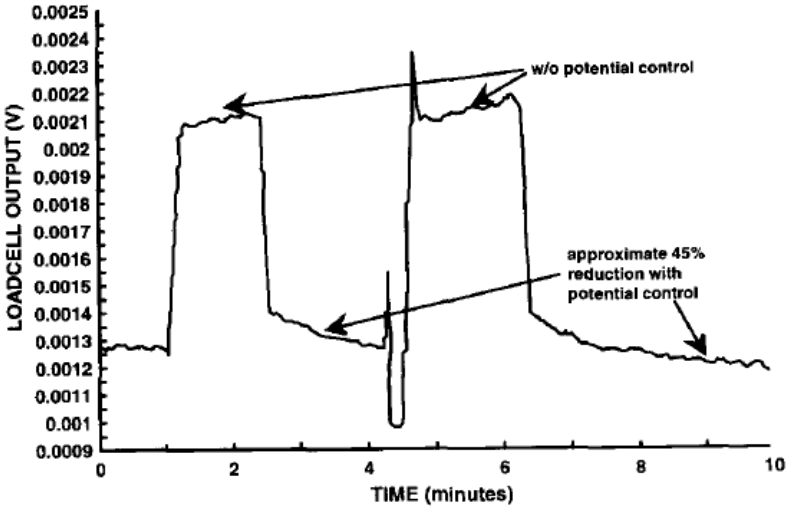

Figure 2.48. Response of friction (represented by the load cell output in the y-axis) *vs.* time. 45% reduction in friction was seen when 1.5 V *vs.* SCE was applied to one of the sliding surfaces [99].

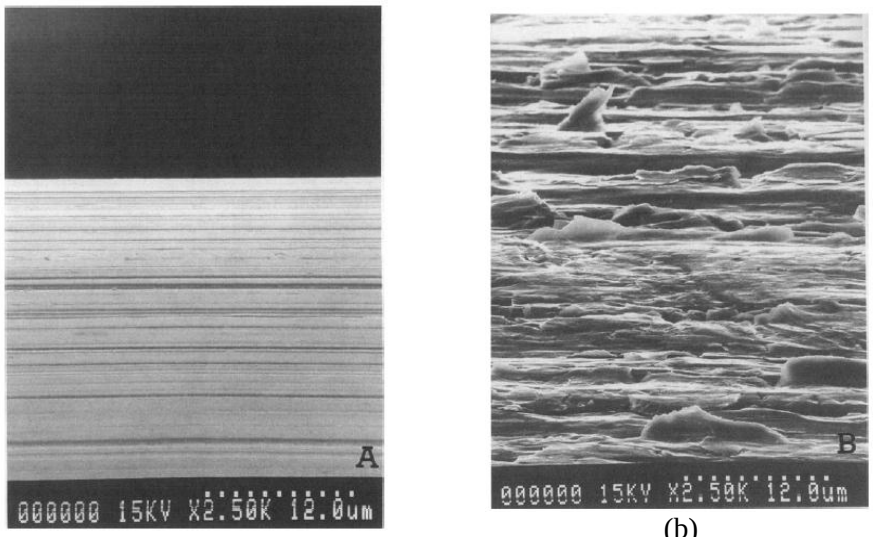

(a) (b)

Figure 2.49. SEM micrographs of surfaces of wires drawn (a) with electrode control and (b) without electrode control from [99].

These effects of friction dependence on actively switching potential which have been reviewed, were due to the control of adsorption of the friction modifiers onto the surfaces. However, the exact mechanism explaining the behaviour of these molecules when interacting with the surfaces remains as an open subject. Some work by Lahann *et al.* [100] reported that by varying the potential, the adsorbed monolayer will undergo conformational changes which can render the surface hydrophobic or hydrophilic (without desorbing the monolayer). However, this was done using a specially modified self-assembled monolayer molecule.

2.7 Controlling Potential to Influence Friction in Other Base Fluids

Tung and Wang [101, 102] simulated the contact between a piston ring and the cylinder wall, up to 100 °C, lubricated by mineral and commercial engine oils in a block on disc contact mode. The disc was made of GM 232-M cast iron (cylinder wall material), while the blocks (3 thin steels equidistantly placed along the circumference) were made of GM 15-M cast iron and SAE 1045 spring steel, which are the materials for the piston ring. The load was quoted as load per length, at 27, 44 and 61 N cm^{-1}. They reported that by applying current through the piston ring material, a lower friction result was found after sliding test. Subsequently, the current was applied *in-situ, i.e.*, while sliding, which also resulted in decrease in friction. It was reported that a smoother surface was produced when current was applied which was due to the increased reaction between the surface and the anti-wear additives in the oil.

Xu and Spikes [103] used a high frequency reciprocating ball-on-disc rig to study the tribological effects of zinc dithiophosphate (ZDDP) in di-ethylhexyl sebacate (DEHS) base

fluid solution, under the influence of the applied potential, at a temperature of 60 °C. The load was 400 g, corresponding to 690 MPa Hertzian mean contact stress (due to 6 mm steel ball on steel disc, both materials were AISI 52100). They reported that the reaction of the anti-wear additive (ZDDP) in the ester based fluid was enhanced when oxidating (positive) potentials were applied, thus decreasing wear. The reduction in friction and wear was attributed to the adsorption of the disulphide, or the enhanced reaction to produce thicker phosphate/thiophosphate anti-wear coating.

2.8 Summary

The drilling industry clearly faces great tribological challenges mainly due to excessive torque and drag generated by the whole weight of the drillstring when sliding against the formation wall or steel casing. These issues have been identified to be influenced by the type of lubricants (drilling mud) used for a particular drilling operation. Therefore, active research is needed to overcome this issue by optimising the components that make up the drilling mud and also in designing the tools to adapt to these conditions.

Due to the long distances of extended reach oil drilling, the tribological problems downhole are also increased due to increased numbers of local contacts between steel/steel along the hole. This direct steel/steel contact poises high friction and wear region, and the viscosity of the mud does not make much contribution to mitigate it. Under boundary lubrication, the most important factor is the presence of adsorbed molecules rather than a localised high viscosity lubricant. The understanding of the boundary lubrication phenomena has long been studied and stimulated investigations into the mechanisms of friction and wear reduction of the adsorbed molecules which react with the surface physically or chemically.

Previous studies have initially established that the adsorption of these molecules can be controlled using electrical potential. However, to extend these results beyond a proof of concept study, a systematic programme of investigation is necessary which includes the actual drilling mud formulations to fully explore the underlying triboelectrochemical processes.

Direct steel/steel contact will cause significant adhesion of the sliding surfaces thus results in high friction, which will dissipate as heat. This can also affect the chemical reactions such as oxidation of the steel surface or the debris, since chemical wear does not itself constitute a wear mechanism and must always be accompanied by some mechanical action to remove the chemical products that have been formed. As a result of the adhesion, material transfer can be obtained between the sliding surfaces, thus no wear occurs. However, these can break away from the contact to forming debris and resulting in wear [104]. The debris can have a higher hardness through work hardening or oxidation and can act as abrasives in the contact. Furthermore, in drilling muds, the presence of bentonite particles in the solution will increase the complication since the relatively hard bentonite particles can cause 2-body abrasion and 3-body indentations to the sliding steels. In addition, during drilling, a well that is not cleaned of cuttings will produce higher friction due to the abrasive rock debris and can be improved by removing it.

The harsh conditions during oilwell drilling demands the simulation of high pressure and high temperature environment. However, there is not much previous work in triboelectrochemistry at elevated temperatures. On one hand, there is a lot of electrochemical work on studying the effectiveness of corrosion inhibitors at high temperatures for downhole applications, such as by Quraishi *et al.* [105, 106] which used temperatures up to 105 ºC in hydrochloric acid. On the other hand, previous tribological work such as by Truhan *et al.* [18] which experimented using drilling muds did not conduct at elevated temperatures. Only Brandon *et al.* [5] conducted triboelectrochemical experiments related to oilwell drilling at elevated temperatures (up to 80 ºC). This is probably due to the difficulties of designing a triboelectrochemical rig which would allow simulation of the high temperature environments. This is because at high temperatures, the reference electrode might be affected, and also the drilling mud will be evaporating which will require constant feeding.

Therefore, this project intends to expand the current undersanding by testing the friction control by electrochemical methods in a simulated downhole conditions. Initial target of 10% reduction was set to be desirable.

3 Methodology

3.1 Introduction

This chapter will introduce the procedures undertaken throughout this project, in order to assess the effects of applied potential on the friction and wear performance, whilst simulating the downhole drilling conditions.

The test setup mainly employed a three electrode electrochemical cell; and a triboelectrochemical rig, which integrated the investigation of mechanical sliding and electrochemical reactions. The practice was made possible by using a pin-on-disc (PoD) rig, available at the nCATS laboratory, in which the incorporation of an electrochemical control was obtained by modifications, *i.e.*, by installing a three-electrode electrochemical cell into the rig. This modification process will also be discussed in this chapter.

Furthermore, details of the the test setup will be presented, including the types of materials used and the lubricant/solution preparation methods. Finally, some insights into the steps taken during the post-test analysis will be discussed, such as the use of Scanning Electron Microscope in the determination of the wear mechanisms.

3.2 Preparation of the Tribological Experimental Setup

This section aims to introduce the pin-on-disc tribometer used in this projec. Explanations of the rig modifications that were implemented will also be presented.

3.2.1 The Pin-on-Disc (PoD) Rig

The PoD rig allowed uni-directional sliding of the steel/steel or steel/sandstone contacts to be studied in either lubricated or dry conditions. Initially, the existing PoD rig as shown in Figure 3.1 was used for dry sliding of steel/steel contacts. The rig consisted of a static pin mounted on a rigid frame which was fixed to the ground. The normal load on the pin could be varied between 40 N and 100 N, which will cause the pin to press against the rotating disc at a required stress. Similarly, the speed of the disc rotation may also be controlled up to 250 rpm. However, the load and speed were kept constant in this study, at 50 N and 11 rpm respectively, to enable cross comparing of the test results under similar experimental conditions.

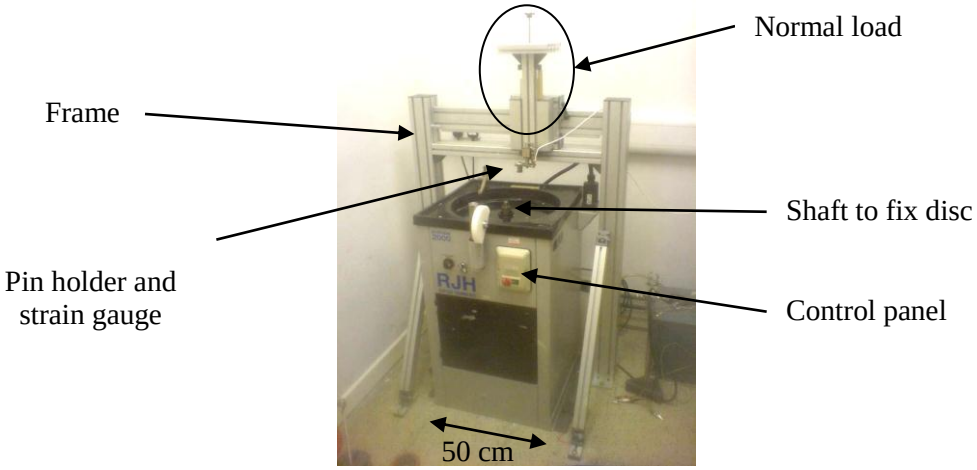

Figure 3.1. The unmodified PoD rig allowing pure mechanical sliding.

3.2.2 Modifications to the PoD Rig

A few modifications to the existing PoD rig were implemented aiming at introducing electrochemical control on the disc or pin, and also improving the robustness of the friction measurements. The major electrochemical modification involved designing a disc holder incorporating a three electrode cell so that an electric potential could be applied to the rotating disc, which should be reliable and free from leaks. In addition, the improvement to the friction measurements particularly involved in minimising the effect of hysteresis found in the rig.

3.2.2.1 Installing the Three Electrode Cell

A summary of the concepts used in designing the triboelectrochemical rig are schematically shown in Figure 3.2. The existing pure mechanical sliding setup, as shown in Figure 3.2 (a), was combined with the three electrode electrochemical cell, Figure 3.2 (b). Therefore, the result of integrating the two is schematically represented in Figure 3.2 (c), in which the potential of the disc can be controlled whilst sliding against the pin.

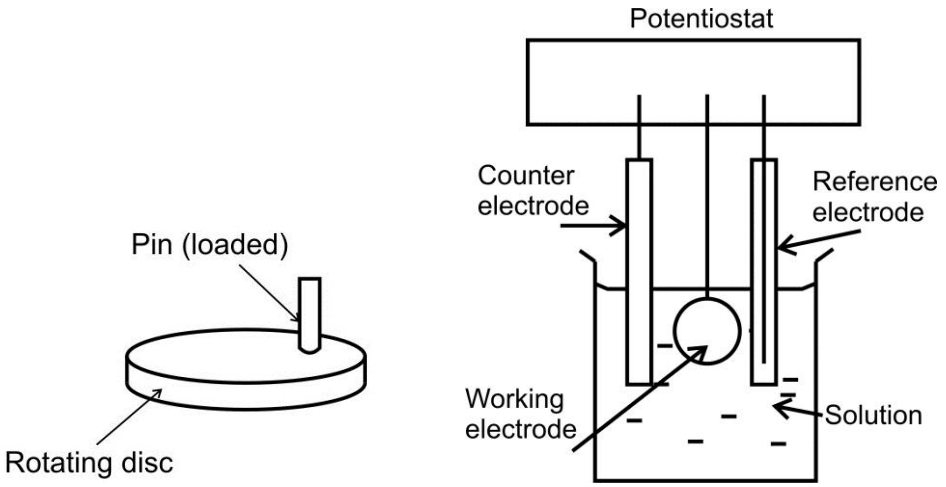

(a) (b)

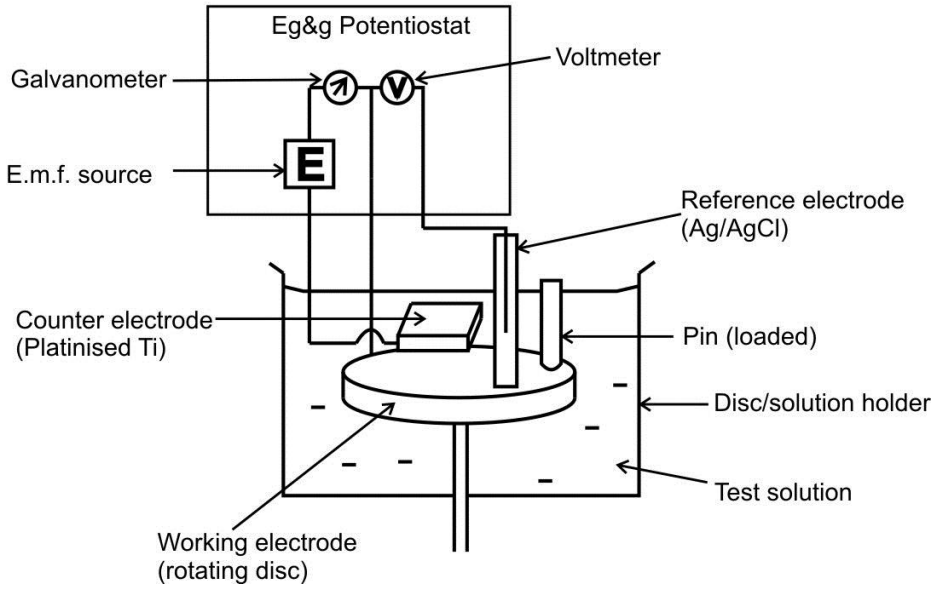

(c)

Figure 3.2. Schematics showing (a) a pure mechanical pin-on-disc; (b) a simple potentiodynamic polarisation apparatus, and; (c) the concept of combined mechanical and electrochemical setup.

There were a few challenges that needed to be addressed in order to bring the concept as shown by Figure 3.2 (c) above into practice. The first challenge was to design a disc holder capable of retaining the test solution, and with the ability to be securely fixed to the shaft beneath the frame. The holder was made with acetal (polymer) which is chemically inert and electrically insulating, whilst providing sufficient strength. Secondly, the test solution must be sealed so that it will not leak in between the base of the holder and the disc, which was achieved using an o-ring seal. Figure 3.3 shows the detailed schematic of the final design.

This study controls the electric potential of the rotating disc, which meant that the connection between the disc and the potentiostat was not straightforward. Therefore, a carbon brush was installed in order for a continuous electrical connection to be made with a slip ring at the bottom of the holder (not shown in figure). The counter electrode was embedded in an acetal block with one face exposed to the test solution. The counter electrode and its holder had two holes to accommodate the pin and the reference electrode.

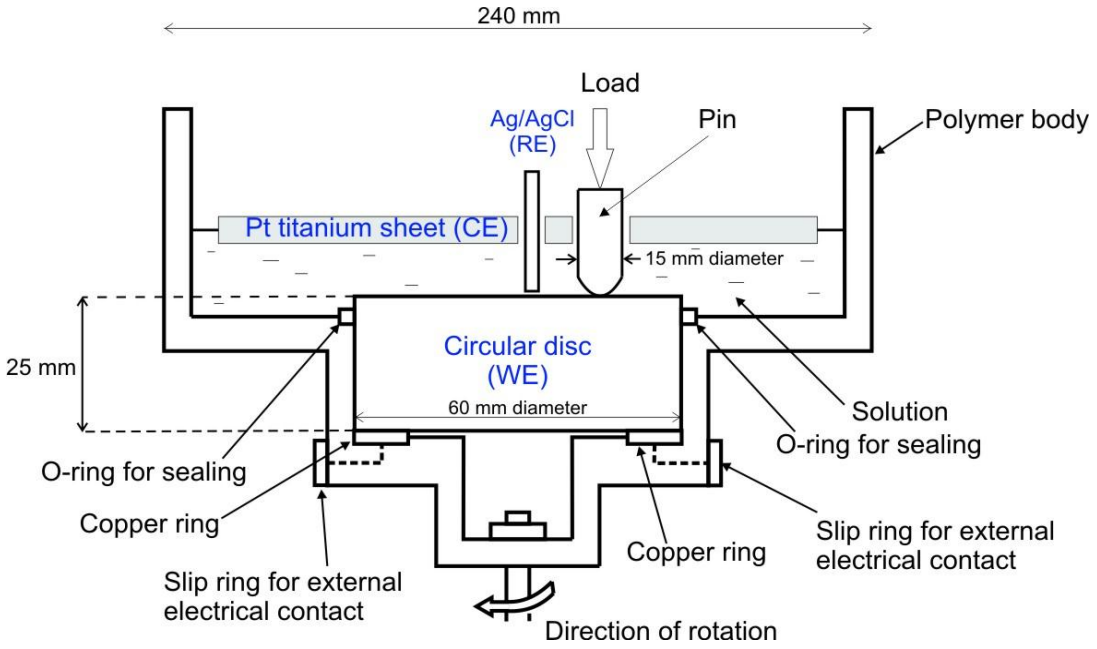

Figure 3.3. Detailed schematic of the designed disc holder incorporating the three electrode cell.

3.2.2.2 Improving the Friction Measurements

i. Improvements to Calibration Procedure/Setup

Discussions with previous users of the inherited PoD rig (as shown in Figure 3.1) in the nCATS revealed that possible improvements could and should be made to produce a more robust friction measurement, particularly by developing the calibration procedure. The previous calibration procedure employed a spring balance manually pulled on the pin to produce a voltage reading. The disadvantage of the system was that a constant load could not be applied and maintained for a period of time, thus the voltage measurement was made on a fluctuating response. Thus, the result of the calibration was plotted as voltage output *vs.* the applied load, as shown in Figure 3.4, which is an essential step prior to running the PoD or sliding tests.

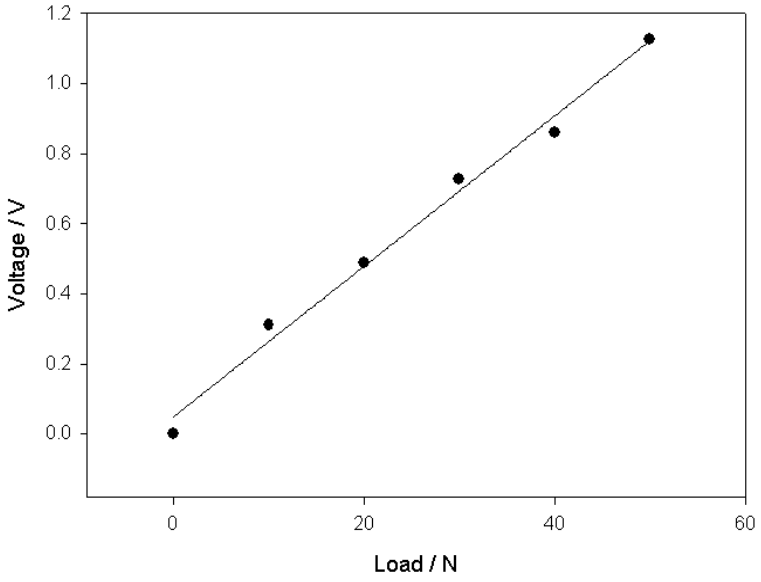

Figure 3.4. Initial calibration result (step loading only).

Another disadvantage of using the initial calibration procedure was the difficulty in establishing effective step loading and unloading which is critically important for detecting hysteresis. Therefore a new system was designed in order that a base capable of supporting weights could be attached to the pin via a pulley, as schematically shown in Figure 3.5, to replace the spring balance. This system was more robust as it does not depend on a manual method for applying force. The installation of the new system (weight-pulley system) enabled a more systematic calibration method to be adopted where the applied load on the pin was gradually increased from 0 to 60 N and *vice versa*. 60 N was chosen because it was well above the normal load used within a typical triboelectrochemical test in this study (50 N). The consequence was a detection of hysteresis during the calibration which clearly necessitated further improvements to the design of the PoD rig, see Figure 3.6.

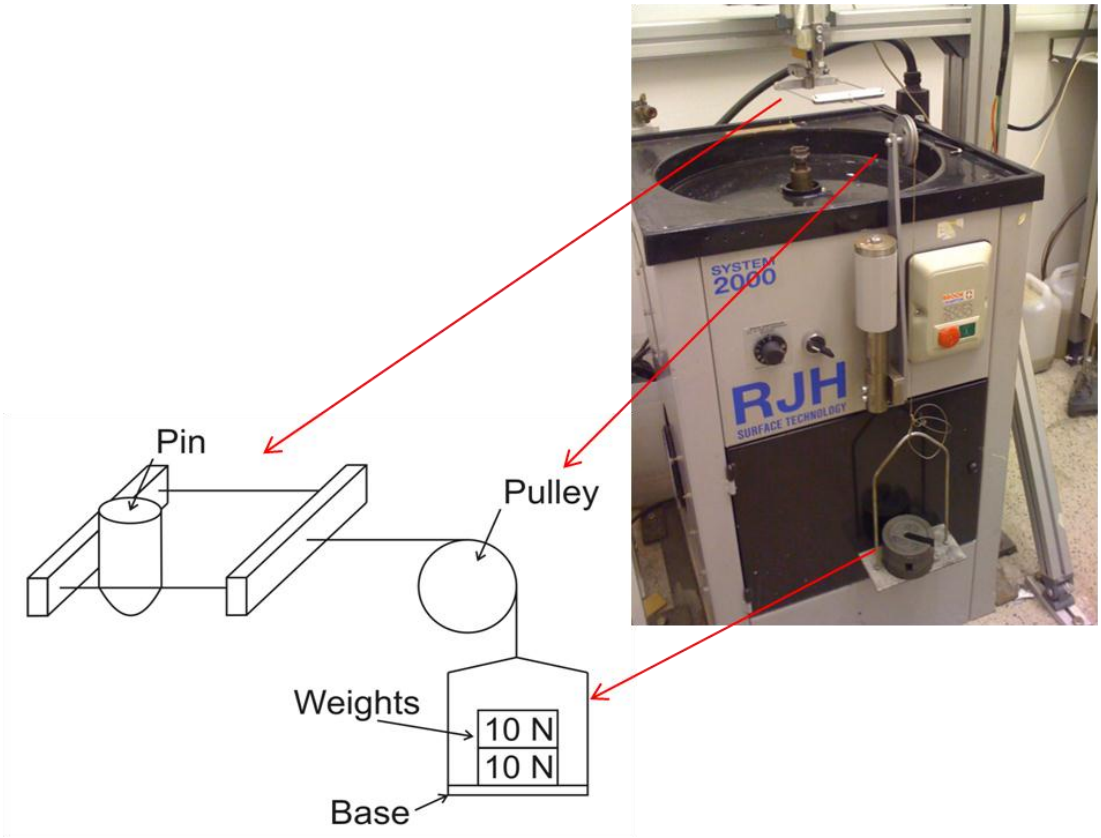

Figure 3.5. The weight-pulley system replacing manual handling.

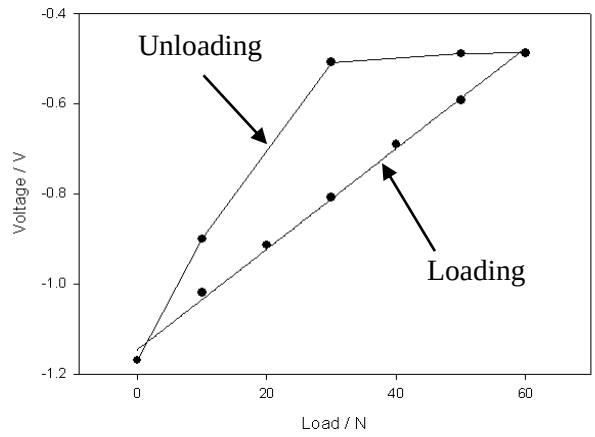

Figure 3.6. Calibration result showing the detected hysteresis during unloading step.

ii. Hysteresis Minimisation

Careful investigation using the improved calibration setup (weight-pulley) concluded that the hysteresis problem was caused by high levels of friction in the pin shaft holder assembly in the rig, see Figure 3.7. The friction hindered the smooth translation of motion from the pin to the load cell, thus the real friction measurement between the pin and disc was susceptible

to error. The hysteresis was observed to be prominent during the unloading process because the load cell could not effectively relax to the appropriate reduced strain due to the shaft friction. The overall effect of the hysteresis could be that, during a PoD test, any reduction in friction (or fluctuation) would not be correctly measured leading to the potential loss of valuable information within each test.

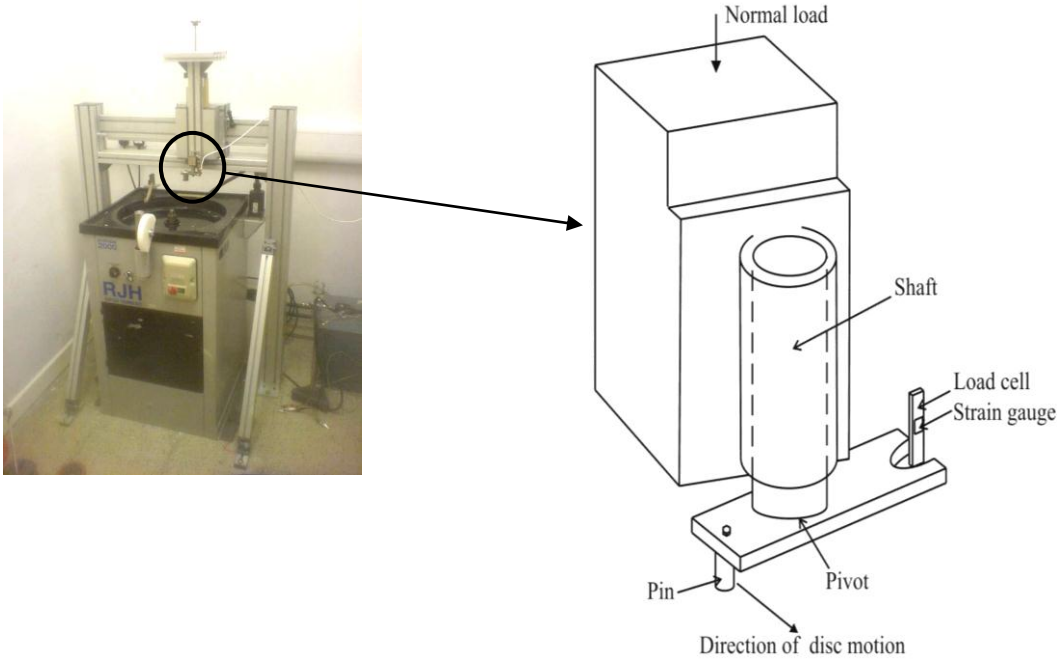

Figure 3.7. Initial design of the pin holder (Design I).

The evolution of the design towards a hysteresis free (or minimum) is summarised in Figure 3.8. Design I had high friction between the shaft and the holder as mentioned, therefore a bearing was implemented into Design II. However, there was still a small amount of hysteresis in the system. The final design (Design III) used a linear ball slider setup manufactured by THK Japan (model LSP 1365), replacing the shaft and pivot setup. The manufacturer claimed that this slider has a very low friction thus was chosen to be tested for feasibility. It is now proven to produce negligible hysteresis, and as such was used henceforth for the whole duration of this project.

Pin Holder Design **Calibration Result**

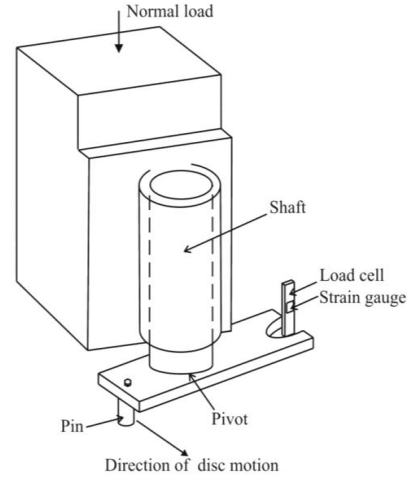

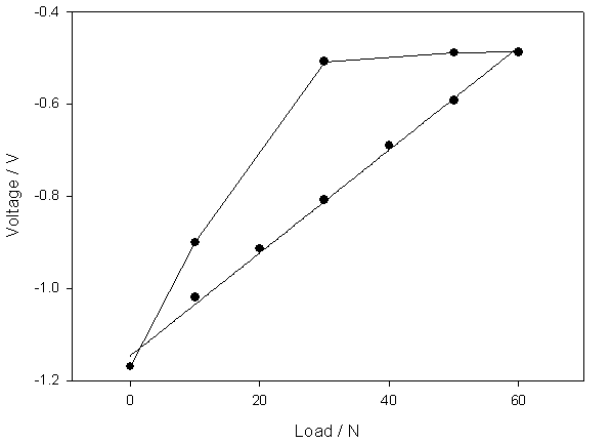

(a) Design I

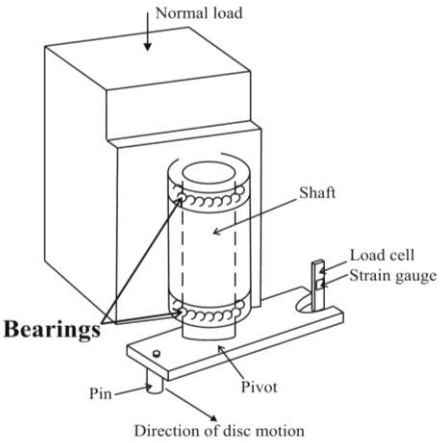

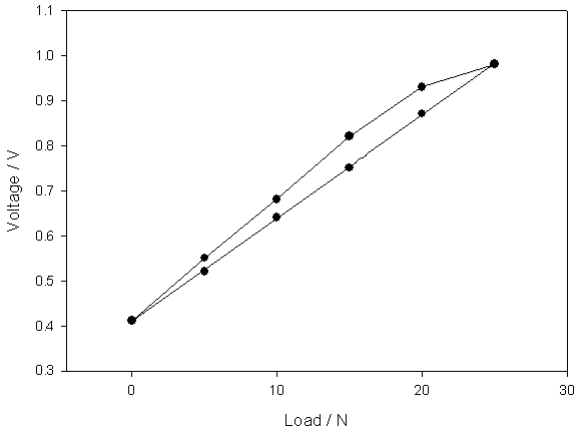

(b) Design II

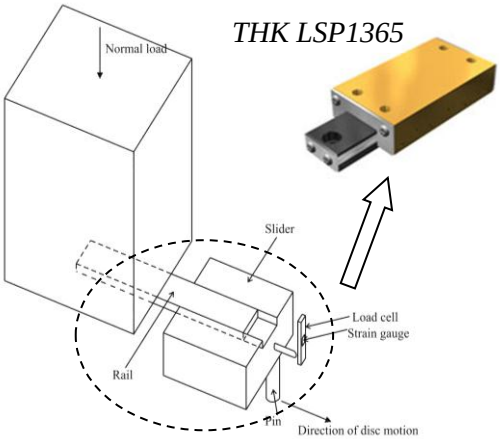

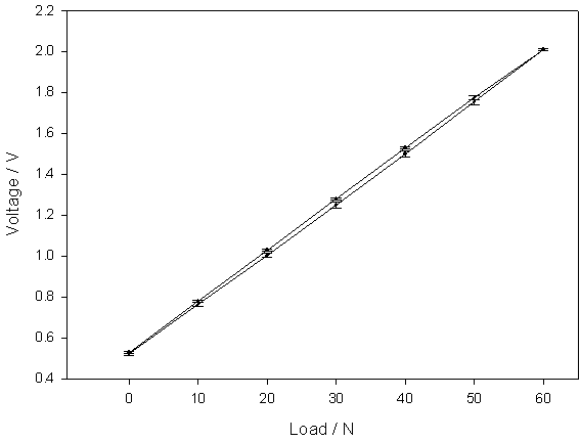

(c) Design III

Figure 3.8. Evolution of the pin holder design. Design III is the final design with the minimum hysteresis, which was employed in every PoD test setup of this project.

A more detailed schematic of the pin holder employed in Design III is shown in Figure 3.9, visualising the sliding motion of the slider along the fixed rail. The slider and rail allowed a degree of freedom along the tangent of the rotating disc hence the frictional force between the pin and disc can be transmitted to the load cell. A pip was installed at the leading edge of the slider to make contact with a rigidly held load cell. The elastic deformation of the load cell was detected by the strain gauge and the output recorded, hence converted to friction.

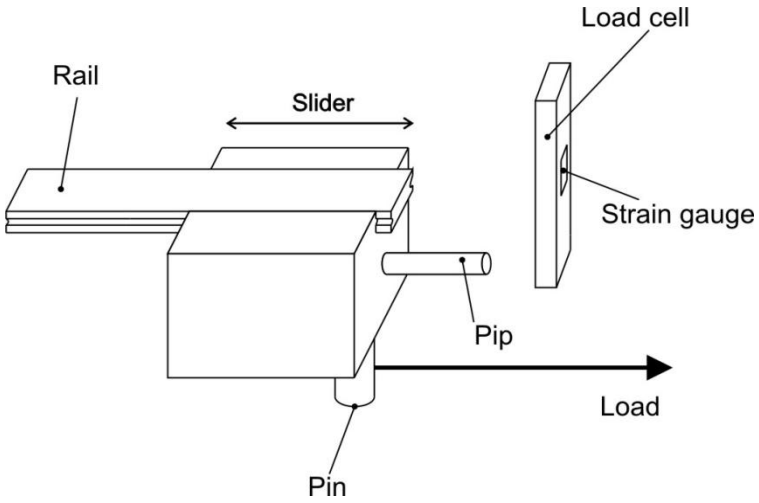

Figure 3.9. Schematic of the final design of the pin holder.

3.2.2.3 Friction Calibration Equation

A general equation relating voltage and friction can be achieved and serves as the basis for any conversion,

$$y = mx + c \qquad \text{eqn. 3.1.}$$

where x is the load in N, y is the voltage in V, m is the slope of the line in V N^{-1}, and c is the y-intercept in V. Therefore, this relationship could be used to represent the trend line from the calibration graph such as shown in Figure 3.10.

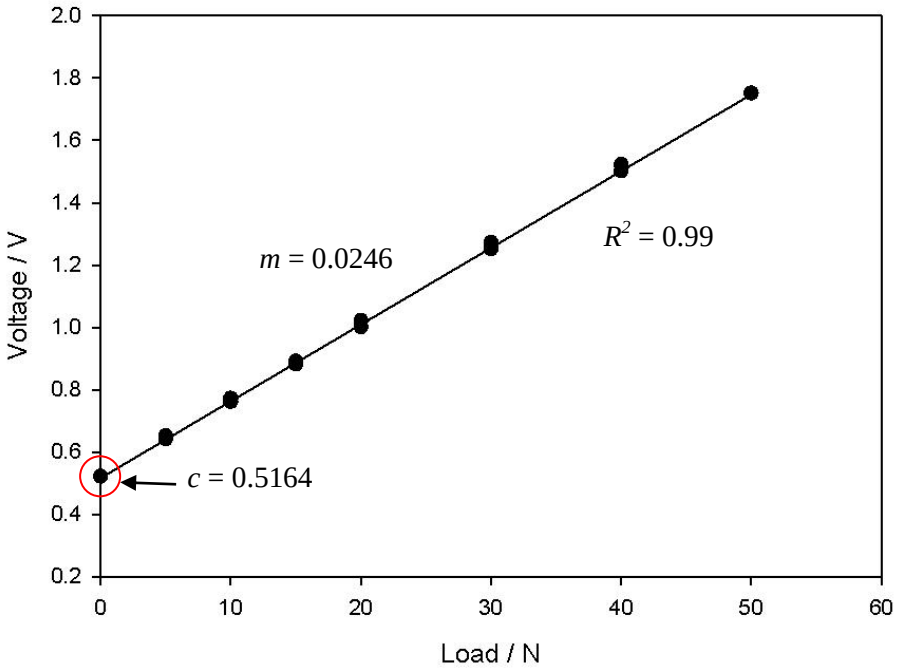

Figure 3.10. A calibration graph of voltage *vs.* applied load. The points show the voltage at discreet loads employing the step loading and unloading procedure. A linear interpolation trend line was fitted to the points.

3.3 General Test Methodology

The overview of the general test methodology is represented by the flowchart shown in Figure 3.11. On the whole, the steps could be grouped into three, *i.e.*, the pre-test, in-test and post-test. The pre-test consists of the steps related to preparing the pre-requisites of the PoD experiments, such as the fabrication of pins and polishing the disc samples. Furthermore, other important test requirements, such as the solutions, were prepared, and the friction calibration was conducted.

The in-test procedure refers to the two main types of tests utilised in this study, which were the (i) pure electrochemical tests, and (ii) triboelectrochemical tests (integrated mechanical and electrochemical methods). Generally, the electrochemical tests were aimed at assessing the behaviour of the steel immersed in the different solutions while being subjected to a potentiodynamic polarisation or open-circuit potential test setup. These tests were conducted in the beaker. However, the triboelectrochemical tests were aimed at investigating the relationship between the electrochemical performance and tribological phenomena, *i.e.*, by conducting the electrochemical tests with the presence of the sliding motion between the pin and disc. The modified PoD rig (as discussed previously in this chapter) was used for performing these tests.

The results of all these tests were analysed in the post-test procedure, which involved statistical interpretation of the electrochemical reactions, as well as physical and chemical examination of the samples. Finally, all of these could be used to devise the conclusions of this project, and therefore would be beneficial for future developments.

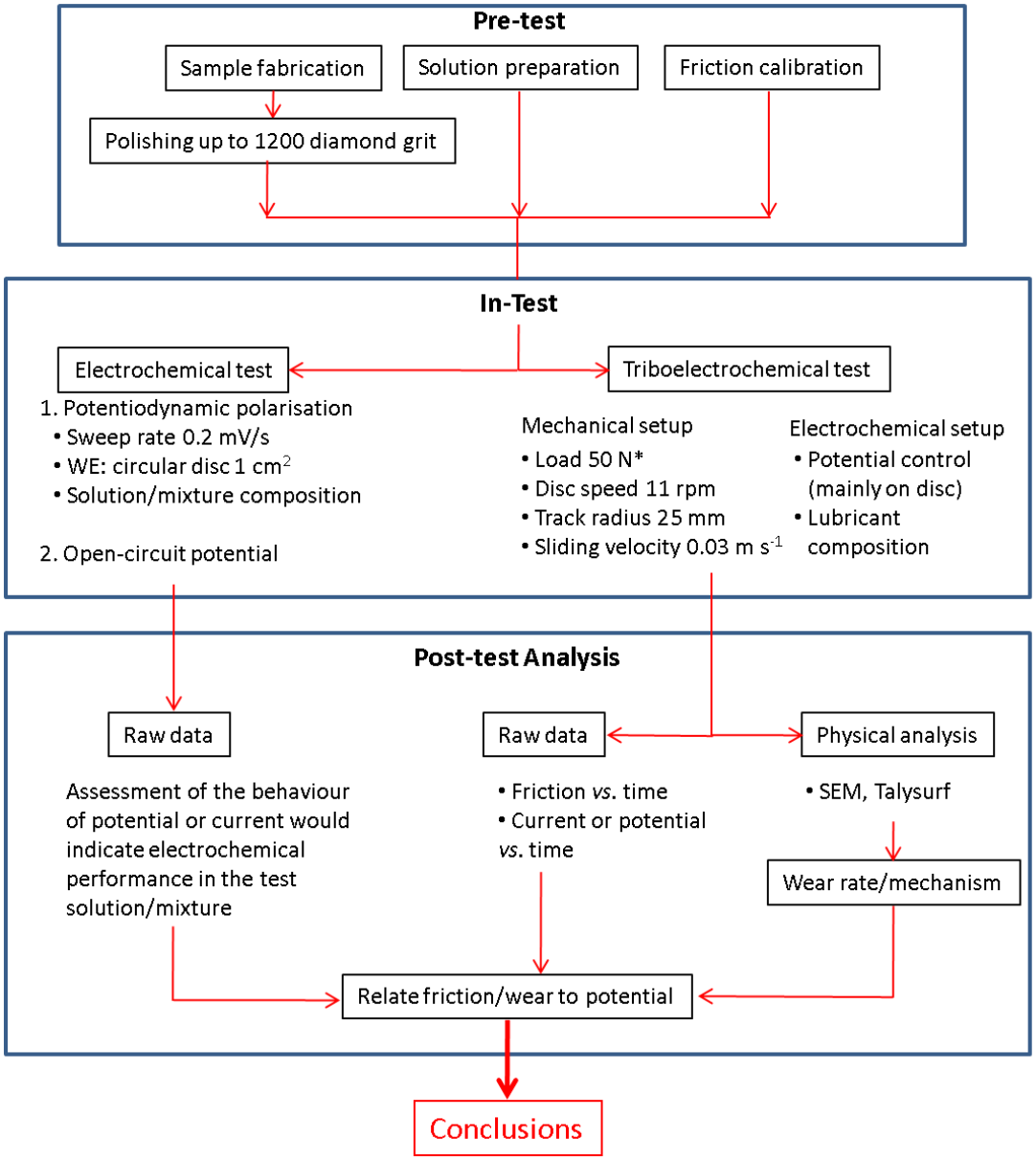

Figure 3.11. Flowchart of the general test methodology employed in this project, showing brief explanations of each step.

3.4 Sample and Solution Preparations

This section (Section 3.4) will report on one of the essential steps involving the preparation for the tests. The important criteria for the design of the pin and disc samples will be presented, such as the geometries and materials used. In addition, the details of the types of lubricants/test solutions used in the experiments, as well as the preparation methods, will also be discussed.

3.4.1 Steel Samples

The geometries of the steel pin and disc samples are schematically shown in Figure 3.12Figure 3.12. The pin tip was machined to a 25 mm radius and subsequently hand polished (see Figure 3.12 (a)). The 60 mm diameter discs (see Figure 3.12 (b)) were polished using magnetic diamond polishing plates by Struers, and the final step was by using 1200 grit. Surface roughness measurements of the polished disc and pin samples were performed using a Taylor Hobson Form Talysurf 120L profilometer and obtained R_a values of 0.04 µm and 0.05 µm, respectively. The contact between the pin and disc would produce an initial Hertzian contact stress of 390 MPa (see Chapter 2 for calculation details).

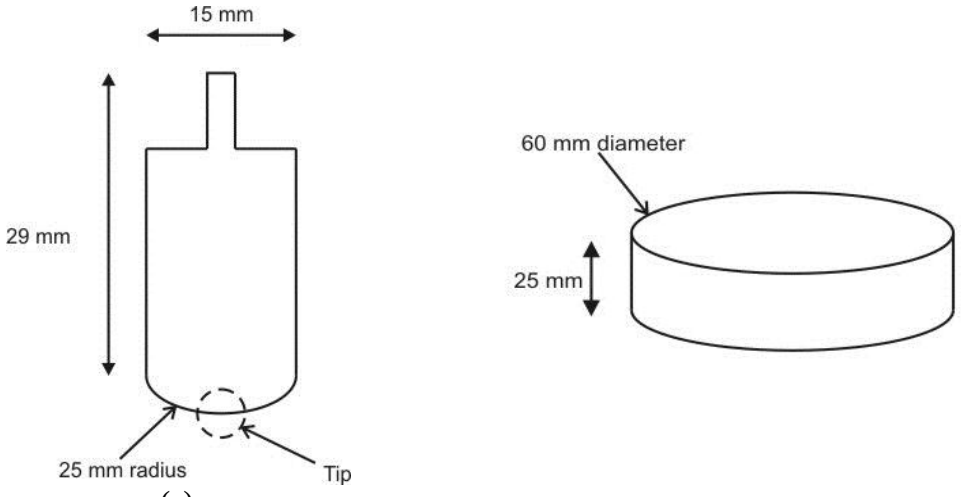

Figure 3.12. Schematic of the pin (a), and; disc (b) used in this study.

Both the pin and disc steel grade was EN 24 steel (BS 970 817M40 equivalent to AISI 4340) and had a chemical composition as shown in Table 3-1 [107].

Element	C	Cr	Fe	Mn	Mo	Ni	P	S	Si
Nominal Composition (%)	0.41	0.8	*	0.7	0.25	1.83	0.02	0.02	0.25

Table 3-1. Nominal composition of the material used (AISI 4340) [107]. *Fe being the balance of the composition.

The pin and disc materials had similar Vickers hardness measurements of around 241 HV. A transverse cross-section of the pin was polished for microstructural analysis. The final polishing was achieved using a 1 µm diamond paste. Subsequently, it was etched in 2% Nital solution for 5 s. The microstructure shows dispersed carbide as a result of tempering following hardening during the manufacturing process, see Figure 3.13.

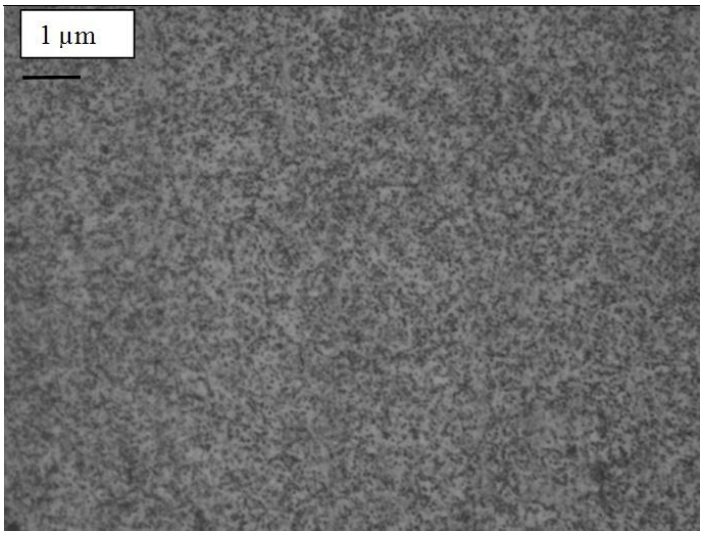

Figure 3.13. Microstructure of the steel after etching in 2% Nital, showing dispersed carbide as a result of tempering following hardening during the manufacturing process.

3.4.2 Sandstone Samples

The steel/sandstone contacts consisted of two arrangements which were (i) sandstone pin/steel disc, and (ii) steel pin/sandstone disc (see Table 3-2). Therefore, pins and discs were fabricated out of the sandstone material, to slide against the steel samples with geometries described earlier. The change in arrangement was particularly to assess the electrochemical and tribological performance when the steel surface area was varied. To achieve this goal, a few extra components were necessary to enable the sandstone pin and disc to be fixed in the rig, which involved the fabrication of a special adaptor and disc holder respectively (see next Subsections 3.4.2.1 and 3.4.2.2).

Steel/sandstone contact arrangement	Pin material	Disc material
i	Steel	Sandstone
ii	Sandstone	Steel

Table 3-2. The two couple arrangements used to simulate the steel/sandstone contact.

3.4.2.1 Fabrication of the Sandstone Pins

The sandstone pins were fabricated to similar design of the steel pin, see Figure 3.1. A steel adaptor was used to clamp the sandstone pin so that it can be installed in the place of the steel pin counterpart. The sandstone pin was cut from a larger sandstone cylinder (nugget sandstone provided by Schlumberger) with the help from the Rock Preparation Lab, at the School of Ocean and Earth Science, University of Southampton. The sandstone pin tip was machined by eye using a steel pin as a guide, due to technical limitations.

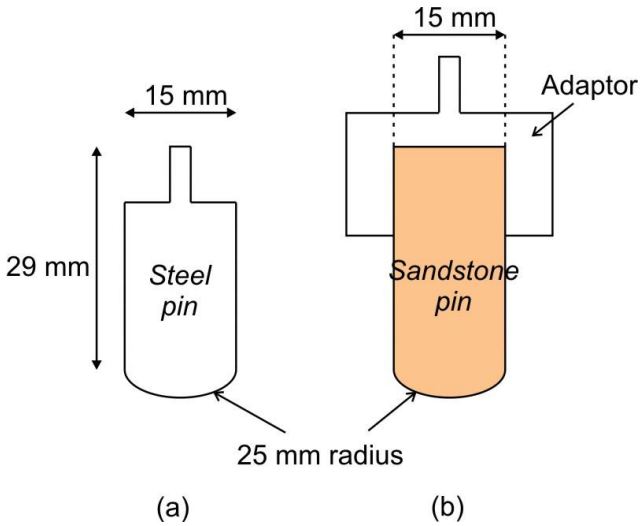

Figure 3.1. Schematic of the (a) steel pin, and (b) sandstone pin with the adaptor for fixing to the pin holder.

3.4.2.2 Fabrication of the Sandstone Discs

The schematic of the sandstone discs and the appropriate holder are schematically shown in Figure 3.2. The sandstone samples were provided by Schlumberger and were sliced into thinner discs to be used in different tests.

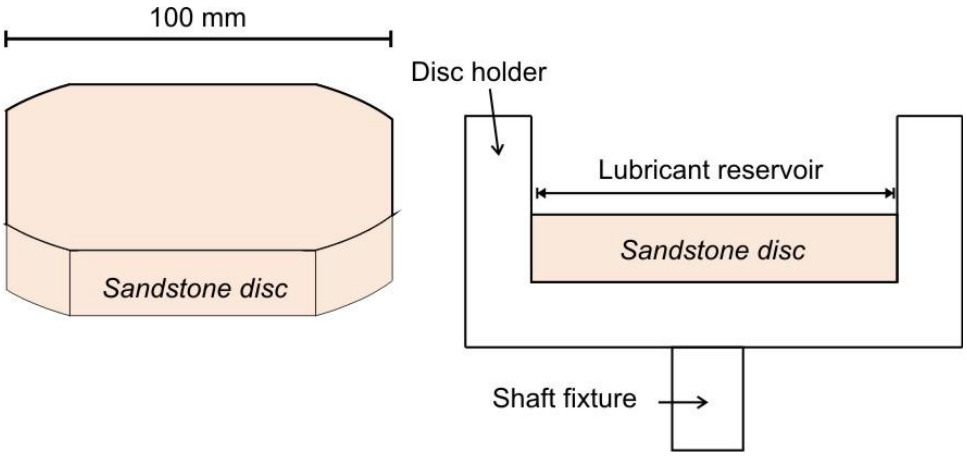

Figure 3.2. Schematic of the sandstone disc with the holder.

3.4.3 Test Solutions

3.4.3.1 List of the Test Solutions Used

Most of the solution pH was set to around 9 to simulate the actual bentonite drilling mud. Table 3-3 briefly lists the details of all the mixtures to be used in the triboelectrochemical experiments. In addition, the other solutions using the alternative additives, namely butyrate, oleate and CTAB were prepared without mixing with the bentonite particles or polymer powder.

Number	Name as will be referred	Constituents			
		NaOH pH 9	Bentonite particles	Octanoate additive	Polymer powder
1	NaOH	Yes	No	No	No
2	OA	Yes	No	Yes	No
3	Bentonite*	Yes	Yes	No	No
4	Bentonite+ octanoate*	Yes	Yes	Yes	No
5	Polymer	No	No	No	Yes
6	Polymer+ octanoate	No	No	Yes	Yes

Table 3-3. Details of the constituent of the solutions used in this study. These are the most important as they constitute the majority of the analysis of this project. * A version incorporating the presence of silica sand particles was also prepared.

The preparation steps of all the solution/mixture are detailed in Table 3-4 below (including the use of alternative additives). The concentrations of the drilling muds (base fluid) were akin to the actual application by industry and relevant technical publications. Particularly, the bentonite particles are typically used at 60 g L^{-1}, whilst the polymer powder (for the polymer based mud) at 4 g L^{-1}. However, for the additives, the octanoate and butyrate concentrations were standardised to 60 mM, whilst the oleate and CTAB were 1 mM. The justification for the choices of additive concentrations will be detailed in the next subsection (Subsection 3.4.3.2).

Test Solution/mixture	Preparation procedure
NaOH	Small quantities of 0.1 M NaOH was added to distilled water to adjust the pH to 9
Octanoate	1 cm^3 of 99% octanoic acid solution was mixed with 73 cm^3 of 1 M NaOH. The mixture was then diluted to 1 L and the pH adjusted to 9 by adding drops of 0.1 M NaOH.
Bentonite*	Bentonite particles were added by small amounts until 60 g to 1 L of distilled water while constantly stirring. The pH was adjusted to 9 by adding drops of 0.1 M NaOH if required.
Bentonite+ octanoate*	60 g of bentonite particles were slowly added to a pre-mixed OA solution while constantly stirring.
Polymer	4 g of the polymer powder was added to distilled water while stirring, producing a gel-like consistency. The powder was provided by MI Swaco, namely Duovis.
Polymer+ octanoate	4 g of the polymer powder was added to the octanoate solution while stirring
Oleate	0.3 g of sodium oleate powder was added to 1 L of distilled water and the pH was adjusted to 9 with 0.1 M NaOH
Butyrate	6.6 g of sodium butyrate powder was added to 1 L of distilled water and the pH was adjusted to 9 with 0.1 M NaOH
CTAB	0.36 g of CTAB powder was added to 1 L of distilled water while stirring with slight heat

Table 3-4. Test solution preparation procedures used in this study. *A version incorporating the presence of 30 g L^{-1} silica sand particles was also prepared.

3.4.3.2 Details of the Friction Modifying Additives

As described in Chapter 2, the adsorption of these friction modifiers onto contacting surfaces is essential to produce a low friction contact. Thus, a few types of friction modifiers were chosen which were (in order of most used):

a) Octanoic Acid

Previous work [92-94] has proven that octanoic acid additive can create a dependence of friction on applied potential. Therefore, this was chosen to produce baseline data and also to test if the phenomenon is reproducible in the drilling mud. The concentration of this additive was set to 60 mM which is equivalent to 1 wt% in water.

b) Sodium Butyrate

The butyrate molecule has a shorther hydrocarbon chain length (4 carbon atoms) cf. octanoate (8 carbon atoms). It was chosen to test the hypothesis that a shorter chain molecule will have greater mobility, and thus might have better reaction to an actively switched potential (during sliding). The concentration of sodium butyrate was 60 mM in order to match the octanoate, and the pH was adjusted to 9.

c) Sodium Oleate

Sodium oleate was chosen as the third additive because the molecules have higher hydrocarbon chain length (18 instead of 8 in octanoate). Therefore, this should enable more friction reduction cf. octanoate, due to the production of a more ordered adsorption layer (see Chapter 2 for more details). The concentration used was 1 mM and the pH was adjusted to 9.

d) Cetyl trimethylammomium bromide (CTAB)

CTAB was chosen due to the positive charge of the functional head group, as opposed to the other three additives which were negative. The purpose was to test the adsorption effect when cathodic potentials are used instead of anodic. The concentration for CTAB was 1 mM and the pH was not adjusted.

In summary, the carbon content of the fatty acid additives decreased in the order of oleate>octanoate>butyrate (summarised in Table 3-5). The hypothesis of using the three additives was that each will have different affinity to the steel surface, and would give different levels of friction (expected to decrease following that order).

Additive Name	**Butyrate (Sodium Butyrate)**	**Octanoate (Octanoic Acid)**	**Oleate (Sodium Oleate)**
Chemical Formula	$NaC_4H_7O_2$	$C_8H_{16}O_2$	$NaC_{18}H_{33}O_2$
Carbon content	4	8	18
Expected friction reduction when present	Low	Medium	High

Table 3-5. The chemical formula of all the additives and the expected friction reduction effects.

3.4.3.3 The Bentonite Particles

The size distribution of the bentonite particles used to formulate the bentonite drilling mud was estimated to be between 10 to 50 μm (see Figure 3.3), and was added at a set 60 g L^{-1} concentration which is typical to that used in the drilling industry. At this concentration, it is reported that the suspended bentonite particles provide a viscosity increasing effect which is useful for carrying the cut formation during drilling [4, 54].

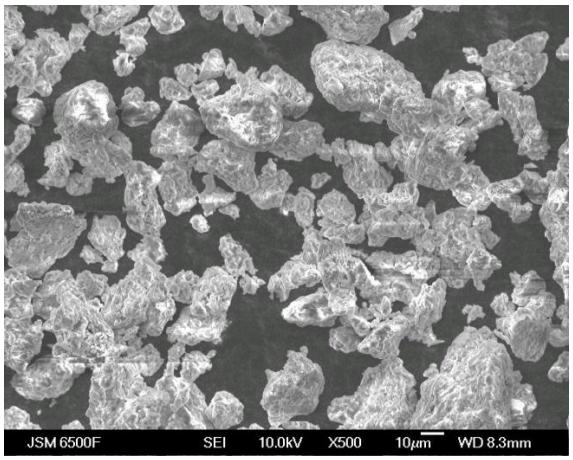

Figure 3.3. SEM micrograph of the bentonite particles before added to the mixture.

To simulate the presence of cruched rock debris (cut formation) which is mixed in the drilling mud, silica sand particles were included in a few formulations at 30 g L^{-1} concentration. The sand particles were provided by Schlumberger and had a mean size of 5 μm.

3.5 In-Test Methodology

This section (Section 3.5) will present the methods undertaken in conducting the main experiments employed in this project. The first part of the experimental series was aimed at establishing the electrochemical performance of the solutions in contact with the steel. Therefore, these tests were mainly conducted in the beaker and will be detailed in Subsection 3.5.1. The second part, however, was to assess the relationship between the electrochemical performance and mechanical phenomena, *i.e.*, with the presence of sliding. It involved conducting experiments in the rig, which will be discussed in the following Subsection 3.5.2.

3.5.1 Electrochemical Tests

3.5.1.1 Potentiodynamic polarisation

The pure electrochemical experiments were conducted using the AISI 4340 steel as the working electrode while immersed in the test solutions (electrolyte). This was in order to assess the electrochemical behaviour of the steel in contact with the different types of solution. Mainly, the test procedure involved polarisation (potentiodynamic) of the steel from –1 V overpotential to +1 V overpotential, in each test solution.

As such, the potentiodynamic polarisation setup is schematically shown in Figure 3.4. The potentiostat used was EG&G 263A Princeton Applied Research. The working electrode had 1 cm^2 area exposed to the electrolyte. The reference electrode was a silver/silver chloride (Ag/AgCl), and the counter electrode was platinised titanium with an apparent surface area of about 80 cm^2. During a simple potentiodynamic polarisation test, the applied voltage is swept at a rate of 0.2 mV s^{-1}. The current was monitored and recorded, subsequently divided by the area of the exposed steel (1 cm^2) to get the current density in A cm^{-2}. A more detailed explanation of the fundamentals of this test method was discussed in Chapter 2.

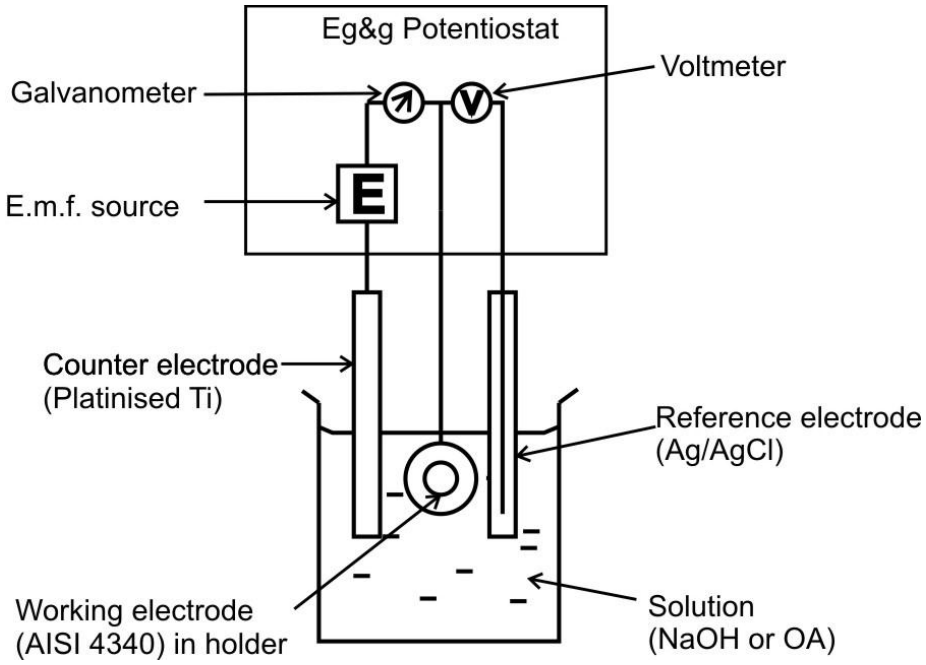

Figure 3.4. Schematic of the electrochemical cell used for simple potentiodynamic polarisation tests.

3.5.1.2 Open-circuit Potential Drift

The open-circuit potential (OCP) drift test involved the immersion of the steel in the test solution without polarising it. The aim was to allow the electrochemical reactions to achieve steady state, whilst monitoring the behaviour of the potential. Therefore, this test was done prior to the potentiodynamic polarisation test.

The absence of polarisation allowed the experimental setup to be slightly simpler than the potentiodynamic polarisation. Particularly, the test setup only requires the steel (working electrode) to be immersed in the solution, with the reference electrode to monitor the potential. Therefore, the counter electrode could be omitted in the test setup. The OCP drift tests were conducted in 1 hr periods, immediately prior to each potentiodynamic polarisation, in which the results could be plotted as the potential *vs*. time graph.

3.5.2 Triboelectrochemical Tests

3.5.2.1 Introduction

Some of the electrochemical experiments discussed previously in Section 3.5.1 were repeated in the PoD rig to assess the reproducibility. Therefore, the test setup of each potentiodynamic polarisation in the rig is shown schematically in Figure 3.5. Note that the pin is excluded in any electrochemical polarisation. Finally, the test was repeated while the rig was rotated at 11 rpm to examine the effect of hydrodynamics (increased mass transport)

to the electrochemical response, since this speed was also typical for any triboelectrochemical test in this study.

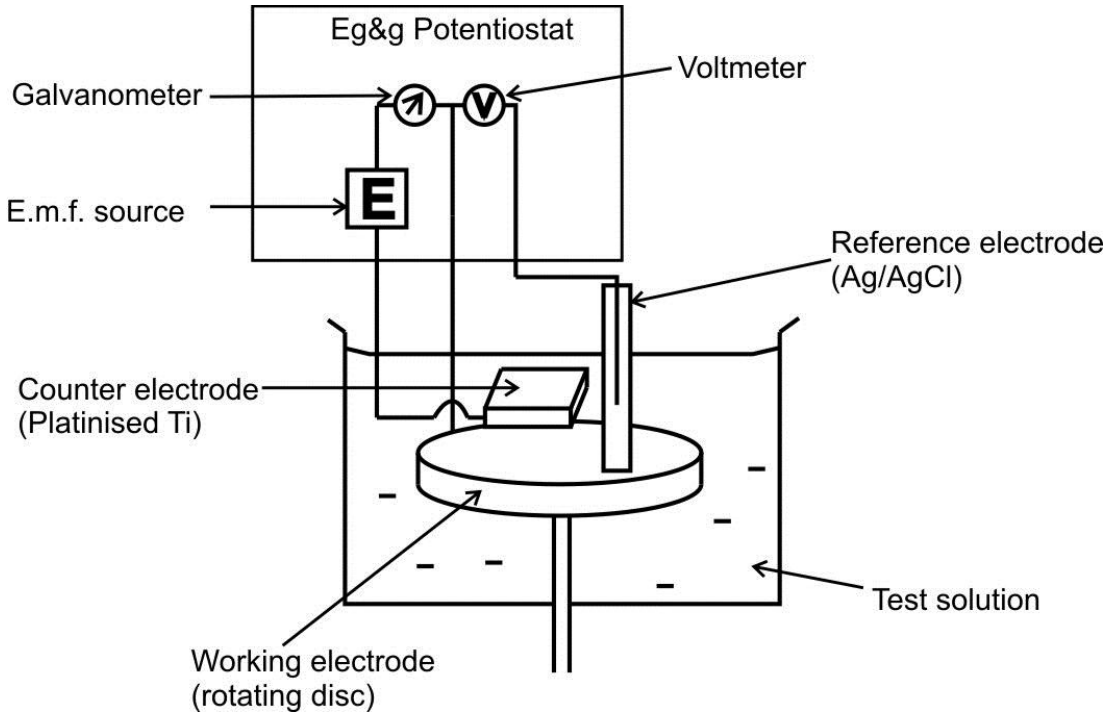

Figure 3.5. A conceptual schematic representation of the test setup for potentiodynamic polarisation in rig.

3.5.2.2 Electrochemical Test Setup

Excluding the tests to assess only the reproducibility of the rig, the electrochemical setup of the triboelectrochemical tests could be listed as follows (see Table 3-6):

Criteria	Explanation
Applied overpotential / V	Between –1 and +1. For example, at –1, –0.54, 0, +0.36, and +1.
Potential application mode	Mainly potentiostatic (one overpotential value throughout the sliding period), apart from the active switching test.
Reactions recorded	Current / A at 1 Hz acquisition, except for the 0 V overpotential test in which potential / V *vs.* Ag/AgCl was recorded

Table 3-6. A list of the electrochemical setup.

3.5.2.3 Mechanical Test Setup

The mechanical setup of the triboelectrochemical tests were 50 N normal load (corresponding to 390 MPa initial Hertzian contact stress) and 0.03 m s^{-1} sliding velocity. The radius of the track was set to 25 mm, which will obtain a 108 m sliding distance after sliding for 1 hr.

3.6 Methodology of the Post-Test Data Analysis

The methods of analysing the results of the experiments will be discussed in this section. In particular, the analysis consisted of evaluating the recorded data during the sliding period which included the friction, potential and current values. Furthermore, physical analysis of the samples was also conducted such as calculating the wear rate of the pins and discs, and imaging by using the Scanning Electron Microscopy (SEM). In addition to this, a chemical analysis of the worn surfaces was also conducted using X-ray Photoelectron Spectroscopy (XPS), especially for observing the tribofilm that was formed during sliding.

3.6.1 Processing the Friction Data

The methods to process the friction raw data is visually shown by the flowchart in Figure 3.6. The recorded *in situ* raw data were in a voltage format, therefore the conversion factor or equation from the calibration procedure during the pre-test (previously discussed in Section 3.2.2.3) was used to convert from voltage *vs.* time, to friction *vs.* time.

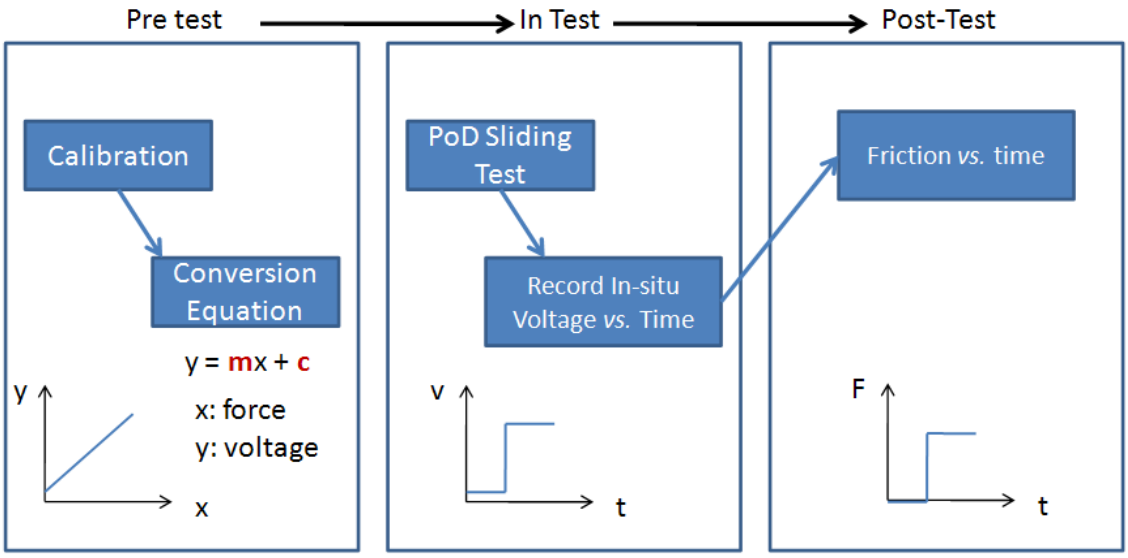

Figure 3.6. Flowchart showing the procedures to convert voltage to friction.

This step can be extended by dividing all data points by the normal load (50 N) to get coefficient of friction, μ, *vs.* time / s. Subsequently, the mean μ (μ_{mean}) can be obtained from the μ *vs.* time data using the equation shown below,

$$\mu_{mean} = \frac{\sum_{i=1}^{i=n} \mu_i}{n} \qquad \text{eqn. 3.2.}$$

where *n* is the number of data points which is 3600 (due to 1 Hz acquisition rate at 3600 s sliding period). Note that only the data during sliding is used to be calculated in eqn. 3.2. The μ_{mean} value from each test was collected and could be plotted against the applied overpotential (most tests were repeated once). This would allow the assessment of the overall influence of potential upon tribological performance. Furthermore, the standard deviation (s.d.) of each friction response could be calculated by using,

$$s.d. = \sqrt{\frac{\sum_{i=1}^{n}(\mu_i - \mu_{\text{mean}})^2}{n}} \qquad \text{eqn. 3.3.}$$

3.6.2 Evaluating the Electrochemical Performance

As discussed earlier, the electrochemical performance from both the pure electrochemical and the triboelectrochemical tests were recorded either as current or potential. As such, separate evaluations are required to investigate the behaviour.

3.6.2.1 Current Density

The recorded *in-situ* current data was in current *vs.* time format. During the post-test, the current was divided by the area of the electrode, which were 1 and 28 cm^2 for the pure electrochemical and triboelectrochemical tests respectively. Therefore, the result would be a current density *vs.* time graph. Figure 3.7 illustrates the procedure of converting the current recorded during a sliding test to current density.

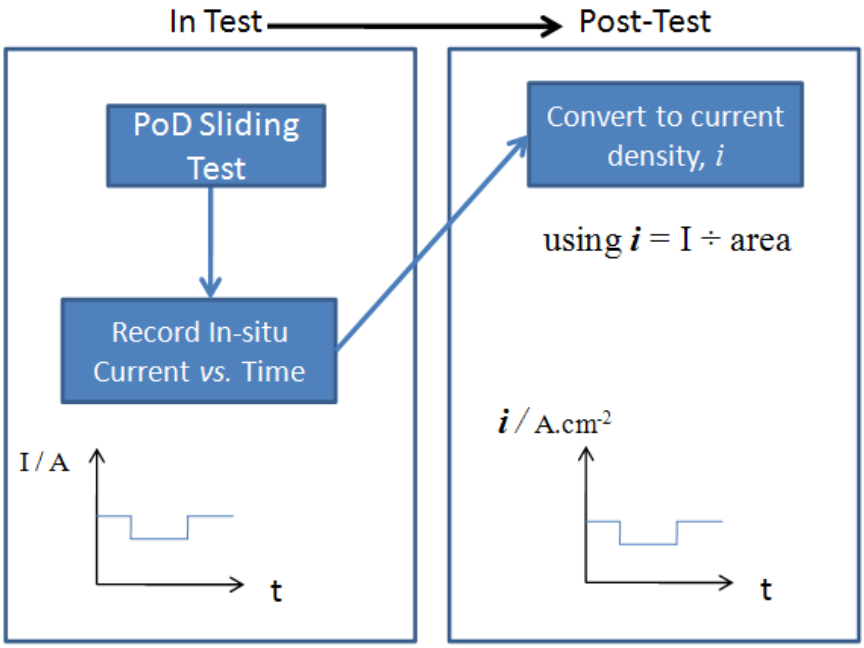

Figure 3.7. Flowchart of converting current *vs.* time to current density *vs.* time.

3.6.2.2 Potential

Potential was recorded during each OCP *vs.* time test in the pure electrochemical setup, prior to each potentiodynamic polarisation. Similarly, potential was also recorded in the triboelectrochemical setup, but only at 0 V overpotential, *i.e.*, the test when no potential was applied (being recorded instead). This data was used without further modification, apart from plotting the potential / V (*vs.* Ag/AgCl) *vs.* time / s graph. However, for the triboelectrochemical tests, the average values of the OCP over the sliding period were calculated to allow quantitative comparison.

3.6.3 Wear Rate of Disc

The transverse profile of the wear track on the disc was measured using a Taylor Hobson Talysurf 120L profilometer at four equidistant positions around the track, as shown in Figure 3.8. The aim was to obtain a mean area of the groove (wear track) to enable volume loss calculation.

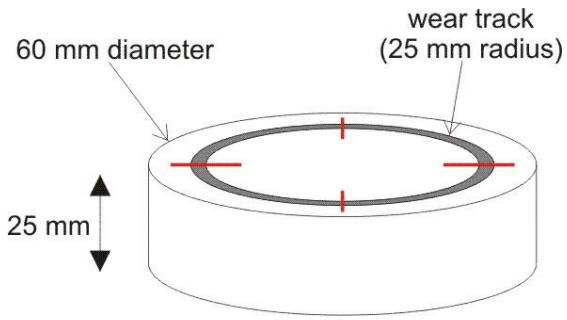

Figure 3.8. Schematic of a tested disc showing four transverse profile lines.

Figure 3.9 shows the expected profile from a wear track scan using the Talysurf. The calculation method assumed that the off wear track surface did not change during the test, therefore it is a suitable plane to base the calculation of the wear track cross-sectional area.

Therefore, from Figure 3.9, the area of the wear track is given by, *a*,

$$a = A_c - (A_a + A_b) \qquad \text{eqn. 3.4.}$$

If a_{mean} is the mean area in m^2 of the four profiles, therefore the volume loss, *V*, along the track can be calculated by this equation,

$$V = 2\pi r a_{mean} \qquad \text{eqn. 3.5.}$$

where *r* is the wear track radius (0.025 m). Thus, the Archard specific wear rate, *k* as discussed in Chapter 2 can be calculated,

$$k = \frac{V}{WL} \qquad \text{eqn. 3.6.}$$

where *W* is the load (50 N), and *L* is the sliding distance (108 m after 3600 s). The unit of *k* is $m^3\ N^{-1}\ m^{-1}$ or can be converted to $mm^3\ N^{-1}\ m^{-1}$ by multiplying with 10^9.

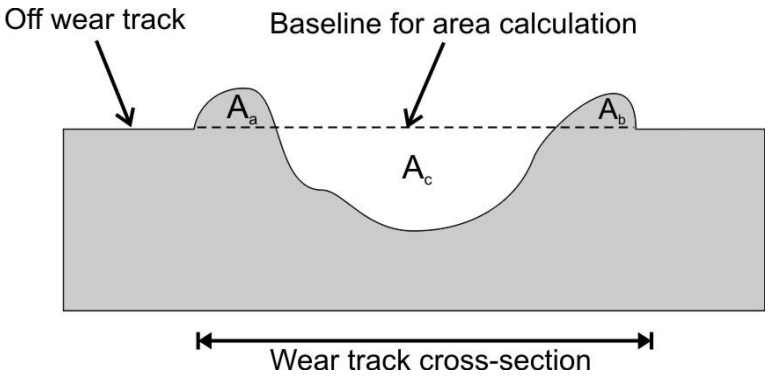

Figure 3.9. Schematic of the wear track cross-sectional view (a single profile).

3.6.4 Wear Rate of Pin

Whilst for the pin, the wear scar diameter can be used to calculate the volume loss of the tip, established using an optical microscope, see Figure 3.10. This is due to the assumption that the pin tip will be worn out during sliding and produces a circular wear scar.

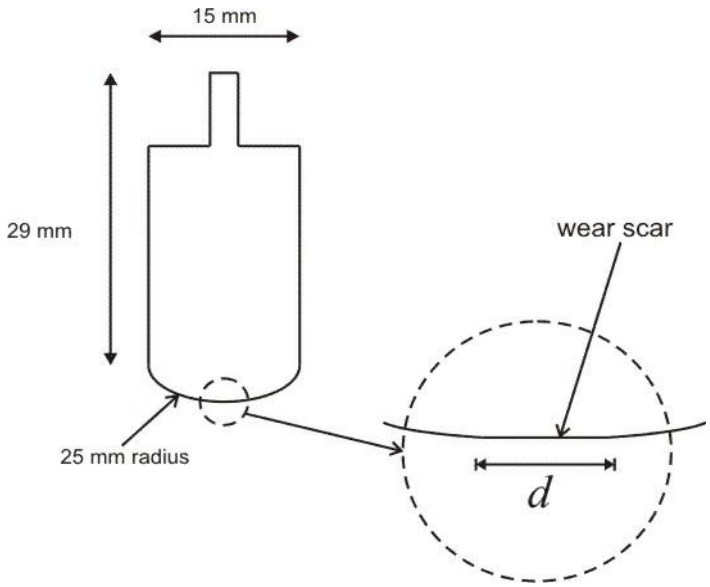

Figure 3.10. Schematic of a tested pin showing the volume lost (wear scar).

Therefore, the calculation of the volume loss was made by the following equation,

$$V = \frac{\pi d}{64R} \qquad \text{eqn. 3.7.}$$

where *d* is the diameter of the wear scar and *R* is the radius of the machined pin tip (0.025 m). Therefore, the value of volume loss obtained from this method can be used to calculate the specific wear rate of the pin using eqn. 3.6, as discussed previously.

3.6.5 Scanning Electron Microscope (SEM) for Wear Mechanism Determination

The Scanning Electron Microscope (SEM) was used to image the wear track of the discs and wear scar of the pins. This was conducted only on the steel samples and was useful over the optical microscope due to the absence of light interference and the ability to focus at high magnifications. The samples were imaged to investigate the type of wear mechanisms involved during the sliding process, at x100, x500, x1000 and with a few at x4000. The SEM model was Joel JSM 6500F thermal field emission.

3.6.6 X-ray Photoelectron Spectroscopy (XPS) for Chemical Analysis

XPS has been used to assess the composition of the tribofilm formed on the samples during sliding tests such as shown by [82, 108]. The presence of the adsorbed tribofilm such as the octanoate molecules used in this project can be particularly detected by observing the peak intensity of the C element in the XPS spectra. This is due to the high C content in the molecules' hydrocarbon chains, and at the functional group in which the C and O have both single and double bonds. Other elements such as O and Fe could also be assessed for secondary evidence. The XPS equipment used was at Cardiff University, model Kratos Axis Ultra-DLD.

3.6.6.1 XPS Sample Preparation

Due to the small test chamber of the XPS equipment, a few special arrangements were needed. This included the fabrication of a new steel disc in which smaller samples were attached to the surface, which were removed after the test for the XPS (see grey circles on the steel disc, in Figure 3.14). Only the octanoate test solution was chosen due to time limitation.

3.6.6.1.1 Fabrication of Special Steel Disc

A steel disc was fabricated so that six bores were available to accept six small inserts made from similar material as shown in Figure 3.14. Three inserts were installed in the wear track to investigate the adsorption of the additives and the relation with the sliding action, while three other inserts off the wear track so that a comparison can be made, *i.e.* between off and on wear tracks within the same disc surface. The inserts were seamless on the disc surface once installed and polished, therefore it was assumed that it will not affect the frictional response during pin-on-disc experiments.

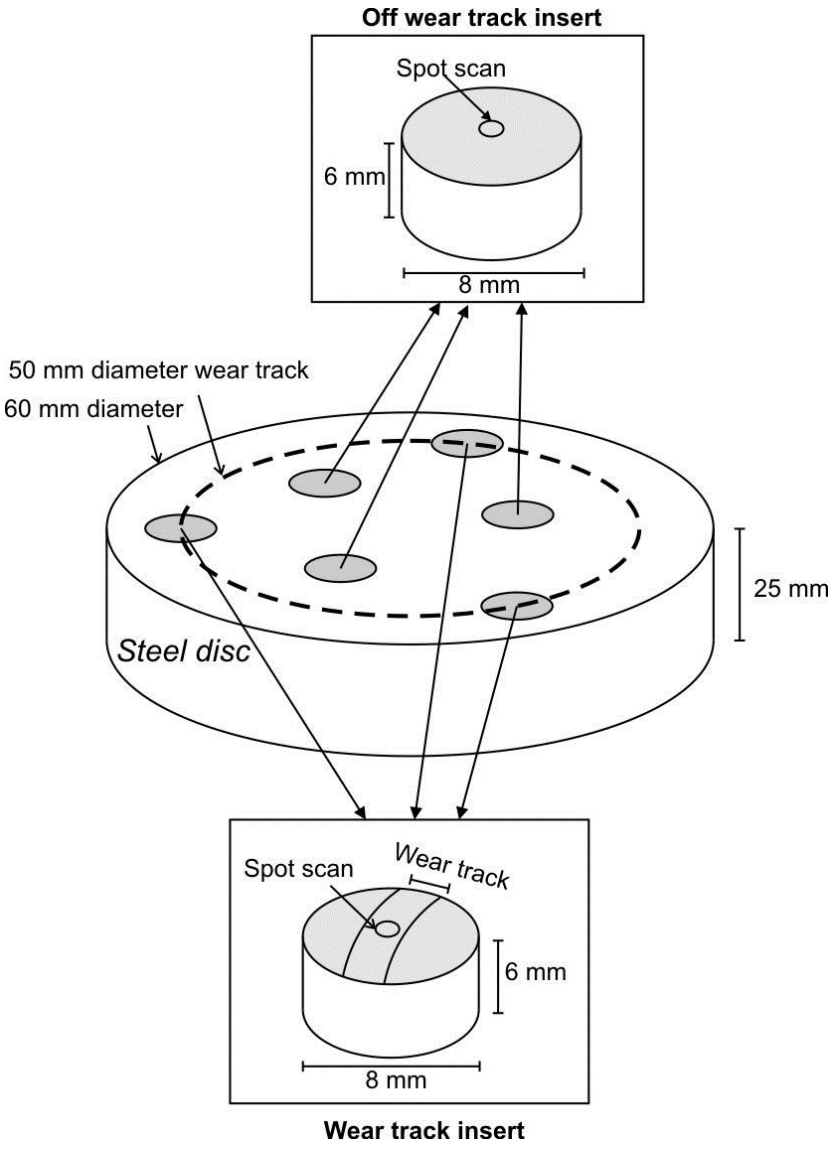

Figure 3.14. Schematic of the implementation of the small inserts on the steel disc for XPS scanning. Three on and off wear track sections/inserts were retrieved from each disc after experiments.

3.6.6.1.2 Sample Polishing and Testing

The discs were polished according to the normal procedures, *i.e.*, mounted on a holder and polished using diamond magnetic discs (Struers) at 80, 120, 600 and 1200 grades. Subsequently, the discs were tested in the PoD rig using the normal procedures. Only three tests were conducted, mainly at –1, 0 and +1 V overpotentials, due to time and technical constraints. However, these tests were considered sufficient to allow the observation of the formation of the octanoate adsorption film with respect to applied overpotential.

3.6.6.1.3 Removing the Inserts

After each experiment, the discs were rinsed with ethanol and stored in a desiccator overnight. Next, the discs were removed from the desiccator and clamped from the sides, up

side down. A flat ended punch was used to hammer out the inserts from the disc, and were stored in small glass tubes.

3.6.6.2 XPS Scanning Methodology

3.6.6.2.1 Angle Resolved Scan for Depth Analysis

It is possible for the XPS to provide compositional information as a function of depth. One of the ways is to tilt and scan the sample at an angle, which is used almost exclusively in photoelectron spectroscopy. Scans are made at different angles and the spectra will then be collected and processed [109]. The angles employed in this study are 90º and 45º as shown in Figure 3.11.

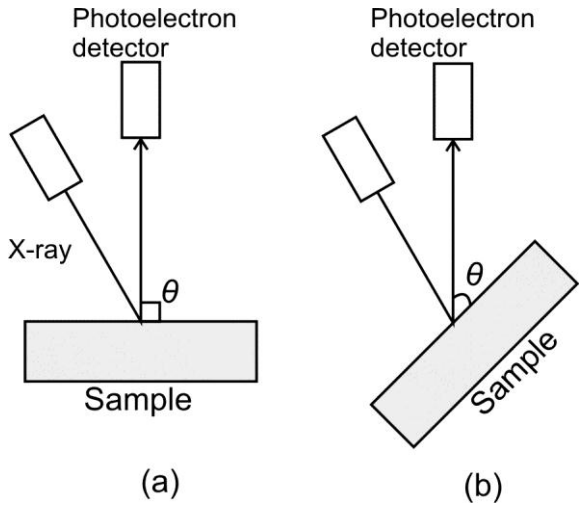

Figure 3.11. Method of conducting the angle resolved scan in XPS at (a) 90º, and (b) 45º. These data can be used to process the compositional analysis in relations to the depth.

3.6.6.2.2 High Resolution Scan

These elements were given special attention for the high resolution (high-res) scan mode: C, O, and Fe. The information in Table 3-7 was used for interpreting the high-res spectra data which was compiled from the literature. The binding energy shows the position of the peaks corresponding to the individual elements, and could provide valuable information about the evidence of adsorption.

Element	Binding Energy / eV	Description
Carbon (C)	283.9 [82]	Ascribed to impurities
	284.1 [82]	Methylene carbon peak indicating presence of organic material
	285.6 [82]	Methylene carbon attached to carboxylic group.
	284.7 [110], 287.1 [111], 287.9 [82]	Characteristic of carboxylic COO^- (indication of adsorption)
	288.0 [82]	Ascribed to symmetrical arrangement of COO^-
	290.0 [82]	Ascribed to asymmetrical arrangement of COO^-, and any unreacted (not chemisorbed) molecules
	288.7 [112], 289.1 [111], 290.2 [82], 293.5 [113]	Characteristic of carboxylic C=O (indication of adsorption)
Oxygen (O)	528.7 [82]	Ascribed to the lattice O^{2-} in the metal oxide substrate
	530.8 [82]	Ascribed to OH^- ions from the Fe-OH
	535.0 [82]	Ascribed to oxygen in the carboxylic molecules
$Fe2p_{3/2}$ (Fe^{2+})	709.6 [82]	Can be used to detect iron oxide, such as Fe_20_3 [114]
$Fe2p_{3/2}$ (Fe^{3+})	711.2 [114], 715.6 [82]	
$Fe2p_{1/2}$	720.4 [82]	

Table 3-7. Details of the important elements and the binding energies that can be used to determine the adsorption of the octanoate molecules which were collected from the literature.

3.6.6.2.3 List of the Insert Samples

The record of the inserts taken to Cardiff University for XPS scanning is shown in Table 3-8.

	Sample Identifier	Sample Description	Sample Measurement Method
1	OA -1 V **ON**	An insert from a rotating disc held at - 1 V overpotential, *on* the wear track.	Spot scans within the wear track at 90° and 45°. It was noted that the spot scan must not be bigger than the width of the wear track (around 1 mm) so that focus only on the wear track.
2	OA -1 V **OFF**	An insert from a rotating disc held at - 1 V overpotential, *off* the wear track.	Spot scans around the surface at 90° and 45°.
3	OA 0 V **ON**	An insert from a rotating disc held at OCP, *on* the wear track.	Spot scans within the wear track at 90° and 45°. It was noted that the spot scan must not be bigger than the width of the wear track (around 1 mm) so that focus only on the wear track.
4	OA 0 V **OFF**	An insert from a rotating disc held at OCP, *off* the wear track.	Spot scans around the surface at 90° and 45.
5	OA +1 V **ON**	An insert from a rotating disc held at + 1 V overpotential, *on* the wear track.	Spot scans within the wear track at 90° and 45°. It was noted that the spot scan must not be bigger than the width of the wear track (around 1 mm) so that focus only on the wear track.
6	OA +1 V **OFF**	An insert from a rotating disc held at + 1 V overpotential, *off* the wear track.	Spot scans around the surface at 90° and 45.

Table 3-8. A list of the samples taken for XPS analysis at Cardiff University with the description and method of scan. OA refers to the test conducted in the octanoate solution.

4 Steel / Steel Contacts in Baseline Solution

4.1 Introduction

This chapter presents the results and analysis of the contact between the steel pin and steel disc (steel/steel). The potential of the disc was controlled between ± 1 V overpotential while the other mechanical conditions such as the sliding distance, load and velocity were kept constant. The other variable of the experiment was the test solution, which included a baseline solution containing pH adjusters to simulate the drilling mud. The additives were included in these solutions to obtain low friction contacts, and most importantly, create the dependence of friction and wear on applied potential. The background understanding was established by mainly incorporating the sodium octanoate additive into the formulation.

This chapter focused on the development of the experiments conducted in the baseline solution (water based) of which the pH was adjusted to 9. Furthermore, the effect of additive was also tested by incorporating 60 mM sodium octanoate in the formulation, which was also used in previous work such as [78, 93-95]. This chapter was aimed at assessing the feasibility of employing potential application to influence the tribological performance, particularly in the modified pin-on-disc tribometer as discussed previously in Chapter 3 - Methodology. Furthermore, this chapter will provide a basis for the discussions of the later chapters, especially when important changes to the test setup were made such as by incorporating a viscosity modifying clay particles in the test solution (bentonite clay to simulate actual drilling mud), and changing the contact couple to steel / sandstone.

4.2 Primary Investigation in Baseline Solutions

4.2.1 Baseline Data Using NaOH Solution

4.2.1.1 The In-situ Coefficient of Friction (μ) *vs.* Time Result

The values of friction were recorded at 1 Hz acquisition rate during each sliding test. The data was then converted into coefficient of friction (dividing by 50 N normal load), and plotted against time / s (see Figure 4.1 which shows only the –1, 0 and +1 V overpotential tests). Generally, the disc rotations were started after 1000 s idle period, allowing the electrochemical reactions to stabilise.

The test at –1 V overpotential (see Figure 4.1 (a)) showed that at start of rotation (1000 s) the initial value of μ (static friction) is 0.11, then increased to 0.40 at 1500 s, and reached a relatively stable value of 0.46 at around 2500 s. The steady state mean μ (μ_{mean}) was also calculated as 0.46 with a standard deviation (s.d.) of 0.03. The start of friction at low values was probably due to the effect of hydrogen ions (H^+) produced on the steel surface giving a low friction contact, although more work is needed to fully understand the mechanism in the contact. However, this phenomenon is not unfamiliar as the hydrogen adsorption has been known to reduce friction in diamond like carbon (DLC) materials such as shown by Gao *et. al* [115].

At 0 V overpotential (see Figure 4.1 (b)), and at the start of rotation, static μ was 0.17 and rapidly increased to 0.50 at 1300 s. The value of μ attained a steady state of 0.46 at 1700 s, which was also the calculated value of μ_{mean} with a s.d. of 0.0142. The higher initial value of μ, and the faster time to reach steady state cf. –1 V overpotential test were probably due to the absence of the promotion of any electrochemical reactions such as the hydrogen ion production before sliding. This was because no potential was applied to enhance any cathodic or anodic reactions.

At +1 V overpotential, the value of static μ at the start of rotation was 0.11. Then, it decreased slightly to 0.09 in a short period of time (at 1100 s), and increased again but to a higher value of 0.50 at 1800 s. The initial low friction behaviour is believed to be due to the prevention of direct steel/steel contact, because of the oxide layer (corrosion) produced during the idle period. However, this layer has been stripped off after a few cycles, which caused a more significant direct steel/steel contact, thus the increase in μ. Finally, from 1800 s onwards, the μ kept on increasing gradually up to 0.55 at the end of the test (at 4600 s). The μ_{mean} was calculated as 0.53 with a s.d. of 0.01. The higher value of the μ_{mean} cf. the previous tests at –1 and 0 V overpotentials was probably due to the entrainment of the oxide

particles in the contact, combined with the constant production of oxide layer on the surface throughout the experiment [116].

The values of μ_{mean} and s.d. from each of the tests conducted in the NaOH test solution can be plotted against the applied overpotential to assess the trend, which will be presented in the next section (Section 4.2.1.2).

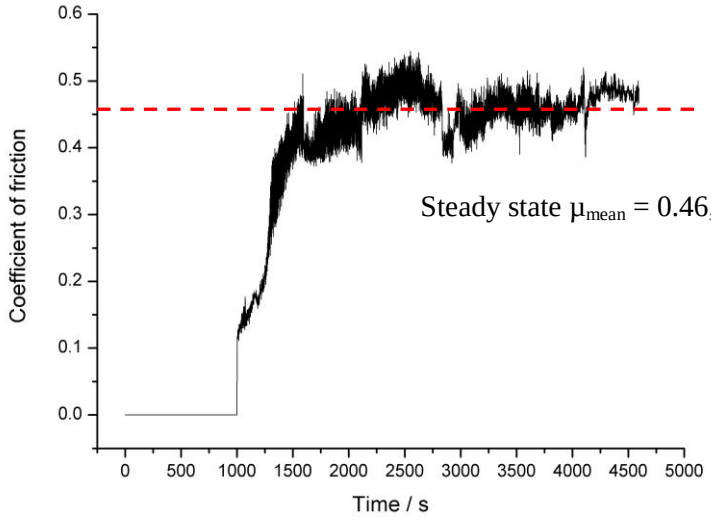

(a)

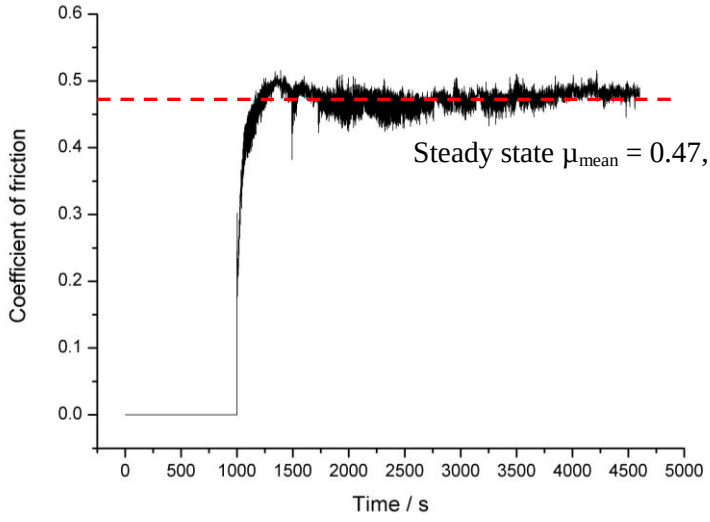

(b)

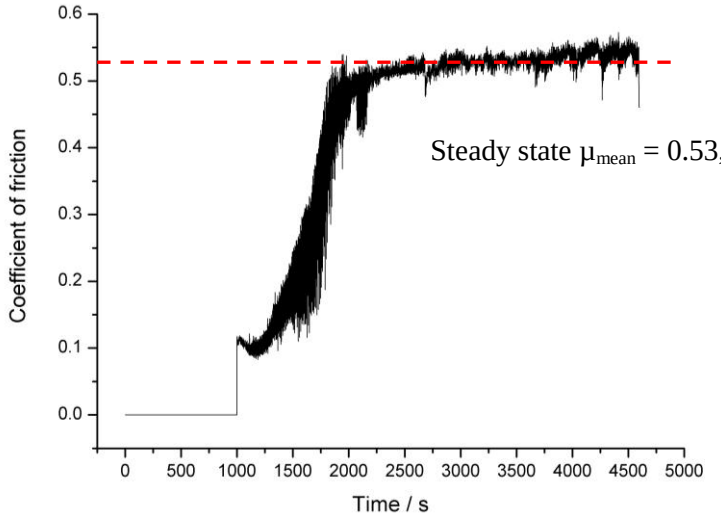

(c)

Figure 4.1. Coefficient of friction (μ) *vs.* time as recorded during the PoD tests in the NaOH test solution at (a) –1 V, (b) 0 V, and (c) +1 V overpotentials. The dashed lines show the mean μ.

4.2.1.2 Static Coefficient of Friction *vs.* the Applied Overpotential

The static coefficient of friction refers to the initial value of the μ when sliding was started, obtained from the μ *vs.* time plot as shown previously. As such, the values of the static μ were collected from each experiment and could be plotted against the applied overpotential / V, as shown in Figure 4.2. It is seen that the values were in the range of 0.1 and 0.2, and did not show any significant dependence on the applied overpotential. However, the lower values at the extreme overpotentials might have been due to the production of hydrogen adsorption or oxide film formation, at –1 and +1 V respectively, as discussed previously. The static μ data can be compared with the values from the other test solution, namely octanoate, which will be discussed later in this chapter.

The analysis of the dynamic friction is essential in examining the effect of overpotential on friction and wear, because it allows a more generic representation of the friction response during the sliding period. Therefore, the next section's discussion (Section 4.2.1.2) will focus on the response of the dynamic friction on the variation of the overpotential between +1 and –1 V.

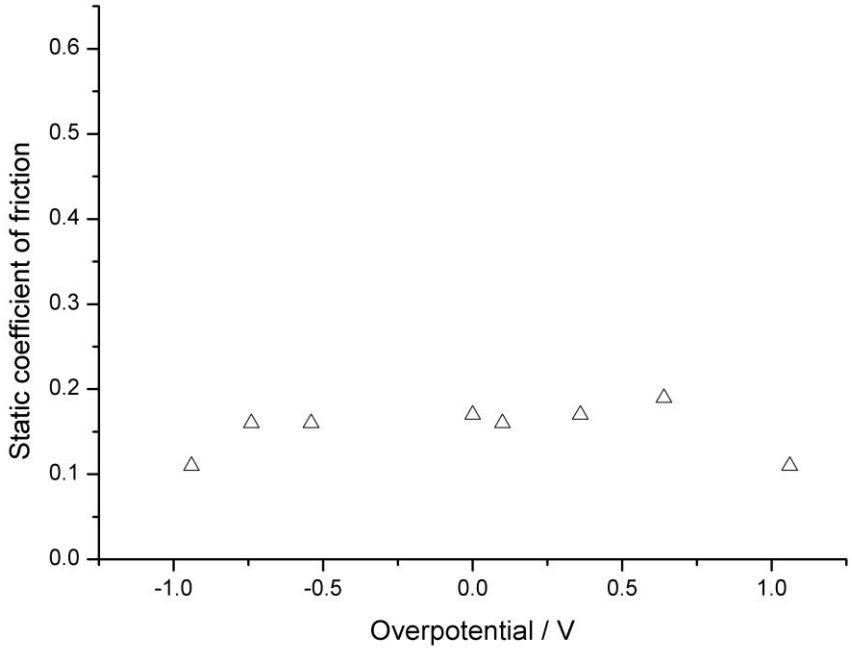

Figure 4.2. Static coefficient of friction *vs.* overpotential for experiments conducted in the NaOH solution.

4.2.1.3 Mean Coefficient of Friction (μ_{mean}) and Wear *vs.* the Applied Overpotential

The dynamic mean coefficient of friction (μ_{mean}) of the tests conducted in the NaOH test solution *vs.* overpotential is shown in Figure 4.3. The data is fitted with a linear function and produced a near horizontal line, with an average value of 0.49. This shows that the friction is independent of the applied potential. Furthermore, the average value is considered high and is expected when there is significant direct steel/steel contact between the pin and disc [74, 92]. This test solution contained no electroactive species and therefore, no effective tribofilm was developed on the contacting surfaces to provide any effective separation [31]. Nonetheless, the levels of μ_{mean} in this system are significantly lower than the value for the dry sliding conditions, which produced μ values around 1.05 within just a few minutes of sliding (result not shown).

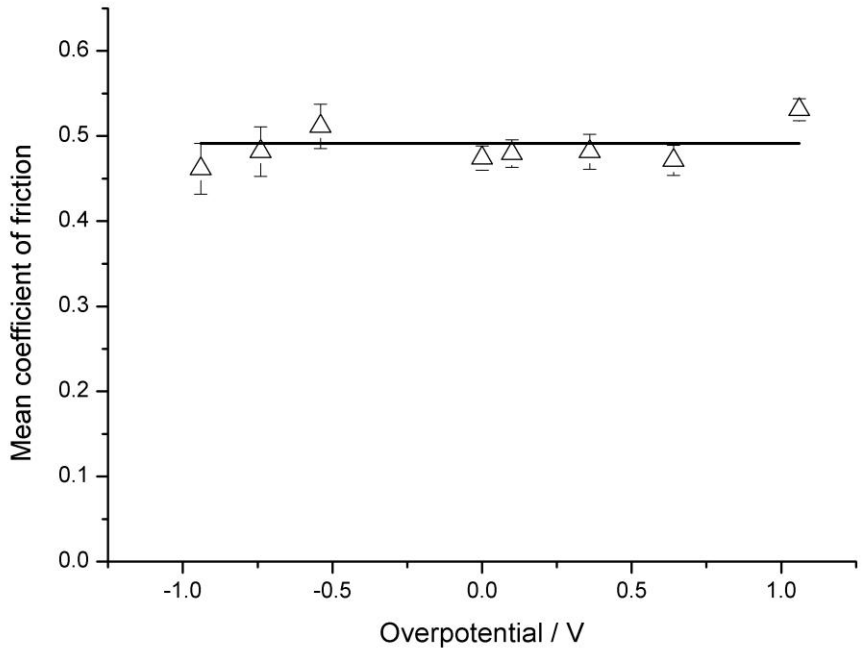

Figure 4.3. μ_{mean} (dynamic friction) *vs.* overpotential of experiments conducted in NaOH solution of steel/steel contact.

Visual observation of the pin and disc at –1 V overpotential showed no corrosion. However, at 0 V overpotential, slight corrosion was seen in the form of thin and patchy black deposits. At +1 V overpotential, corrosion was more severe and present in the form of thin yellow and light brown deposits. However, these corrosion features were only seen in the area where no contact was made during the tests, *i.e.*, off the wear scar (pin) and wear track (disc). The area where contact was made showed a relatively shiny surface with the presence of grooves. This was due to the constant removal of the oxide film in the contact during the mechanical

sliding. The oxide film and other corrosion products in the wear track were cleaned to reveal the underlying surface by using a cloth soaked in a solution of 10^{-3} M Mercaptobenzimidazole in 1 M H_2SO_4, from ref. [117].

A more in depth investigation of the wear mechanism was conducted by Scanning Electron Microscopy (SEM) analysis. The SEM micrographs of the pins showed that adhesion was found on all surfaces (within the wear scars) regardless of overpotential, which can be seen in Table 4-1 (only –1, 0 and +1 V overpotential ones are shown). The adhesion is indicated by the plucked appearance. This probably explains the mechanism of contact, which was the direct steel/steel, occurring between the asperities of the pin and disc. However, no significant evidence of adhesion was seen on the discs at the same magnification level, probably due to the incorporation of the wear debris onto the disc surface, or transfer of pin material onto disc. Furthermore, the pin surface was in continuous contact, therefore was at a higher temperature than the disc which only had intermittent contact.

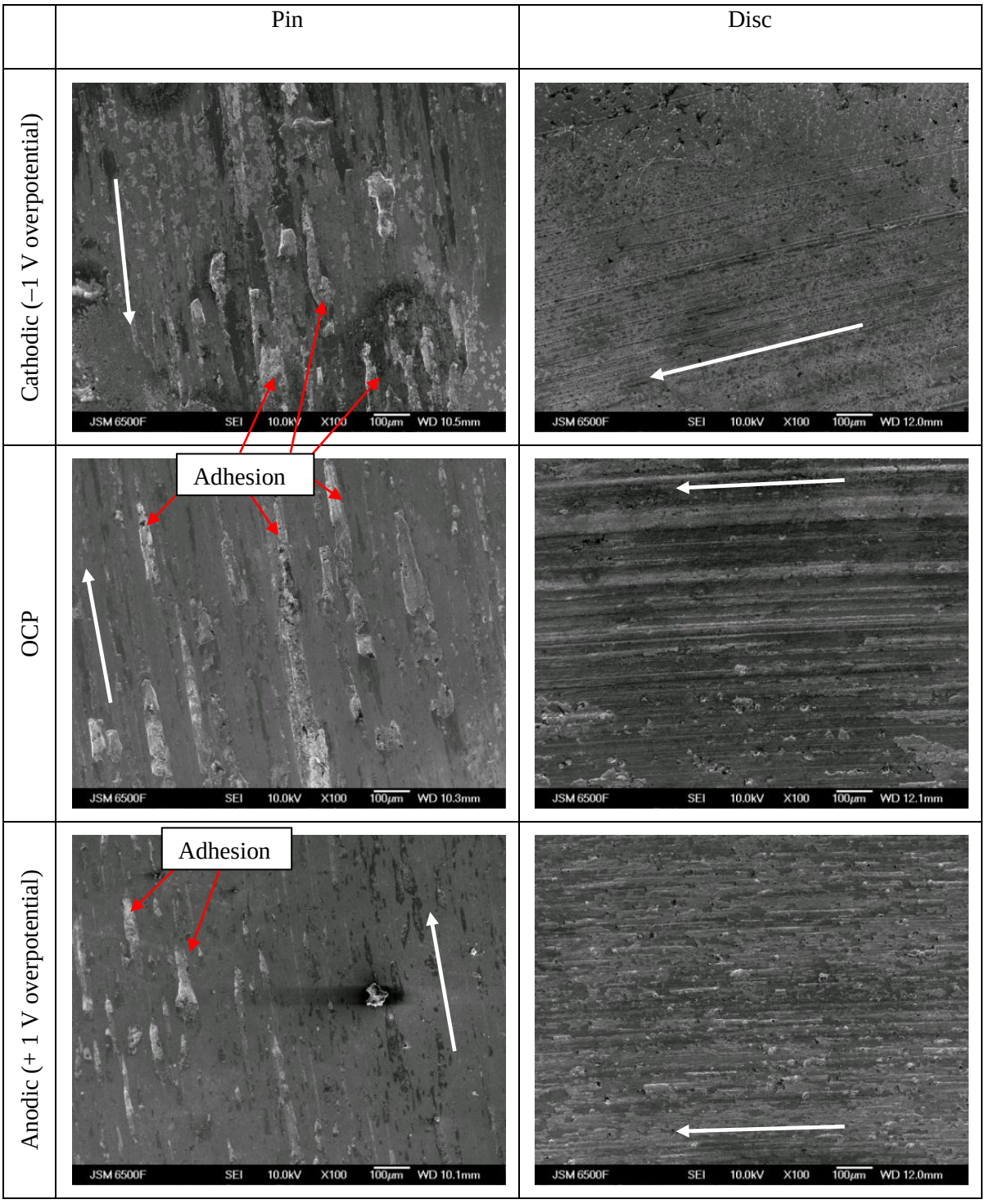

Table 4-1. SEM micrographs (x100 magnification) of the pins and discs of the NaOH test solution at cathodic and anodic overpotentials and OCP. White arrows indicate direction of motion.

Higher magnification images of the disc wear track (x1000) at –1, 0 and +1 V overpotentials are shown in Figure 4.4, which correspond to the contents of the third column in Table 4-1. At –1 V overpotential (see Figure 4.4 (a)), the surface is relatively smooth which was probably due to the inhibited corrosion reaction. Furthermore, this smooth texture might indicate that the wear mechanism was predominantly plastic deformation. These concur with the immunity zone in the Pourbaix diagram (see Figure 2.21 in Chapter 2), thus supporting that the wear mechanism was abrasion, with the absence of metal dissolution and oxide films (due to corrosion). In addition, there is evidence of small islands of slightly darker colour, found across the micrograph, which probably suggest material transfer from the pin onto the disc. The magnitude of current density recorded during sliding, was in the order of 10^{-3} A cm^{-2}, which could account for the cathodic reactions, such as the hydrogen evolution.

However, at 0 V overpotential (see Figure 4.4 (b)), the texture of the surface is less smooth, which suggested that corrosion reactions such as oxide film formation occurred during test. This was also supported by the Pourbaix diagram, which showed a possibility of oxide formation (corrosion zone). Furthermore, evidence of material transfer is not apparent from the micrograph cf. test at –1 V overpotential, probably due to the presence of the oxide film in between the contact.

Figure 4.4 (c) shows the disc micrograph at +1 V overpotential, in which pit formation and metal dissolution were observed probably due to the enhanced corrosion reaction during the test. The pits were probably showing evidence of corrosion reactions found preferentially around the carbide of the steel. This could also be supported by the magnitude of current density, which was in the order of 10^{-2} A cm^{-2}, *i.e.*, an order of magnitude higher cf. –1 V overpotential test. Although the direction of current was reversed (anodic as opposed to cathodic), the higher current value indicated higher electrochemical reactions, *i.e.*, possibly the mixture of oxide formation and oxygen evolution. Furthermore, the nature of the iron oxide film, which was less robust than, for example, chromium oxide in stainless steel, also contributed to the relatively high reaction rate. Therefore, these might suggest that the wear mechanism was a combination of complex interaction between mechanical sliding and corrosion, which will be discussed next.

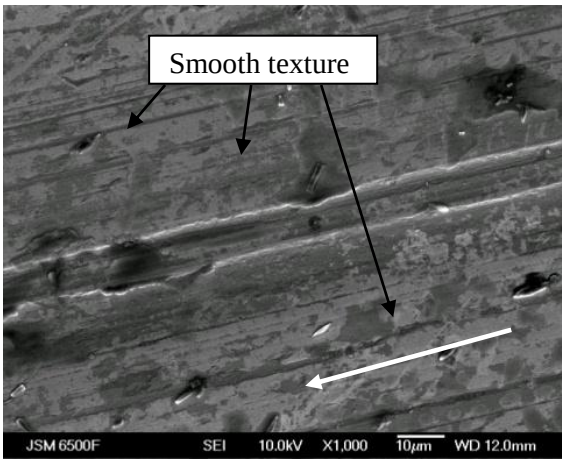

(a)

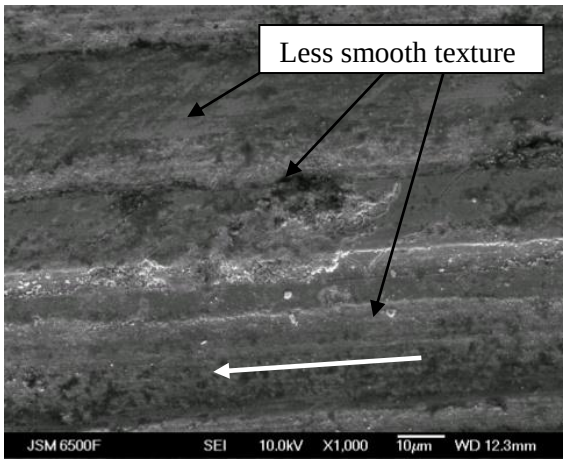

(b)

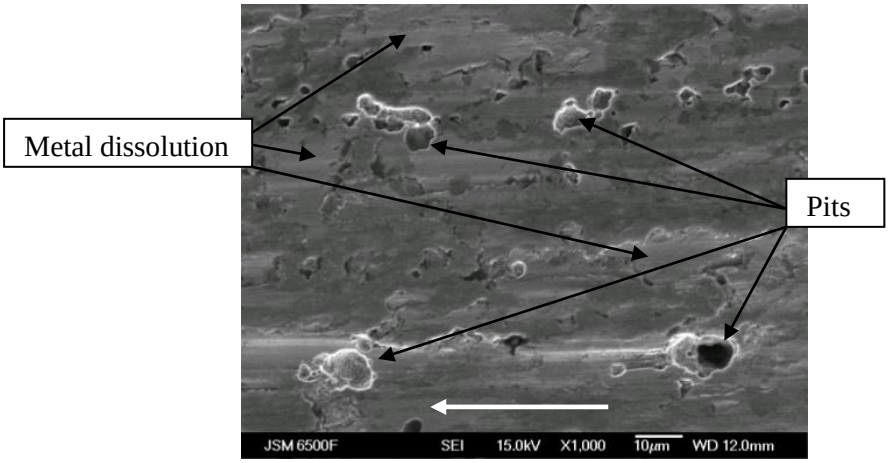

(c)

Figure 4.4. SEM micrographs (x1000 magnification) of the discs of the NaOH test solution at (a) cathodic of –1 V overpotential, (b) OCP of 0 V overpotential, and (c) anodic of +1 V overpotential. These disc micrographs correspond to the x100 magnification from Table 4-1. Arrows indicate direction of motion.

The quantification of the pin and disc specific wear rates with regards to the applied overpotential are shown in Figure 4.5. The pins show that the wear rates are all in the mild wear region, *i.e.*, within 10^{-15} $m^3 N^{-1} m^{-1}$ (see Figure 4.5 (a)).

However, the disc wear rates showed an increase from 10^{-15} $m^3 N^{-1} m^{-1}$ at cathodic (negative) overpotentials to up to two orders of magnitude higher values, at more anodic (positive) overpotentials (see Figure 4.5 (b)). This increase was probably due to the enhanced metal dissolution as the application of anodic potential (pure corrosion and/or wear due to corrosion). In addition to this, the s.d. showed an increasing trend from cathodic to anodic overpotentials. The reason was probably due to the higher general corrosion on the disc at more anodic overpotentials, therefore increasing the variation in the individual wear profile measurements along the wear track. Similar result was also seen by Mischler *et. al* [118] who used a reciprocating rig to assess the tribo-corrosion behaviour of alumina/carbon steel tribopair in NaOH pH 11. They reported that the wear was negligible when cathodic potential was applied, in contrast to a significant volume loss (wear) when anodic potential was applied. Furthermore, they concluded that only plastic deformation was found at cathodic potential which explained the negligible wear, whilst the production of oxide film at anodic reduced the ductility of the surface which caused the higher material removal. Thus, this could offer the explanation in the trend of mean and s.d. of the disc wear rates in Figure 4.5 (b). Further investigation into this behaviour was conducted by Favero *et. al* [119] who utilised an alumina/316L stainless steel tribopair in a reciprocating rig, lubricated by 0.5 M sulphuric acid. They reported that the wear rate of the anodic steel sample was an order of magnitude higher than cathodic. The phenomenon was explained due to the production of the passive film (at anodic), which introduced internal stress in the near surface substrate, whilst obstructing the movement of dislocations. Thus, they concluded that these mechanical degradation were also important underlying processes leading to total wear, *i.e.*, not just the corrosion.

There are two possible reasons for the discrepancy in the wear rate trends for the pin and disc. The first is due to the difference in wear rate calculation methods. The method of calculating the material loss from the disc wear track was by using a profilometer, which accounts for the off wear track as a baseline. This might cause some error at anodic overpotentials since the off wear tracks are also covered with oxide layers. Whereas, the pin wear rate was obtained by calculating the geometric volume loss from the radius of the wear scar. However, this method is not completely free from error since it assumes an ideal condition, such as a completely circular wear scar, and does not account for other changes such as plastic deformation.

The second reason for the discrepancy is probably due to the control of potential of the disc by connecting it constantly to the potentiostat. Thus, at more anodic overpotentials, the disc surface will be having constant oxidation reactions such as metal dissolution, while the pin might have had intermittent reactions due to the indirect connection. Therefore, the disc will result in more material loss compared with the pin.

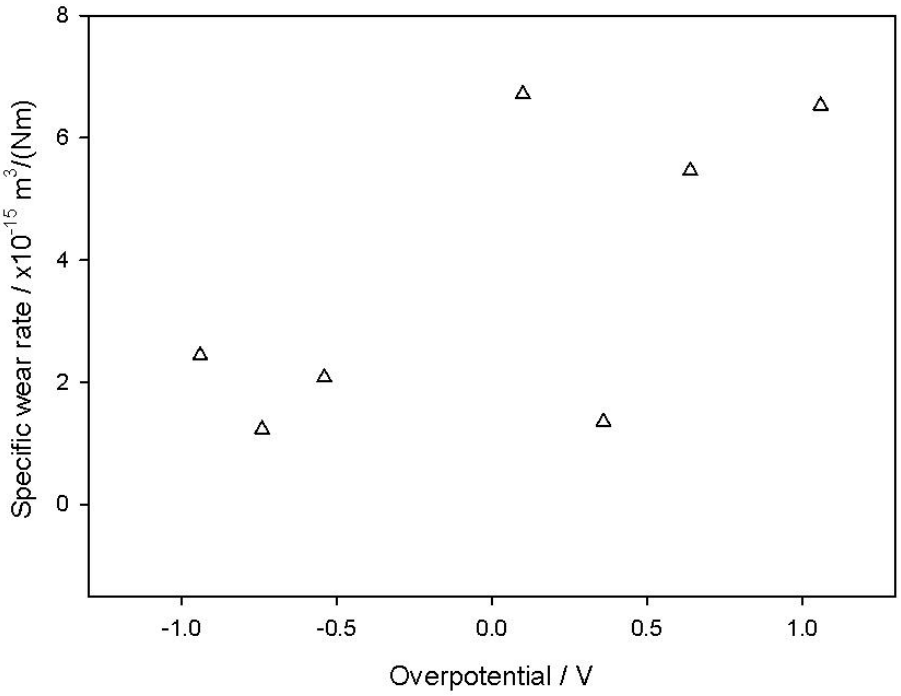

(a)

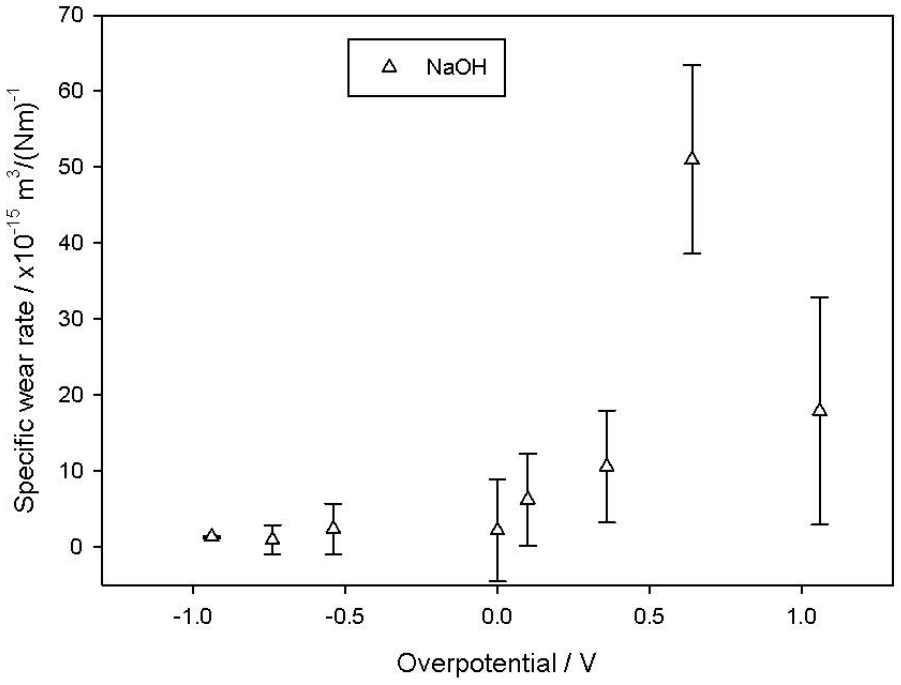

(b)

Figure 4.5. Specific wear rates *vs.* overpotential from the NaOH test solution of the (a) pins, and (b) discs.

4.2.2 Effect of the Octanoate Additive on Tribological Perfomance

Previous work [92-94] has proven that the octanoate additive can create a dependence of friction on applied potential. Therefore, this additive was chosen to be added to the baseline solution (NaOH) so that it can be compared and contrasted with the baseline without the incorporation of additive. Furthermore, similar experimental procedures were applied to the solution with the additive, namely the application of overpotential in the range of ± 1 V to the rotating disc. This was mainly to assess the sensitivity of the friction and wear response towards overpotential application.

4.2.2.1 The In-situ Coefficient of Friction (μ) *vs.* Time Result

The result of μ *vs.* time / s after incorporating the octanoate additive into the test solution is shown in Figure 4.6 (only the –1, 0 and +1 V overpotentials are presented). Generally, all the calculations of μ_{mean} in this test set were based upon the whole rotation period, due to the relatively stable friction responses produced. This was in contrast with the NaOH test, in which only the steady state values were used to calculate the μ_{mean} . As such, other calculations, presented later in this thesis, will be based upon the whole rotation period for simplicity and consistency.

At –1 V overpotential, and at the start of rotation, the value of μ was at 0.15 and gradually increased to around 0.40 at 1500 s, where it stabilised (see Figure 4.6). The μ_{mean} and s.d. values are 0.39 and 0.07 respectively which are listed in Table 4-2. These also correspond to the highest μ_{mean} and s.d. values in this test set, compared with the tests at 0 and +1 V overpotentials. This was because direct steel/steel contact occurred between the pin and disc, due to the repulsion of the octanoate additive away from the surface and preventing the formation of a tribofilm [93]. Although, this value of μ_{mean} was still lower than any of the NaOH tests as discussed previously, which suggested that there might be some small amount of adsorption on the steel surface.

At 0 V overpotential, μ at start of rotation was at 0.11 and gradually attained a relatively lower steady state (cf. the –1 V overpotential test) of 0.16 at 1700 s. Furthermore, the values of μ_{mean} and s.d. are significantly reduced by around 60% compared with the –1 V overpotential test, to 0.16 and 0.03 respectively. This was due to the significant reduction of the direct steel/steel contact by the presence of the octanoate additive adsorption film or tribofilm.

At +1 V overpotential, μ started at 0.12 and attained steady state by a relatively short time to 0.15 (at 1300 s). In addition, the μ_{mean} and s.d. were slightly lower than the 0 V overpotential test, at 0.15 and 0.0142 respectively. This shows that the application of anodic overpotential

could improve the frictional response, but only marginally. These results are consistent with Brandon *et al.* [93] who reported that the μ_{mean} to be around 0.16 and 0.14, at OCP (*i.e.*, 0 V overpotential) and +1.00 V *vs.* SHE respectively. This also agrees with Duffy *et. al* [74] who tested an iron/steel sliding contact in 60 mM sodium octanoate under applied anodic potential, and utilised a surface vibrational spectroscopy to study the adsorbed layer. It was reported that the octanoate molecules form islands of iron octanoate monolayers on the steel surface (tribofilm). Furthermore, the application of anodic overpotentials could increase the thickness of the iron octanoate with time [94, 95], which could result in a better separation of the direct steel/steel contact.

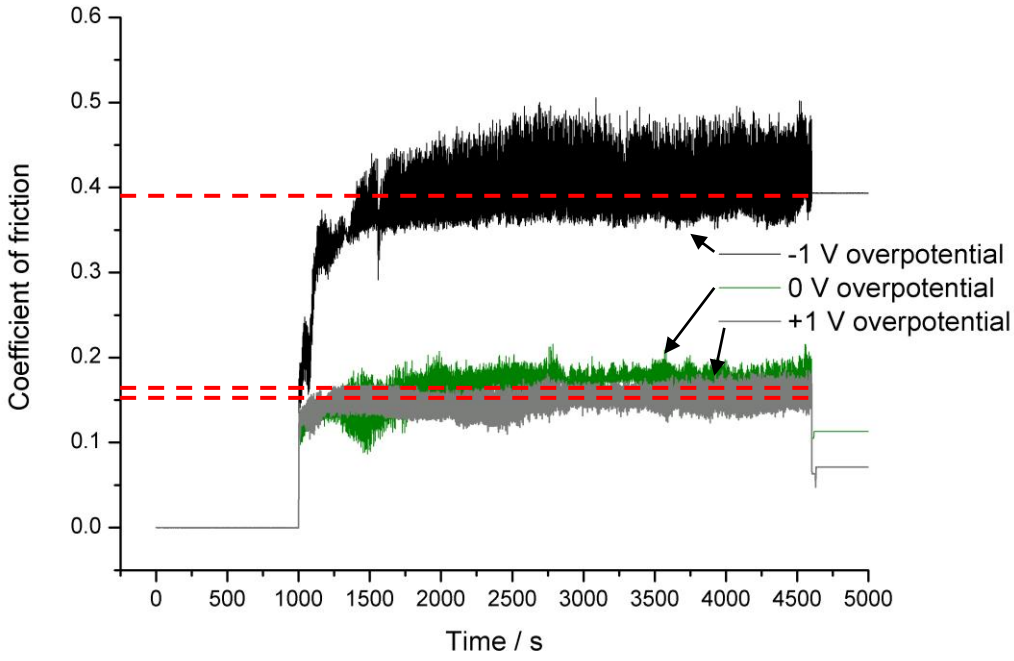

Figure 4.6. Coefficient of friction (μ) *vs.* time as recorded during the PoD tests in the octanoate test solution at (a) –1 V, (b) 0 V, and (c) +1 V overpotentials. The dashed lines show the calculated μ_{mean}.

Overpotential / V	μ_{mean}	s.d.
–1	0.39	0.07
0	0.16	0.03
+1	0.15	0.01

Table 4-2. The values of μ_{mean} and s.d. of the octanoate test solution at –1, 0 and +1 V overpotentials, corresponding to the dashed lines in Figure 4.6

4.2.2.2 Static Coefficient of Friction *vs.* the Applied Overpotential

The static coefficients of friction of both the NaOH and octanoate tests vs. overpotential are shown in Figure 4.7. Generally, it is shown that the static friction was reduced when the octanoate additive was present. This was probably due to the production of the tribofilm on the disc surface was developed before the contact with the pin was made, at the beginning of each test. Therefore, this might have caused a slight reduction in the levels of direct steel/steel contact initially. However, the next section (Section 4.2.2.3) will explore the response of the dynamic friction on overpotential which is more representative of the whole sliding processes, and will aid in a more accurate discussion of the effects of potential on tribological performance.

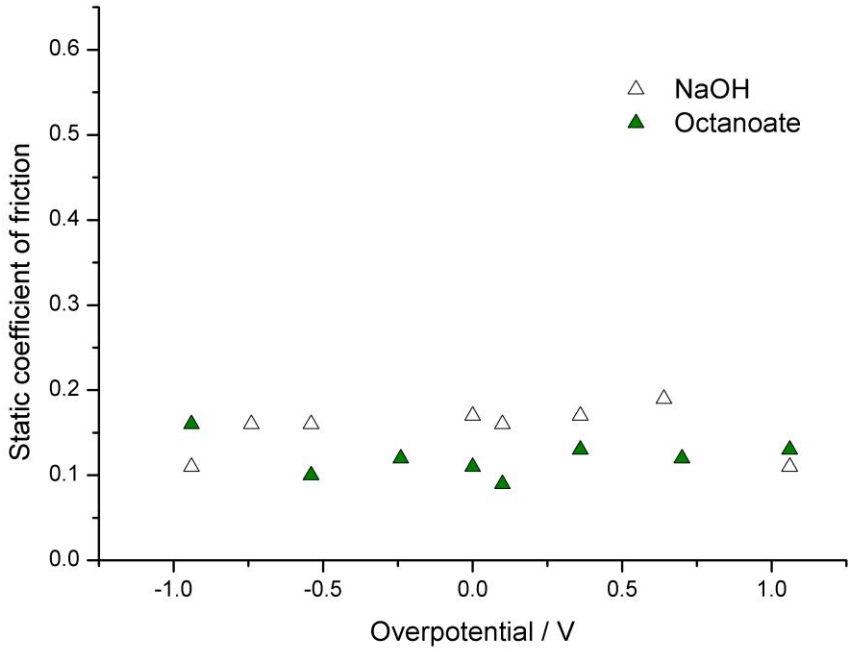

Figure 4.7. Static coefficient of friction *vs.* overpotential for experiments conducted in the NaOH and octanoate solutions. Generally, the octanoate test gave lower static friction compared with the NaOH.

4.2.2.3 Mean Coefficient of Friction (μ_{mean}) and Wear *vs.* the Applied Overpotential

The effect of adding the octanoate additive to the μ_{mean} (dynamic coefficient of friction) *vs.* overpotential trend can be seen in Figure 4.8, in which a clear dependence of friction on overpotential was observed, agreeing with previous findings [93, 94, 120]. Generally, the trend shows that the values of friction were high when cathodic overpotentials were applied. This was due to the octanoate additive being repelled from the surface, preventing the

formation of the tribofilm, thus resulting in significant amount of direct steel/steel contact. Conversely, low friction was obtained at more anodic overpotentials, due to the additives forming effective tribofilm to separate the contacts. This trend was not seen in the NaOH test set, because of the absence of the electroactive friction modifying additives such as this octanoate. In contrast, the variation of overpotential in the NaOH test solution only promoted the cathodic reactions (*i.e.*, hydrogen evolution or reduction of oxygen) or anodic reactions (metal dissolution or oxide formation), when cathodic or anodic overpotentials were applied respectively. The products of these reactions were probably not beneficial in reducing the friction and wear compared with the case when the octanoate additive was present.

It is noted that at 0 V overpotential, the μ_{mean} in the octanoate test solution was reduced by 66% compared with the NaOH test (*i*.e, from 0.47 to 0.16). This meant that even at no applied potential the friction could be reduced significantly, owing to the inherent nature of the octanoate molecules adsorbing at the steel/solution interface to influence the tribological behaviour, by forming a robust tribofilm.

It is interesting that the μ_{mean} at –1 V overpotential had a relatively large difference with the μ_{mean} at around –0.5 V overpotential, *i.e.*, having values of 0.39 and 0.20 respectively. This means that the transition point from high to low mainly occurred in between these two points. This steep transition behaviour was also seen by He *et. al* [98], who utilised a ball-on-plate tribometer lubricated by an aqueous solution containing 1 mM sodium dodecyl sulphate additive. They reported that the transition between high and low μ (0.45 and 0.10 respectively) occurred only within a small potential range, *i.e.*, between –0.4 and 0 V *vs.* Standard Calomel Electrode, while the values of μ outside this range did not show much change.

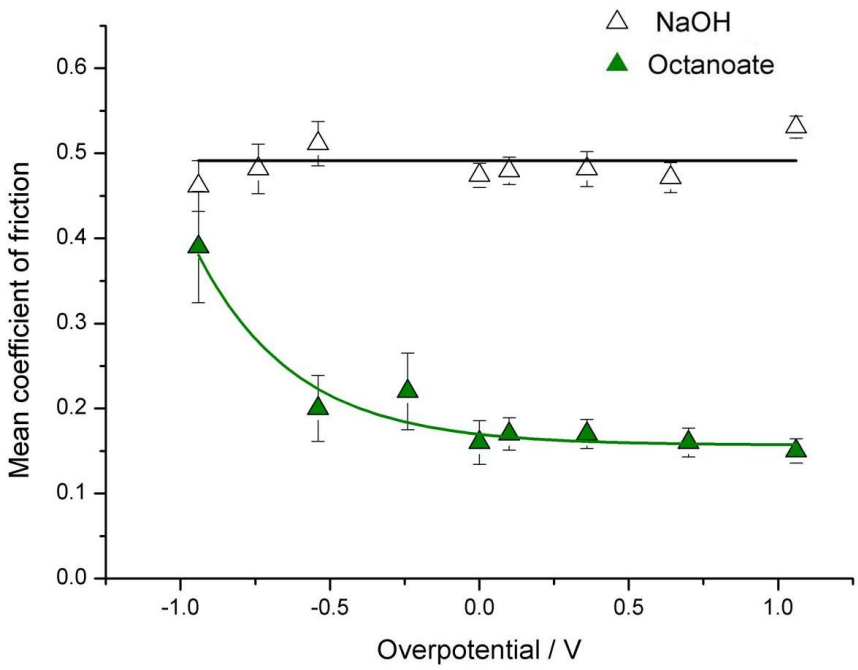

Figure 4.8. μ_{mean} (dynamic friction) *vs.* overpotential of experiments conducted in NaOH and octanoate test solutions of steel/steel contact.

The SEM micrograph of the pin at –1 V overpotential showed evidence of gross adhesion (see Table 4-3 which shows only the –1, 0 and +1 V overpotentials). The corresponding disc wear track also showed some evidence of adhesion. Therefore, these might suggest that direct steel/steel contact occurred, which also resulting in the highest friction in this test set.

The pins at 0 and +1 V overpotentials showed relatively smooth wear scars. Plus, the disc wear track features were not significantly changed compared with the off wear track, which suggested that there were less damage caused by the sliding action. In particular, the +1 V overpotential disc wear track shows that the grinding marks from the sample preparation process (polishing) are still present, with evidence of black deposits which might be the residual tribofilm or compacted debris.

By comparing the micrographs of the previous NaOH, and this octanoate (Table 4-1 and Table 4-3 respectively), it is apparent that the presence of the octanoate additive significantly reduced corrosion (metal dissolution and oxide formation) due to the formation of the octanoate adsorption film (tribofilm), which stifled further electrochemical reactions. Furthermore, this tribofilm was also effective in decreasing the direct steel/steel contact at the same time. The evidence of the tribofilm could also be given by the EDX scan which was performed on both the cathodic and anodic disc wear tracks (see Figure 4.9). It showed that the detection of carbon was only seen on the anodic disc wear track. Assuming that the detected carbon was from the octanoate molecules, this suggested the absence of the

tribofilm at cathodic, and presence at anodic. Although, the limitation of EDX is that it only detects the elements and its relative concentrations, but there was no specific indicator for the origin of the elements (*i.e.*, originated either from the tribofilm or not). Therefore, Chapter 6 will discuss on the use of X-ray Photoelectron Spectroscopy (XPS) to investigate the formation of the tribofilm more accurately, which will detail on the chemical state of the molecules.

	Pin	Disc
Cathodic	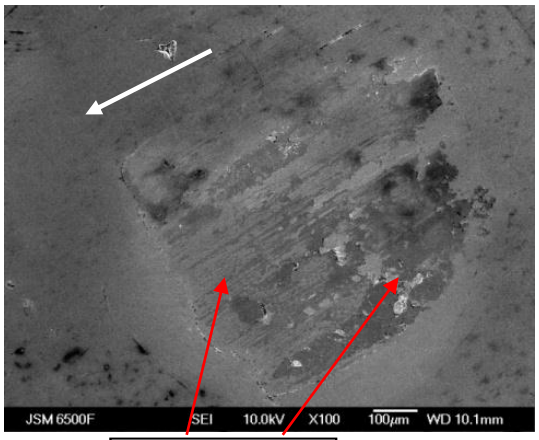	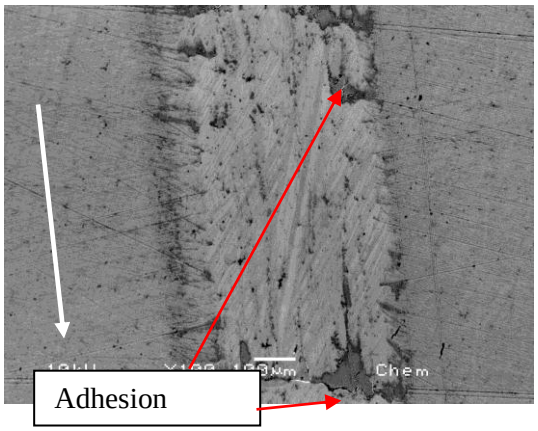 Adhesion
OCP	Adhesion 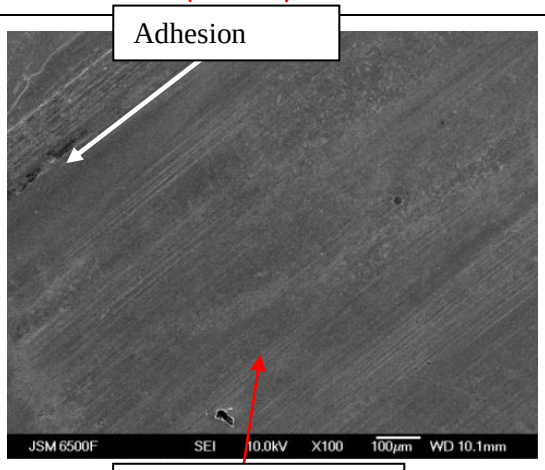	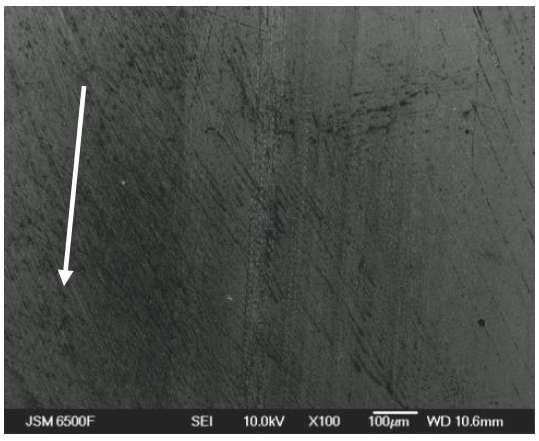
Anodic	Smooth wear scars 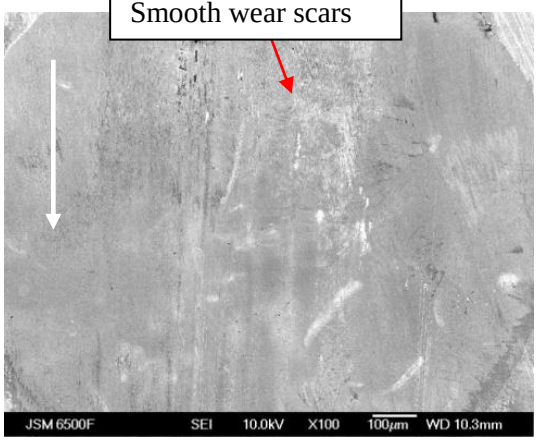	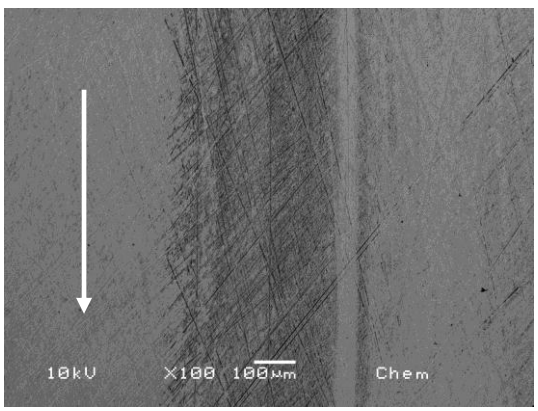

Table 4-3. SEM micrographs (x100) of the pins and discs of the octanoate test solution at –1, 0 and +1 V overpotentials.

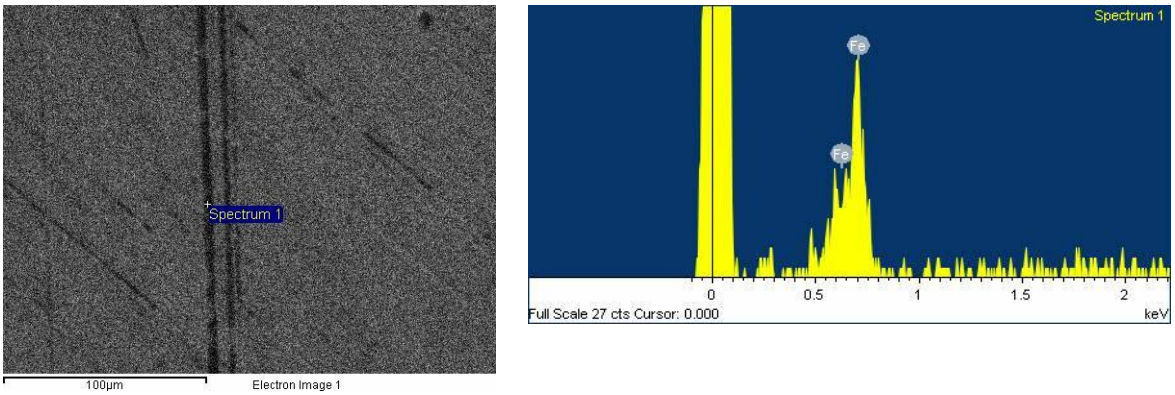

(a)

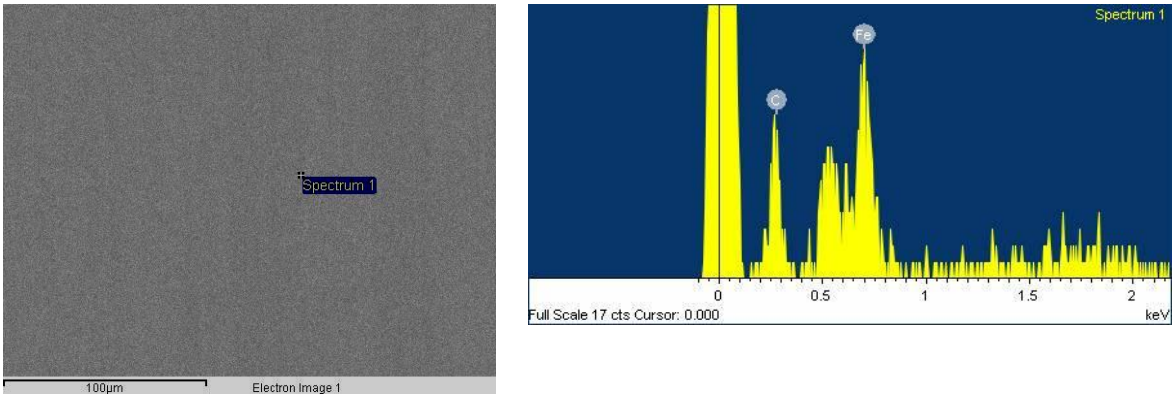

(b)

Figure 4.9. Results of EDX analysis performed within the wear track of a (a) cathodic disc, and (b) anodic disc in the octanoate test. Carbon peak was seen only in the anodic disc wear track and was not seen in cathodic, probably due to the detection of the octanoate molecules (tribofilm).

The specific wear rates of the pins in NaOH and octanoate test solutions are shown in Figure 4.10 (a). Generally, the wear rates of the pins in the octanoate test are lower than the NaOH. As mentioned earlier, this was probably due to the reduced direct steel/steel contact and lower corrosion rate. The reduction in both of these effects might have caused the lower material loss during the sliding action.

In contrast, the wear rates of the discs are similar between the NaOH and octanoate tests, but only at cathodic overpotentials (see Figure 4.10 (b)). At anodic overpotentials, the values of octanoate tests remained low while the NaOH increased considerably. The increase in the NaOH disc wear rates was probably due to the increased corrosion combined with significant removal of the steel surface by the sliding action. Similarly, the s.d. of the NaOH tests also increase significantly at more anodic overpotentials, which might indicate larger variations of the profile along the wear track, due to the severe general corrosion. Conversely, the low values of the octanoate disc wear rates were probably due to the reduction in both the corrosion and direct steel/steel contact, due to the formation of tribofilm. Moreover, it is seen that the s.d. of the octanoate tests were similar across the overpotential, which

suggested that the protection by the tribofilm also caused less variations in the wear track profile. Therefore, this might suggest that the tribofilm was robust, and forms a relatively homogenous layer on the steel surface. The discussion on the chemical state of the octanoate tribofilm will be detailed in Chapter 6.

The results of the pin and disc wear rates can also be explained in terms of the conventional tribo-corrosion term, *i.e.*, by using eqn. 2.13 (from Chapter 2),

$$T = Q_m + C + S + A$$

where T is the total wear rate which is the data presented in Figure 4.10, and C is the solids free flow corrosion rate which could be calculated from electrochemical tests. The terms S and A refer to 'synergy' (wear due to corrosion) and 'additive' (corrosion due to wear) [35]. Particularly, in the NaOH solution at anodic overpotential, the value of C was higher cf. the octanoate at anodic overpotential by two orders of magnitude, which was shown from the potentiodynamic polarisation plot (will be discussed later in this thesis). Furthermore, the absence of a corrosion inhibitor might have caused higher values of S and A as well, since the steel does not have the ability to form a protective passive layer. Therefore, in overall, the result was a higher wear rate than when octanoate additive was present.

It is interesting that, for the NaOH tests, the trend of the μ_{mean} (previously in Figure 4.8) showed a significant difference to the pin and disc wear rates (Figure 4.10 (a) and (b)), *i.e.*, the values of the μ_{mean} were unchanged across the overpotential, whilst the wear rates marked a significant increase at anodic overpotentials. The reason for the unaffected friction was probably that the overpotential either caused bare steel contacts at cathodic, or presence of oxide film at anodic, which were both ineffective in providing a good boundary lubricating condition. Conversely, the increase in the wear rates at anodic overpotentials was the result of the higher corrosion rate, and its complex combination with mechanical sliding, as discussed previously.

Similarly, for the octanoate tests, the trends of the μ_{mean} (see Figure 4.8) also showed disparities with the pin and disc wear rates (see Figure 4.10). Particularly, the friction trend showed a decrease at more anodic overpotentials, but generally, the wear rates were relatively low (both pin and disc) at all overpotentials. However, the reduction in the s.d. of the disc wear rates at more anodic overpotentials might be related to the lower friction (see Figure 4.10 (b)). The low s.d. indicated the smaller profile variations along the wear track, while the low friction indicated the low shear strength of the contact, in which both were probably due to the increased effectiveness of the tribofilm, in reducing the direct contact.

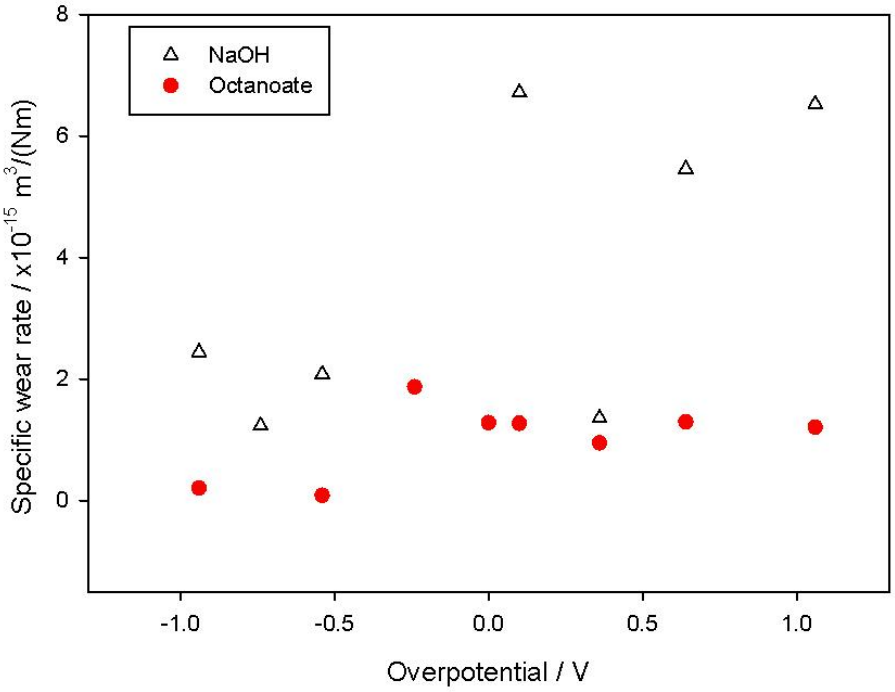

(a)

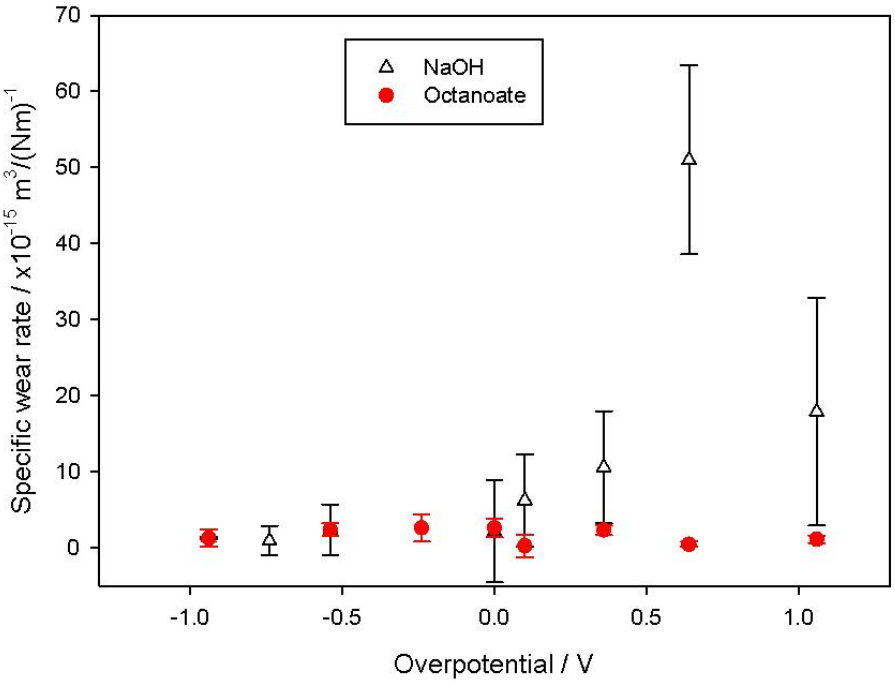

(b)

Figure 4.10. Specific wear rates from the NaOH and octanoate test solutions of the (a) pin, and (b) disc.

4.2.3 Profile of Disc Wear Tracks

The cross sectional profile of the disc wear tracks from the NaOH and octanoate tests are shown in Table 4-4 (at 0 V overpotential only). It can be seen that the width of the NaOH wear track is around 1.2 mm, and contains a lot of peaks and valleys. This was probably due to the direct steel/steel contact which caused high adhesion and resulted in plastic deformation, or the pin material being transferred onto the wear track. This agrees with the SEM micrographs as shown previously in Table 4-1, and Figure 4.4 (b), which showed features of grooves and less smooth texture probably owing to the severity of the sliding contact.

In contrast, the octanoate disc wear track showed fewer peaks and valleys. Furthermore, it also formed a relatively defined wear track with a maximum depth of 0.2 µm and about 1 mm wide. This might also indicate an absence of the pin material transfer onto the wear track, as was seen in the NaOH test. These suggested the work of the tribofilm protecting from direct steel/steel contact and adhesion.

NaOH	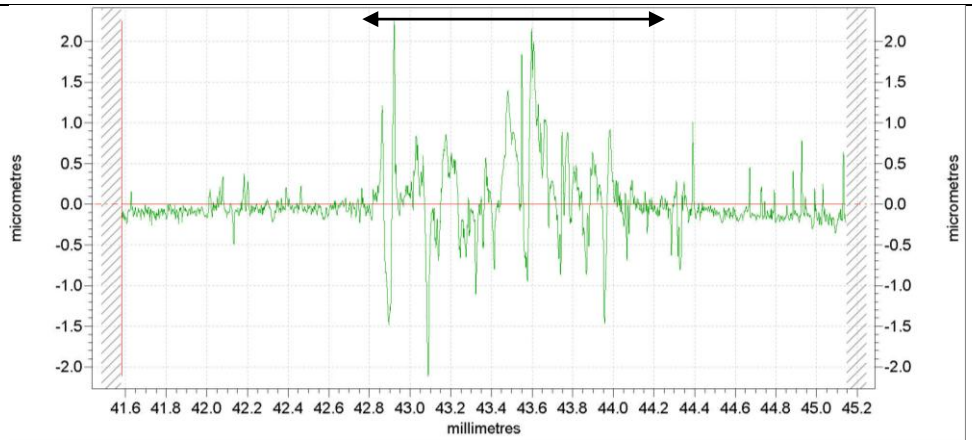
Octanoate	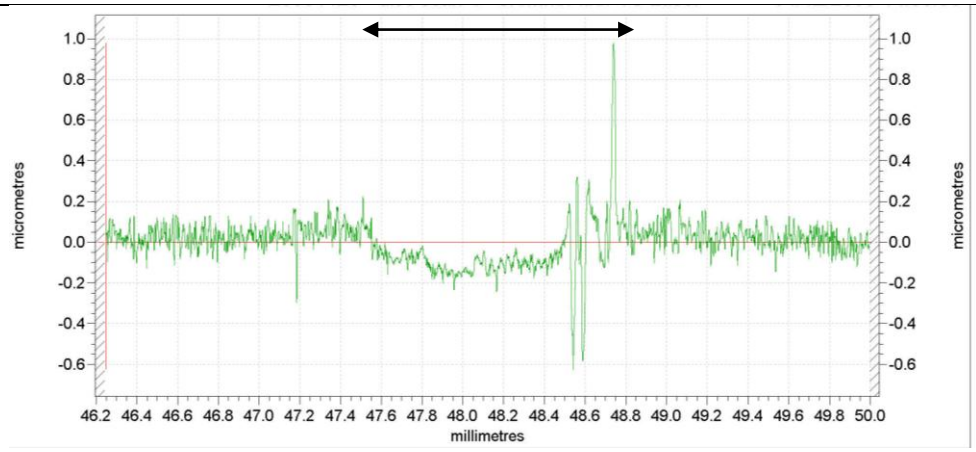

Table 4-4. Profile of the wear track of the discs at OCP (0 V overpotential) from the NaOH and Octanoate tests. Arrows show the wear track width.

4.2.4 Schematics of the Mechanism of Contacts in the NaOH and Octanoate Test Solutions

The schematic of the mechanisms of contact between the pin and disc in the NaOH and octanoate test solutions are shown in Table 4-5, which consist of both the cathodic and anodic contact overpotential conditions. At cathodic overpotentials, the NaOH test undergoes a direct steel/steel contact of the asperities. A similar situation is observed in the octanoate test due to the repulsion of the additive from the contact. This causes adhesion between the pin and disc and could potentially cause relatively severe abrasion of the contacting surfaces.

On the other hand, at anodic overpotentials (also including no potential application), the NaOH test will experience significant corrosion. This is due to the material being mild steel, which does not contain passivation behaviour to inhibit corrosion. Furthermore, the formation of metal oxide film (corrosion) is not suitable to provide an effective separation of contact, which explains the independence of friction on applied overpotential in this test set (which is in agreement with Mischler *et.al* [121]). To the contrary, the octanoate test will produce octanoate adsorption films (tribofilms) on the surface which will inhibit direct steel/steel contact of the asperities, resulting in low friction and wear. This is the key difference between these two test solutions, in which the presence of additive allows the friction to be affected by controlling the surface potential, owing to the octanoate being electroactive (anion or negative charged).

	Cathodic overpotentials	Anodic overpotentials
NaOH	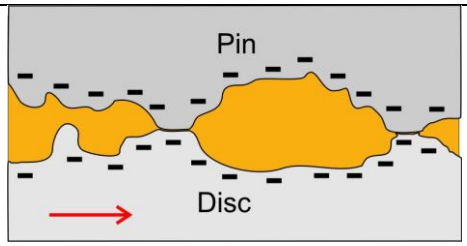	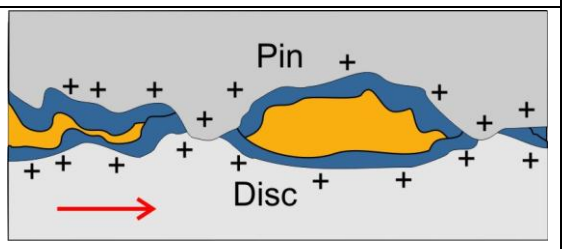
Octanoate	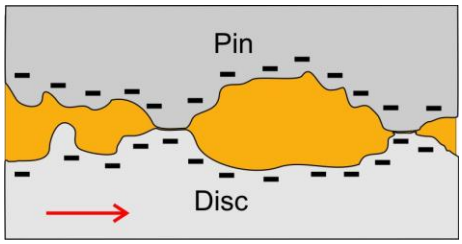	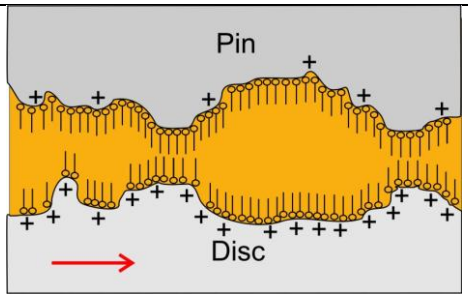

Table 4-5. Schematic of contacts in the NaOH and octanoate test solutions at cahodic and anodic conditions.

4.3 Investigating the Effect of Other Additives

Up to this point, only the octanoate additive has been employed to test the effect of applied overpotential on friction and wear. In principle, there are a few criteria of the additive molecules that are important for friction and wear reduction, therefore this section will aim to explore some of these. For example, the length of the carbon chains are important in providing lubrication by separating the direct contact, thus oleate and butyrate additives are used to test a longer (18 carbon atoms) and shorter (4 carbon atoms) chains respectively, cf. the octanoate (8 carbon atoms). Furthermore, all of these additives are negative charged, therefore a positive charged additive, cetyl trimethylammoniumbromide (CTAB), was tested to see if it is able to produce low friction when adsorbed onto the cathodic sites as opposed to anodic. Thorough investigation of the wear rate and wear mechanisms of the tests conducted using these additives will be incorporated in future work.

4.3.1 Oleate

The result of using the oleate additive showed that friction is independent of applied overpotential (see Figure 4.11). This is probably due to the adsorption of this additive which takes place on both cathodic and anodic sites, thus is readily adsorbed regardless of surface potential. This agrees with previous work [106, 122] that tested oleic acid derivatives and reported that the molecules behave as a mixed type corrosion inhibitor (adsorbing on anodic and cathodic sites).

However, the levels of friction were lower than any other additives that have been used, *i.e.*, the values of μ_{mean} were around 0.09. The lower friction was expected since the oleate molecules have longer carbon chain length than the octanoate, thus imparting a stronger tribofilm, and is more effective in separating the direct steel/steel contact. There are a few mechanisms of friction reduction suggested in the literature such as the ability of the oleate molecules to form a bi-layer arrangement, formation of a more oriented arrangement or the increased repulsion between the carbon chains which were adsorbed on both contacting surfaces [31, 74]. However, the results in Figure 4.11 probably suggest that using a molecular structure with a higher chain length will result in low friction contacts, but does not necessarily mean that the friction could be controlled by varying the surface potential.

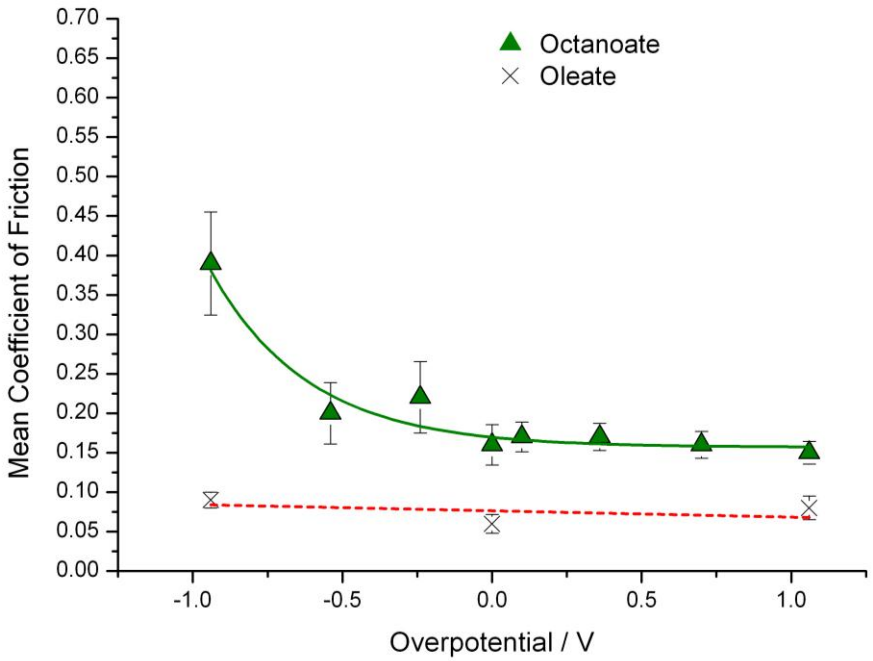

Figure 4.11. Mean μ *vs.* overpotential of experiments conducted in octanoate and oleate test solutions of steel/steel contact. The solution with the oleate additive generally has the lowest friction.

The micrographs of the disc wear tracks from the oleate tests are shown in Table 4-6. At –1 V overpotential, a first look at the wear track at x100 magnification shows that the surface was mildly abraded with only 100 μm width of grooves. The reason for only the middle part of the wear track being seen was probably due to the highest concentration of stress in the contact between the pin and disc. However, a closer look at the middle at x4000 magnification revealed a smooth texture with a few small grooves.

At 0 V overpotential, the surface of the wear track at x100 shows a smoother texture cf. the other tests in this set, *i.e.*, the –1 and +1 V overpotentials. It is interesting that this test also gave the lowest friction, as previously shown in Figure 4.11. The reason is not clear, but this might suggest that the oleate additive forms an effective tribofilm naturally and the application of any overpotential would cause a small disruption in the process. Similarly at the higher magnification, generally a smooth surface of the wear track is observed with the presence of some fine grooves. Furthermore a relatively deep groove is seen which is believed to be due to the normal variation within the wear track.

At +1 V overpotential, the x100 magnification micrograph shows that the general texture of the wear track is smooth, but with the presence of a few grooves in the middle of the wear track. A closer look in the middle at x4000 magnification revealed a surface which has a few deep grooves probably due to some direct steel/steel contact during sliding.

In summary, at x100 magnification, and across the overpotentials, all the wear tracks show no evidence of adhesion and are mildly abraded. At higher magnification of x4000, the micrographs revealed that the grooves in the wear track have similar width of around 1 μm, particularly for the 0 and +1 V overpotential tests. Furthermore, as discussed previously, there was little variation in the frictional response among these three overpotentials. Therefore, as mentioned earlier, these suggest that the oleate additive adsorb onto the contacting surfaces in all cases, thus, resulting in the similar wear mechanisms at all applied overpotential. However, the lowest friction was achieved at no potential application, suggesting a formation of a naturally robust tribofilm.

	X100	x4000
Cathodic (–1 V overpotential)	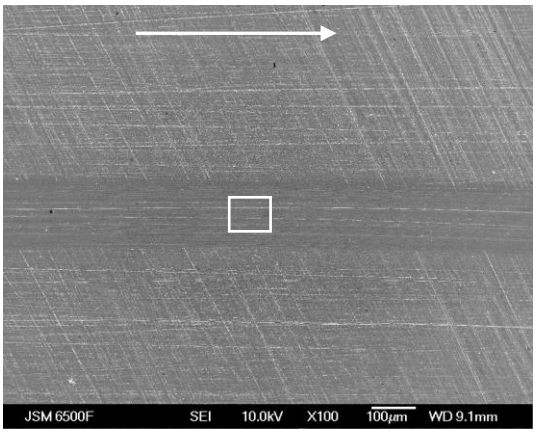	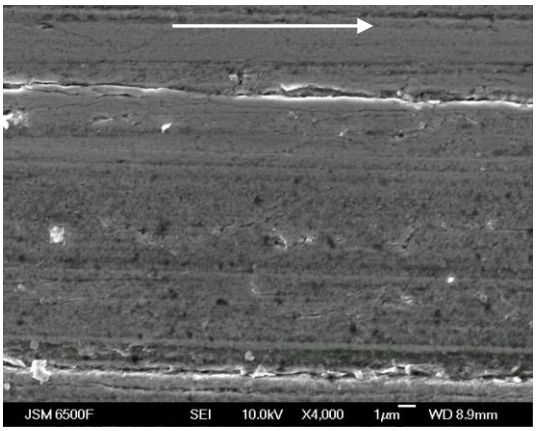
OCP (0 V overpotential)	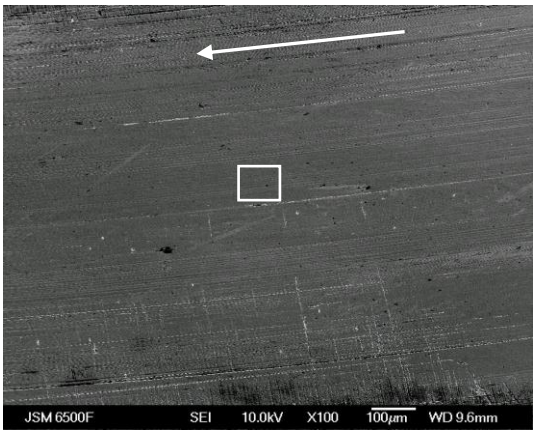	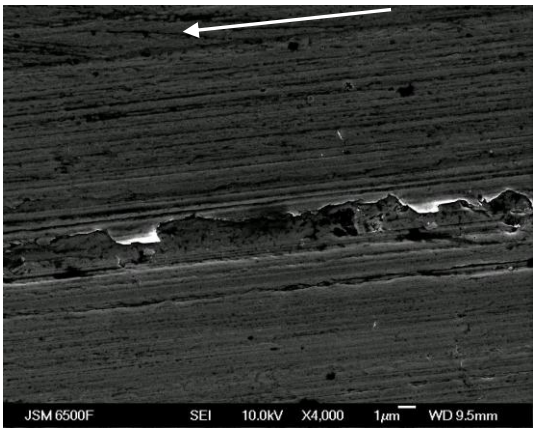
Anodic (+1 V overpotential)	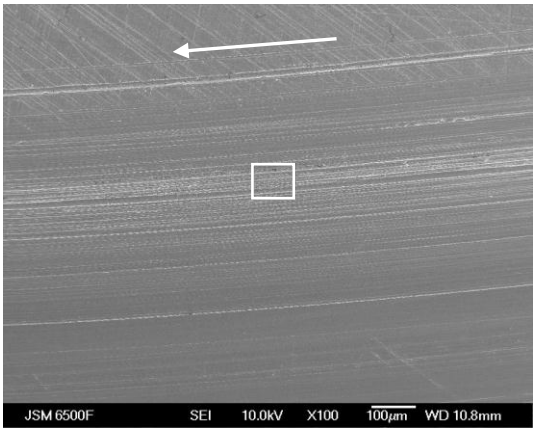	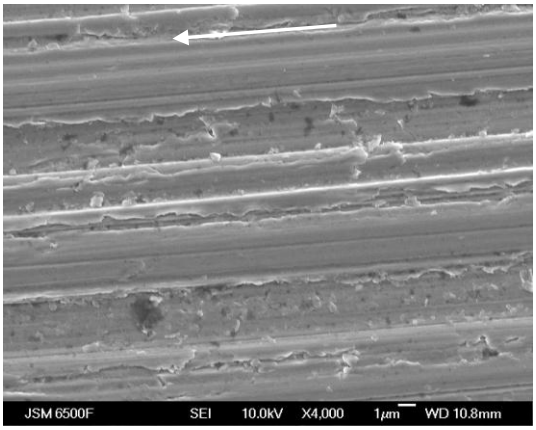

Table 4-6. SEM micrographs of the disc wear track from the oleate tests. Arrows show the direction of motion while the boxes show the approximate area that were zoomed in at x4000 magnification.

–1 V overpotential	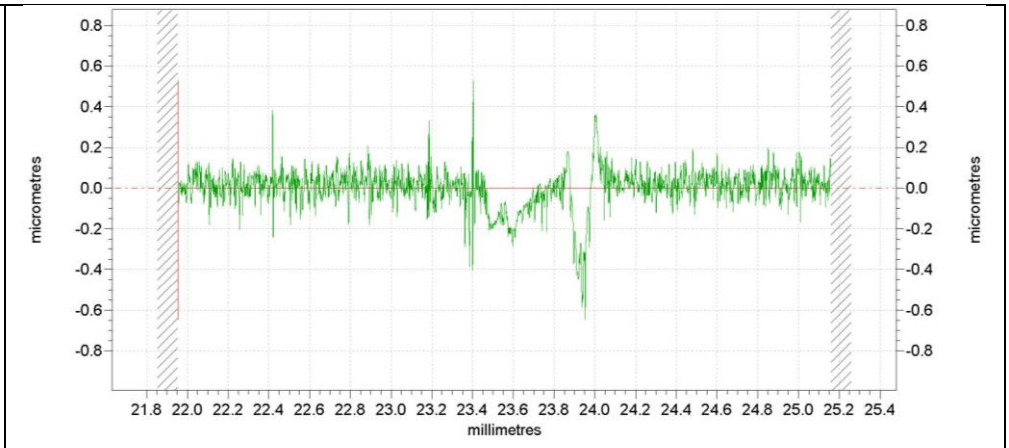
0 V overpotential	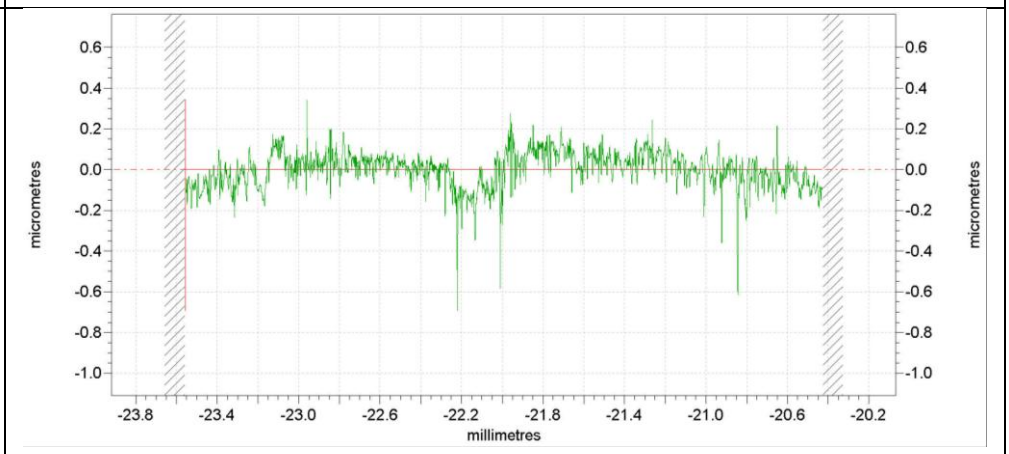
+1 V overpotential	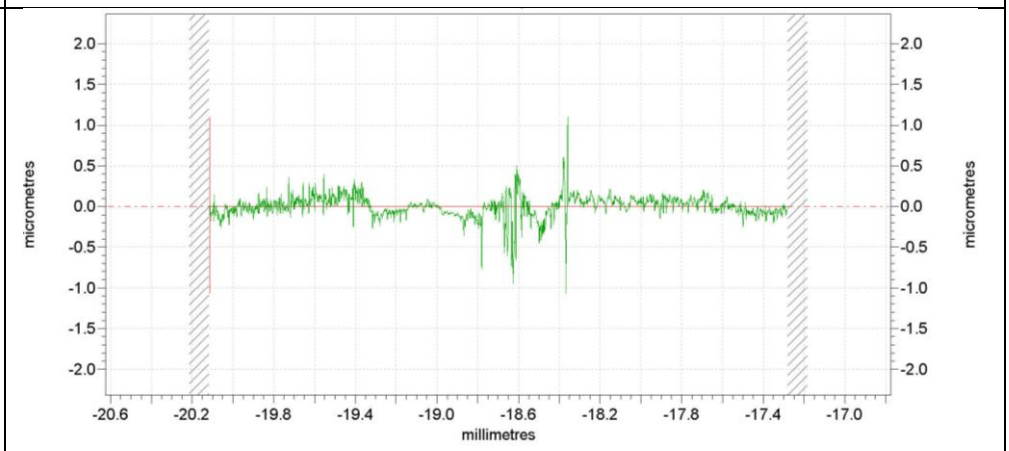

Table 4-7. Profiles of the wear track of the discs from the tests incorporating the oleate additive.

In addition, the micrographs of the pins are shown in Table 4-8. Generally at x100 magnification, and across the overpotentials, the pin wear scars show smooth feature in the middle, and some abrasion marks around the outside of the tailing edge. There was no evidence of adhesion in the middle of the wear scars which might suggest that there was no significant direct steel/steel contact. These micrographs also show that the abraded area around the outer of the wear scar becomes relatively larger at +1 V overpotential.

Furthermore, the x4000 micrographs of the abraded area show that the number of grooves increased especially at more anodic overpotentials, along with a noticeable increase in roughness. This might suggest that some direct steel/steel contact occurred. However, more work is needed to obtain a concrete conclusion of the phenomena found in this test set.

	x40	x4000
Cathodic (–1 V overpotential)		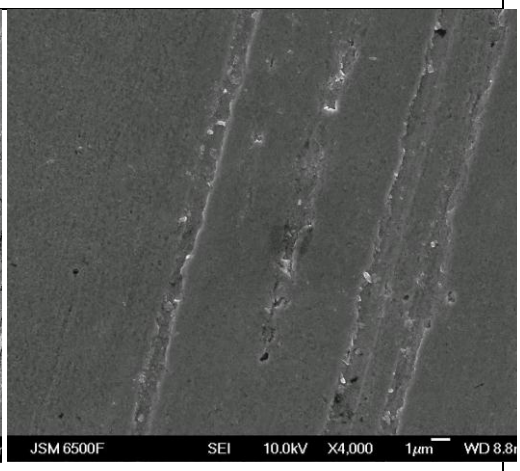
OCP (0 V overpotential)	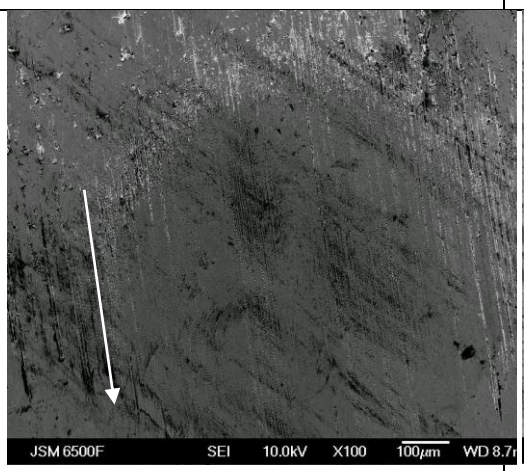	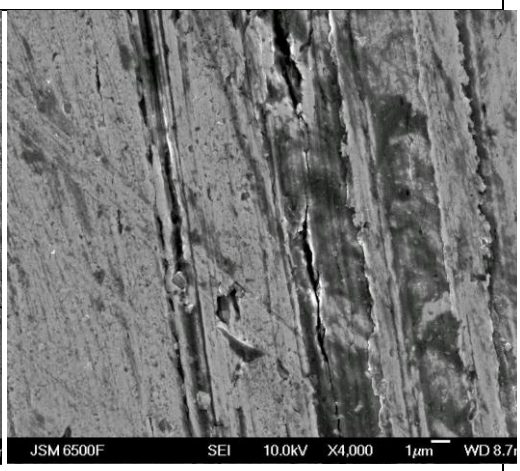
Anodic (+1 V overpotential)	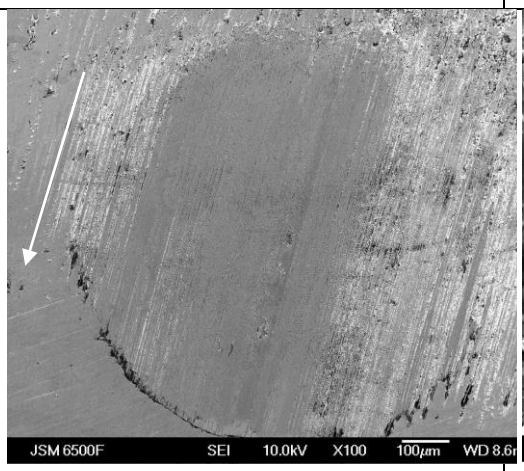	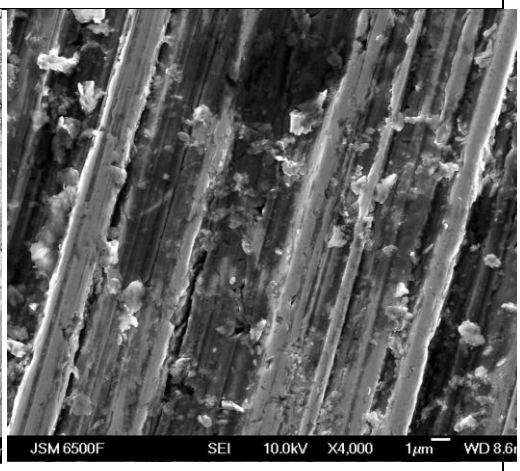

Table 4-8. SEM micrographs of pin samples from the oleate tests. The arrows show the direction of pin motion.

4.3.2 Butyrate

The result of employing the butyrate as an additive is shown in Figure 4.12, in which it is superimposed with the octanoate test results. Generally, it can be seen that the butyrate has similar trend to the octanoate, with regards to having the transition of high friction at cathodic overpotentials to low friction at more anodic overpotentials. However, in this solution, the transition point is seen at the 0 V overpotential, as opposed to the highest cathodic overpotential in the octanoate test. Furthermore, the reduction of μ_{mean} from 0.35 to 0.25, *i.e.*, by 28%, is less than for the octanoate test makes the butyrate a less favourable lubricant compared with octanoate with regards to reducing friction.

However, one advantage of the butyrate is that the transition of high to low friction can be achieved by applying a relatively small magnitude of anodic overpotential. This would be useful, and it is worth to be considered for further investigations.

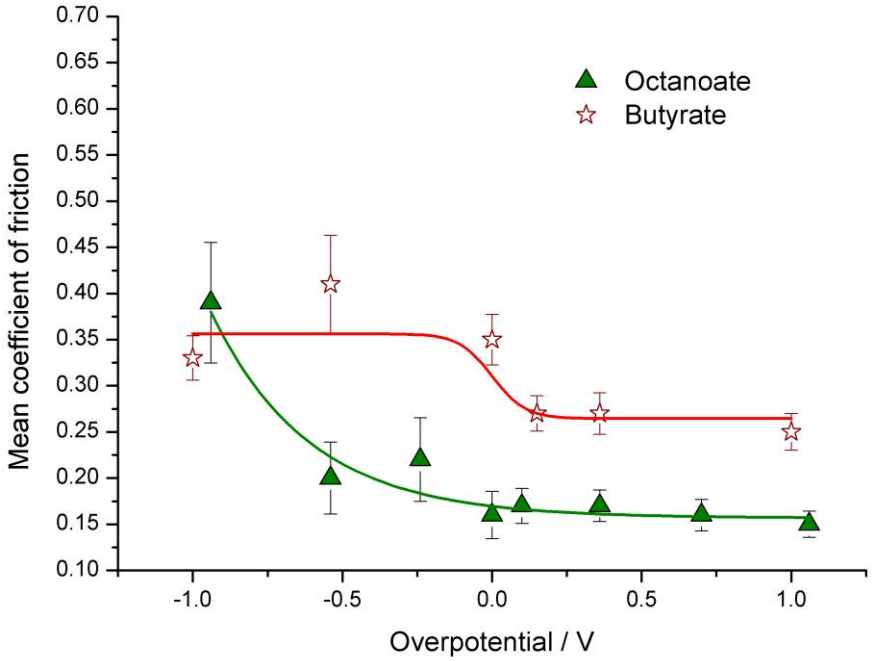

Figure 4.12. Mean μ *vs.* overpotential of experiments conducted in octanoate and butyrate of steel/steel contact

4.3.3 Cetyl Trimethylammoniumbromide (CTAB)

The effects incorporating the CTAB additive on the results of μ_{mean} *vs.* overpotential graph is shown in Figure 4.13, which is superimposed on the octanoate and butyrate test results. The trend of friction reduction is reversed in this case, with the transition from high friction to low obtained at cathodic applied overpotential. In particular, at –1 V overpotential, the value of μ_{mean} was 0.32, which was lower than at the 0 V overpotential (0.42). This reduction, which is by 25%, suggests that the additive adsorbs onto the cathodic sites, forming a tribofilm to reduce the direct steel/steel contact, thus producing the low friction. This agrees with the assumption that the positive charged additive could adsorb onto the surface when cathodic overpotentials are applied and affects the tribological performance. It is also notable that the CTAB is able to reduce the friction at just 1 mM concentration, cf. 60 mM in the octanoate and butyrate test. This is probably due to the small amount of additive molecules which are actually needed to form a complete monolayer on the surfaces in contact. Further investigation into the effects of concentrations are needed to support this finding.

At +1 V overpotential, the value of μ_{mean} increased slightly to 0.45 with respect to 0.42 at 0 V overpotential. This might suggest that some of the CTAB is readily adsorbed at 0 V and will be repelled when anodic overpotential is applied, resulting in the slight increase in friction. Visual observation of the test at +1 V overpotential showed that the solution colour changed to yellow. This might suggest that there was some iron dissolution from the steel surface (oxidation or corrosion process), thus changing the colour of the solution.

These results are interesting because as far as the author is concerned, there is no previous work relating to testing the CTAB as an additive, either in a normal tribometer or with potential control. However, these results also proved that it is possible to control friction by employing the CTAB additive, especially in obtaining friction reduction at cathodic overpotential, as opposed to anodic for the butyrate and octanoate tests. Therefore, this area can be explored to improve the current understanding of the phenomena.

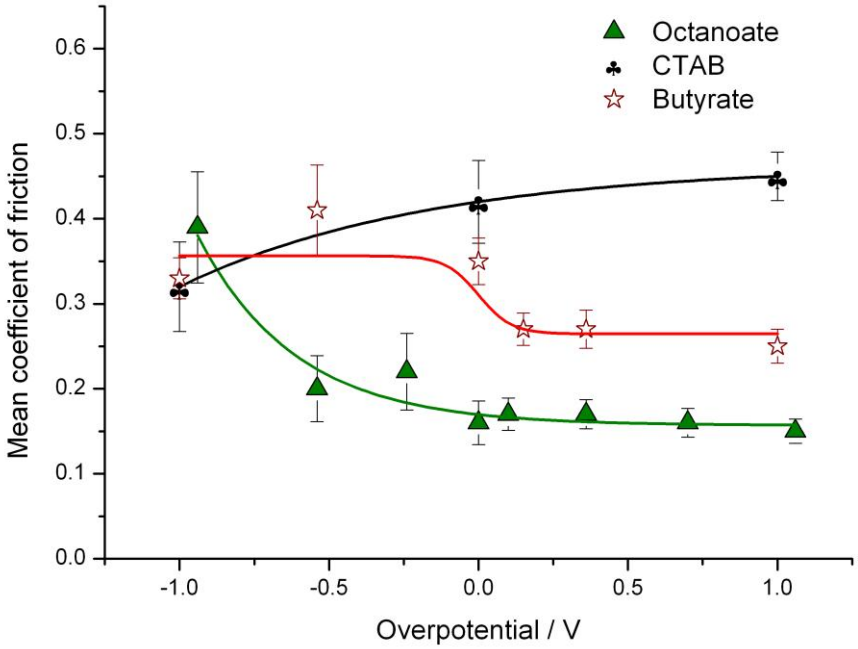

Figure 4.13. Mean μ *vs.* overpotential of experiments conducted in octanoate, CTAB and butyrate of steel/steel contact

4.4 Active Switching Experiment

The following part of this chapter will report on the experiments conducted with the active switching control of the overpotential without stopping the disc rotation. This is to test the mobility of the additive molecules and to study the feasibility of employing this technique to actively control friction and prevent stick-slip or vibration induced by sliding.

The octanoate additive was tested following the extensive investigation previously, which showed positive outcome in achieving a control over the friction response by varying the overpotential. However, the previous investigation employed the application of a constant overpotential value in each sliding test (lasted 1 hour). Therefore, this section explores the effects of actively switching the overpotential between –1 and +1 V within a test. The aim was to examine the reversibility of the adsorption film (tribofilm) and mobility of the molecules due to the change in overpotential. In short, high friction was expected when –1 V overpotential was applied, whereas low friction was expected at 0 and +1 V overpotentials.

Similarly, the butyrate additive was also chosen due to its ability to reduce friction in the previous experiment (see Section 4.3.2). Furthermore, the aim was also to assess the reversibility and mobility of the butyrate additive compared with the octanoate. The smaller size of these molecules compared with octanoate was assumed to allow for better mobility, but the reversibility depends on the chemical reactions on the steel surface which needs further investigation.

Mainly, the test procedure involved application of the overpotential at –1 V for 300 s (5 minutes), followed by a switch off. Then, after about 200 s, +1 V overpotential was applied for another 300 s which was also followed by a switch off. The disc rotation was not stopped during these steps. Finally, this cycle was repeated two times to assess the reproducibility of the friction response.

4.4.1 Octanoate Additive

The applied overpotential which was switched between ± 1 V in the octanoate test solution is shown on the top of Figure 4.14, whilst the friction response is on the bottom. It is seen that the response of friction is fairly close to the switching of overpotential, in which a low friction is achieved whenever +1 V overpotential is applied, and high friction when more cathodic is applied. The levels of friction are also in agreement with the previous tests conducted in the potentiostatic mode. That is, the low values of μ are expected to be around 0.16 whilst the high is around 0.39.

During the first switch, when the overpotential was turned on from 0 to –1 V, the μ showed a response of 100 s to achieve steady state at around 0.39. The relatively slow response was probably due to the slow action of removal of the octanoate tribofilm which was strongly adsorbed on the surface. The application of the cathodic overpotential might have aided the film removal process by hindering the replenishment of new octanoate molecules to adsorb and form a tribofilm. However, when the overpotential was turned off to 0 V, the μ showed an abrupt decrease to around 0.19 in 54 s. This probably suggests that on the elimination of the cathodic overpotential, the octanoate molecules are readily and quickly adsorbed onto the surfaces. Application of +1 V overpotential resulted in a small drop in μ to 0.13, but gradually increases to 0.17 despite the potential. The reason is not clear at the moment, but it is probably due to the temporary formation of a thicker or denser tribofilm which can be removed by the sliding action.

During the second switch, which started with the overpotential turned on from 0 to –1 V, the response of μ is significantly delayed cf. the first switch. The μ is shown to gradually increase and attain a steady state at 0.39 just before the overpotential was turned off back to 0 V. This probably suggests that the action of removal of the tribofilm becomes more difficult over time in which the reason is not clear. Subsequently, when the overpotential was turned on to +1 V, the levels of μ decreased from 0.20 to 0.15 but gradually increased, as seen in the first switch.

During the third switch, when –1 V overpotential was applied, the transition of μ from low to high was significantly delayed cf. the previous two switching cycles. Similarly, the reason is probably due to the increase in difficulty of removing the tribofilm formed during the previous cycle, as time increased. Furthermore, the steady state was reached at around 0.42 which was slightly higher than the previous cycles, probably suggesting that once the tribofilm was removed in this third cycle, revealed a relatively rougher substrate (probably due to corrosion or adhesion) which produced higher friction upon direct contact. At switch off, the μ decreased abruptly to 0.21 which was again probably due to the spontaneous adsorption of the octanoate additive forming a tribofilm. At application of +1 V overpotential, μ slightly decreased to 0.15.

Therefore, it can be postulated that the response of μ towards overpotential switching is time dependant, *i.e.*, the delay in the μ response becomes higher as time progresses. This is probably due to the adhesion of the tribofilm to the surface becoming stronger because of the increased chemisorption of the octanoate additive on the steel substrate, and the properties of the tribofilm could also be altered by the sliding contact. He *et. al* [98] employed a AISI 304 stainless steel/zirconia tribocouple, immersed in 1 mM aqueous sodium dodecyl sulphate

(SDS) utilising a rotating balls-on-disc contact mode. They reported that the friction response followed the sinusoidal wave form of the applied potential very closely, in which the delay was short, reaching a minimum of 0.2 s. Furthermore, the values of μ at high and low levels were 0.45 and 0.10 respectively, corresponding to the application of +1.6 V and +0.9 V (cell voltage). However, in another publication, He *et. al* [123] utilised a few techniques such as the quartz crystal microbalance, atomic force microscopy and lateral force microscopy to assess the adsorbed dodecyl sulphate additive. Thus, they concluded that the adsorption of the additive was completely reversible in their system. This is different from the octanoate in which it was reported to form an iron octanoate adsorption film, which is probably less reversible [74, 78]. Furthermore, they concluded that the additive adsorb in a stripe-shaped aggregates which is probably more effective in reducing friction, compared with a relatively less ordered octanoate adsorption film [74, 95]. However, the use of SDS is not feasible in light of applying into drilling operations due to the harsh downhole conditions [124].

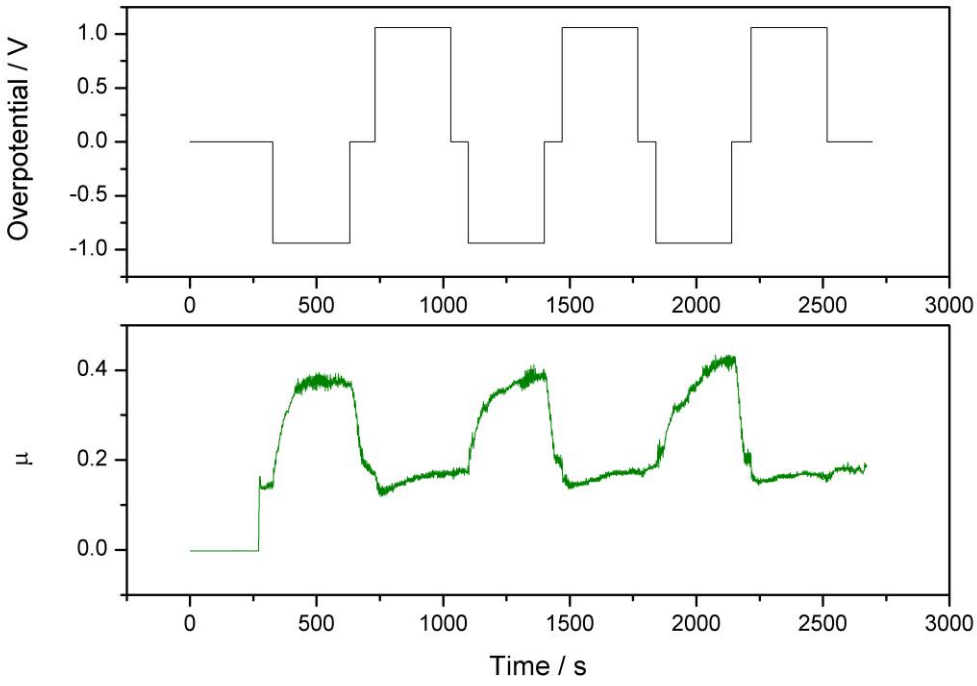

Figure 4.14. Active switching between ± 1 V overpotentials in the octanoate solution, showing (a) the applied overpotential on the top graph, and (b) the response of μ on the bottom graph.

4.4.2 Butyrate Additive

The result of the active switching procedure in the butyrate test solution is shown in Figure 4.15. The first switch starts with the application of –1 V overpotential at around 300 s. Consequently, there was a gradual increase in μ up to 0.40 at the end of the –1 V overpotential application. This might suggest a relatively slow desorption process of the previously adsorbed butyrate which occurred before the overpotential application. When the overpotential was turned off from –1 to 0 V, the μ was seen to drop gradually. The drop continued to a final value of 0.31, at the end of the subsequent +1 V overpotential application. This slow drop in friction might suggest that the butyrate additive reformed the tribofilm in a longer period of time cf. octanoate.

At the start of the second switch, *i.e.*, when –1 V overpotential was applied at 1100 s, μ was seen to increase rapidly from 0.31 to around 0.45. This is interesting since it might suggest that the adsorbed butyrate additive was spontaneously desorbed at the application of cathodic overpotential. Afterwards, the μ reduced slightly to 0.40 where it attained steady state. When the overpotential was switched off, the μ started to drop gradually. This drop continued after the start of +1 V overpotential, and reached 0.32 at the point where the overpotential was switched off. The general trend of friction during this second switch shows a more responsive result towards the overpotential control. This probably suggests that the butyrate additive has stabilised in the system.

The third switch shows that the friction response obtained in the second switch is reproduced. This probably suggests that the butyrate additive is relatively reversible cf. the octanoate. The reason that similar response was not seen during the first switch, is probably suggesting that the butyrate additive has not reached a stable condition during that time.

Generally, the levels of friction obtained from this active switching test are higher compared with the potentiostatic test results as discussed earlier in Section 4.3. In particular, this test shows that the values of μ at low and high are around 0.31 and 0.40 respectively, but the potentiostatic tests showed that the values were around 0.25 and 0.33 when –1 V and +1 V overpotentials were applied respectively. However, it can be seen that the friction response of the butyrate active switching test did not reach steady state at every overpotential change within the set timeframe. Therefore, this might account for the difference in the friction levels, compared with the potentiostatic tests which had more time to allow for stabilisation.

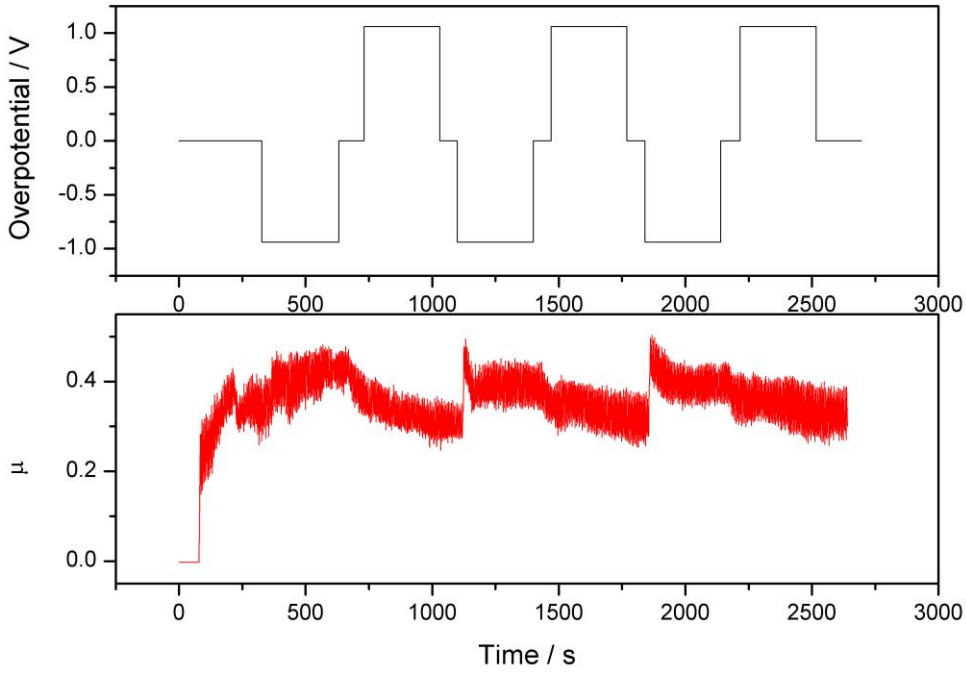

Figure 4.15. Active switching between ± 1 V overpotentials in the butyrate solution, showing (a) the applied overpotential on the top graph, and (b) the response of μ on the bottom graph.

4.4.3 Stability of the Friction Response during Active Switching

To investigate the stability of the friction response at each overpotential application, the standard deviation (s.d.) could be used as a good indicator of the levels of perturbation, *e.g*, a high s.d. would suggest a high friction perturbation probably due to excessive vibration or stick-slip. Therefore, Table 4-9 lists the s.d. calculated from the octanoate and butyrate friction responses, which correspond to each applied overpotential during the active switching cycles.

The values of s.d. of octanoate at –1 V overpotential were 0.06, 0.05 and 0.07 at the first, second and third cycles respectively (see column 3 in Table 4-9). These indicate that there was a fair amount of perturbations in the friction response, which was probably due to the vibration caused by some direct steel/steel contact. However, after switching off the –1 V overpotential (thus 0 V overpotential), the values of s.d. were 0.07, 0.08 and 0.09 at each cycle respectively, which were all higher than prior to the switch off. This was due to the large drop in friction from high (μ of 0.39) to low (μ of 0.16), which caused the increase in the s.d. calculation, *i.e.*, not due to vibrations or stick slip. However, application of +1 V overpotential at all cycles resulted in a reduction in the values of s.d. to 0.01. This suggests that the friction response was stabilised and the perturbation was reduced, probably due to

the thicker or denser tribofilm. Finally, the s.d. remained at 0.01 whenever the +1 V overpotential was switched off to 0 V at every cycle, suggesting that the tribofilm remained effective.

In contrast, the values of s.d. of butyrate showed little variation with applied overpotential across the three cycles, in overall. The highest s.d. was when –1 V overpotential was applied at the first cycle, which was due to the initially slower process of butyrate desorption, as discussed previously.

Therefore, these results show that the friction response in octanoate could be stabilised during the application of anodic overpotential, whereas no significant change was seen in the butyrate response. This was probably due to the octanoate being a good boundary lubrication additive owing to the longer carbon chain length.

Cycle no.	Overpotential / V	S.d. of octanoate	S.d. of butyrate
1	–1	0.06	0.05
	0	0.07	0.04
	+1	0.01	0.04
	0	0.01	0.03
2	–1	0.05	0.04
	0	0.08	0.04
	+1	0.01	0.04
	0	0.01	0.04
3	–1	0.07	0.04
	0	0.09	0.04
	+1	0.01	0.04
	0	0.01	0.04

Table 4-9. List of the standard deviations of the μ responses calculated at every applied overpotential during each cycle (showing both octanoate and butyrate tests).

4.5 Summary

The results from the pin-on-disc setup, incorporating the three electrode electrochemical cell confirms that friction control by electrical potential is achievable. The rig allowed friction coefficient measurements at a fixed load while controlling the interfacial potential of the disc, and the tribometer permitted assessment of friction–time relations and the tenacity of the iron octanoate film.

To summarise the findings that have been presented in this chapter, the analyses can be separated according to the solution constituents.

i. NaOH (additive absent), and octanoate (additive present) solutions

Generally, all NaOH tests yielded much higher coefficient of friction compared with octanoate tests for the same applied overpotentials. Friction was reduced in the octanoate solution when anodic overpotentials were applied due to a production of a low friction tribofilm of iron octanoate. Furthermore, the tribofilm has the ability to reduce wear of both pin and disc. In addition, a change in the overall wear mechanism was found to have occurred between tests conducted in octanoate and NaOH solutions. The EN 24 steel (AISI 4340) was prone to corrosion in the NaOH solution and was exacerbated by application of a relatively high anodic overpotential. Whereas in the octanoate solution, the additives adsorb on the disc and react to produce iron octanoate which offers protection to corrosion and direct steel/steel contact, reducing both friction and wear.

ii. Feasibility of Alternative Additives

The oleate additive was advantageous in producing the lowest friction of all the test solutions used in this project. However, no dependence of friction on overpotential was observed, probably due to the natural behaviour of the molecules to form a strong bond with the substrate and shows no reaction towards variation in overpotential.

The shorter alkyl chain length additive (butyrate) was able to reduce friction by a relatively small amount cf. the octanoate. However, it allows the control of friction to be obtained by applying a relatively small magnitude of overpotential. This might open the possibility for developing this type of additive so that it can be used in this project's test setup.

The positive charge additive (CTAB) can also reduce friction when cathodic overpotential was applied, but not to a significant extent cf. the octanoate. However, this shows that the reduction of friction could also be obtained when cathodic overpotential is applied in a solution containing a positive charged additive.

iii. Active Switching Experiment

The test using the octanoate test solution showed that the friction response followed the overpotential variation quite closely. However, there was some lag in the friction response, which increased with time. This was probably due to the increased tenacity of the octanoate molecules after a period of time.

The butyrate test solution did not show a close response of the friction towards overpotential switch as much as the octanoate. The reason is not clear at the moment, but it is probable that the butyrate stabilises in a longer period of time, and does not show a quick response within the set timeframe.

5 Steel / Steel Contacts in Drilling Mud

5.1 Introduction

The previous chapter (Chapter 4) has established the feasibility of controlling friction and wear by varying the applied overpotential. Therefore, this chapter aimed at expanding the understanding beyond the use of the baseline solutions which were NaOH pH 9, and 60 mM sodium octanoate at pH 9. Therefore, this Chapter 5 was a step further into assessing the feasibility of this technique for applications related to the drilling operations.

This chapter presents the results of the tests conducted in the simulated drilling muds, namely by incorporating bentonite particles in the constituent. Similar test methods as presented in Chapter 4 were employed in order to assess the reproducibility of the test results, such as the sliding speed (0.03 m s^{-1}), normal load (50 N), overpotential range (± 1 V). However, a few key adjustments were made to investigate the influence of applied overpotential on the response of friction and wear. Particularly, the constituent of the drilling mud was formulated such that it simulated a baseline mixture containing only viscosity enhancer (bentonite), in which subsequently, the octanoate additive was incorporated. Furthermore, silica (sand) particles were also added to simulate the crushed rock during drilling, which in real practice becomes intermixed with the drilling mud and could increase tool wear when entrained in sliding contacts (or become abrasive particles for erosion-corrosion mechanisms).

Another type of drilling mud formulation was also included in this chapter, which replaces bentonite clay with a polymer based additive. However, this polymer mud was not investigated as much as the bentonite mud due to time constraint.

5.2 Bentonite Drilling Mud

5.2.1 Bentonite Drilling Mud without Additive

5.2.1.1 Mean Coefficient of Friction (μ_{mean}) and Wear *vs.* the Applied Overpotential

The effect of applied overpotential on friction in the bentonite drilling mud is shown in Figure 5.1. The μ_{mean} values are generally higher than the NaOH tests. This was generally due to the absence of any friction reducing additive such as the octanoate, and the presence of the relatively hard bentonite particles in the mixture which were entrained in the contact causing two-body abrasion. Furthermore, the error bars of the bentonite tests are also

relatively larger than the NaOH tests which generally shows that the friction response had more perturbations, *i.e.*, were less stable, compared with the NaOH tests.

The data was fitted with linear interpolation and showed a relatively weak dependence of friction on overpotential. At cathodic overpotentials, the μ_{mean} decreased slightly, from 0.58 to 0.52 at 0 and –1 V overpotentials respectively. Visual observation of the setup at the end of test and with rotation stopped, revealed an area of thinner (less viscous) drilling mud above the disc whereas the sides had normal consistency. This behaviour suggested that the bentonite particles were repelled from the cathodic disc (owing to the particle's negative charge), thus causing smaller number entrained particles in the contact. Furthermore, it is seen that the friction (μ_{mean}) increased as the overpotential was more anodic than 0 V, *i.e.*, to a maximum of 0.60 at +1 V overpotential. In this condition, the amount of entrained particles was relatively high owing to the increased attraction between the anodic disc and the bentonite particles, resulting in higher friction.

Visual observation of the disc surface at cathodic overpotential after rinsing showed shiny surfaces, which was similar to the octanoate tests, but with larger wear track widths. However, at anodic overpotentials showed production of mud cake, which was due to the agglomeration of the bentonite particles. The mud cake was assessed by hand and showed a relatively soft material, which had a slightly similar consistency as wet pot clay. The mud cake increased in density at higher values of anodic overpotentials, especially at +1 V. Furthermore, a trench was observed in the mud cake, around the track of the pin. These were suggestions of the bentonite particles being entrained in the contact which potentially could affect the friction. An insight into the mud cake formation will be presented later in this chapter (Section 5.2.1.3).

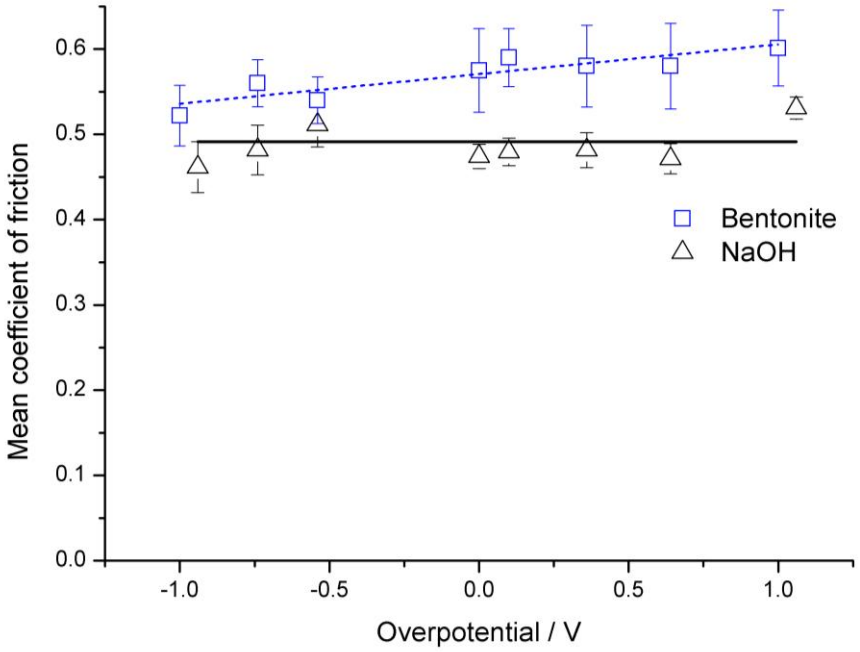

Figure 5.1. Mean μ *vs.* overpotential of experiments conducted in NaOH, and bentonite drilling mud.

To aid in comparing and contrasting, the micrograph of the pins and discs from the drilling mud tests are arranged in Table 5-1. Focusing on the pins at –1, 0 and +1 V overpotentials showed evidence of particle abrasion (two-body abrasion), which suggested that the bentonite particles were entrained in the contact. However, the difference of the pin feature across the overpotentials is difficult to ascertain. This is probably due to the potential control was made on the disc only, which left the pin floating (unless in contact with disc which was assumed intermittent).

The general feature of the disc wear track at –1 V overpotential was relatively smooth, which suggested that the bentonite particles were entrained to a lesser extent into the contact due to being repelled from the surface. This is because the bentonite particles are negatively charged and are sensitive towards surface potential [12, 125]. Furthermore, at this potential, corrosion was suppressed due to the reduced oxidation reactions, such as the metal dissolution and oxide formation. Visual observation after the sliding test (rotation stopped) showed that the drilling mud immediately above the disc became slightly less viscous than the bulk which suggested that the particles were repelled away to the sides. There is some occasional evidence for particle indents in the wear track (see micrograph) which shows that the contact is not completely free from the effect of entrained particles.

At 0 and +1 V overpotential, focusing on the disc wear tracks, abrasion due to the entrained particles (two-body abrasion) becomes apparent while being severe at +1 V. Furthermore,

visual observation of the disc at the end of tests showed corrosion in the form of black deposits, being more prolific at +1 V overpotential.

The feature of the disc wear track at +1 V overpotential suggested that there was a high plastic deformation, combined with the particle abrasion and corrosion. Furthermore, observation at the end of the sliding test revealed that a mud cake was produced on the disc surface and at the leading edge of the pin, owing to the attraction of the bentonite particles to the positive disc (agglomeration). This offers the explaination of how the anodic (positive) overpotential can influence the wear mechanism and high levels of friction by attracting more bentonite particles into the contact.

	Pin	Disc
Cathodic (–1 V overpotential)	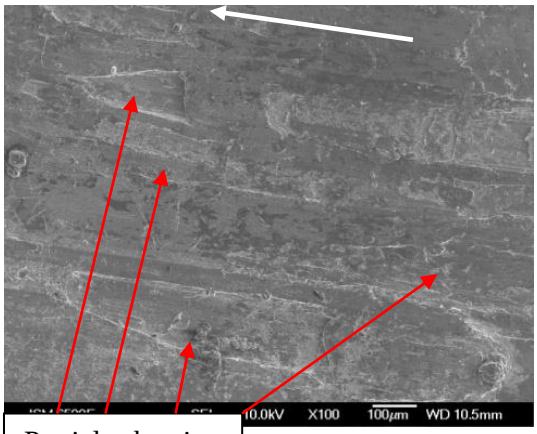	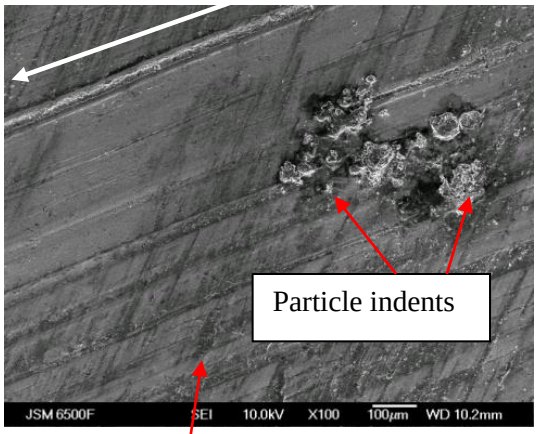
OCP (0 V overpotential)	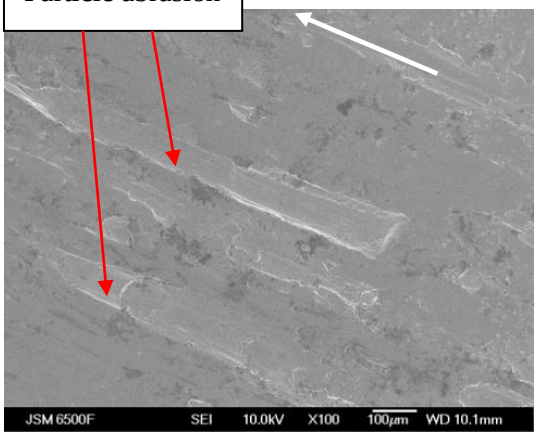	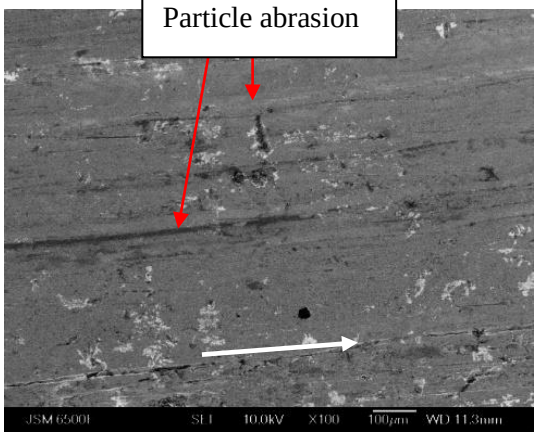
Anodic (+1 V overpotential)	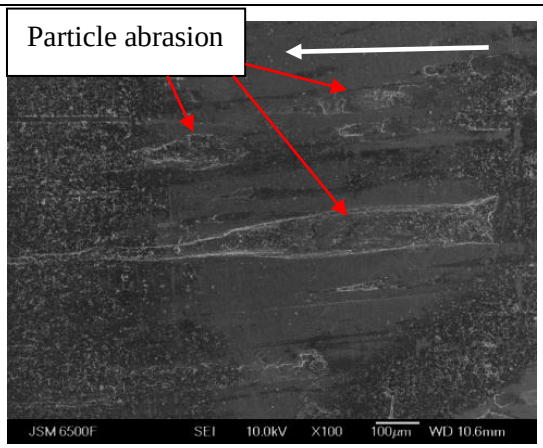	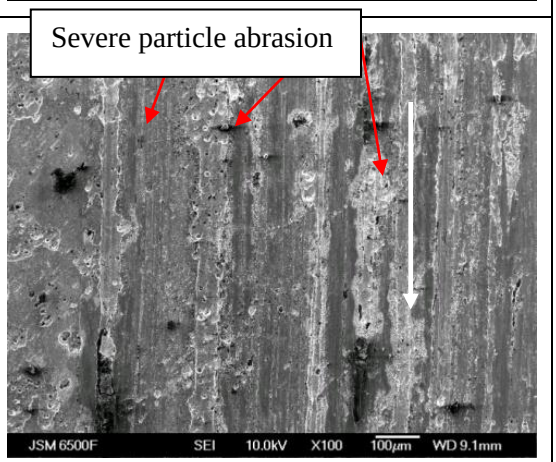

Table 5-1. SEM micrographs (x100) of the pins and discs of the bentonite test solution at -1, 0 and +1 V overpotentials. White arrows indicate direction of motion.

Higher magnification of the disc wear tracks are shown in Figure 5.2 (x1000). The micrograph of –1 V overpotential shows the feature of particle indent which is similar to a crater (see Figure 5.2. (a)). At 0 V overpotential, evidence of particle abrasion is seen in the wear track, with some corrosion (see Figure 5.2 (b)). At +1 V overpotential (see Figure 5.2 (c)), severe plastic deformation is seen, with evidence of small features of indents scattered around the wear track. This was probably due to the combined action of corrosion and increased bentonite particle entrainment, both promoted by the application of anodic overpotential.

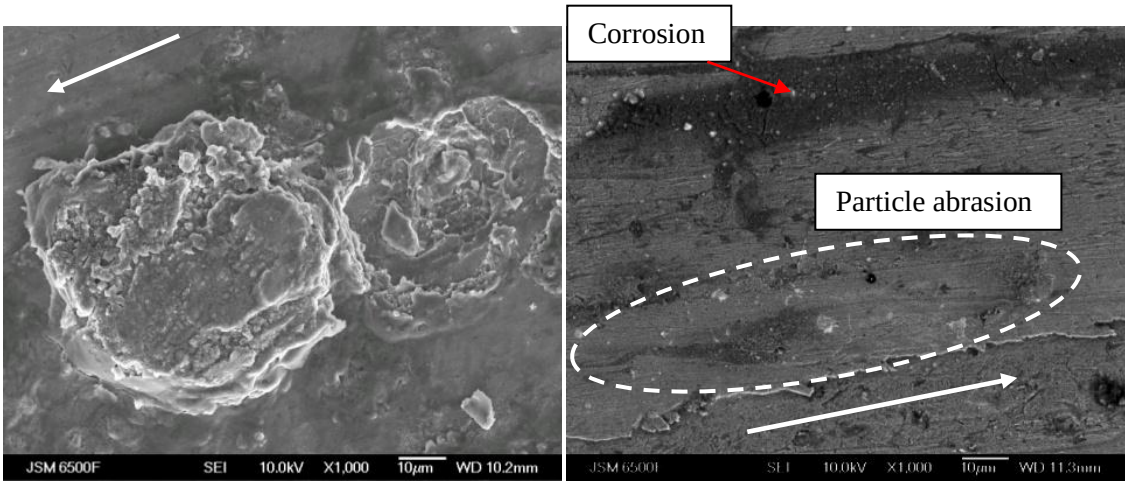

(a) (b)

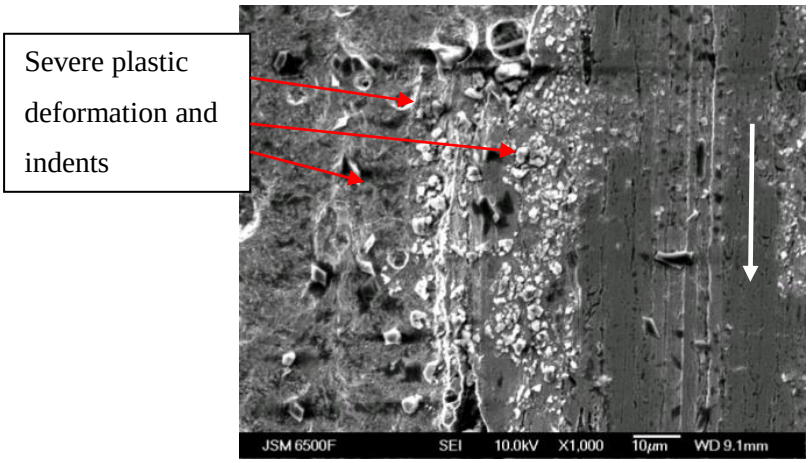

(c)

Figure 5.2. SEM micrographs (x1000 magnification) of the discs of the bentonite test at (a) –1 V overpotential, (b) 0 V overpotential, and (c) +1 V overpotential. These disc micrographs correspond to the x100 magnification from Table 5-1.. Arrows indicate direction of motion

The wear rates of the pins and discs of the bentonite and NaOH tests are shown in Figure 5.3. It is evident that the pin wear rates of both bentonite and NaOH tests are relatively similar, *i.e.*, within the same order of magnitude of 10^{-15} m^3 N^{-1} m^{-1} (see Figure 5.3 (a)). However, there might be some errors, due to the geometrical method used in the calculation of the volume loss. Furthermore, the alternative gravimetric method of calculating the pin volume loss is not suitable to replace the geometrical (pin cap) method. This is due to the significant corrosion of the NaOH pins, which most probably will cause an error in the mass loss (gravimetrical) measurement. Previous work in tribo-corrosion relating to sliding contacts in aqueous solutions mostly employed ceramic such as alumina or zirconia as the counterface, which were usually reported as having negligible wear, thus the wear rates were not calculated, such as shown by [98, 118, 119]. However, Brandon *et al* [93, 94] were of the few who used steel counterface, but they utilised a corrosion inhibitor (such as octanoate) in their solution. Thus, corrosion was controlled and did not cause significant error in their method of calculating the counterface wear rate (pin volume loss determined by geometrical method).

The bentonite disc at cathodic, *i.e.*, at –0.5, –0.7 and –1 V overpotentials, show slightly larger wear rate values compared with the NaOH tests (see Figure 5.3 (b)). This was probably due to the entrained particles in the bentonite mixture causing more material loss. However, at 0 V overpotential, the disc wear rate had a negative value, which means that probably there was material gain, although, by a small amount. This was probably due to corrosion which produced iron oxide, in combination with severe plastic deformation causing material gain, as discussed previously. The bentonite discs at anodic overpotentials are omitted in the figure, because of the severe corrosion that resulted in the difficulty in obtaining accurate volume loss from the wear track profile. The next section will briefly present the phenomena of material gain found on the discs at anodic overpotentials.

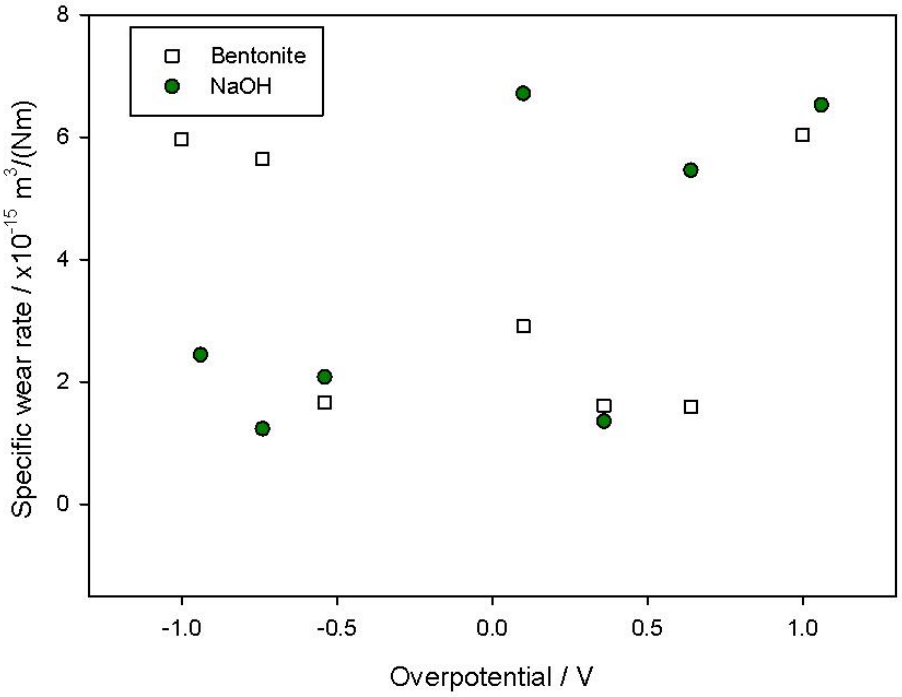

(a)

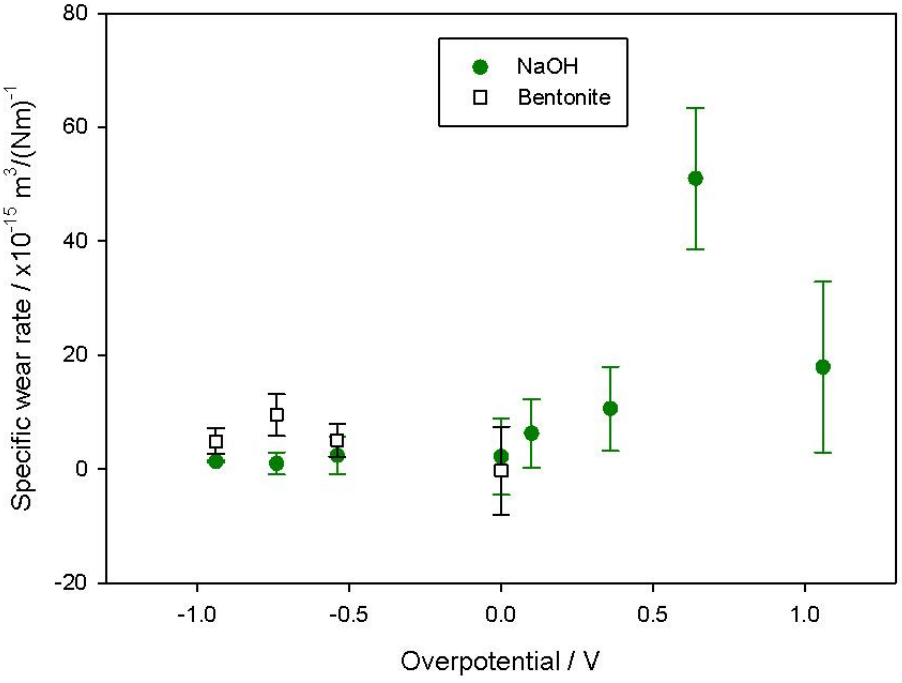

(b)

Figure 5.3. Specific wear rates from the bentonite and NaOH test solutions of the (a) pin, and (b) disc.

5.2.1.2 Difference in the Wear Track Profiles of the Cathodic and Anodic Discs

The profile of the disc wear tracks at –1, 0, and +1 V overpotentials of the bentonite tests are shown in Table 5-2 (obtained using the Talysurf). At cathodic overpotential, the wear track is at the same level as the off wear track, *i.e.*, unworn surface. However, there are a small number of peaks and valleys in the wear track which could have been due to particle abrasion and direct steel/steel contact. However, it is not obvious from this profile that there is a net a material loss as shown by the wear rate. This was probably due to the wear rate was calculated as the mean from four different profile measurements on the wear track, in which the shown profile is only one of them and is a typical example.

At 0 V overpotential, the profile of the disc wear track looks similar to the cathodic test at –1 V overpotential, with the wear track at the same level as the off wear track. However, wear rate calculation showed that there is a small material gain, *i.e.*, a negative wear rate as discussed previously. This might have been due to the material transfer from the pin or particle embedment onto the disc surface. Furthermore, once again, it could also be due to the variations along the wear track (four different profiles on the track) which resulted in a negative value of the mean.

At +1 V overpotential, there is clear evidence of material gain on the wear track which might also indicate material transfer or particle embedment. This was probably due to the increased severity of particle abrasion, direct steel/steel contacts and corrosion as discussed previously. The off wear track also shows some evidence of pits (valleys) probably due to corrosion, which agrees with the findings of visual observation and SEM micrograph.

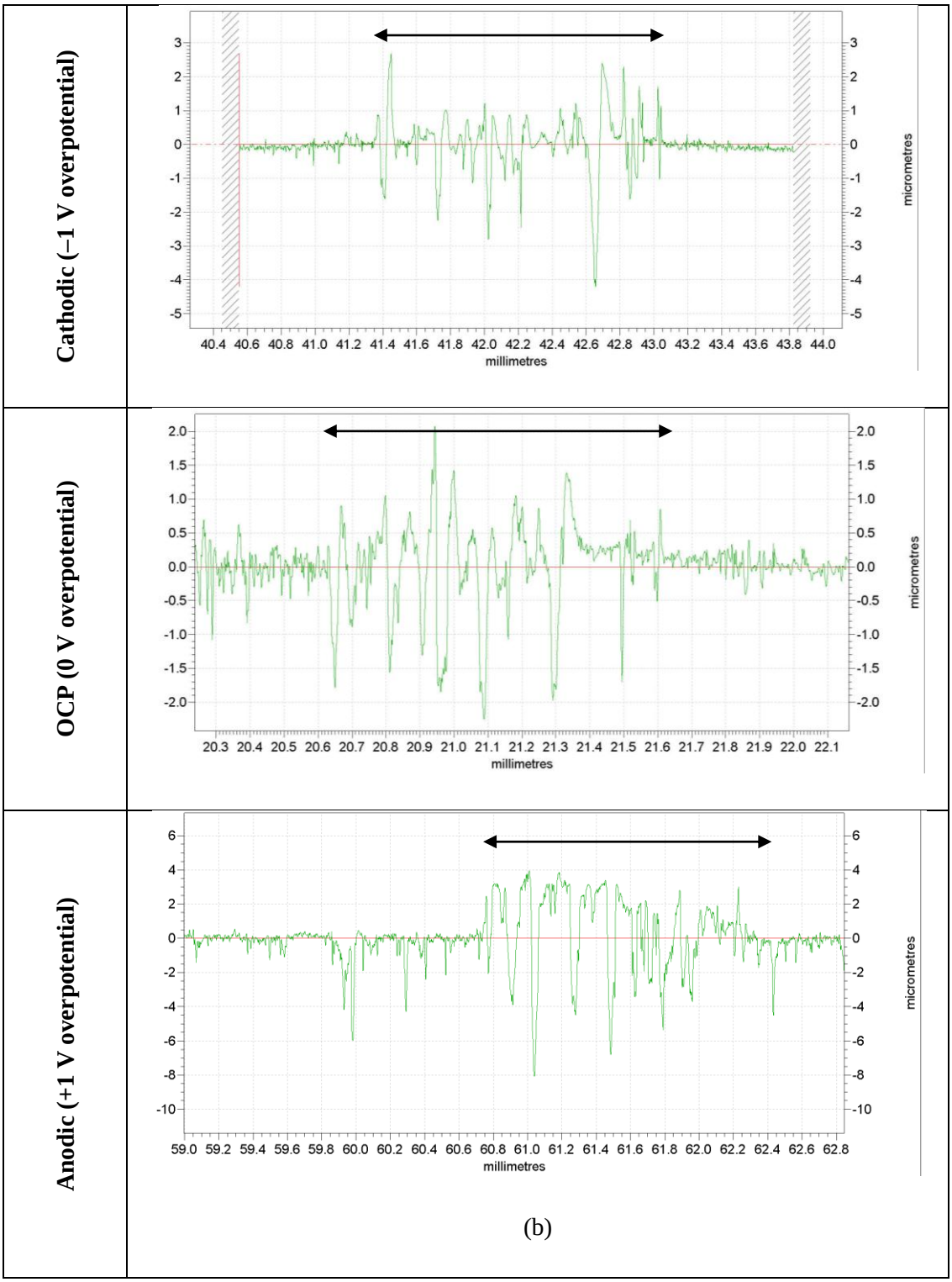

(b)

Table 5-2. Profile of the wear track on the discs tested in the bentonite drilling mud at cathodic overpotential, OCP, and anodic overpotential. Arrows showing the width of wear track.

5.2.1.3 The Formation of Mud Cake

The discs which were retrieved from the cathodic overpotential tests showed a generally clean and relatively shiny surface, slightly similar to the cathodic discs from the NaOH and octanoate tests. However, the width of the wear track was larger with visible grooves within the wear track. This was easily seen even before rinsing the disc in tap water. This was probably due to the inhibited corrosion reaction similar to all test solutions.

However, the discs which were experimented at anodic overpotentials in the bentonite tests showed productions of mud cake on the surface, when observed at the end of the tests. Figure 5.4 shows an example of the mud cake which was formed during the +1 V overpotential test. It is seen that the pin created a trench in the mud cake, and after rinsing revealed a wear track on the disc which was severely grooved and had black deposits (see Figure 5.4 (b)).

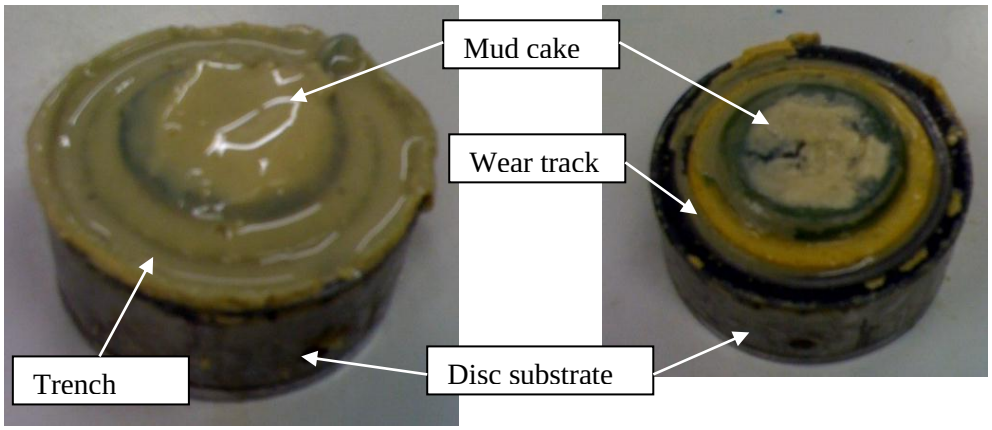

Figure 5.4. Images of the discs showing the mud cake formed after the +1 V overpotential test (a) as retrieved from test, and (b) after rinsing with tap water.

In addition, the effect of this mud cake on the pin is schematically shown in Figure 5.5. Tests with low anodic overpotential values such as +0.54 V showed that a relatively small particle build up was produced at the leading edge of the pin, owing to the action of ploughing the mud cake which was formed on the disc (see Figure 5.5 (a)). However, at higher values, especially at +1 V overpotential, created larger particle build up at the leading edge.

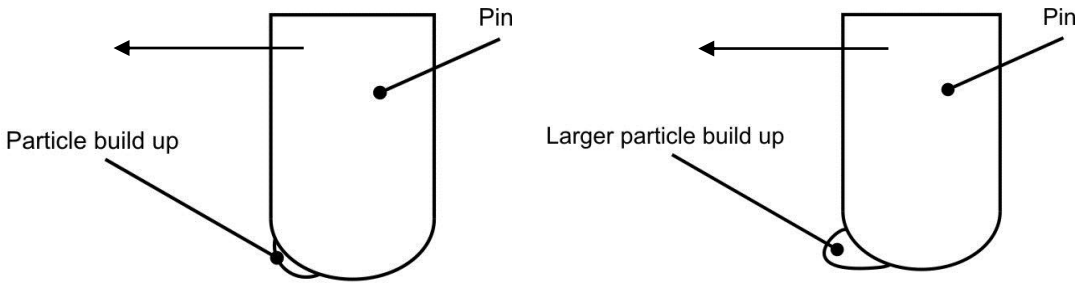

(a) (b)

Figure 5.5. Schematic of (a) small, and; (b) large particle build up as a result of lower and higher anodic overpotentials respectively. This was found at the leading edge of the pin. The arrows show the leading edge of the pin.

Therefore, as discussed previously, the production of mud cake might suggest that there was a higher number of bentonite particles which could be entrained in the contact during sliding. This would result in an increased amount of two-body abrasion due to the particles, thus probably resulting in higher resistance to grooving, which could explain the higher friction, overall. Furthermore, in theory this would create a severely abraded wear scar and wear tracks because the bentonite particles were relatively harder than the steel. Consequently, this was confirmed by the SEM micrographs as shown previously, and more evidence will be shown later in this chapter relating to this issue.

5.2.2 Effect of the Octanoate Additive on the Bentonite Drilling Mud

5.2.2.1 Mean Coefficient of Friction (μ_{mean}) and Wear *vs.* The Applied Overpotential

The simple formulation of the drilling mud consisting of distilled water and bentonite particles showed a weak dependence of friction on applied overpotential. Similarly, the primary investigation in the baseline solutions presented earlier in Chapter 4, involved the incorporation of the octanoate additive into the formulation to impart the dependence of friction on overpotential. Therefore, this section will present the effects of adding the octanoate additive into the drilling mud formulation itself, with particular focus on the performance of friction and the change in wear mechanisms.

The effect of incorporation of the octanoate additive into the drilling mud (thus bentonite+octanoate) on friction response can be seen from Figure 5.6. The bentonite+octanoate data was fitted with a sigmoidal curve and showed a high μ_{mean} value at cathodic overpotentials, particularly at –1 and –0.5 V overpotentials, which had similar values to the bentonite drilling mud as discussed previously (μ_{mean} around 0.56). Again, the reason is believed to be due to the repulsion of the octanoate additive from the disc surface, leaving the surface susceptible to two-body abrasion by the bentonite particles (no tribofilm formation).

The friction value dropped dramatically at –0.2 V overpotential and attained low values at more anodic overpotentials. This was believed to be due to increased adsorption of the octanoate additives, forming tribofilm which separated the direct steel/steel contact and reducing abrasion. Furthermore, it was also observed that the friction perturbations decreased at anodic overpotentials, which can be shown by the smaller error bars, especially at +1 V overpotential. This might suggest an increased effectiveness of the tribofilm, maybe by forming a thicker or denser film [95].

It is interesting that the values of μ_{mean} at the anodic overpotentials are comparable with the octanoate test (*i.e.*, particle free system reported in Chapter 4), considering the number of abrasive bentonite particles in this mixture. The possible explanation for this behaviour is that the adsorption of the octanoate additives passivated the disc surface, which resulted in no sites to attract the bentonite particles when applying anodic overpotentials. This is supported by the low values of current density recorded during the experiments, which was also in the same magnitude as the octanoate test, *i.e.*, in 10^{-6} A.cm^{-2} (will be discussed in detail in Chapter 8). This low current density values might suggest that the tribofilm with

similar characteristics such as density and thickness was produced in both solution types, regardless of the presence of the particles.

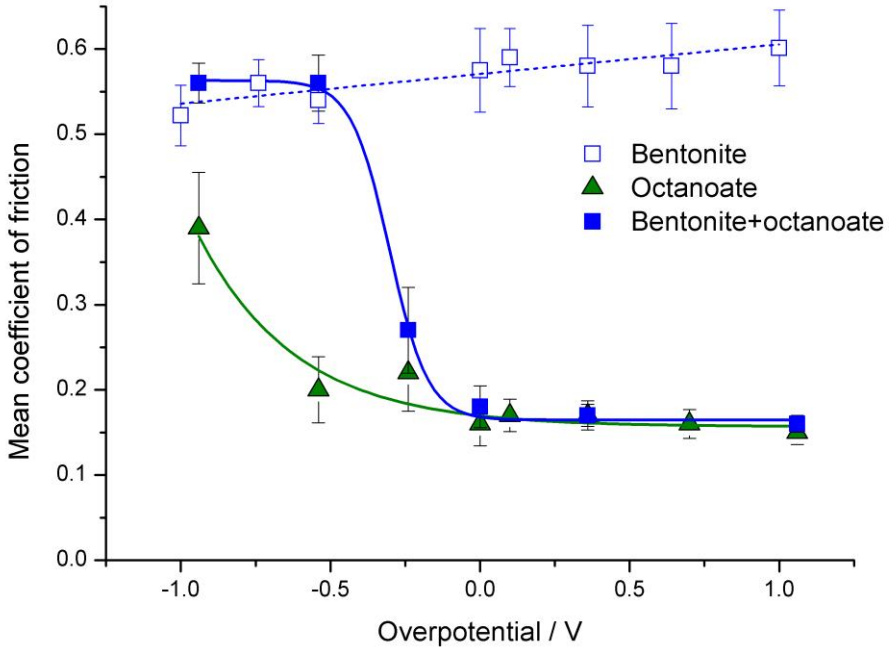

Figure 5.6. μ_{mean} *vs.* overpotential of experiments conducted in the octanoate (from Chapter 4), bentonite, and bentonite+octanoate test solutions.

The SEM micrographs of the pins at 40 and 500 magnification times are shown in Table 5-3. The grooves of the pin wear scars are relatively wide at –1 V overpotential test, which can be seen from the x40 micrograph. These were probably due to the entrainment of the bentonite particles causing increased levels of two-body abrasion. Furthermore, there is evidence of delamination when observed at the higher magnification (x500), which might suggest adhesion due to the direct steel/steel contact. This test also gave the highest friction in the sliding test as discussed previously, with a μ_{mean} value of 0.56.

At 0 V overpotential, the grooves on the wear scar are medium, and adhesion was not found when viewed at the higher magnification (x500) micrograph. Furthermore, at +1 V overpotential, the grooves were even smaller (narrowest) which can be seen in both the x40 and x500 micrographs. The presence of grooves at 0 and +1 V overpotentials is believed to suggest that the sliding was not totally immune to particle abrasion. However, the lower levels of abrasion and adhesion might suggest the effective formation of the octanoate tribofilm on the contacting surfaces, separating direct steel/steel contact and reducing the severity of particle abrasion. In addition, the low friction given by these conditions as

discussed previously are supporting this hypothesis (μ_{mean} values of 0.18 and 0.16, at 0 and +1 V overpotentials respectively).

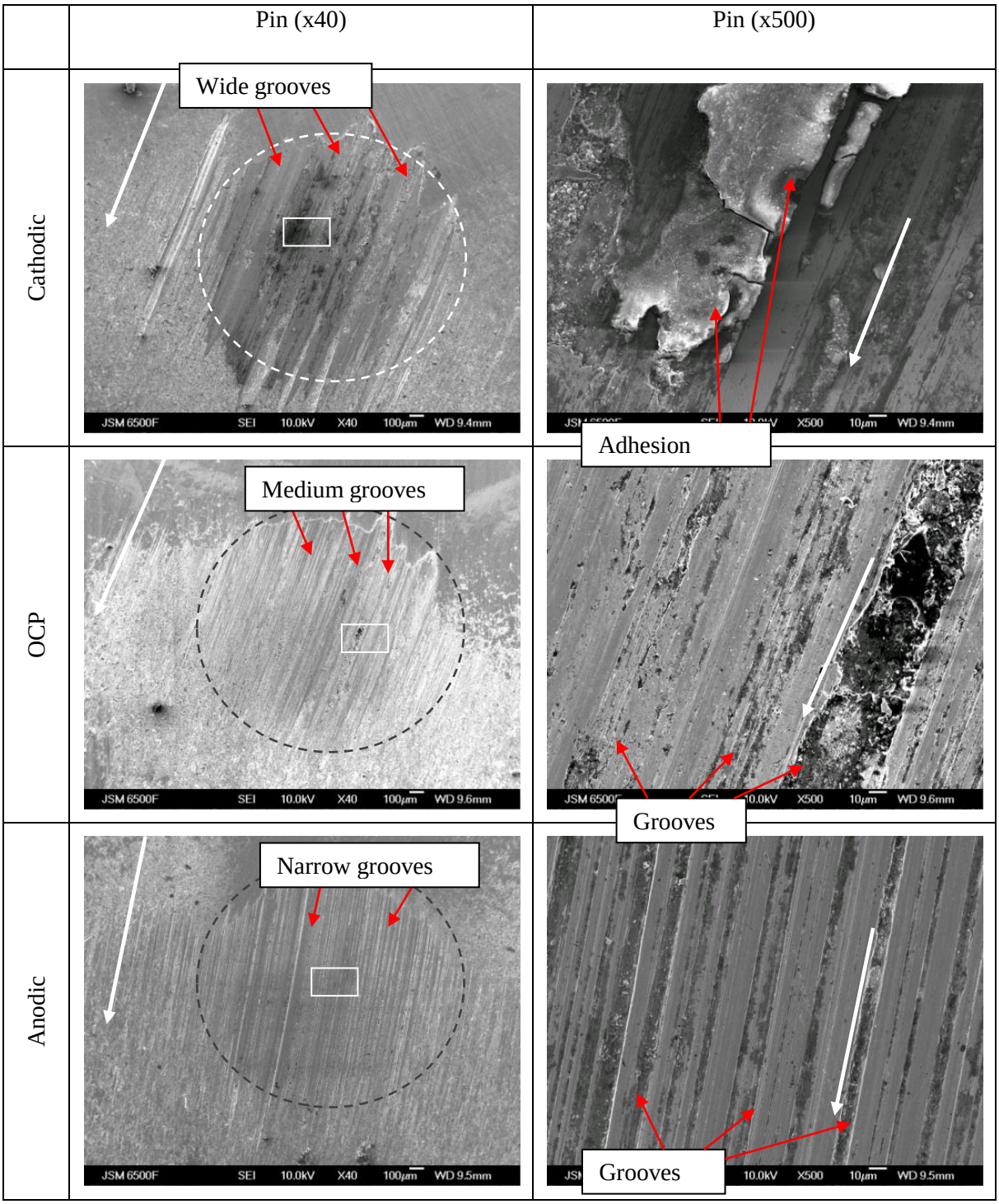

Table 5-3. SEM micrographs (x40 and x500) of the pin and disc samples tested in the bentonite+octanoate mixture. White arrows show the direction of motion, dashed circles show the nominal wear scar and the white boxes show the focused area (approximate).

The disc micrographs also indicated that there might be matching groove sizes with the pin wear scars (see Table 5-4). Particularly, there is an observed change in groove width from relatively wide, medium to narrow, at –1, 0 and +1 V overpotentials respectively, as previously seen on the pins. For example, it is seen that the grooves at +1 V overpotential are relatively narrower than the other tests. Similarly, this might be attributed to the work of the tribofilm, where it might have been effectively formed at more anodic overpotentials.

The EDX scans on both the cathodic and anodic disc wear tracks are shown in Figure 5.7. Two spectra were obtained from each disc, focusing on the area within the groove and on the plane surface. The results showed that the spectrum within the groove (spectrum 1 on Figure 5.7 (a) and (b)) indicated the presence of more elements, particularly Si and Al. This might be due to the trace of the bentonite particles, which suggested that the groove was the result of particle abrasion. Outside the groove (spectrum 2 on Figure 5.7 (a) and (b)), there were indications of Fe, O, and C only, which were expected for the surface of steel (similar to the octanoate spectra as shown previously in Section 4.2.2 in Chapter 4). However, the presence of C on the cathodic disc was not expected, because of the assumption that the tribofilm was absent (see Figure 5.7 (a)). Therefore, this possibly suggests that the C might be detected from other sources (such as carbides or contamination film). Alternatively, this might suggest that the octanoate molecules were not completely repelled from the surface, but formed a weak arrangement of adsorption film, which was not robust for boundary lubrication. This opens the door to further investigation.

	Disc (x500)
Cathodic	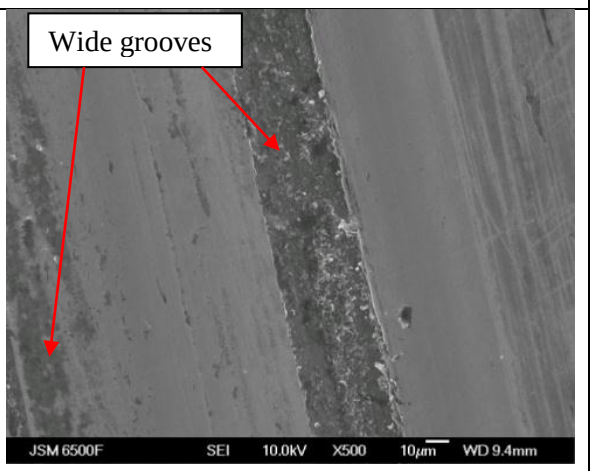
OCP	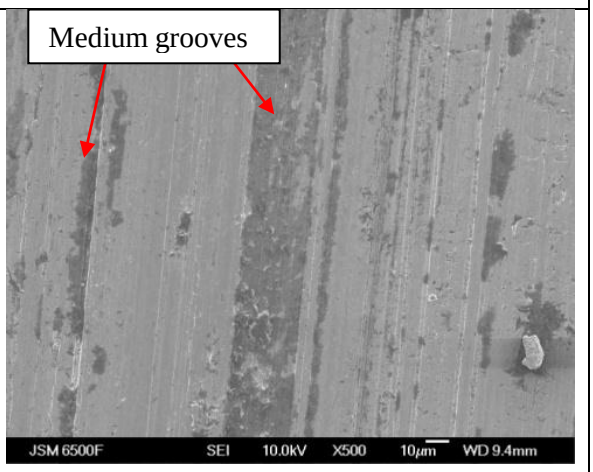
Anodic	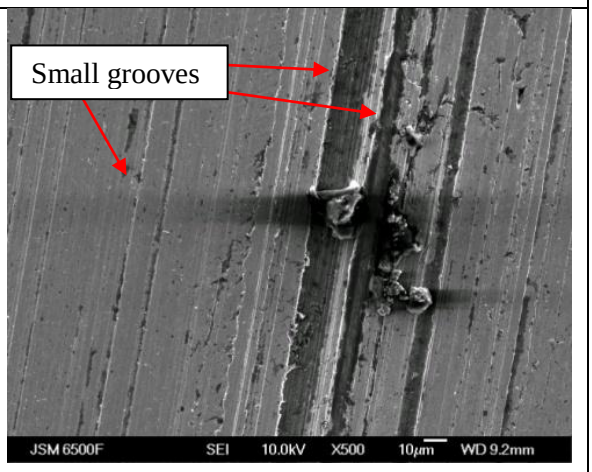

Table 5-4. SEM micrographs (x500) of the disc tested in the bentonite+octanoate tests.

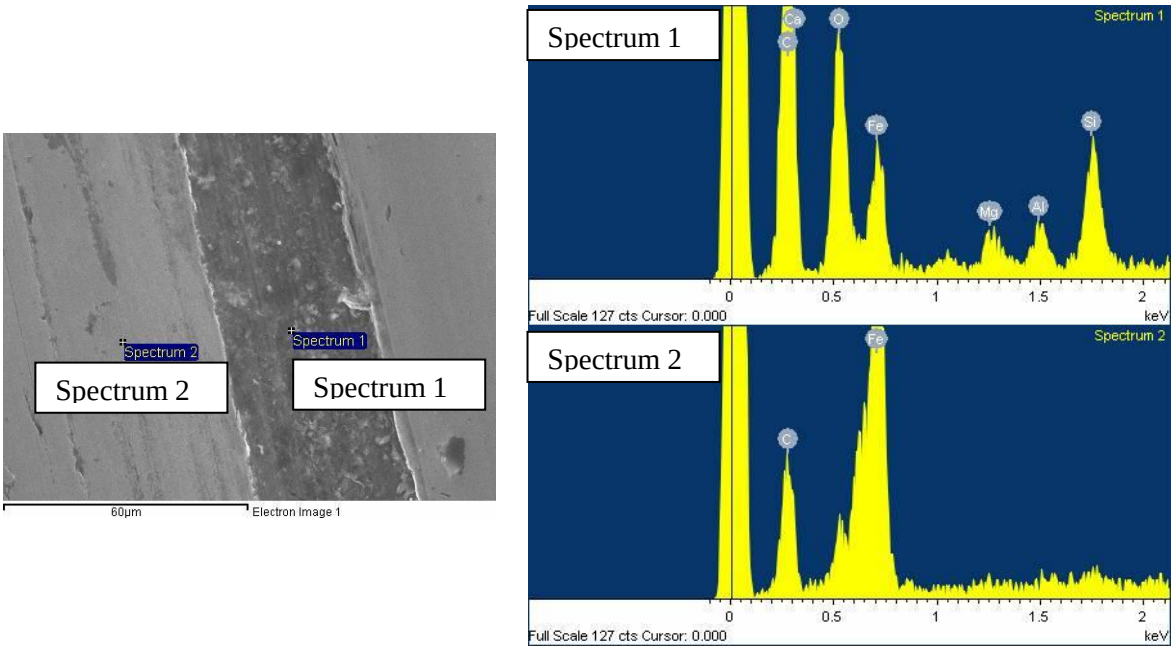

(a)

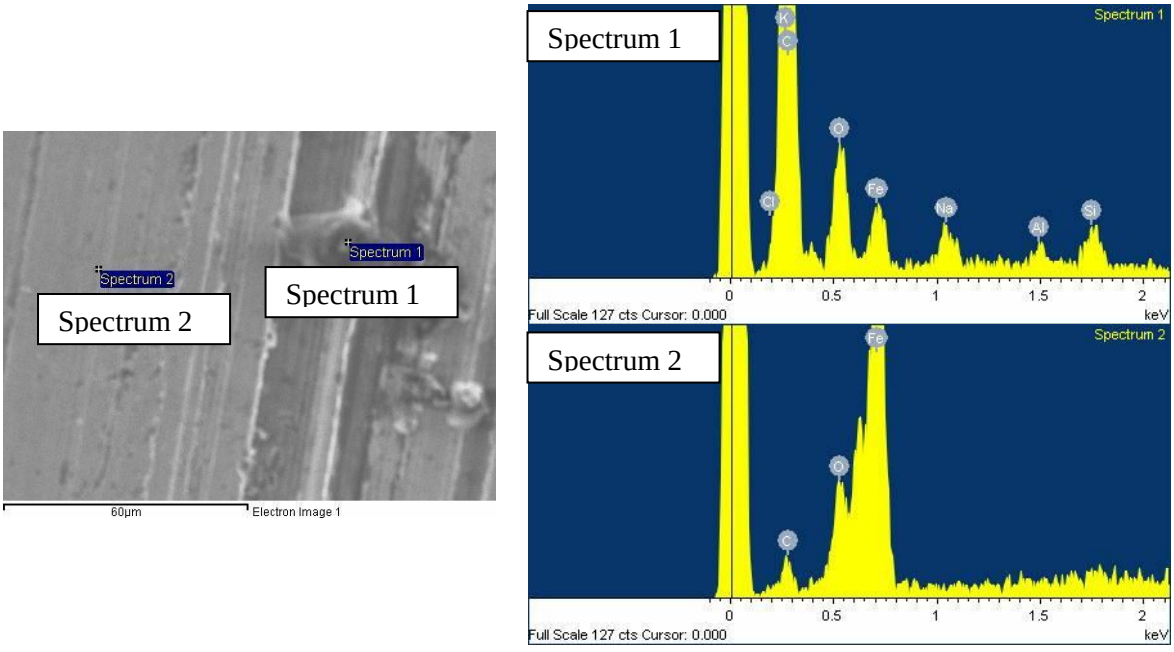

(b)

Figure 5.7. Results of EDX analysis performed within the wear track of a (a) cathodic disc, and (b) anodic disc in the bentonite+octanoate tests, with spots taken on a groove and on a plane surface.

The wear rate of the pins and discs of the bentonite+octanoate tests are shown in Figure 5.8, with the inclusion of the values from the bentonite drilling mud and octanoate (from chapter 4) test results. Generally, it is seen that the pin wear rate could be arranged in descending order as bentonite > bentonite+octanoate > octanoate (see Figure 5.8 (a)). This shows that the two-body abrasion due to the bentonite particles were high in the bentonite drilling mud, but could be reduced by the presence of the octanoate additive, probably due to the

formation of effective tribofilm in the contact. Expectedly, the octanoate tests produced the lowest wear rates due to the absence of abrasive particles in the solution.

Generally, the bentonite discs wear rate shows that at cathodic overpotentials, the values are the highest among the three (see Figure 5.8 (b)), which is in agreement with the results of the pin wear rates as shown in Figure 5.8 (a). However, the material gain at 0 V and more anodic overpotentials were only seen on the bentontie discs (not on pins). This was probably due to the increased electrochemical reactions, combined with the higher particle entrainment, as discussed previously.

The values of the disc wear rates follow the descending order from bentonite > bentonite+octanoate > octanoate, similar to the pin wear rates. This might suggest that whenever additive is present, the tribofilm was formed on both the pin and disc surfaces, thus producing similar wear mechanisms. Particularly for the bentonite+octanoate discs, the lower wear rate compared with the bentonite discs suggested the effective work of the tribofilm reducing direct steel/steel contact, particle abrasion and corrosion (metal dissolution or oxide formation).

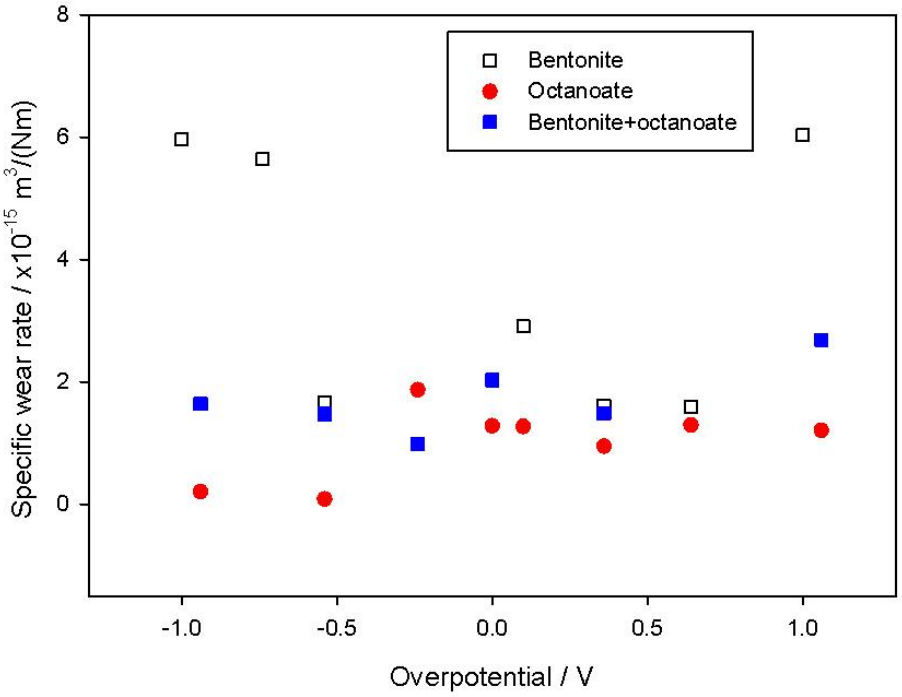

(a)

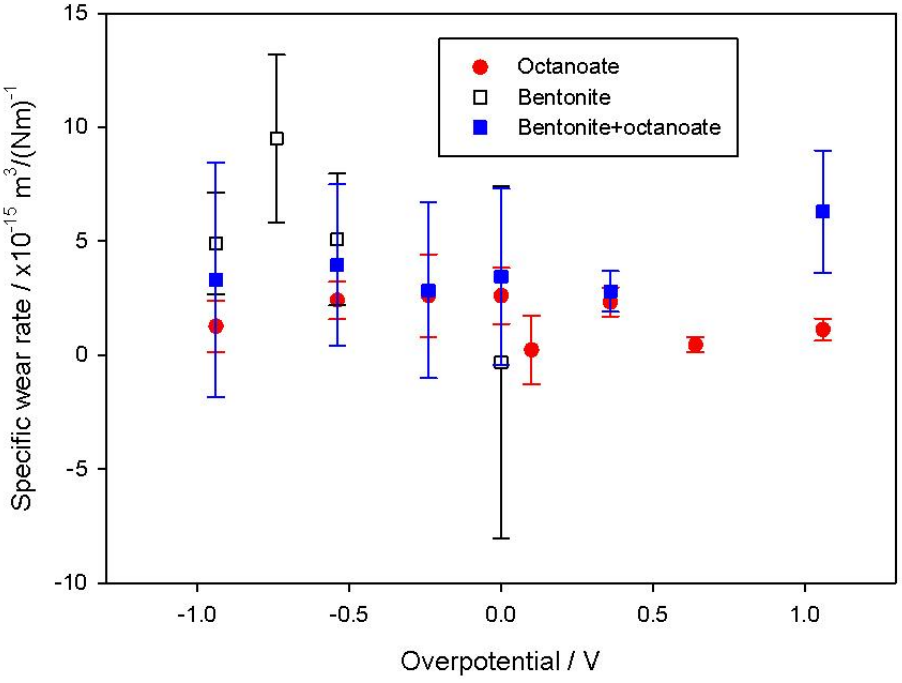

(b)

Figure 5.8. Specific wear rates from the bentonite and bentonite+octanoate test of the (a) pin, and (b) disc. Bentonite anodic overpotential discs were omitted due to severe corrosion that resulted in the difficulty in obtaining accurate volume loss.

5.2.2.2 Profile of Wear Tracks

The profiles of the disc wear track of the bentonite and bentonite+octanoate tests are shown in Table 5-5 (only 0 V overpotentials tests are shown). The bentonite test shows a wear track with a width of 2 mm, and a maximum depth of 3 µm. There is also evidence of some peaks higher than the off wear track baseline, probably showing material gain due to material transfer from pin or particle embedment.

The bentonite+octanoate test shows a relatively narrower wear track of 1.6 mm, and a reduced maximum depth to around 2 µm. This might be due to the protection by the tribofilm from particle abrasion and direct steel/steel contact. However, there is evidence of an increase in the height of the peaks compared with the bentonite test, in which the actual reason is not clear. However, only a general comparison can be made using these profiles as they do not account for the complete variations along the wear track. This is one of the disadvantages of using a pin-on-disc test rig, in which the produced wear track is relatively large and the surface profile might not be homogeneous throughout, cf. other rigs producing smaller and more controllable wear track such as the reciprocating contact mode.

Bentonite	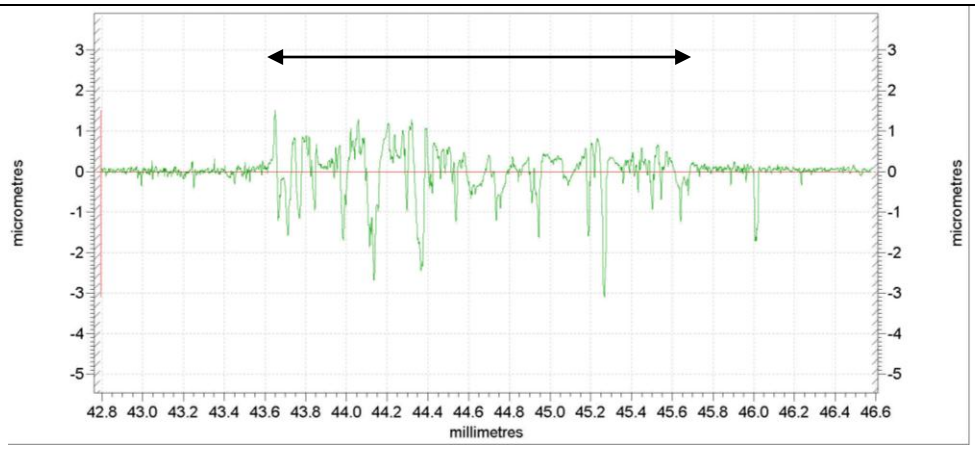
Benttonite+octanoate	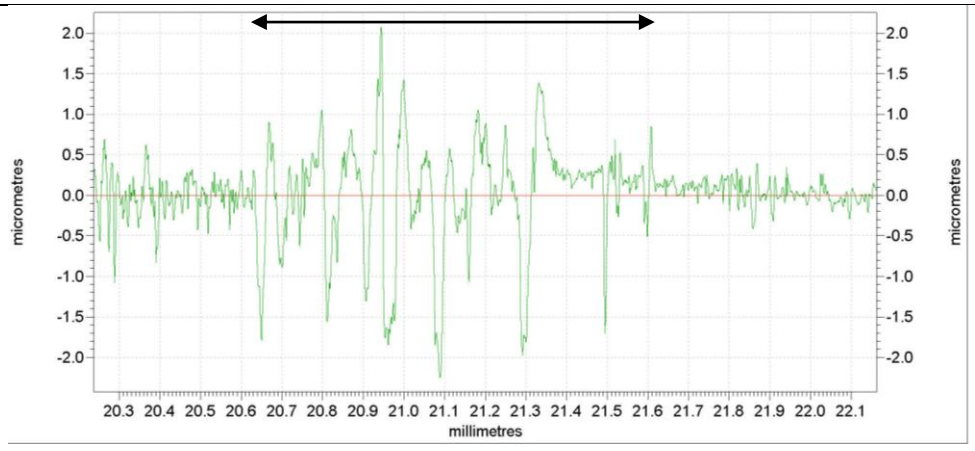

Table 5-5. Profile of the wear track of the discs at OCP (0 V overpotential) from the bentonite and bentonite+octanoate tests. Arrows show the wear track width.

5.2.3 Effect of Adding Silica Sand Particles into the Bentonite Drilling Mud with and without Additive

In realistic downhole drilling conditions, the drilling mud will be carrying sand particles which are the result of the drilling processes, from the bottom of the whole to the surface. Therefore it is reasonable in laboratory experimental setups to incorporate the sand particles (silica) in the drilling mud to simulate this rock debris. For example, such work were shown by Thakare [13] and Bello *et. al* [126] who utilised a micro abrasion rig to test the abrasion characteristics of different concentrations of silica sand particle suspensions in distilled water.

5.2.3.1 Mixture Consisting Bentonite and Silica Sand Particles (without Additive)

The effect of adding 3 wt % silica particles (5 μm mean diameter) into the bentonite drilling mud (thus bentonite+silica), to the μ_{mean} *vs.* overpotential performance is shown in Figure 5.9. It is evident that the bentonite+silica tests at –1, 0 and +1 V overpotentials lie exactly on the same trendline of the bentonite tests. Therefore, this shows that the addition of the silica particles did not have any effect on the frictional responses, with respect to the variation in the applied overpotential. This is probably due to the silica particles not having affinity for surface potential as opposed to the bentonite particles, because silica is inert (not charged).

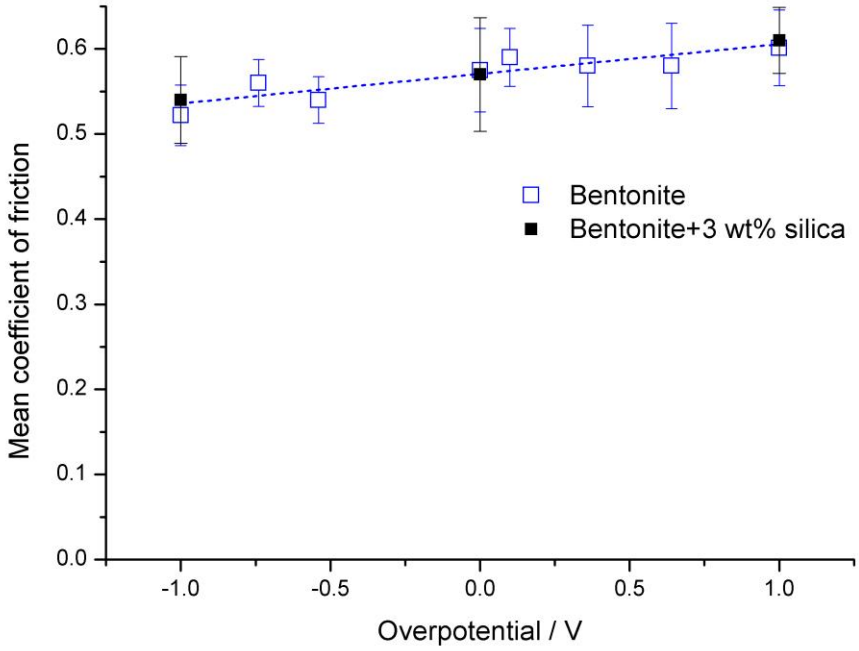

Figure 5.9. μ_{mean} *vs.* overpotential of experiments conducted in the bentonite and bentonite+silica (3 wt% silica sand) mixtures. Graph showing the bentonite+silica test results lying on the same trendline of the bentonite tests.

Therefore, a question arises whether the silica particles were actually entrained in between the pin and disc contact or not. To corroborate this, investigation of the worn surfaces might offer some insightful information. The SEM micrograph of the disc at –1 V overpotential shows a severely abraded wear track at x500 magnification (see column 2 in Table 5-6). However, this is not seen in the bentonite test at –1 V overpotential (see column 3 in Table 5-6), which instead shows a feature that is predominantly smooth, with rare cases of particle indents. Therefore, this might suggest that the levels of abrasion are actually higher in bentonite+silica than the bentonite tests.

Furthermore, at +1 V overpotential, the bentonite+silica disc wear track also shows a severely abraded wear track (grooved) with the presence of numerous particle indents (relatively more than the corresponding bentonite test). This was probably due to the effect of increased bentonite particles entrainment in the contact, which was combined with the higher amount of entrained silica particles suspended in the mud. In addition, at this anodic overpotential, corrosion was also significant which could have contributed to the severity of the observed worn surface, by forming an iron oxide layer or by metal dissolution.

Higher magnification micrographs (x4000) of the bentonite+silica tests show clear evidence of formation of grooves at –1 V overpotential, whilst particle indents are seen prolific at +1

V overpotential (see Figure 5.10). These two distinct features might suggest that at –1 V, the predominant wear mechanism was two-body abrasion, whilst at +1 V more particle was entrained thus causing multiple indentation, in combination with grooving.

Visual observation of the discs at -1 V overpotential showed a relatively shiny disc. However, at more anodic overpotentials, corrosion was present along with the production of the mud cake which bear resemblance to the observations of the bentonite tests. These probably suggest that the presence of the silica particles did not cause any change to the electrochemical reactions. However, some significant differences are seen in the disc micrographs cf. the bentonite tests, which might suggest that the addition of the sand particles caused some change in the wear mechanism.

	Bentonite+silica Disc	**Bentonite Disc**
Cathodic (–1 V overpotential)	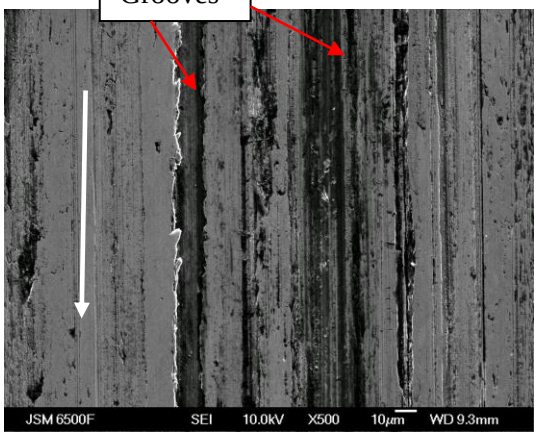	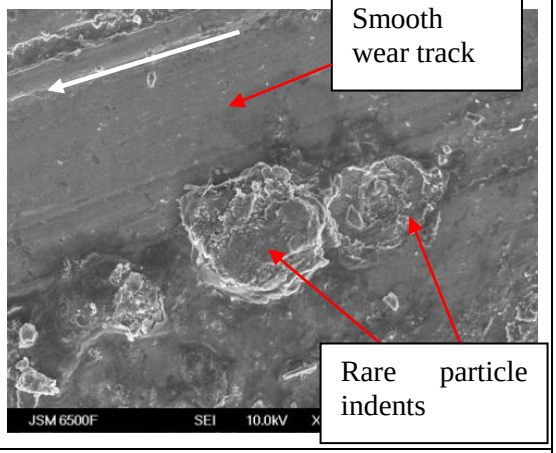
Anodic (+1 V overpotential)	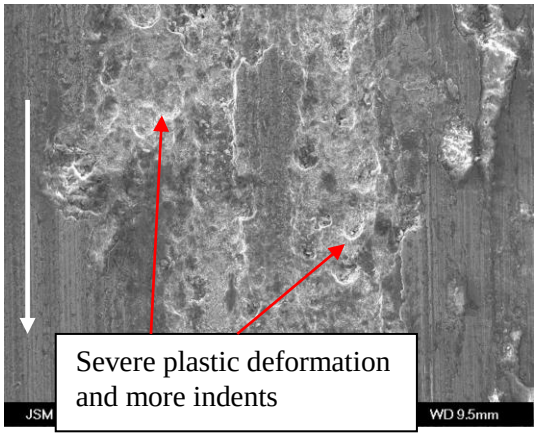	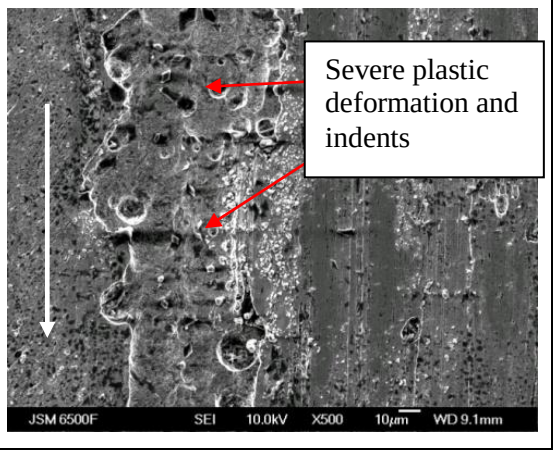

Table 5-6. SEM micrographs (x500) of the disc wear track tested in the bentonite+silica and bentonite mixtures. White arrows show direction of motion.

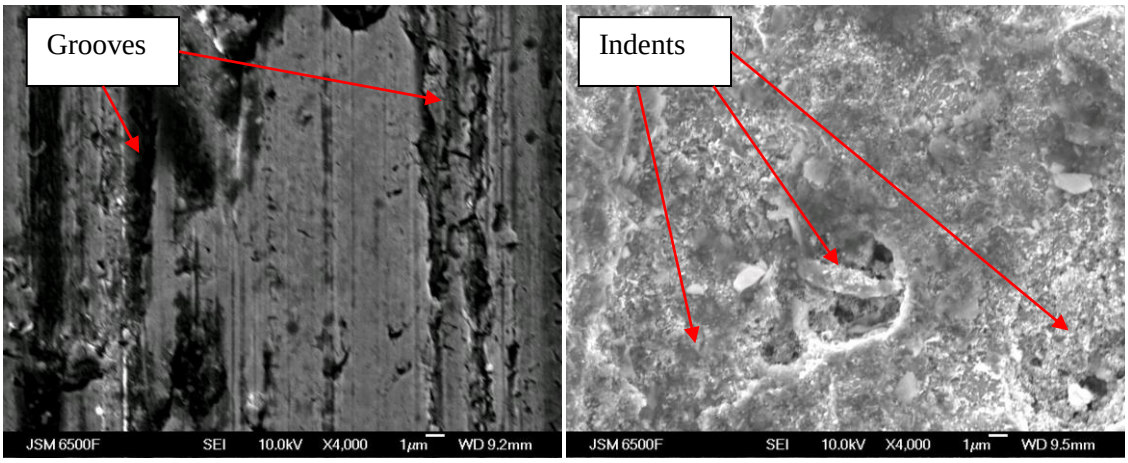

(a) (b)

Figure 5.10. SEM micrographs of the bentonite+silica disc wear tracks at higher magnification (x4000) of the (a) –1 V, and (b) +1 V overpotentials. These micrographs correspond to the items in column 2 of Table 5-6.

5.2.3.2 Mixture Consisting Bentonite and Silica Sand Particles with Addition of Octanoate Additive

This section will present the results of tests which were related to the formulation comprising both the bentonite and silica sand particles, with the addition of the octanoate additive, *i.e.*, bentonite+silica+octanoate. This adds to the previous discussions on the effects of employing the bentonite+silica drilling mud in the test procedures. As discussed earlier in this chapter, the octanoate additive could add beneficial characteristics to the solution being tested, therefore this section will explore the drilling mud incorporating this additive. It is worth noting that this formulation is the closest simulation to downhole conditions with regards to this project thus far. Namely, the simulation consists of the presence of viscosity enhancer (bentonite particles), friction modifier (octanoate additive), and the cuttings debris (silica particles).

The result of the presence of octanoate additive in the bentonite+silica+octanoate test, namely on the μ_{mean} *vs.* overpotential performance is shown in Figure 5.11. Generally, in contrast to the bentonite tests, it is evident that the dependence of friction on overpotential could be produced.

The trend line shows a transition from a high friction region at cathodic overpotentials to low friction region at anodic. This behaviour was similar to the results of the silica free mixture, *i.e.*, the bentonite+octanoate tests as discussed previously. This shows that the presence of octanoate additive could result in friction reduction regardless of any type of added particles

(combination of bentonite and silica sand). Therefore, it means that the tribofilm was effective in these conditions, in reducing particle abrasion and direct steel/steel contact. Furthermore, the similar trend was probably partly due to the inert silica sand particles which are insensitive towards the steel surface.

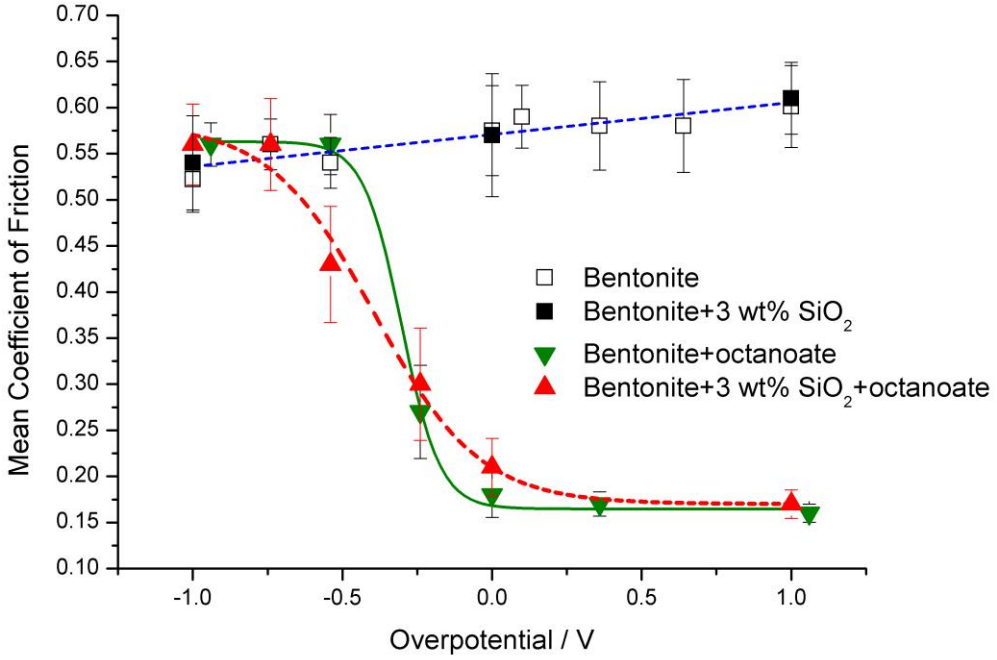

Figure 5.11. Mean μ *vs.* overpotential of experiments conducted in bentonite, bentonite+silica, bentonite+octanoate and bentonite+octanoate+silica tests.

The SEM micrographs of the pins and discs (x40 magnification) of the bentonite+octanoate+silica tests at –1, 0 and +1 V overpotentials are shown in Table 5-7. At –1 V overpotential, the pin generally has a slightly larger and more edged (less circular) wear scar compared with the other overpotentials tests (see column 2 in Table 5-7). Furthermore it shows evidence of adhesion in the wear scar, which is also seen in the disc wear track (see column 3 in Table 5-7). The reason is probably due to the direct steel/steel contact between the pin and disc, combined with the particle abrasion due to entrainment of both bentonite and silica sand particles.

At 0 V overpotential, the pin wear scar is relatively more circular shaped, and less evidence of adhesion was seen. Furthermore, the disc wear track shows grooves with very small amount of adhesion. These suggest the reduction of direct steel/steel contact and a lower level of particle abrasion, which was probably due to the production of an effective tribofilm on the surfaces.

At +1 V overpotential, evidence of adhesion on the pin wear scar is at its lowest. However, the general feature of the grooves is similar with the test at 0 V overpotential, and also gave similar values of μ_{mean}. This might suggest that the tribofilm's effectiveness is already at its best at 0 V overpotential, and application of +1 V only resulted in marginal improvements. This improvement, as discussed previously, might be due to a thicker or denser tribofilm produced.

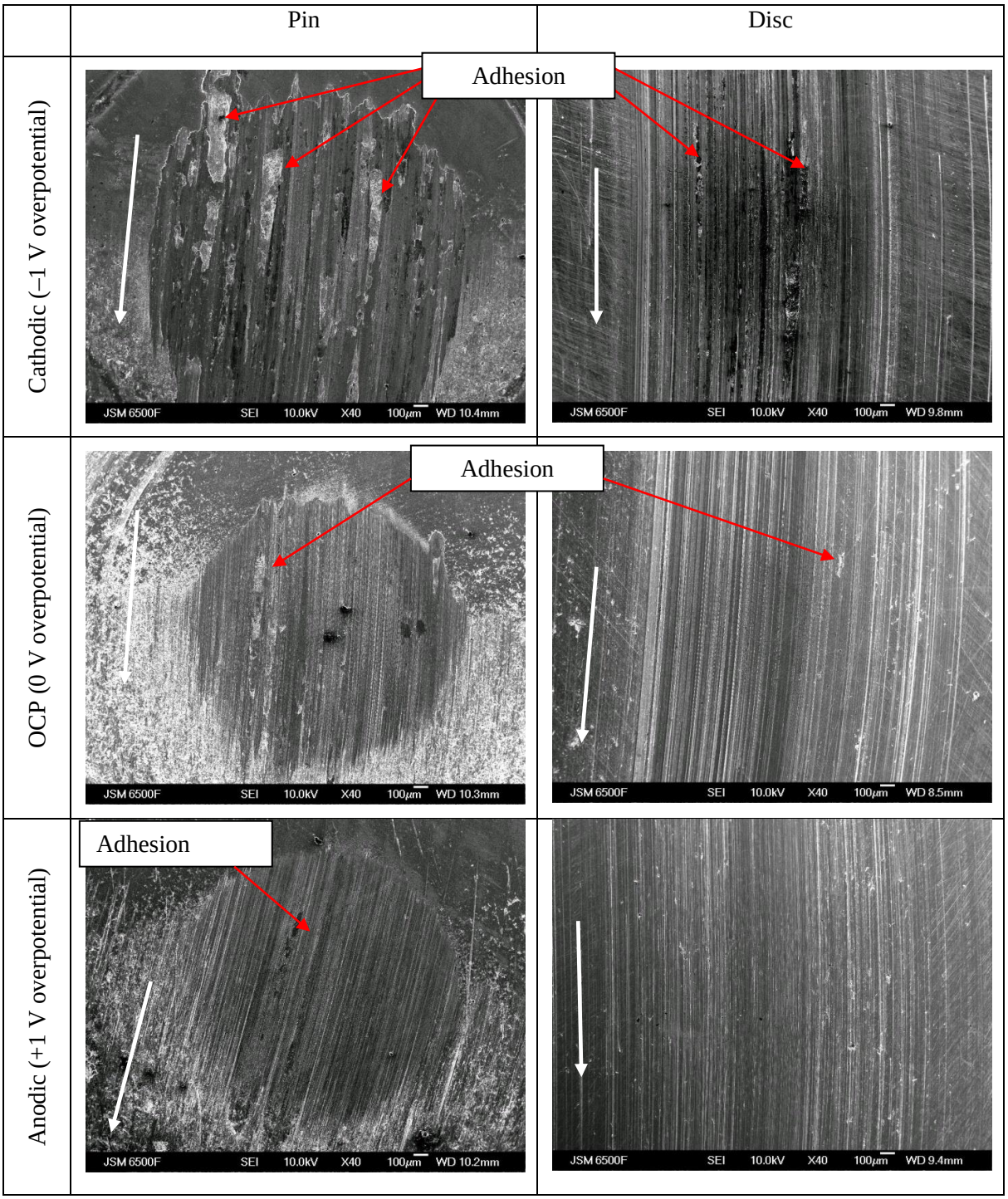

Table 5-7. SEM micrograph at low magnification (x40), of pin and disc samples tested in the bentonite+octanoate+silica mixture. White arrows indicate direction of motion.

The micrographs of the pin and disc samples shown previously in Table 5-7 were focused at higher magnification (x4000), and tabulated in Table 5-8. At –1 V overpotential, the pin wear scar surface shows a relatively rough texture compared with the disc wear track. This was probably due to the constant contact of the whole pin tip surface, whilst the disc only had small and localised contact, during the sliding test. Thus, it might have caused more

severe wear on the pin. Both the pin and disc showed evidence of grooves probably due to the abrasion of particles (two-body). These observations might suggest the unprotected sliding surfaces (by the tribofilm), thus caused the significant direct steel/steel contact and particle abrasion.

At 0 V overpotential, both the pin and disc show that generally there are reductions in the rough surface texture cf. the –1 V overpotential test. This might suggest less adhesion, due to the formation of the tribofilm. However, more grooves are seen in these micrographs which could have been revealed due to the smoother general texture. Furthermore, it might also suggest that since there was less adhesion between the steel surfaces, more sand particles could have been entrained in between the contact, but the friction was still low due to the tribofilm formation.

Finally, at +1 V overpotential, the pin and disc micrographs show the lowest amount of rough surface texture in this test set. Therefore, this might support that the formation of a thicker or denser tribofilm on the surfaces to increase the efficacy of reducing the direct steel/steel contact. Furthermore, the number of grooves has also increased, but they are mainly shallow which can be seen in between the larger ones. The reason for the increased amount of grooves might be explained in two ways, similar to the 0 V overpotential. Firstly, the smoother surfaces could have caused the presence of the grooves to be revealed, *i.e.*, more clearly seen cf. the case when the surface is rougher. Secondly, the number of entrained sand particles might have increased, although, the protection by the tribofilm was still effective.

In summary, it is seen that as the overpotential changed from –1 to +1 V, the pin wear scars and disc wear tracks show that there are reductions in the amount of rough features. This might suggest that less adhesion was produced in the contacts at more anodic overpotentials, which was probably due to the increased tribofilm effectiveness in reducing direct steel/steel contact, which agree with previous discussions using the baseline solutions. However, the effect of increased number of particles observed at more anodic overpotential is not understood clearly at the moment and remains as a hypothesis.

	Pin wear scar	Disc wear track
Cathodic (–1 V overpotential)	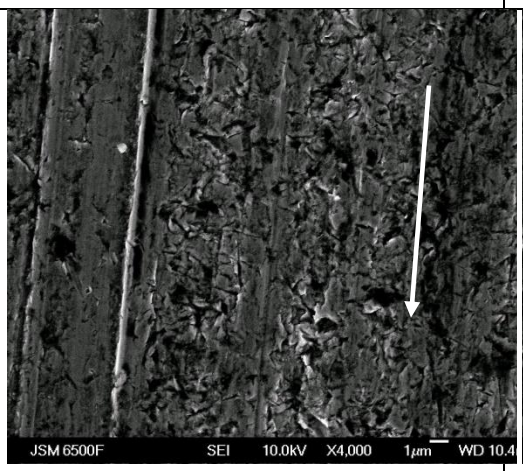	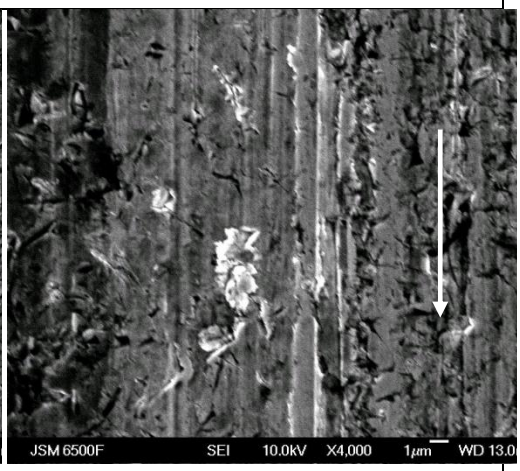
OCP (0 V overpotential)	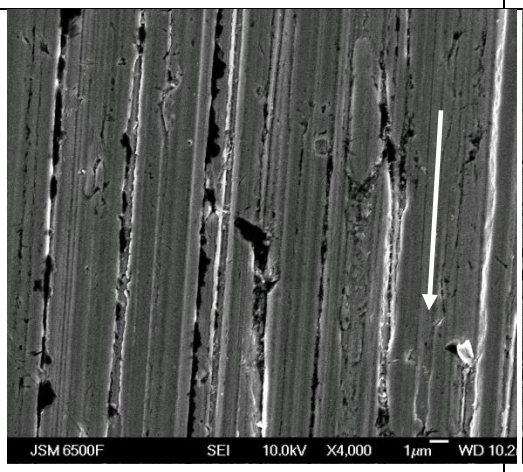	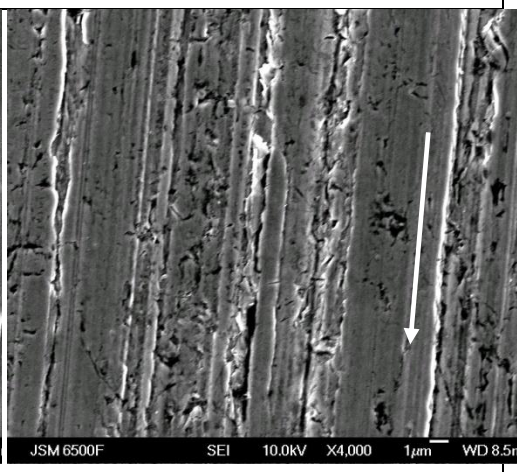
Anodic (+1 V overpotential)	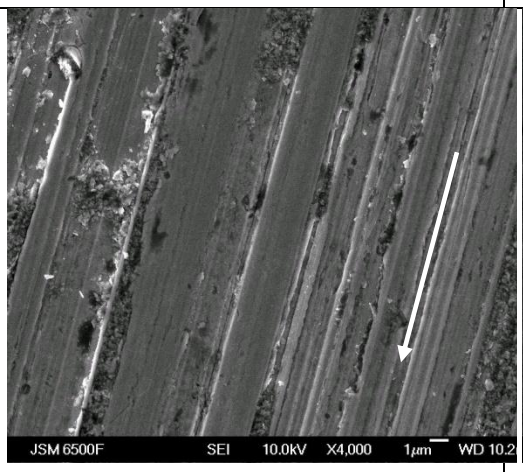	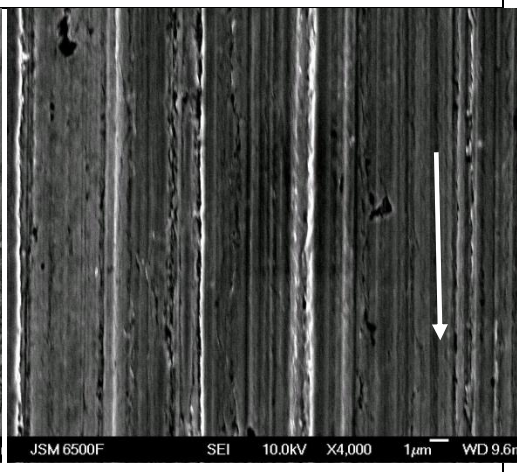

Table 5-8. SEM micrographs at higher magnification (x4000) of pin and disc samples tested in the bentonite+octanoate+silica mixture.

5.2.4 Summary of the Mechanisms of Contacts in the Bentonite Drilling Mud

Based on the discussions of the μ_{mean} *vs.* overpotential graphs, and corroborations from micrographs, a general understanding of the mechanisms involved in the contacts has been reached. Particularly, the contacts can be categorised into drilling mud with additive and without additive. Furthermore, these can be classified according to the overpotentials applied, *i.e.*, either cathodic or anodic.

The schematic of the contacts based on the friction and wear responses are shown in Table 5-9. The contact mechanism at cathodic overpotential is similar between the tests with or without the octanoate additive. This is due to the repulsion of the octanoate additive away from the surface to prevent the formation of a tribofilm. Furthermore, hydrogen evolution is likely on the surface, which was neither effective in causing a reduction nor an increase in friction. Wear of the cathodic samples were also seen to be low irrespective of the magnitude of the overpotential, although Akonko *et. al* [127] who used a pin-on-disc tribometer employing 304 stainless steel in 3.5 wt% NaCl reported that a higher cathodic potential could cause embrittlement of steel, thus resulting in higher wear.

However, at anodic overpotentials, a few key differences are seen in the contact mechanisms. In short, in the additive free contacts, the application of anodic overpotentials promotes the oxidating electrochemical reactions such as metal dissolution and metal oxide formation on the surfaces. This oxide film is not effective in providing boundary lubrication for separating direct steel/steel contacts. Furthermore, the amount of bentonite particles entrained in the contact will be increased, due the enhanced steel surface attraction with the negatively charged bentonite particles. In contrast, in the presence of the additive, the anodic electrochemical reactions are inhibited due to the adsorbed film (tribofilm). Therefore no corrosion was produced as verified by visual observation, *i.e.*, showing a relatively smooth surface. Furthermore, this will also reduce the entrainment of bentonite particles due to the absence of free surface charge to attract particles onto the steel surface.

The silica sand particles, however, are charge neutral and are not expected to exhibit charge dependency as the bentonite particles. However, the silica particles are mixed well with the bentonite drilling mud, therefore an increased amount of bentonite entrainment is likely to result in increased silica particle as well. This was shown previously in the micrographs, that the incorporation of silica particles caused the production of a relatively higher number of grooves within the wear scar and wear track, compared with the tests excluding the silica in the drilling mud. Although triboelectric charging could cause sand particles to attain

positive or negative charges, but it requires a broad distribution of sizes, such as found in sand storm and dust devils [128].

	Cathodic overpotential	Anodic overpotential
No additive	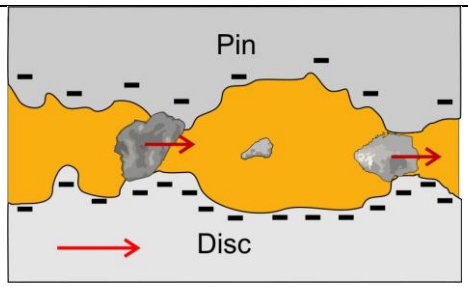	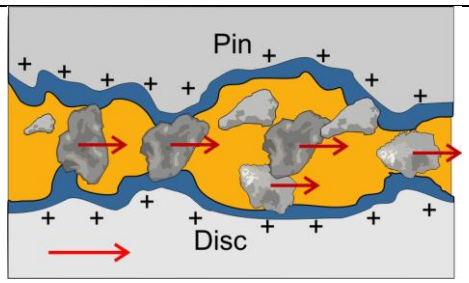
With additive	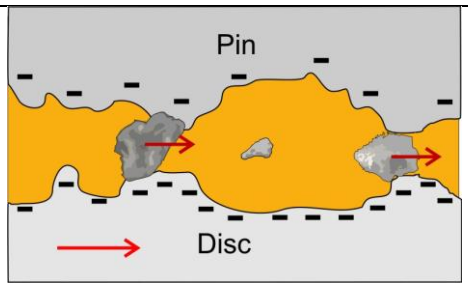	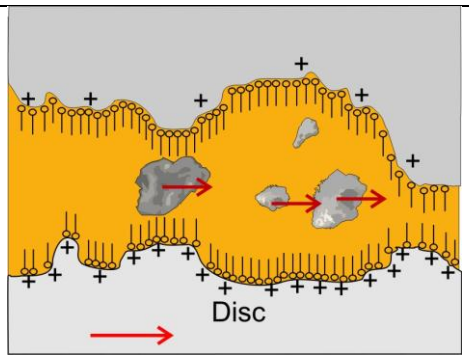

Table 5-9. Schematic of the contacts between the pin and disc at cathodic and anodic overpotentials for the no additive tests (bentonite and bentonite+silica), and the additive present tests (bentonite+octanoate and bentonite+silica+octanoate)

5.3 Polymer Drilling Mud

The polymer drilling mud offers an alternative to the bentonite drilling mud, which allows the achievement of a lower friction (thus lower torque and drag) during the drilling operations. The lower friction is probably due to the absence of abrasive particles cf. the bentonite drilling mud, amalgamated with the incorporation of various types of friction modifying additives. Therefore, the polymer mud was tested in this investigation, mainly by diluting a powder under the commercial name of Duovis, supplied by MI-Swaco, and further with the addition of the 60 mM octanoate additive. The viscosity of the mud has similar behaviour as the bentonite mud, in which the viscosity will decrease at elevated shear stress (shear thinning).

The effect of employing the polymer mud on the results of μ_{mean} vs. overpotential plot is shown in Figure 5.12. The lowest μ_{mean} of 0.20 in the polymer mud was found when the value of overpotential was at –1 V (most cathodic). The reason is not clear at the moment, since the composition of the polymer powder used to make the mud is unknown. It is known that polyglycol and fatty acid are constituent parts, but no details of which type and molecular weight. This trend is the opposite of the octanoate test, which gave the highest μ_{mean} at this overpotential. This shows that at more cathodic overpotentials, the polymer mud lubricity is enhanced, which was probably due to the production of a tribofilm in favour of the cathodic sites (for adsorption).

At more anodic overpotentials, the values of μ_{mean} increased gradually, and the highest μ_{mean} value is 0.37 at +1 V overpotential. It also gave the largest error bar in the polymer mud test set, thus indicating a higher friction perturbation. Visual observations showed that a deposit of green elastic material on the disc surface, probably due to the oxidised polymer mud. Furthermore, this deposit might have caused some impedance to the replenishment of mud into the contact, thus causing the higher friction. This μ_{mean} value is similar to the highest value in the octanoate test (which was at 0.39), suggesting a similar contact mechanism occurred in which no effective tribofilm was formed, *i.e.*, significant direct steel/steel contact between the pin and disc.

With the incorporation of the octanoate additive, friction was generally reduced, especially at more anodic overpotentials. This probably suggests that an octanoate tribofilm was formed during sliding. Furthermore, a similar trend was seen cf. the octanoate test, in which the highest friction was found at the highest cathodic and then gradually reduced as the overpotential became more anodic. However, the range of μ_{mean} in the polymer+octanoate test is between 0.27 and 0.14, which is smaller than the octanoate test which was between 0.39 and 0.15. This smaller range was probably due to the combined action of the lubricious

polymer mud with the octanoate additive, producing a better separation of the direct steel/steel contact in all cases. All of these suggest that the octanoate additive is effective in the polymer+octanoate mud, and that it inhibited the electrochemical reactions preventing oxidation such as those found in the polymer mud test without additive.

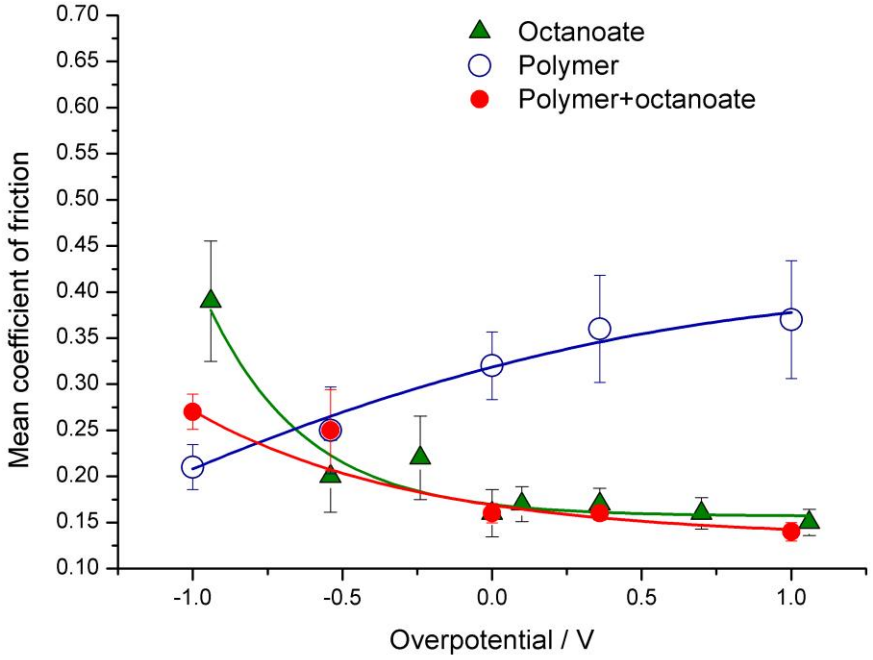

Figure 5.12. Mean μ *vs.* overpotential of experiments conducted in the Polymer solutions of steel/steel contact. Octanoate data is included from Chapter 4for comparison.

The micrographs of the disc wear tracks from the polymer mud tests (without additive) at –1 and +1 V overpotentials are shown in Table 5-10. At –1 V overpotential, the micrograph at x100 magnification shows that the wear track is lightly grooved with no signs of adhesion, which also gave the lowest friction as discussed previously. Delamination is not seen even at x500 magnification. This suggests that there was no severe direct steel/steel contact occurred, probably due to the formation of an effective tribofilm by any of the polymer mud's constituent which is unknown.

However, at +1 V overpotential, signs of adhesion were seen in the wear track, both at x100 and x500 magnifications. This contact also gave the highest friction in the previous discussion. This suggests that there was significant direct steel/steel contact. As discussed previously, the reason might be due to the oxidation of the polymer mud which impedes the flow of new mud in the contact, thus making the formation of a tribofilm difficult. Furthermore, it is also possible that the additive responsible for producing the tribofilm in the

polymer mud is repelled away from the contact. However, this explanation is not solid because there is not enough information regarding the polymer mud's constituent thus lack of verification.

	x100 magnification	**x500 magnification**
-1 V	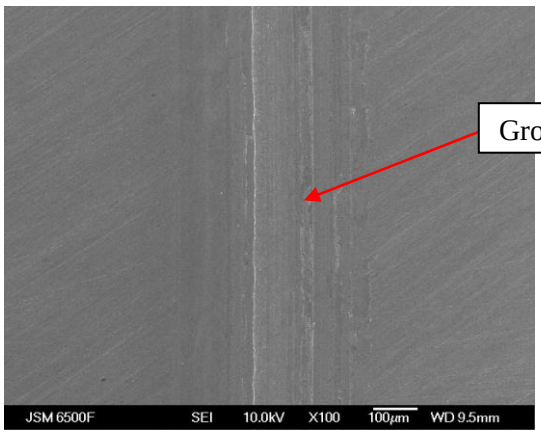	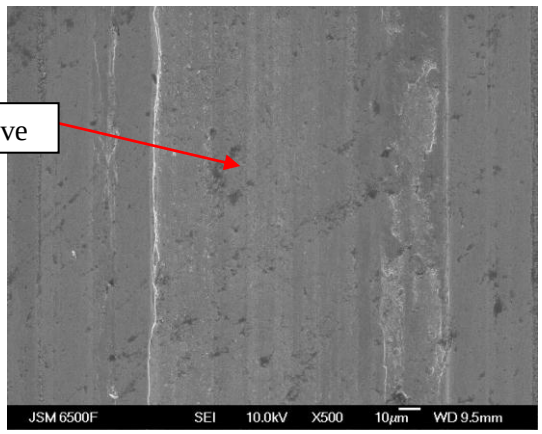
+1 V	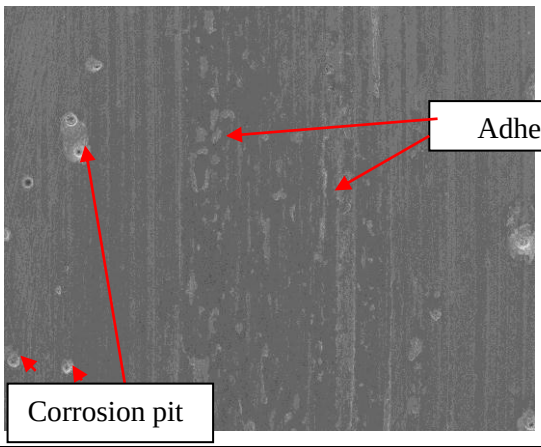	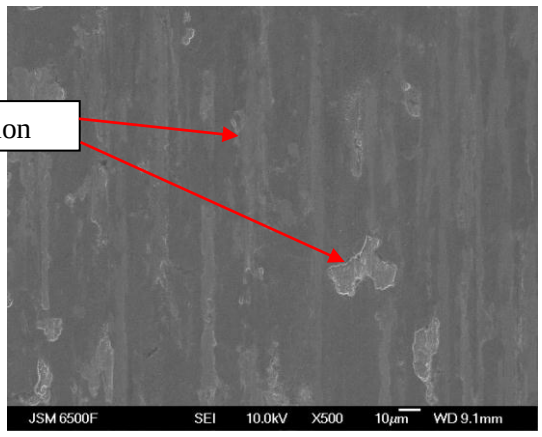

Table 5-10. SEM micrographs of the disc wear tracks in the polymer mud tests.

The SEM micrographs from the polymer+octanoate tests are shown in Table 5-11. At –1 V overpotential, the disc at x100 magnification shows a wear track which is relatively deep. Furthermore, the x500 magnification revealed that there was no delamination, despite the highest friction produced in the test set. The value of μ_{mean} was 0.27, which was higher than the polymer without additive test of the same overpotential *i.e.*, μ_{mean} at 0.20. This probably suggests that the formation of a tribofilm was not complete thus causing a small degree of direct steel/steel contact occurred.

Conversely, at +1 V overpotential, the disc wear track at x100 magnification shows that the wear track is less defined and is shallower than the –1 V test. The micrograph at x500 magnification also shows that the polishing marks from the preparation processes are still present, within the wear track. The lowest friction was also given in this contact condition

(μ_{mean} = 0.14). Therefore, this probably suggests that the octanoate formed an effective tribofilm to further separate direct steel/steel contact.

	x100 magnification	**x500 magnification**
-1 V	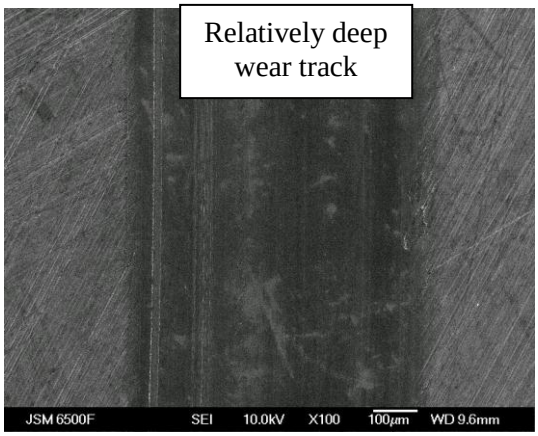	
+1 V	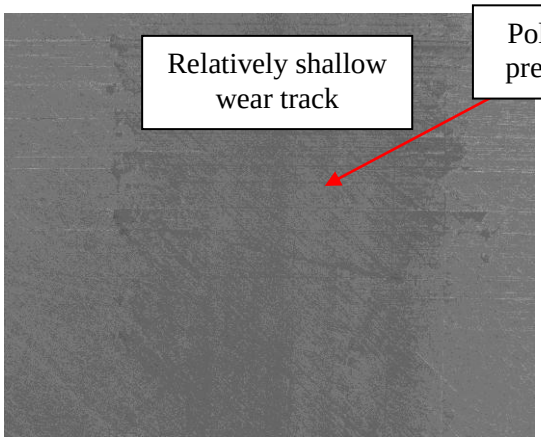	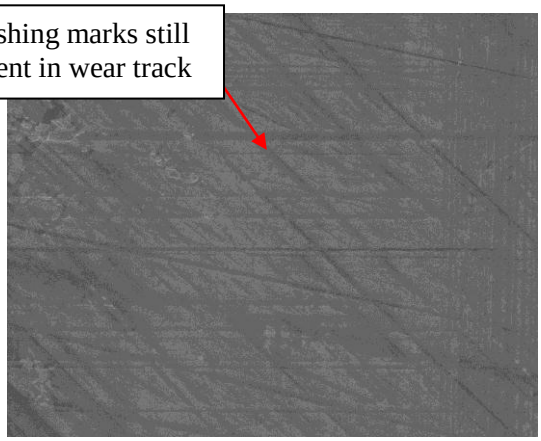

Table 5-11. SEM micrographs of the disc wear tracks in the polymer+octanoate mud tests.

5.4 Summary

iv. Investigation of the Bentonite Based Formulation

The bentonite drilling mud tests showed a weak dependence of friction on overpotential. Slightly lower friction was obtained at cathodic overpotential due to the repulsion of the bentonite particles from the contacting surfaces. Conversely, a slight increase in friction was obtained when anodic overpotential was applied due to the increased number of particle attraction and entrainment in the contact. However, the level of friction in this test set was considered high compared with the tests employing octanoate additive in the formulation.

When present, the octanoate additive reduced friction significantly in the drilling mud, especially when more anodic overpotentials were applied. This was believed because of the production of the tribofilm. Furthermore, the additive appears to mitigate the two-body abrasion of the bentonite and sand particles, seen by the decrease in the friction values and the reduction of the severity of the worn surfaces, which show the robustness of the formed tribofilm.

v. Investigation of the Polymer Based Mud Formulation

The polymer drilling mud produced lower friction than the bentonite counterpart, and can be further reduced by the presence of the octanoate additive, especially when anodic overpotentials were applied. This indicated that the adsorption film is also effective in the polymer fluid. The lowest friction of this test set was found when the highest anodic overpotential was applied, which was probably due to the synergistic action of the naturally lubricious polymer and the friction modifier (octanoate).

6 XPS Analysis of the Adsorbed Octanoate Additives

6.1 Introduction

Previously, Chapter 4 had presented the experimental results relating to the effects of applied overpotential on the friction and wear performance in the NaOH and octanoate test solutions. Therefore, this chapter intends to explain the mechanism of friction and wear reduction due to the octanoate adsorption, by characterising the chemical state of the tribofilm formed on the steel surface. Particularly, only the tests conducted in the baseline octanoate solution were employed in performing the XPS measurements. The other test solutions, such as the bentonite and polymer drilling mud (discussed in Chapter 5) were not assessed due to time as well as technical limitations because of the scans being carried out by an external body (Cardiff University).

This section (Section 6.1) will present brief information on the XPS equipment setup and the methods used to process the data. The subsequent sections will present the results of these analyses.

6.1.1 Size of Spot Scan

All the spot scan sizes were standardised to 700 µm diameter. This was primarily to allow accurate assessment of the ON wear track samples which were about 1 mm wide. Therefore, a smaller spot size would allow only the area within the wear track to be assessed.

6.1.2 Analysis of Data from the 45° and 90° Scan Angles

As discussed previously in Chapter 3, the sample surfaces were scanned at a direct angle and tilted, which corresponded to 90° and 45° respectively (with respect to the sample surface). This was to allow comparison between the detection of atoms at the adsorption film-substrate interface, and the atoms from the top layer of the adsorption film or the substrate itself.

6.1.3 Justification of the Use of Carbon, Oxygen and Iron in Analyses

The XPS measurement consisted of an initial broad inspection (survey spectra) of the ON and OFF wear tracks. The purpose was to detect all types of elements present on the surface, including any tribo species. Once that had been established, a graph of the intensity of all the detected elements could be plotted against the binding energy. Afterwards, only four

elements were chosen, namely carbon, oxygen, iron and sodium in which high resolution scans were conducted. The first three elements are important because both carbon and oxygen can be used to confirm the additive adsorption, while the iron can be used for supporting evidence. Sodium is considered as secondary information since it could not be used as a strong argument for explaining the effects of adsorption.

6.1.4 Qualitative and Quantitative Investigation of the Elements

The investigation of the elements obtained from the XPS measurements could be done either qualitatively or quantitatively. Qualitative involved the assessment of the intensity *vs.* binding energy graphs to identify any noticeable changes associated with the peaks (elements), from the samples at different overpotentials, which did not incorporate any calculations. This would allow a quick and general assessment of the trends of the elements with regards to changes with overpotential. In contrast, quantitative investigation refers to the assessment of the relative concentrations of the elements which were calculated from the raw data, *i.e.*, derived from the intensity *vs.* binding energy graphs. This would provide a better assessment of the small changes which occurred in the elemental concentrations.

6.2 General (Qualitative) Investigation of the ON and OFF Wear Tracks from the Survey Spectra

6.2.1 Assessment of the ON Wear Track for Evidence of Adsorption

6.2.1.1 90° Scan Angle

The XPS survey spectra of the ON wear tracks across the –1, 0 and +1 V overpotentials, from both the 90° and 45° scan angles are listed in Table 6-1. The 90° dataset (see column 2 in Table 6-1.) showed a noticeable increase in the intensities of the carbon peaks from –1 V to +1 V overpotential. This might be related to the increase in the amount of adsorption of the octanoate additive at more anodic overpotentials [112].

Similarly, the intensity peaks for sodium showed an increasing trend across the overpotentials, *i.e.*, it was absent at –1 V, but was present at 0 V and +1 V overpotentials (with a slightly higher peak at +1 V). The higher peaks of sodium and carbon at more anodic overpotentials might indicate the higher concentration of sodium octanoate (additive molecule).

However, no significant changes were observed in the oxygen peaks across the overpotentials. Similarly, there was no change in the trend of the iron peaks. Thus, a more thorough investigation of the oxygen and iron at 90° scan angle is essential for a complete understanding of the chemical nature of the surface, particularly in detecting any small changes in the concentrations. This can be done by quantifying their relative concentrations, and further examining the trends associated with these elements which will be presented later in this chapter.

6.2.1.2 45° Scan Angle

The 45° dataset (see column 3 in Table 6-1) shows that the survey spectra at –1 and 0 V overpotentials have lower signal-to-noise ratio (S/N), *i.e.*, larger noise, compared with their counterparts from the 90° dataset. Generally, the lower S/N was probably because of the lower emission angle due to the sample tilt angle of 45°, during the XPS measurement [129, 130]. However, at +1 V overpotential, the S/N seems to be similar between 45° and 90° despite the tilt angle, which was probably due to low surface roughness. The close relationship between surface roughness and levels of noise was demonstrated by Martín-Concepción *et. al* [130], who reported that a surface with lower roughness would yield higher S/N, *i.e.*, produce lower levels of noise. The reduction in surface roughness at more anodic overpotentials were probably due to the production of a more effective tribofilm, reducing direct steel/steel contact and adhesion.

Furthermore, within this 45° dataset, qualitative observations across the –1, 0 and +1 V overpotentials show that the S/N had increased gradually (steady reduction in the overall levels of noise). This trend might again be explained by the reduction in surface roughness of the wear track from –1 to +1 V overpotentials, which could be corroborated by the friction and wear performance as discussed in Chapter 4.

The individual elements carbon, oxygen and iron do not show any trends from –1 to +1 V overpotentials. However, the sodium peak is absent at –1 V, and were present at 0 V and +1 V overpotentials, which was also seen in the 90° dataset. The sodium trend might suggest an increase in detection of sodium octanoate molecules at more anodic overpotentials. However, it is difficult to ascertain this since the sodium peaks need to be correlated with the carbon peaks which on the contrary do not show any apparent trends.

Therefore, the lack of extractable information from this 45° dataset has led to further analysis of the ON wear tracks being focused on the 90° dataset only. In short, quantitative investigation of the individual elements of carbon and oxygen, which will be presented later, will account for the 90° dataset to allow a direct comparison with the results from the OFF wear track.

V	90° Scan Angle	45° Scan Angle
-1	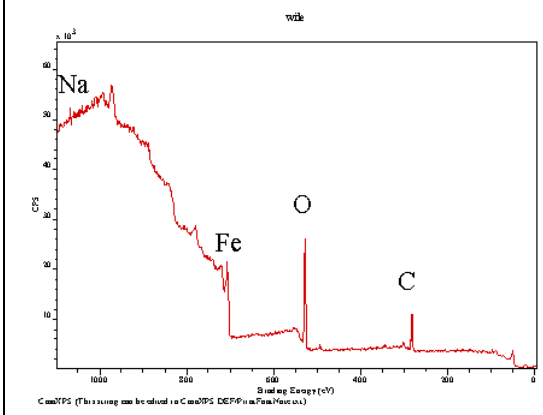	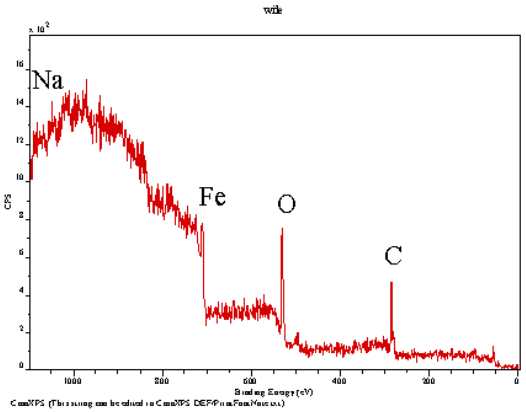
0	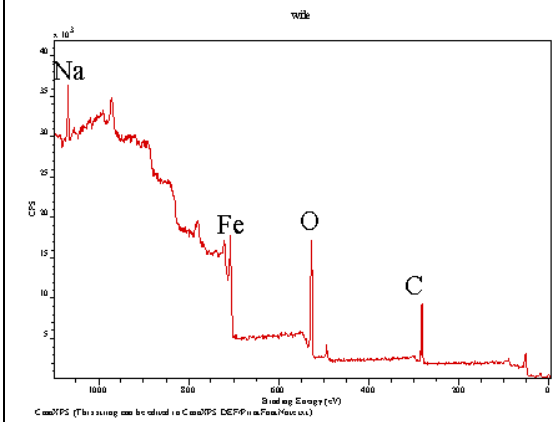	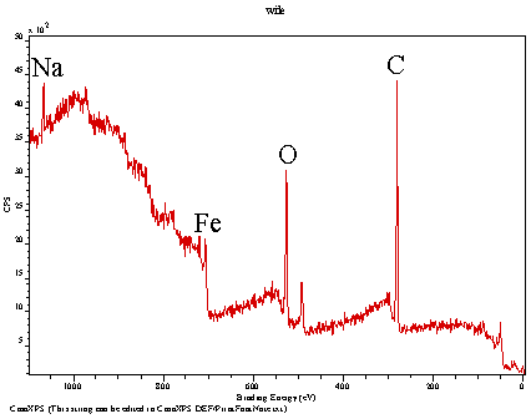
1	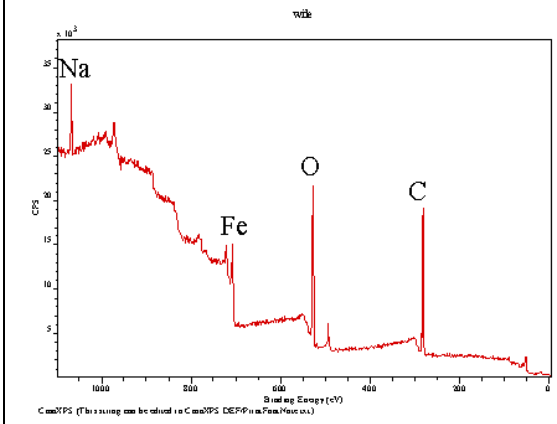	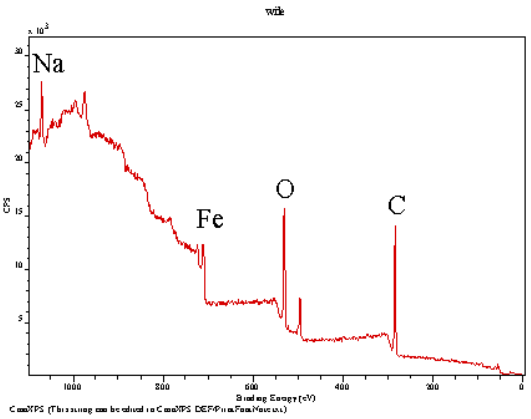

Table 6-1. XPS survey spectra of the inserts from the ON wear track conducted at -1, 0 and +1 V overpotentials, showing both datasets from the 90° and 45° scan angles.

6.2.2 Assessment of the OFF Wear Tracks for Supporting Information of Adsorption Film

The OFF wear track samples were analysed so that it could be used to obtain supporting information to aid the understanding of the behaviour of the octanoate tribofilm found ON the wear track.

6.2.2.1 90° Scan Angle

The XPS survey spectra of the OFF wear tracks across the –1, 0 and +1 V overpotentials, both from the 90° and 45° scan angles are listed in Table 6-2. The 90° dataset (see column 2 in Table 6-2.) showed a noticeable increase in the intensities of the carbon peaks from –1 V to +1 V overpotential. This might suggest the increase in adsorption of the octanoate additive OFF the wear track at more anodic overpotentials. Furthermore, this trend is similar to the ON wear track at 90°, as discussed previously. Therefore, this might suggest that the tribofilm formed on the whole surface, regardless of ON or OFF wear track, with an increase in thickness when more anodic overpotentials where applied.

No significant changes were observed in the oxygen peaks across the overpotentials. This behaviour was also seen in the ON wear track sample. Similarly, there was no change in the trend of the iron peaks. Therefore, a quantitative assessment of the data is required to detect any small changes. This could then be compared with the ON wear track results.

6.2.2.2 45° Scan Angle

The 45° dataset (see column 3 in Table 6-2) shows that there is no change with regards to the S/N across the –1, 0 and +1 overpotentials. In contrast, the ON wear track showed that the S/N was high at –1 V and decreased at +1 V overpotentials, as discussed previously. This was probably because of the relatively smooth surface area of all the samples due to the absence of mechanical sliding, thus allowing the conservation of the surface finish obtained during the preparation processes (polishing). Therefore, potentially there would have been less effect on the levels of noise, as were previously observed in the ON wear track cases.

Interestingly, the carbon peaks have an opposite trend compared with the 90° dataset, in which the intensities dropped gradually from –1 to +1 V overpotentials. Similarly, the oxygen peaks were also showing a decrease. There is no clear reason for this behaviour and will need to be incorporated into future work to fully understand the nature.

V	90° Scan Angle	45° Scan Angle
-1	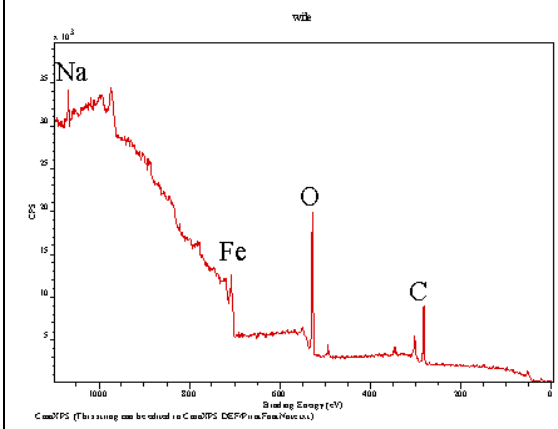	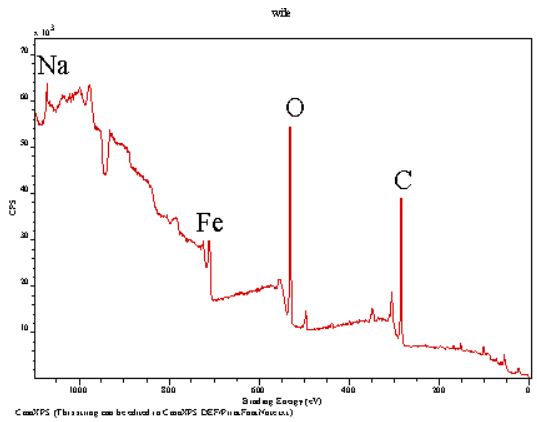
0	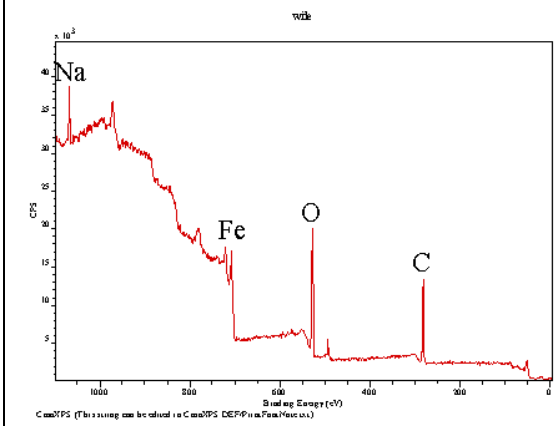	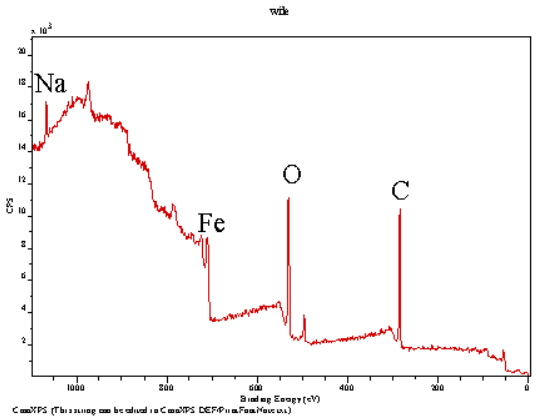
1	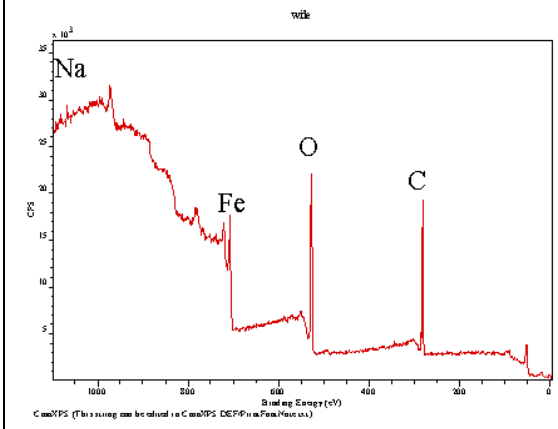	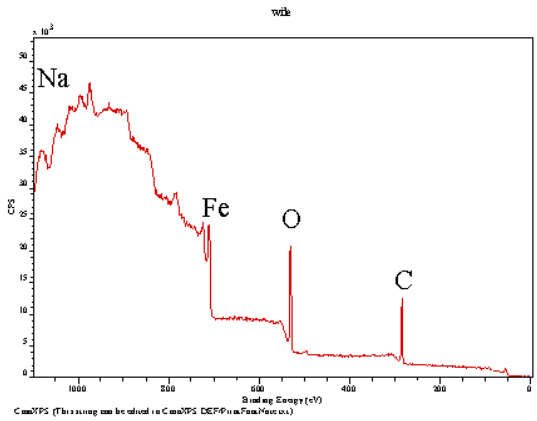

Table 6-2. XPS survey spectra of the inserts from the OFF wear track conducted at -1, 0 and +1 V overpotentials, showing both datasets from the 90° and 45° scan angles.

6.3 Quantitative Investigation of the Carbon and Oxygen from the Survey Spectra

The analytical software (Casa XPS) allowed the concentrations of the carbon and oxygen to be calculated by processing the survey spectra. Therefore, the relative concentrations were tabulated which consist of the data from the ON and OFF wear tracks, and across the –1, 0 and +1 V overpotentials. The following discussions will include only the 90° datasets due to the presence of trends in the dataset with respect to the change in overpotential, as discussed in the previous section. Furthermore, this will make comparing and contrasting less complicated, in order to study the behaviour of the octanoate additive at different overpotentials. The quantitative investigation of the carbon and oxygen will aid in a more accurate understanding of the surface phenomena, compared with the general qualitative investigation of the survey spectra as discussed in the previous Section 6.2.

The disc surface concentrations of carbon and oxygen are shown in Figure 6.1 (a) and (b), respectively. Generally, the trend of the carbon concentration (Figure 6.1 (a)) shows an increase from –1 to +1 V overpotential for both ON and OFF wear tracks. The carbon is believed to be detected from the adsorption film, therefore this trend might suggest that the adsorption of the additive increased [82, 112] as the overpotential was more anodic (positive). This confirms the observation during the qualitative investigation, in which an increase in the peak of carbon was seen at more anodic overpotentials. Thus, a further investigation could be conducted by examining the high-resulotion spectra of the carbon element which will be presented in the next subsection (Subsection 6.4.1). This examination would allow some insight into the probable arrangement type of the additives on the surface.

The general trend of the oxygen concentration is the opposite of the carbon, for both the ON and OFF wear tracks, showing a decrease in the concentration from –1 V to +1 V overpotential (see Figure 6.1 (b)). This trend might suggest that generally, the formation of iron oxide was stifled at more anodic overpotentials both ON and OFF wear tracks, due to the increased adsorption of the octanoate additive. However, ON the wear track, the concentrations were slightly higher than the OFF wear track at –1 and 0 V overpotentials, but was lower at +1 V. This probably suggests that the adsorption of octanoate additive ON the wear track increased, *i.e.*, tribo-enhanced, at +1 V overpotential, which resulted in the lower iron oxide layer formation.

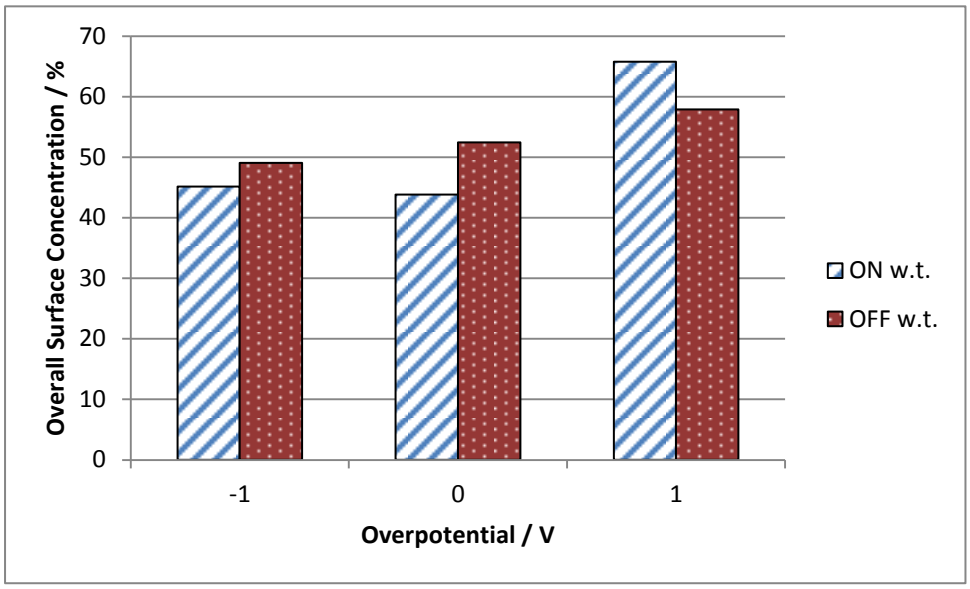

(a)

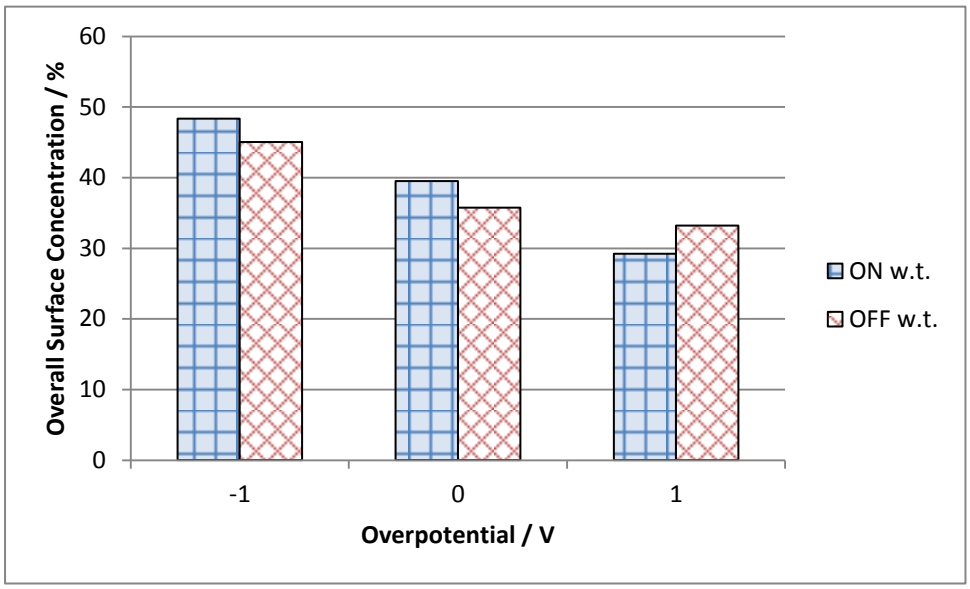

(b)

Figure 6.1. The concentration of the (a) carbon and (b) oxygen with respect to the other scanned elements, namely Fe and Na. The plotted results are from the inserts ON and OFF wear track at –1, 0 and +1 V overpotentials.

6.4 Examination of the High Resolution Spectra

Investigation of the effects of octanoate additive adsorption on steel has so far concentrated on the analysis of the survey spectra. Thus, an in depth analysis of the high resolution spectra, namely of the carbon and iron would allow supporting evidence for the results obtained previously. The reason for assessing the high resolution spectra of carbon is because the spectra can be easily deconvoluted to show different chemical states. Furthermore, the iron would allow the assessment of the nascent steel surface, and whether if there was any adsorption or not.

6.4.1 Quantitative Investigation of the Carbon from the High Resolution Spectra

To further investigate the evidence of adsorption, carbon can be divided into the ones detected from the hydrocarbon chain (C–C peak at 284.1 eV); and from the functional head group (C–O and C=O peaks at 288.0 eV and 290.2 eV respectively). This data is shown in Figure 6.2 (90° dataset only). At –1 V overpotential, and for both ON and OFF wear tracks, the carbon from the hydrocarbon chains (front row) gave a minimum, corresponding to the maximum in the detection of the functional group (back row). Furthermore, at this overpotential, the highest friction was obtained in the sliding tests. Alternatively, at +1 V overpotential, the alkyl chain detection was at the maximum while the functional head group was at the minimum, which also gave the lowest friction in the sliding test.

Therefore, these findings suggest that there might be a correlation between the distribution of the carbon detected from the functional and chain groups with the friction and wear response. To explain the link of these XPS findings with the tribological response, the discussion can be based on the possible arrangements of these molecules when adsorbed onto the steel surface. In particular, it is known that a closely-packed and ordered arrangement is essential for low friction and wear reduction [74], thus the following discussion will be related to this point of view.

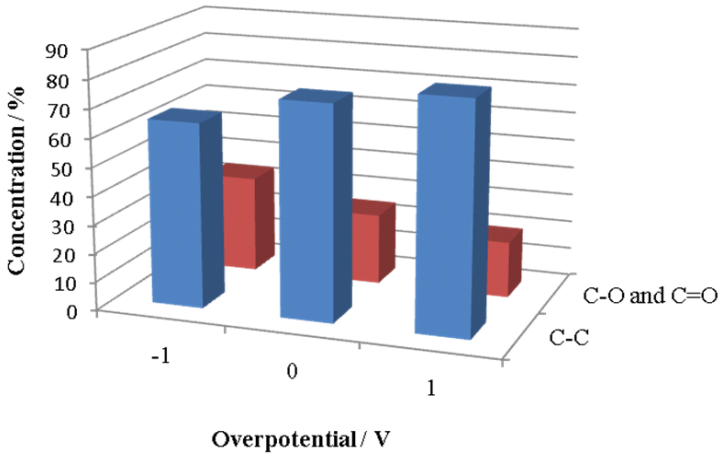

(a)

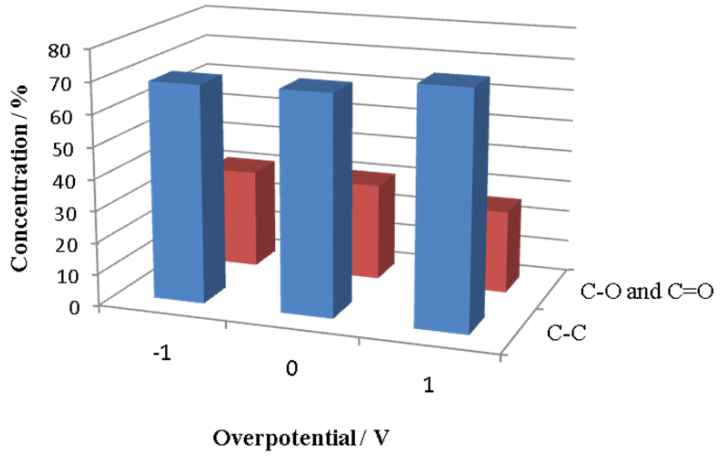

(b)

Figure 6.2. Surface carbon concentration on the disc at –1, 0 and +1 V overpotentials from (a) ON and (b) OFF wear track. The carbon assigned to functional groups are denoted by C–O and C=O; while hydrocarbon chains denoted by C–C.

Therefore, it is probable that the octanoate additive, although not entirely repelled from the surface, constitutes an adsorption film which is loosely packed and disordered at –1 V overpotential, as schematically represented in Figure 6.3 (a). This is due to X-ray penetration through the adsorption film and exciting high amount of core electrons from the carbon in the functional group.

However, a more densely packed and ordered adsorption film such as illustrated in Figure 6.3 (b) would probably mean that the X-rays would mostly excite the core electrons from the carbon in the hydrocarbon chain. Thus resulting in a higher proportion of carbon originated from the chain to be detected. Therefore, a this arrangement is believed to be the possible explanation supporting the low friction contacts at more anodic overpotentials. This is in agreement with Duffy *et. al* [74] who reported the formation of islands of iron octanoate.

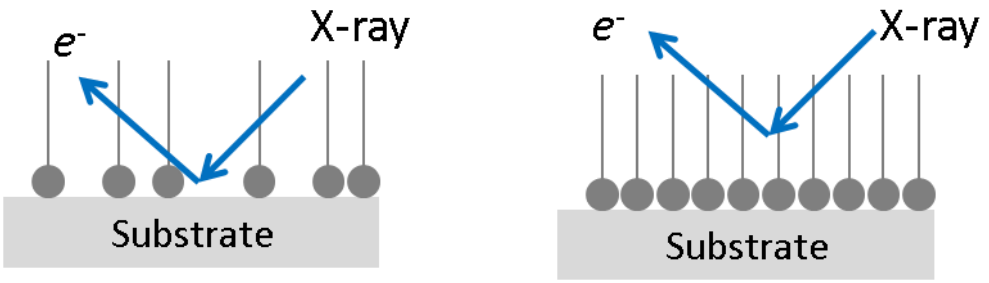

(a) (b)

Figure 6.3. Schematic of the adsorbed molecule arrangement showing (a) loosely packed and (b) densely packed which produced the high and low friction respectively.

6.4.2 Qualitative Investigation of the Iron from the High Resolution Spectra

The high resolution spectra of the iron from the 90° dataset comprised of more peaks compared with carbon. Therefore, it was not easily deconvoluted into separate peaks and made discrimination of the chemical state of the iron atoms difficult. Therefore, the high resolution spectra of iron could only be assessed qualitatively. Hence, Figure 6.4 shows a collection of the high resolution spectra of the iron elements from the ON and OFF wear tracks, and with an arrow pointing to the peak corresponding to the detection of bare iron (Fe^0). It is clear that for the ON wear track, the height of the bare iron peaks were diminishing from –1 V to +1 V overpotential. This can be a supporting argument for the increased adsorption of the octanoate additive at more anodic overpotentials, consequently coating the surface. This is in agreement with the previous discussions in this chapter, especially in the trend of carbon atoms which suggested an increase in the number of octanoate adsorption at more anodic overpotentials.

However, OFF the wear track, the difference was not as dramatic across the overpotentials, probably due to the absence of mechanical interference. For example, at –1 V overpotential (Figure 6.4), the ON wear track registered a higher Fe^0 peak compared with the OFF wear track. Initially, both the ON and OFF wear tracks would have similar levels of Fe^0, but the mechanical sliding had removed a thin adsorption or oxide layer and exposed the nascent steel surface ON the wear track (hence increased Fe^0 peak). However, the Fe^0 peaks OFF the wear track showed a reduction at +1 V overpotential, as was found ON the wear track, which might suggest a higher adsorption of octanoate coating the surface. Generally, these behaviours probably show that the ON and OFF wear tracks had almost similar reactions with the application of overpotential, *i.e.*, increased amount of octanoate adsorption at more anodic overpotentials. However, the presence of sliding ON the wear track might have caused some changes to the physical and chemical state of the surface (such as the removal of oxide layer or small amount of adsorbed octanoate).

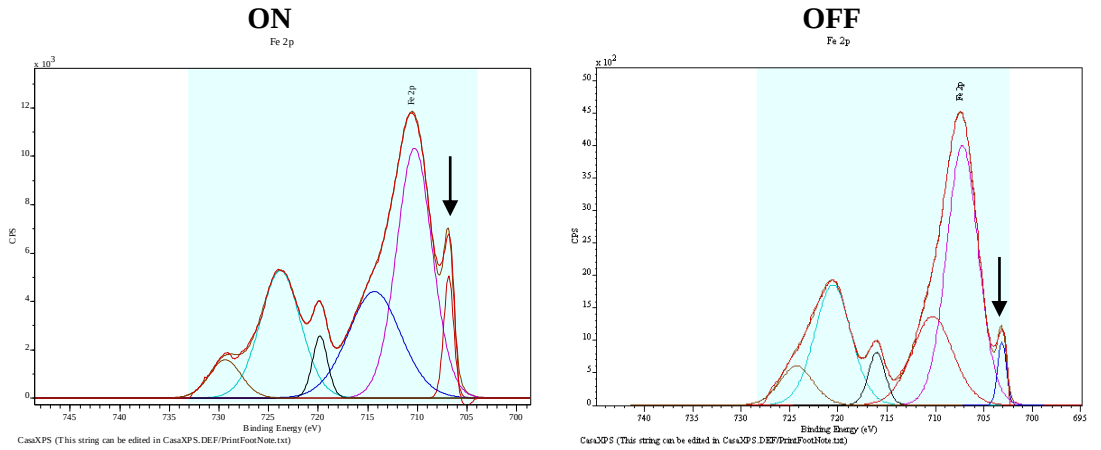

(a) - 1 V overpotential

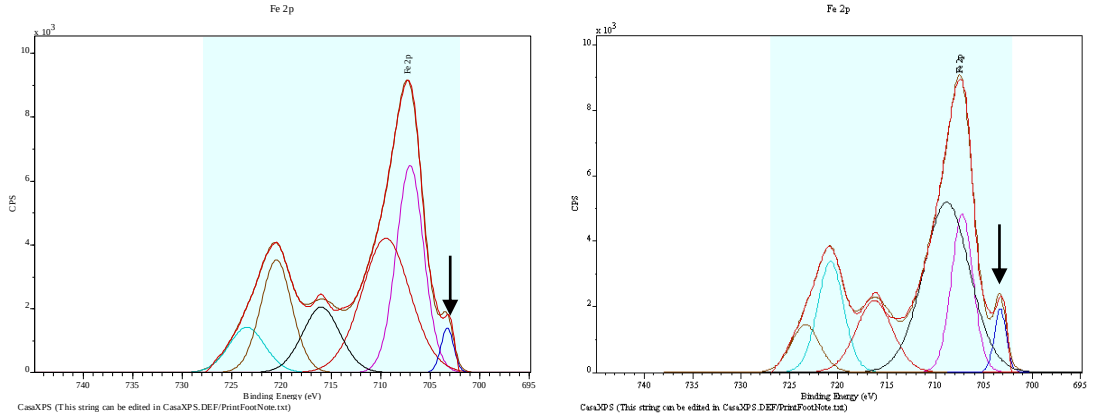

(b) 0 V overpotential

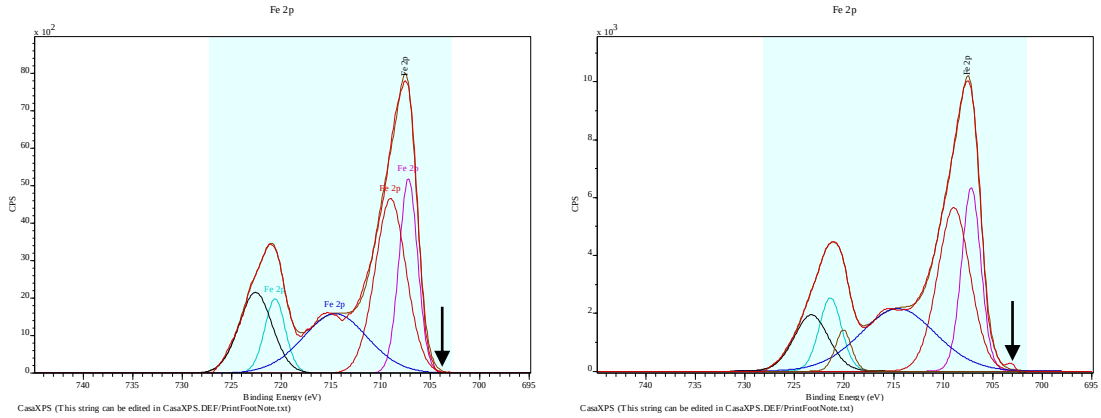

(c) +1 V overpotential

Figure 6.4. High-resolution XPS spectra of the oxygen element at (a) –1 V, (b) 0 V, (c) +1 V overpotentials, ON and OFF wear track insert. The arrow indicates the peak corresponding to the detection of bare iron (Fe^0).

6.5 Summary

Detailed analysis of the survey spectra revealed that only the set of scans conducted at 90° angle were able to provide insightful illustrations of the trends in carbon, iron, sodium and oxygen. The reason could be due to the sensitivity of the XPS equipment, in which a 45° scan would have resulted in the detection of mostly the atoms on the top layer of any sample, thus overlooking the interface between the adsorption film and the substrate [131].

Analysis of the surface carbon and oxygen concentrations of the ON and OFF wear track surfaces provided a good indication for the adsorption of the octanoate additive, forming an effective tribofilm. In brief, the relative concentration of carbon was seen to increase at more anodic overpotentials, suggesting a higher amount of octanoate adsorption. Furthermore, this correlates with the reduction in oxygen concentration at more anodic overpotentials suggesting lower oxide layer formation due to the inhibition by the adsorbed octanoate additive.

Furthermore, detailed analysis of the distribution of the carbon atoms (from the high resolution spectra) either as the hydrocarbon chain or functional head group assisted in hypothesising on the type of arrangement of the additives, which influenced the tribological phenomena. It was hypothesised that a loosely packed and disordered octanoate adsorption was formed at cathodic overpotentials, in contrast to a more densely packed and ordered adsorption film at more anodic overpotential forming a more robust tribofilm.

Finally, the supporting points from the iron element analysis agree with the carbon and oxygen discussions and provided an additional indicator of adsorption. Particularly, this was shown through the reduction in the detection of bare iron at more anodic overpotentials due to the surface probably being coated by the octanoate additive (tribofilm).

All of these were in agreement with the previous discussions in Chapter 4 – Steel / Steel Contacts in Baseline Solutions, and helped especially in understanding the mechanism of friction and wear reduction obtained by incorporating the octanoate additive.

7 Steel / Sandstone Contact

7.1 Introduction

This chapter presents the pin-on-disc test results conducted mainly by employing the steel/sandstone contact couple, as opposed to steel/steel, which was the focus of the previous chapters. The steel/sandstone simulates the contact between the drillstring and the rock formation during the open-hole drilling process. The sandstone materials were provided by Schlumberger.

The NaOH and bentonite drilling mud where chosen as the lubricants and were briefly tested to obtain baseline data. Furthermore, the bentonite+octanoate (bentonite drilling mud with octanoate additive) was tested in order to assess the reproducibility of friction control by applying potentials. These three lubricants were chosen due to limitations to the number of available sandstone samples for testing.

The types of contact arrangements were sandstone pin *vs.* steel disc and vice versa, *i.e*, steel pin *vs.* sandstone disc. The former arrangement simulated the sliding motion between a rotating drillstring against the formation wall, in which the steel observes intermittent contact area whilst the formation observes a continuous contact (see Figure 7.1). The latter arrangement was aimed at assessing the readsorption effect on steel, when subjected to a continuous contact, as opposed to intermittent where the tribofilm could reform prior to the subsequent contact. This was due to the assumption that adsorption forms only on the steel surface.

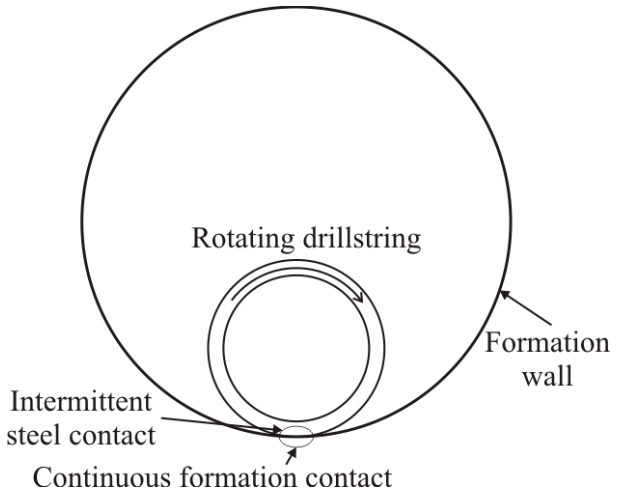

Figure 7.1. Schematic of the sliding contact between a rotating drillstring and the formation wall, showing the area where the steel is subjected to intermittent contact, whilst continuous on the formation.

Application of ±1 V overpotentials were made on the steel sample in each case (either steel disc or steel pin). Therefore, the effects of applying potential onto the static steel pin, or rotating steel disc were assessed, particularly in the performance of friction and wear, and whether the octanoate additive could be controlled in either case. Other test procedures such as the sliding velocity and normal load were similar to the steel/steel couple tests.

7.2 Sandstone Pin / Steel Disc Arrangement

The results of the sandstone pin/steel disc couple in NaOH, bentonite and bentonite+octanoate are shown in Figure 7.2. The bentonite drilling mud showed a linear increase of μ from –1 to +1 V overpotentials, which was similar to the trend found in the steel/steel contact. Visual observation of the disc surfaces after testing at –1 V overpotential showed no evidence of corrosion and some presence of bubbles in the mud, believed to be hydrogen gas which was generated by the cathodic potential at the steel surface (see eqn. 2.8 in Chapter 2). This would have resulted in a change in the pH of the drilling mud which can have an undesirable effect on the suspended bentonite, thus changing the viscosity. Furthermore, in service, the high concentration of hydrogen gas might cause an increase in tool corrosion and failure downhole, such as hydrogren embrittlement [12, 59]. These effects are being ignored at the moment in light of establishing the behaviour of these additives at different overpotentials. However, the disc at +1 V overpotential showed that there was a formation of thick mud cake (around 5 mm), due to agglomeration of the bentonite particles which could have caused the increase in friction. Corrosion products were also found on the disc as thin black deposits, underneath the mud cake.

For the bentonite+octanoate test, the range of μ_{mean} was between 0.90 and 0.27, at –1 and +1 V overpotentials respectively. This range was generally larger than the steel/steel contact type as discussed in Chapter 5, *i.e.*, between 0.56 and 0.16. The highest μ_{mean} value was similar to that obtained for NaOH at 0 V overpotential. This suggests that for the cathodic overpotential the octanoate additive was repelled from the surface in the bentonite+octanoate, leaving surface unprotected from the direct contact between steel and sandstone. This can also be seen in the SEM micrograph of the disc samples of the bentonite+octanoate, shown in Table 7-1. The surface of the disc at –1 V overpotential was apparently rougher than at 0 and +1 V overpotential, probably due to the direct contact between the pin and disc combined with high levels of particle abrasion.

The bentonite+octanoate showed that application of anodic overpotentials resulted in markedly lower friction. The lowest μ of 0.19 was found when +0.36 V overpotential was

applied, followed by 0.27 at +1 V overpotential. This was the opposite of what was expected and may be due to the slight variation in the fabrication of the sandstone pin. Nonetheless, these values were smaller than at 0 V overpotential (μ_{mean} = 0.32) and also had smaller error bars (more stable friction perturbations during sliding), indicating the formation of a more robust tribofilm.

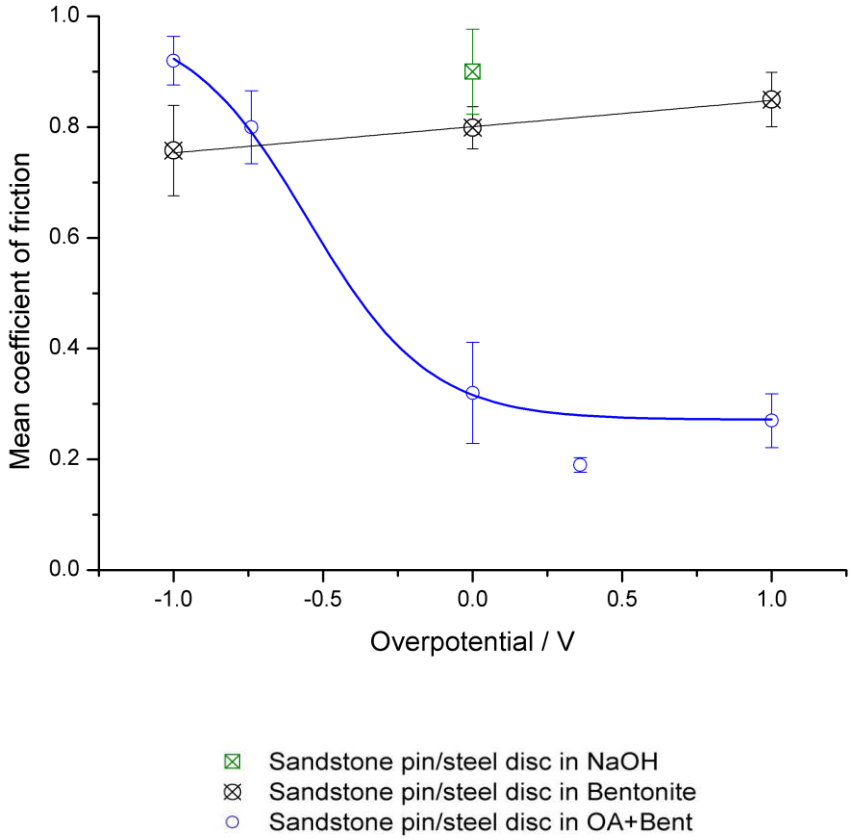

Figure 7.2. Mean coefficient of friction *vs.* overpotential for the sandstone pin/steel disc couple in the NaOH, bentonite and bentonite+octanoate test solutions.

Overpotential / V	SEM micrograph of steel disc surfaces
–1	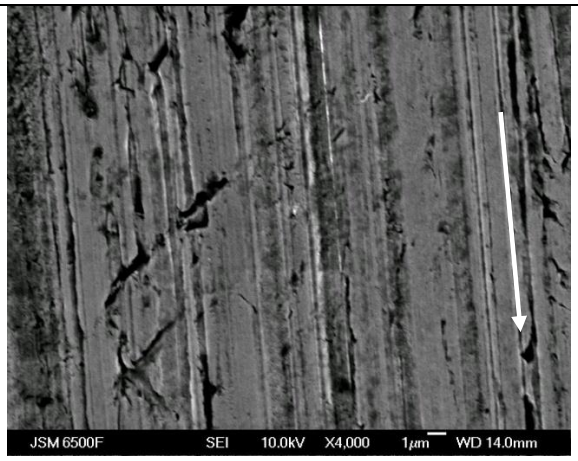
0	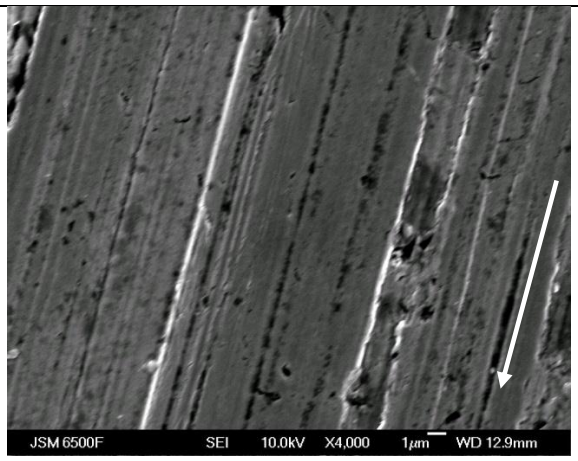
+1	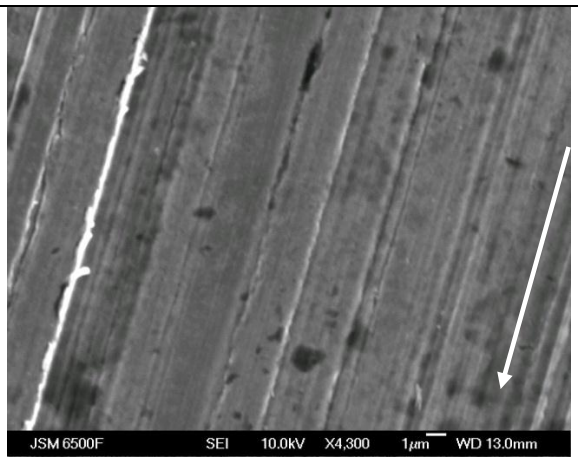

Table 7-1. SEM micrographs (x4000) of the disc surfaces at –1, 0 and +1 V overpotentials for the sandstone pin/steel disc couple in bentonite+octanoate. The white arrows indicate the direction of disc motion.

The wear rates of the sandstone pins in the bentonite+octanoate are shown in Figure 7.3. These pins had wear rate values within the order of 10^{-14} mm^3 N^{-1} m^{-1}, which were higher than the steel pin counterpart in the steel/steel contact type, by an order of magnitude (see Chapter 5). The reason is probably due to the constant shearing action of the sandstone pin tip, which was in contact with the steel disc. This is because generally, sandstone has a relatively low shear strength (around 3 MPa) owing to the microstructure of the sandstone grains, which caused the high material removal during the sliding test [8, 132]. There is a trend of increasing pin wear rate at more anodic overpotentials, in which the reason is not clear. However, the values were within the same order of magnitude, which might suggest that the change is not significant.

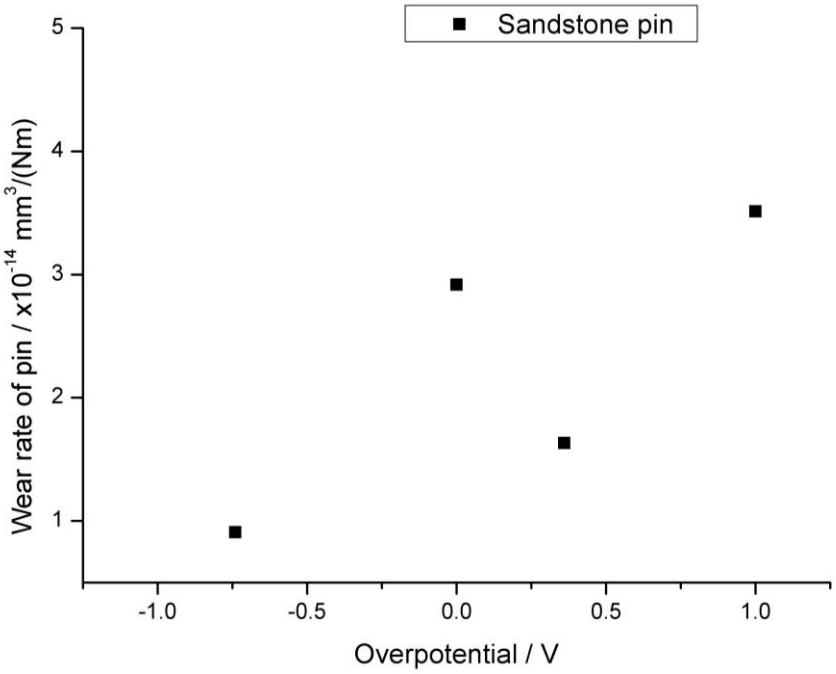

Figure 7.3. Specific wear rates of the sandstone pins sliding against steel discs in bentonite+octanoate, calculated by the geometrical method.

The mechanism of contact in the sandstone pin/steel disc arrangement is shown in Figure 7.4. At cathodic overpotentials, direct contact occurs between the asperities of the sandstone pin and steel disc, which causes high friction (see Figure 7.4 (a)). On the contrary, at anodic overpotentials, an octanoate adsorption film forms on the steel disc, therefore reducing the direct contact of the asperities, hence the reduction in friction (see Figure 7.4 (b)). It is assumed that the adsorption fim, or tribofilm, does not form on the sandstone surface, which might explain the generally higher friction levels compared with the steel/steel couple presented in Chapter 5. In the steel/steel contact, the tribofilm can form on both the surfaces of pin and disc, causing a more effective lubrication.

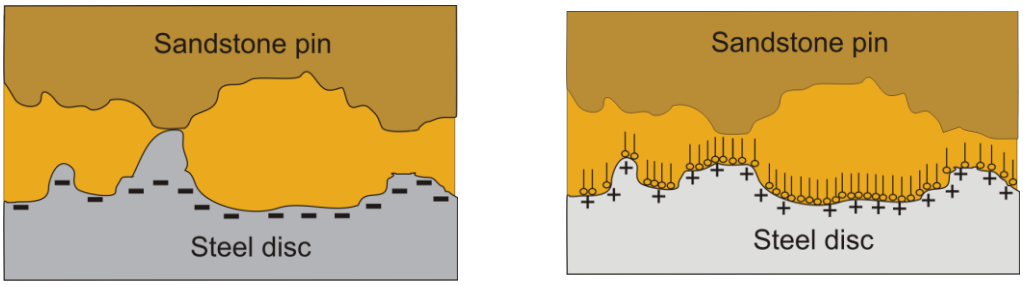

(a) (b)

Figure 7.4. Schematic of the mechanism of contact in the sandstone pin/steel disc contact at (a) cathodic, and (b) anodic overpotentials where the tribofilm was formed.

7.3 Steel Pin / Sandstone Disc Arrangement

The results of reversing the contact arrangement to steel pin/sandstone disc in the bentonite+octanoate are shown in Figure 7.5, superimposed onto the previous results. The trend of friction for steel pin/sandstone disc was similar to the previous sandstone pin/steel disc contact arrangement. However, the range of μ has shifted to between 0.60 and 0.20 (reduction from between 0.90 and 0.27). The explanation for the reduction in the trend was probably due to the steel pins producing wear debris which were relatively soft, and might deform easily, cf. the sand debris produced by the sandstone pins. Therefore, this would have probably caused a less severe two-body abrasion in the contact (details will be discussed later in this section).

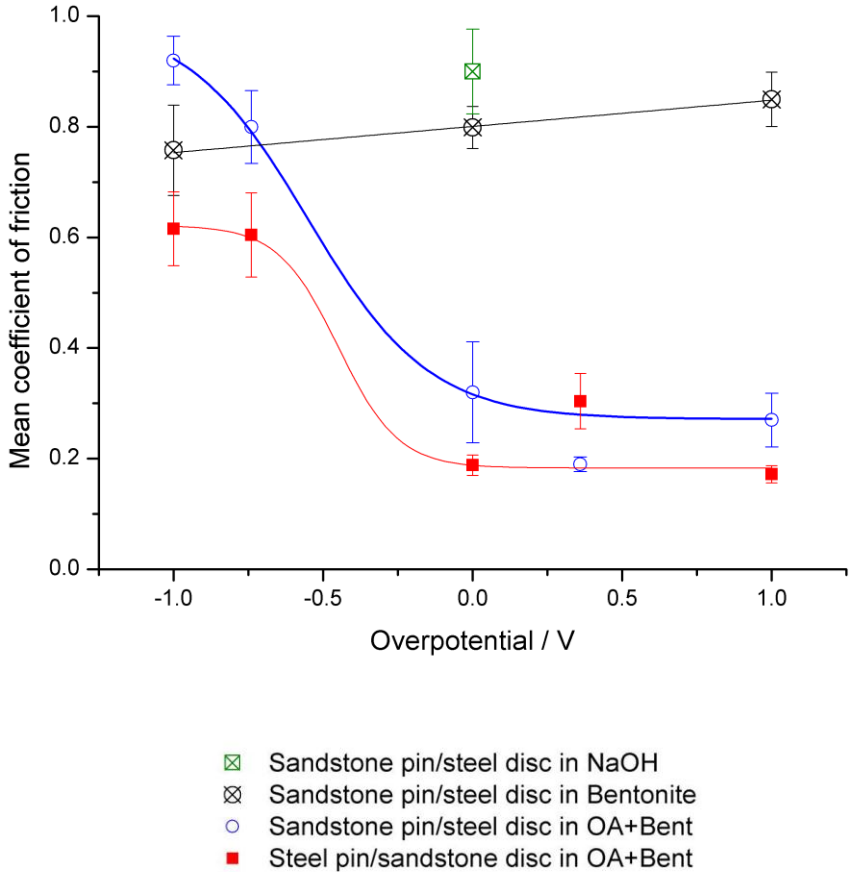

Figure 7.5. Mean coefficient of friction *vs.* overpotential for both sandstone/steel couples in the NaOH, bentonite and bentonite+octanoate test solutions.

Visual examination of the sandstone discs showed no significant wear. However, a detailed surface profilometry analysis was performed, thus the profiles of the sandstone disc wear tracks are shown in Figure 7.6. The results show that the ON wear track profiles were difficult to distinguish from the OFF wear track, due to the porous sandstone material which can be falsely considered as a part of the disc wear. Nevertheless, the surface profiles suggest that no significant wear of the discs occurred, despite the sandstone having low shear strength. The absence of wear was probably due to the shear stress being distributed across the relatively large disc surface. On the contrary, for the sandstone pin (in the previous arrangement), the entire surface of the pin tip was in contact, therefore the grains were probably easier to be removed.

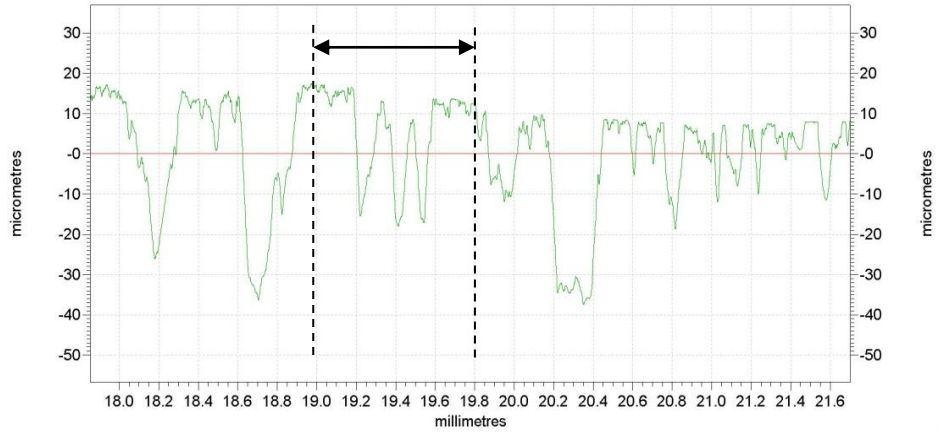

(a) –1 V overpotential

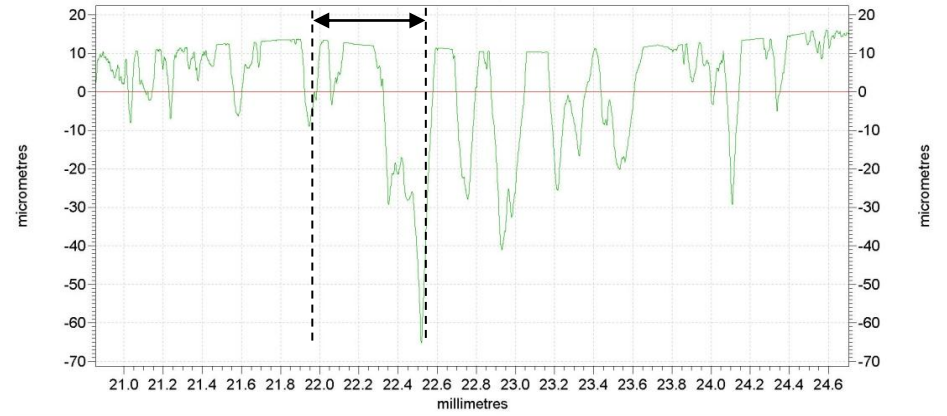

(b) 0 V overpotential

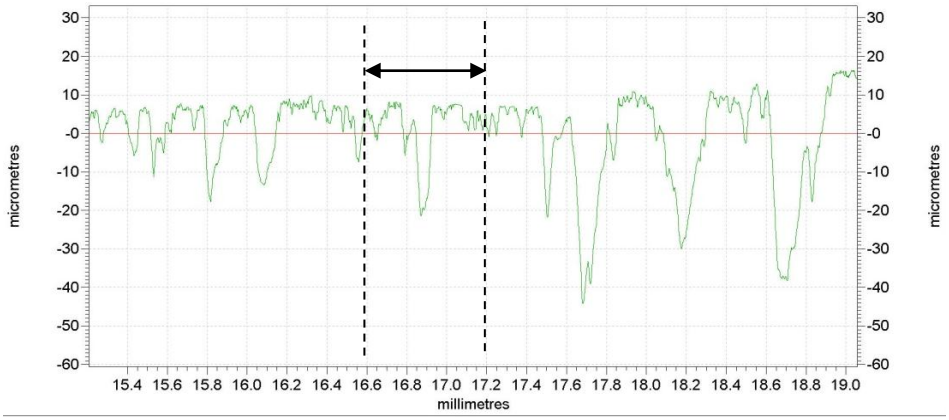

(c) +1 V overpotential

Figure 7.6. Profile of the wear track of the sandstone discs in bentonite+octanoate, at (a) –1 V, (b) 0 V, and (c) +1 V overpotentials. The double ended arrows indicate the width of the wear tracks.

The wear rates of the steel pins were in the order of 10^{-14} mm^3 N^{-1} m^{-1}, as shown in Figure 7.7, which were also higher by one order of magnitude compared with the steel/steel contacts in bentonite+octanoate (as reported in Chapter 5). This was probably due to the increased levels of abrasion by the sandstone disc. However, these values were comparable with the sandstone pins (from the previous sandstone pin/steel disc arrangement). This is interesting

because although sandstone is made of sand particles, which were harder than steel, the rate of material losses of the two types of pins were similar. This supports the previous discussions that the sandstone pins are susceptible to wear due to the low shear strength.

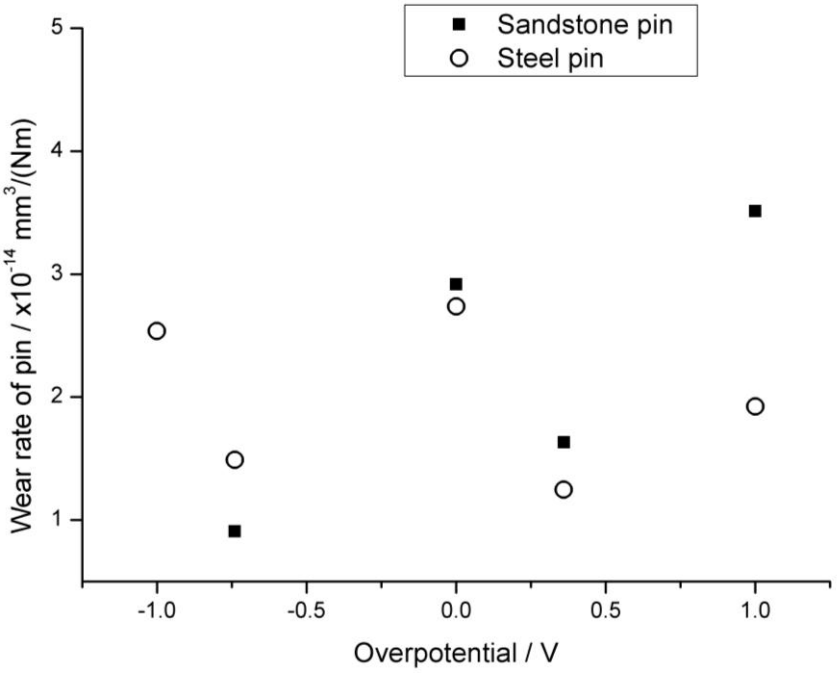

Figure 7.7. Specific wear rates for pins in the steel/sandstone contact arrangement in bentonite+octanoate, calculated by the geometrical method.

Therefore, the general difference between the wear mechanisms of the two contact arrangements, *i.e.*, the steel pin/sandstone disc, and sandstone pin/steel disc, is schematically shown in Figure 7.8 (irrespective of overpotential). In the former arrangement, the sandstone disc is resistant to wear. However, the steel pin produces wear debris which are relatively soft cf. sand, and when entrained, could deform plastically, and might not contribute to two-body abrasion (see Figure 7.8 (a)). In the latter arrangement, the sandstone pin and steel disc would probably produce wear debris, which become mechanically mixed in the contact (see Figure 7.8 (b)). The harder sand wear debris could cause two-body abrasion, which might explain the generally higher friction trend shown in the μ_{mean} *vs.* overpotential graph (see previous Figure 7.5). Generally, in both cases, the porosity of the sandstone material could probably act as traps for particles (sand or bentonite), which could have contributed to the increase in two-body abrasion, raising the levels of friction and wear cf. the steel/steel contacts (as presented in Chapters 4 and 5).

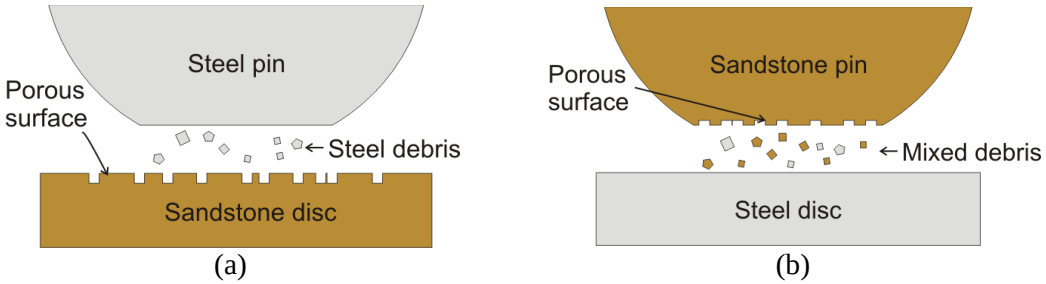

Figure 7.8. Schematic of the wear mechanism of the two contact arrangements in bentonite+octanoate, showing (a) steel pin/sandstone disc, and (b) sandstone pin/steel disc. The bentonite particles are excluded in schematic for clarity.

7.4 Summary

The control of friction in the steel/sandstone contact couples was achievable using the bentonite+octanoate drilling mud. Similar trends of the high friction at cathodic overpotentials and low friction at anodic were found, which were similar to the steel/steel contacts. This showed that the principle of operation was similar regardless of the material and contact type, as long as the formulation of the solution is the same. However, the range of the reduction in friction depended upon the contact material arrangement; with sandstone pin/steel disc having the largest of between 0.90 and 0.20, and the steel pin/sandstone disc between 0.60 and 0.20.

Quantification of the wear rates of the discs were difficult as was the case for the steel/steel contacts, due to the lack of defined wear track to calculate the volume of material loss. This might be improved by increasing the sliding time or load (contact stress).

However, both the steel and sandstone pins in this chapter showed higher wear rates by an order of magnitude cf. the steel pin counterpart in the steel/steel contact (as in Chapter 5). The steel pin wear was probably due to the sandstone counterface's abrasive nature. In contrast, the sandstone pin wear was due to the relatively lower shear strength of the sandstone material, which resulted in an easily fractured pin tip.

Generally, the higher friction levels and wear rates of this steel/sandstone couple cf. the steel/steel, were due to the adsorption film forming only on one surface, which reduced the effectiveness of lubrication. Furthermore, the harder sandstone, and the abrasive wear debris, might also contribute to the difference.

8 Investigation of Electrochemical Performance of the Additives

8.1 Introduction

This chapter presents the discussions of the analysis conducted only on the electrochemical part of this project, which included the results obtained from the pure electrochemical tests, and the triboelectrochemical tests. The electrochemical tests were aimed at assessing the behaviour of the steel exposed to all the solutions with and without the additives. Therefore, this enabled an understanding of the response of potential and current, which was essential before any sliding experiment could be performed. Furthermore, it allowed the observations of the important phenomena such as adsorption in a static condition, thus could be used to aid the interpretation of the tests in the presence of mechanical interference (sliding).

The first set of electrochemical tests which will be presented in this chapter were aimed at assessing the robustness of the modified rig, in terms of producing a reliable electrical connection between the potentiostat and the rotating disc, as discussed in the previous chapters. This was done by investigating the reproducibility of the test results conducted in beaker and rig (omitting the pin).

In addition, the electrochemical response which was recorded during each sliding test was assessed. This included comparing the levels of current density with the results obtained from the pure electrochemical tests conducted in beaker, *i.e.*, in the absence of sliding. These results have been used to establish correlations of the electrochemical performance with the tribological phenomena. For example, the evidence of formation of the adsorption film at a certain potential could be seen in the electrochemical test, thus would explain the tribological performance in the sliding test whilst applying similar potential. These analyses incorporated the steel / steel (including the active switching test) and steel / sandstone contacts.

8.2 Electrochemical Tests to Assess the Modified Rig

The electrochemical experiments conducted in the beaker were performed using controlled steel specimens as the working electrode, and having 1 cm^2 of exposed surface area. In addition, to assess the reproducibility of the results in the modified rig, these experiments were repeated in the rig, employing the steel disc as the counter electrode which had 28 cm^2 of exposed surface area.

In theory, the difference of both conditions due to the surface area could be minimised by quoting the current density / A cm^{-2} instead of the current / A. Furthermore, the behaviour of the open-circuit potential was expected to be the same, as it is not affected by surface area.

8.2.1 Initial Experiments Conducted in Beaker and the Modified Rig in Static Conditions

The open-circuit potential (OCP) *vs.* time tests conducted in the baseline NaOH solutions show that the potentials gradually decreased with time, as shown in Figure 8.1. In the beaker, the potential on initial immersion was around –0.38 V *vs.* Ag/AgCl which reduced to a steady-state value of around –0.48 V after 1000 s. The NaOH result in the rig was similar, but it started from a higher potential value at –0.25 V *vs.* Ag/AgCl and achieved a slightly lower steady-state of –0.55 V. The difference is probably due to the minor variations in the surface finishing processes, and the different cell setup which might have caused voltage drops.

The octanoate tests showed a reverse effect, in which the potential increased with time after immersion. In the beaker, the potential was –0.23 V *vs.* Ag/AgCl at initial immersion and rapidly increased to a steady-state value of –0.19 V in just 200 s. On the other hand, when repeated in the rig, the general trend was similar, but the steady-state potential increased to a slightly higher value at –0.16 V *vs.* Ag/AgCl. However, the increase in potential in both beaker and rig indicated that the octanoate adsorption was achievable and more importantly detectable in both conditions.

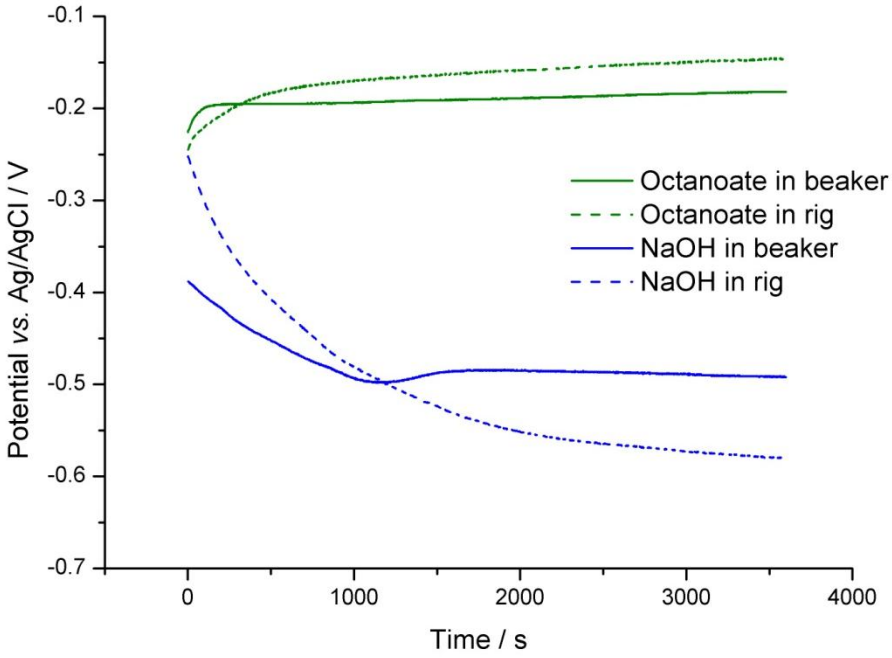

Figure 8.1. Open-circuit potential *vs.* time before potentiodynamic polarisation. Tests were conducted in NaOH and octanoate solutions. Tests were repeated in the rig (without rotation) to assess reproducibility.

The results of the potentiodynamic polarisation tests are shown in Figure 8.2. The E_{corr} for the NaOH solution in beaker was –0.34 V *vs.* Ag/AgCl. In the cathodic region (below the E_{corr}), there is an indication of a limiting current density, denoted by the very small change in current density over a wide variation of potential, *i.e.*, between –0.6 to –1.0 V *vs.* Ag/AgCl. The value of this limiting current density was around 10^{-5} A cm^{-2}. Whilst for the anodic region (above the E_{corr}), a limiting current density was also apparent at 10^{-4} A cm^{-2}. Visual observation of the steel sample after the polarisation test showed significant corrosion as patches of brown and black deposits, which was related to the higher current in the anodic region.

The octanoate showed a similar reaction to the NaOH test in the cathodic region (both in beaker). However, it had a slightly higher E_{corr} value at –0.28 V *vs.* Ag/AgCl cf. –0.34 V in NaOH. Furthermore, at the anodic region, the limiting current density was also seen, and had lower values by two orders of magnitude compared with the NaOH test, *i.e.*, at 10^{-6} A cm^{-2}. The higher E_{corr}, and lower anodic current density were suggesting evidence of octanoate adsorption at the anodic sites. Visual observation also showed no corrosion which confirms that the adsorption film provided effective corrosion inhibition.

The repeated NaOH test in the rig shows that the anodic limiting current density is higher by an order of magnitude than the beaker test. Visual observations of the steel disc after test showed a severely corroded disc, which might explain the higher current density.

Conversely, the repeated octanoate test in the rig showed a slightly lower current density in the cathodic region, while successfully reproducing the low current density in the anodic region which was indication of the adsorption on the disc surface.

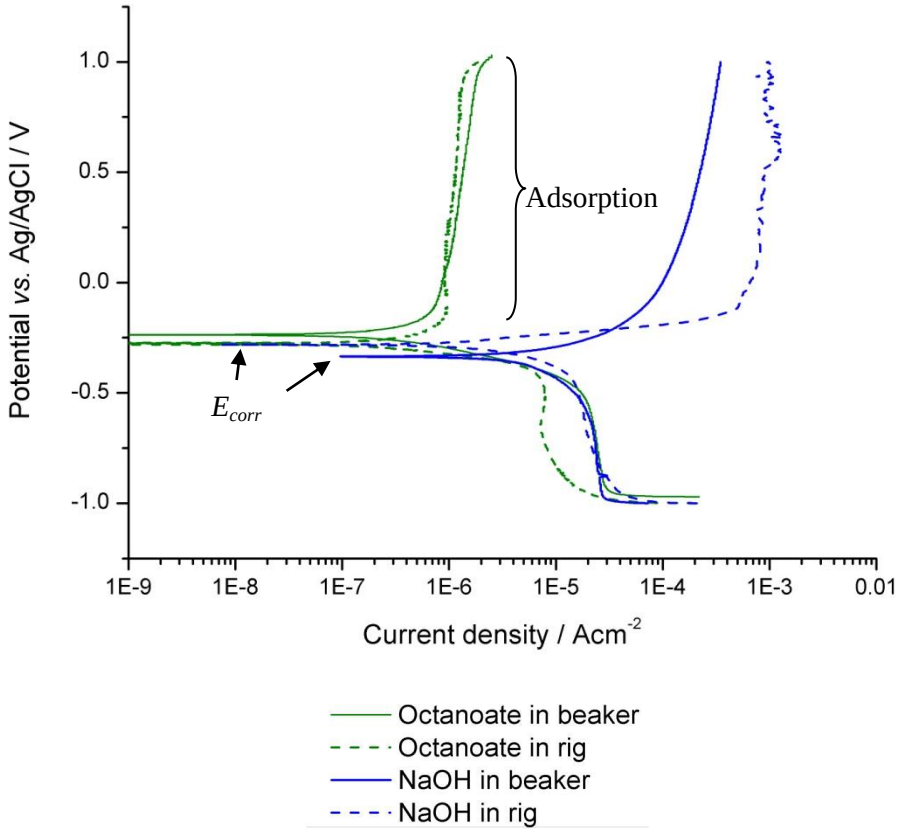

Figure 8.2. Potentiodynamic polarisation tests conducted in the NaOH and octanoate solutions. Tests were repeated in the rig (without rotation) to assess reproducibility.

In summary, the NaOH and octanoate electrochemical test results were reproducible in the modified rig with minor difference. Therefore, the design of the rig was concluded to be robust and could produce reliable electrochemical results under static conditions. The next subsection8.2.2 will present the effect of rotating the disc to the electrochemical reactions, in the absence of the pin.

8.2.2 Experiments Conducted in the Modified Rig with Rotation

The electrochemical tests in the octanoate solution as reported in 8.2.1 were repeated with the disc rotated, in order to simulate the conditions of the pin-on-disc dynamic motion (omitting the pin). Furthermore, the electrical connection between the disc and potentiostat during motion was assessed, by observing the changes to the electrochemical reactions due to the hydrodynamic effects.

The effect of disc rotation at 10 rpm on the OCP *vs.* time result is shown in Figure 8.3. The rotation caused the potential to immediately reach a high value upon immersion cf. the static condition, at –0.19 V *vs.* Ag/AgCl, which was probably due to the effect of increased mass transport. Furthermore, an increase in the noise was also seen (potential noise is shown by the oscillation around a mean), but the mean value was relatively stable at –0.19 V *vs.* Ag/AgCl. This noise was believed to be the result of the hydrodynamics of the solution, *i.e.*, due to the flow of fluid which could affect the kinetics of the molecules. Furthermore, the noise levels were rising with time, the reason for this is not clear. However, the overall value of the potential was still close to the static condition, which means that the rotation did not cause significant changes to the electrochemical response except for the probable increase in mass transport.

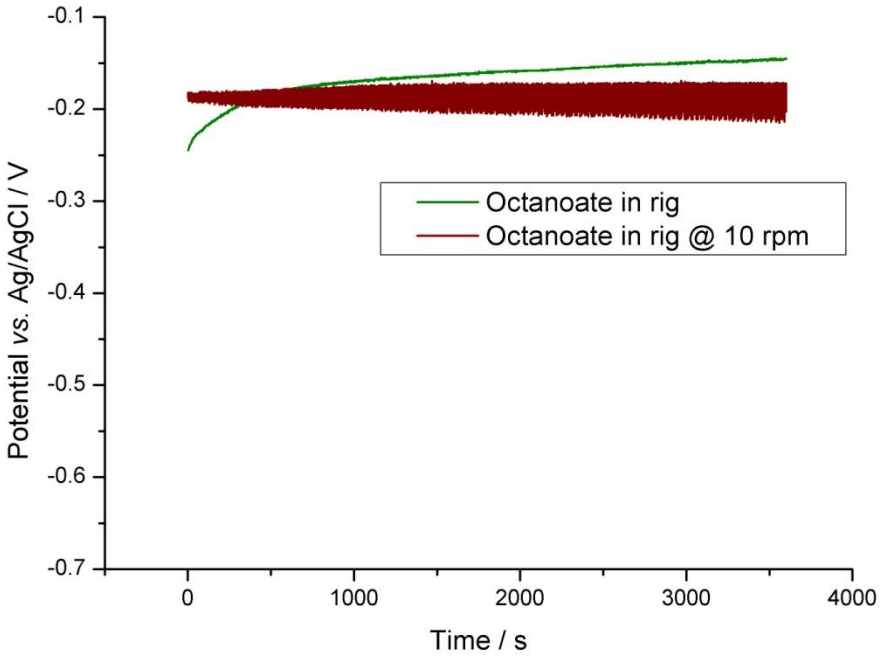

Figure 8.3. Open circuit potential *vs.* time before potentiodynamic polarisation in octanoate and in the rig setup. Comparison with the static and dynamic (disc rotation) behaviours.

The subsequent potentiodynamic polarisation test results are shown in Figure 8.4 (octanoate only). The rotation had caused the E_{corr} value to slightly increase to –0.19 V *vs.* Ag/AgCl compared with –0.28 V during static, most probably due to the effect of enhanced cathodic reaction. This was seen in the increase in the current density in the more cathodic region during rotation, which was probably due to the increase in mass transport. The anodic region, however, showed no difference between rotation and static, which implied that the adsorption can also be controlled while rotating the disc.

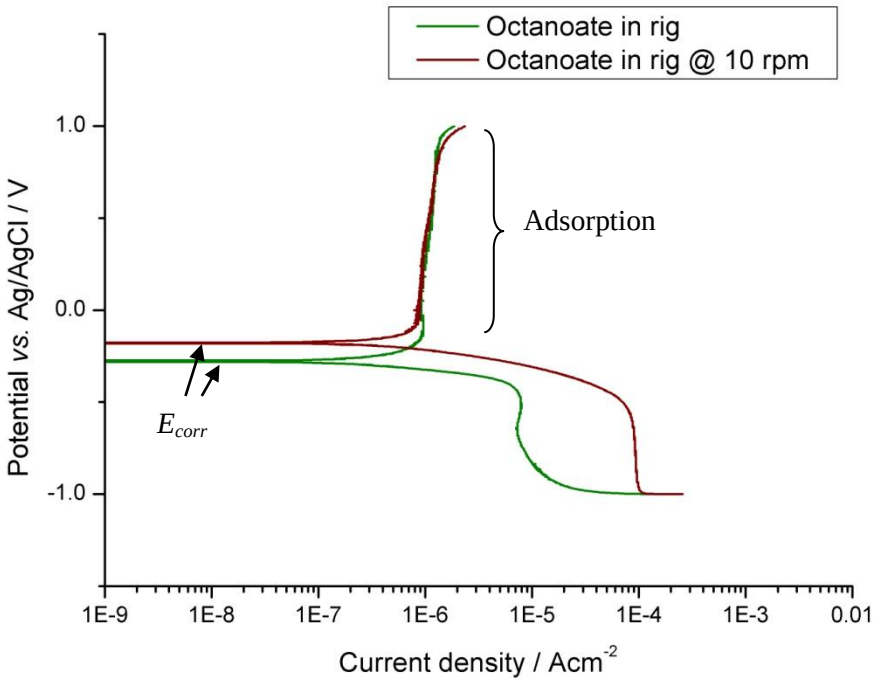

Figure 8.4. Potentiodynamic polarisation conducted in the octanoate test solution and in the rig setup. Comparison between the static and dynamic (disc rotation) behaviours.

8.3 Establishing the Background Understanding by the Electrochemical Tests in the Drilling Mud

This section (Section 8.3) will present the results of the electrochemical tests (OCP *vs.* time and potentiodynamic polarisation) conducted in the drilling mud (in beaker). The previous section discussed on the behaviour of the baseline solutions with and without the presence of additive, *i.e.*, the NaOH and octanoate solutions respectively. Therefore, this section will present the analysis of the electrochemical reactions in the drilling mud, which also included the tests incorporating the octanoate additive in the formulation. In addition, these tests were conducted in the two types of drilling mud which are widely used in industry, the bentonite based and polymer based.

8.3.1 Bentonite Drilling Mud

In the OCP *vs.* time test, the potential for bentonite drilling mud was at –0.43 V *vs.* Ag/AgCl at the start of test and decreased to a steady-state value around –0.71 V within 800 s (see Figure 8.5). This potential value was lower than the NaOH as previously discussed (at –0.50 V *vs.* Ag/AgCl), therefore suggesting that the bentonite particles have an effect on the potential, most probably due to the negative charge of the particles interacting with the positive charged disc. However, when the octanoate additive was present (bentonite+octanoate), the overall value of the potential increased to around –0.35 V *vs.* Ag/AgCl. The increase was close to the trend of the octanoate test, and was also higher than the NaOH, which might suggest that the additive was responsible for this behaviour. This was probably due to the adsorption of the octanoate molecules which inhibited the steel surface regardless of the presence of bentonite particles.

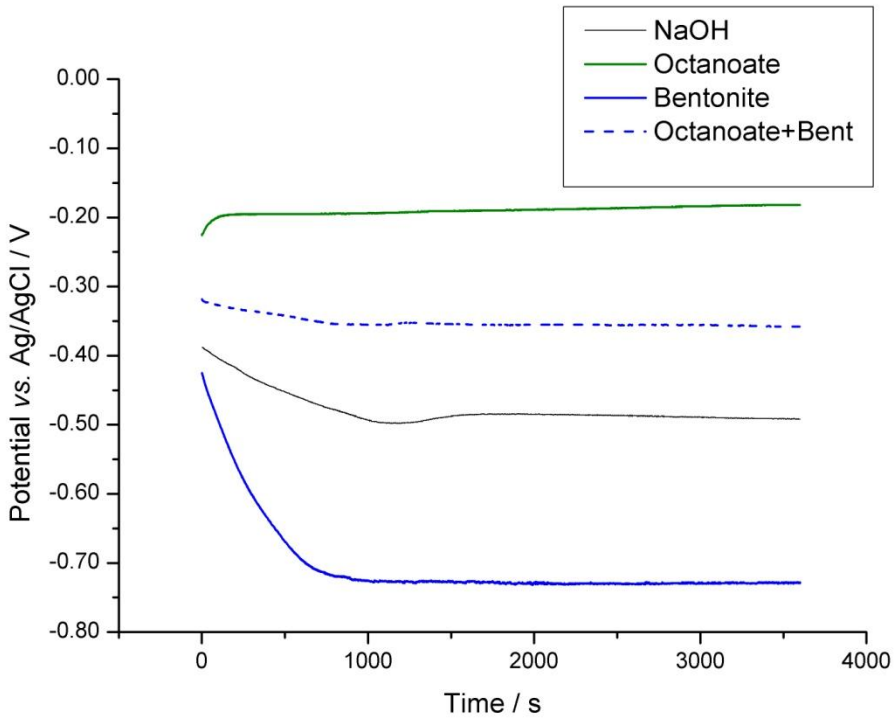

Figure 8.5. Open-circuit potential *vs.* time which was recorded before the octanoate, bentonite and bentonite+octanoate beaker tests

The potentiodynamic polarisation test results in the bentonite drilling mud showed a significant reduction in the value of E_{corr} to –0.60 V *vs.*Ag/AgCl compared with NaOH at –0.34 V *vs.* Ag/AgCl (see Figure 8.6). In the anodic region (above the E_{corr}), the limiting current density was 10^{-3} A cm^{-2} which was an order of magnitude higher than the NaOH. This was probably due to the increased anodic reactions by the incorporation of the bentonite particles which where negatively charged. Visual observation showed production of mud cake due to the agglomeration of the bentonite particles at anodic potentials, which suggested that the particles were attracted to the steel.

In the bentonite+octanoate solution, the E_{corr} decreased to around –1.00 V *vs.* Ag/AgCl, which was lower than the bentonite (without additive) test at –0.60 V *vs.* Ag/AgCl. However, the anodic region showed that there was a limiting current density at 10^{-6} A cm^{-2}, which was similar to the octanoate test previously. Therefore, this might also indicate the adsorption effect in the bentonite+octanoate, despite the presence of the bentonite particles. This was a positive result since it showed that the adsorption film can also be found in this case, which potentially could reduce friction and wear.

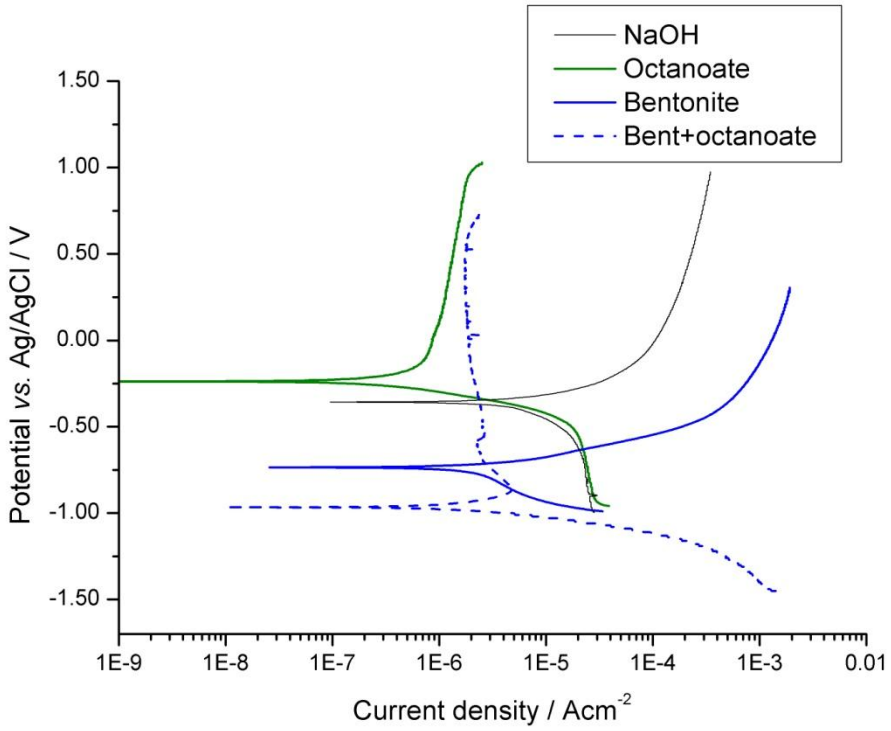

Figure 8.6. Potentiodynamic polarisation tests conducted in the octanoate, bentonite, and bentonite+octanoate in beaker.

8.3.2 Polymer Drilling Mud

The OCP vs. time for the polymer mud test is shown in Figure 8.7 (solid red line) which has a similar trend to the bentonite (solid blue line), *i.e.*, having initially higher values of potential which decreased over time. However, the polymer mud potential started at around –0.61 V *vs.* Ag/AgCl at immersion, which was lower than bentonite, but attained steady-state after around 900 s at a relatively higher value (cf. bentonite) at –0.65 V *vs.* Ag/AgCl.

The addition of the octanoate additive (therefore polymer+octanoate) resulted in an increase in the overall value of the potential to around –0.30 V *vs.* Ag/AgCl, which was also slightly higher than the bentonite+octanoate. This indicated that the adsorption of the octanoate additive was developed in the polymer+octanoate formulation as found in the particle (bentonite) based drilling mud. However, the trend was still lower than the octanoate test (solid green line), which might suggest that the polymer mud contained some chemical species which affected the overall electrochemical reaction. The details of this effect are not conclusive since the actual composition of the polymer mud is not known.

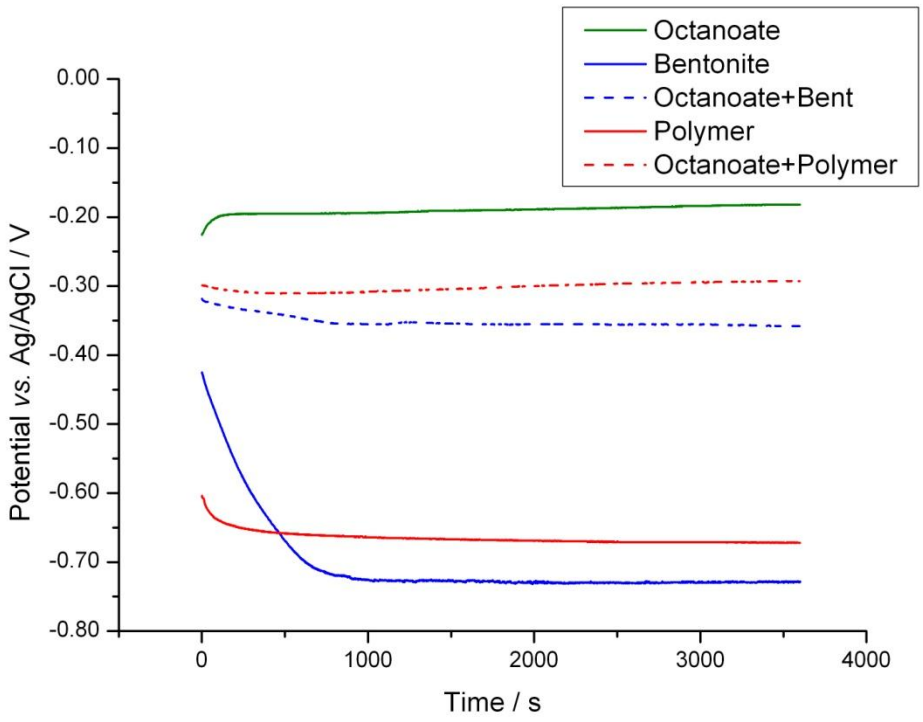

Figure 8.7. Open circuit potential *vs.* time of octanoate, bentonite, bentonite+octanoate, polymer and polymer+octanoate beaker tests.

The result of the potentiodynamic polarisation test in the polymer mud showed that the E_{corr} value was at –0.90 V *vs.* Ag/AgCl, which was close to the value of the bentonite+octanoate test at –1.00 V *vs.* Ag/AgCl (see Figure 8.8). Furthermore, in the more anodic region, the current density was around 10^{-5} A cm^{-2} but an abrupt increase was seen when the potential was at 0.25 V *vs.* Ag/AgCl (transpassive behaviour). Visual examination of the sample after the test showed a few small corrosion pits on the surface, which was the likely cause of the increase. Addition of the octanoate additive (polymer+octanoate) caused an increase in the E_{corr} value to –0.57 V *vs.* Ag/AgCl. Furthermore, the trend of the current density at the anodic region was similar to the bentonite+octanoate, *i.e.*, showing a limiting current density value in the order or 10^{-6} A cm^{-2}. In addition, the transpassive behaviour was not seen in this test. Visual observation confirmed the absence of corrosion pits on the steel surface. Therefore, these might suggest the octanoate additive formed an adsorption film in the anodic region, which was similar to the results of bentonite+octanoate (dashed blue line) and also the octanoate (solid green line).

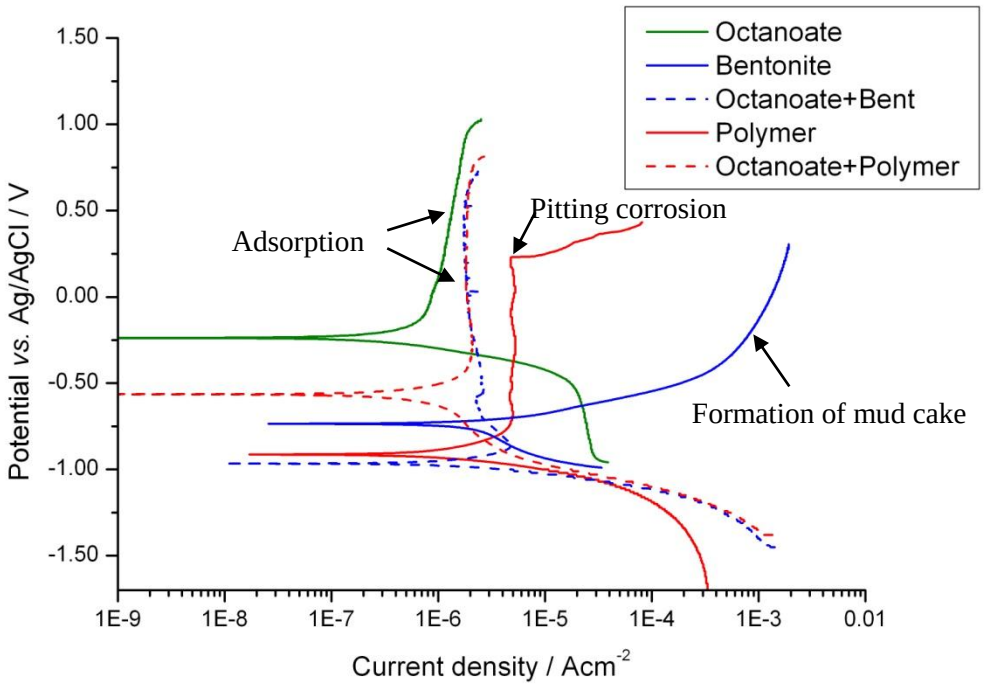

Figure 8.8. Potentiodynamic polarisation tests conducted in the octanoate, polymer, bentonite, bentonite+octanoate, and OA+Polymer in beaker.

8.4 Expanding the Background Understanding by Performing Tests in Alternative Additive Solutions

This section will present the results of the electrochemical tests conducted in the solutions incorporating the alternative additives, namely butyrate, oleate and cetyl trmethylammoniumbromide (CTAB). These additives were chosen in order to assess the effect of molecular structure on the tribological performance. Therefore, this chapter will discuss the electrochemical behaviour of these additives in the OCP *vs.* time and potentiodynamic polarisation tests. This would allow comparison with the behaviour of the test solutions incorporating the main additive used in this project (octanoate).

The results of the OCP *vs.* time conducted using the alternative additive solutions (butyrate, oleate and CTAB) are shown in Figure 8.9. The butyrate started with a potential value similar to the octanoate at around –0.23 V *vs.* Ag/AgCl and continued to increase to a fairly stable value at –0.15 V *vs.* Ag/AgCl. Compared with the oleate or CTAB, the response of butyrate was similar to the octanoate, probably due to the similar concentrations being used of 60 mM, as opposed to 1 mM for the others. Furthermore, butyrate and octanoate share similar molecular structures, but the only difference is that the butyrate consists of a shorter alkyl chain length than the octanoate by half, *i.e.*, four carbon atoms instead of eight in the molecule.

The oleate additive also showed an increasing trend of potential with time, having a similar trend to that of the butyrate. However, the oleate trend is about 0.15 V lower, probably due to the lower concentration of the additive. Furthermore, the slightly different molecular structure of the oleate molecules could also affect this potential behaviour, *i.e.*, due to the longer alkyl chain length with an additional double bond cf. either octanoate or butyrate.

The CTAB, however, showed an opposite response, in which the potential dropped constantly from –0.34 V to –0.57 V *vs.* Ag/AgCl from start to end of test. The behaviour was probably due to the positive charge of the additive, as opposed to negative on octanoate, oleate and butyrate. Furthermore, the structure of CTAB is more complex compared with the others, which could also account for the difference in the behaviour.

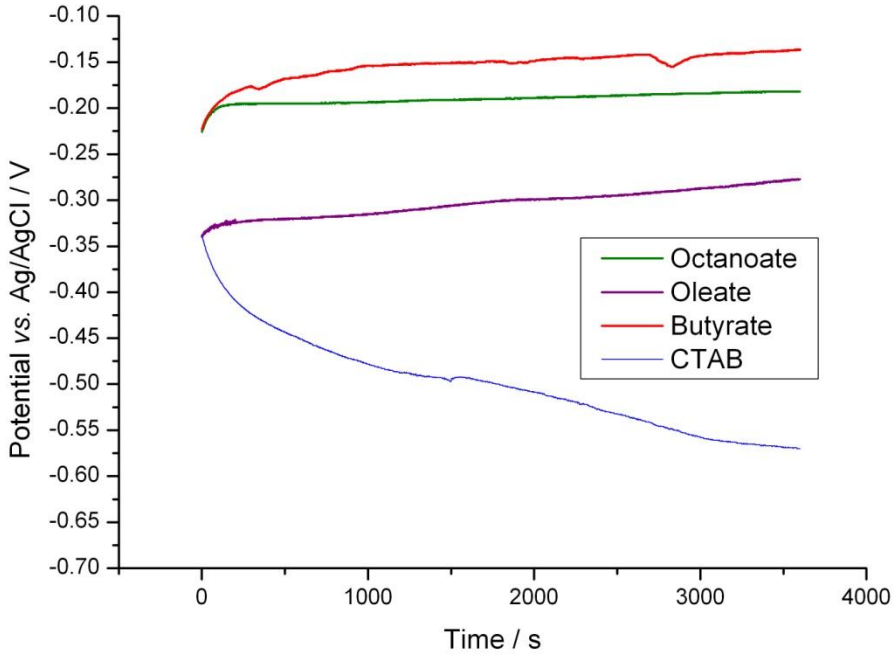

Figure 8.9. Open circuit potential *vs.* time prior to potentiodynamic polarisation tests conducted in octanoate, butyrate, oleate and CTAB solutions in beaker.

The subsequent potentiodynamic polarisation test results using the alternative additives are shown in Figure 8.10. The E_{corr} of oleate was –0.29 V, whilst butyrate and CTAB shared the same value at –0.38 V *vs.* Ag/AgCl. The more anodic region of both the butyrate and oleate showed evidence of adsorption of the additives, illustrated by the low values of current density (current limiting). These were expected due to the negative charged additives which adsorb onto anodic sites, similar to the octanoate. The CTAB, however, showed a high value of current density in the more anodic region, which meant that no adsorption was found on the surface, due to the positive charge of the additive.

All of these results signified that the adsorption of the butyrate and oleate could potentially be obtained by applying the anodic potentials, thus could affect friction and wear in the sliding test. However, there was no clear evidence of adsorption of the CTAB in the more cathodic region since there was no significant reduction of current density shown in the potentiodynamic polarisation test result, despite it being a positive charge additive.

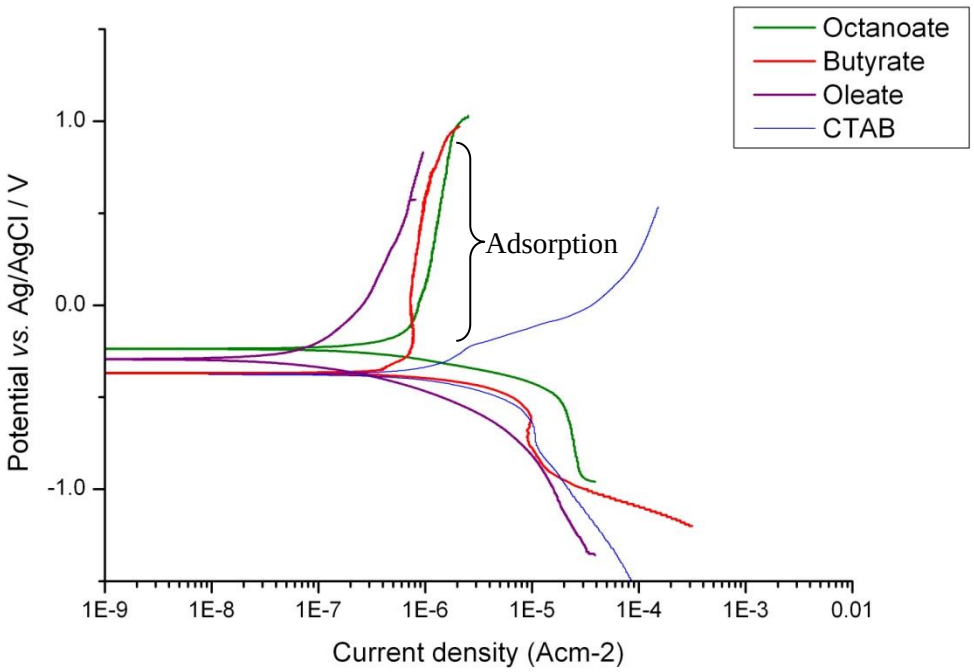

Figure 8.10. Potentiodynamic polarisation tests conducted in the octanoate and alternative additives of butyrate, oleate and CTAB.

8.5 Analysis of the Electrochemical Performance during the Steel / Steel Contacts

This section will discuss the electrochemical performance of the tests conducted in the presence of the sliding motion between the pin and disc (triboelectrochemical), particularly for the steel/steel contact pairs. This would differ from the previous discussions in this chapter which have focused only on the pure electrochemical tests, *i.e.*, in the absence of sliding. The procedure involved recording of the behaviour of potential or current which was obtained during the sliding tests. Theoretically, mechanical actions such as sliding or impact on the surface could influence the electrochemical behaviour, thus, these records can be used to better understand the contact mechanism. Therefore, the analysis of these records could be used to relate to the friction and wear performance as discussed in Chapter 4, *e.g.*, the evidence for adsorption of the octanoate additive could be assessed from the current trends, therefore would strengthen the discussion of the previous chapters. In short, this section will revisit the discussions of Chapter 4, by explaining the results of friction and wear from the analysis of the electrochemical performance (potential and current density).

8.5.1 Assessment of the Magnitude of Current Densities for Evidence of Tribofilm Formation

8.5.1.1 Tests Conducted in the Octanoate Solutions

The current densities that were measured during the PoD tests at –1, –0.54, +0.36 and +1 V overpotentials, using the octanoate as the additive are shown in Figure 8.11. At –1 V overpotential, the current densities in all of the solutions were relatively high (around 10^{-3} A cm^{-2}). However, at –0.54 V overpotential, generally the values were reduced by a small amount, except for NaOH. This was generally expected since the lower magnitude of potential would result in less promotion of cathodic reactions such as the reduction of water or hydrogen evolution. However, the NaOH showed no difference, probably because it had the least dissolved ions, thus showed less sensitivity towards potential.

On the other hand, at anodic overpotentials (+0.36 and +1 V), the current densities were all high, especially at +1 V overpotential due to the higher promotion of anodic reactions. However, the current densities were seen to reduce significantly whenever the octanoate additive was present. In most cases, the reductions were by two orders of magnitude (see bentonite+octanoate and OA+Polymer) cf. the solutions without additive, *i.e.*, NaOH, bentonite and polymer. Furthermore, these values of current density agree with the results of the pure electrochemical test which were conducted in the beaker, discussed previously in this chapter. Therefore, all of these probably suggested the formation of the octanoate

adsorption film, inhibiting the electrochemical reactions either in the presence or absence of sliding motion. In addition, it supported the previous claim that this film could act as an effective tribofilm, due to the tenacity of the film when being subjected to abrasion.

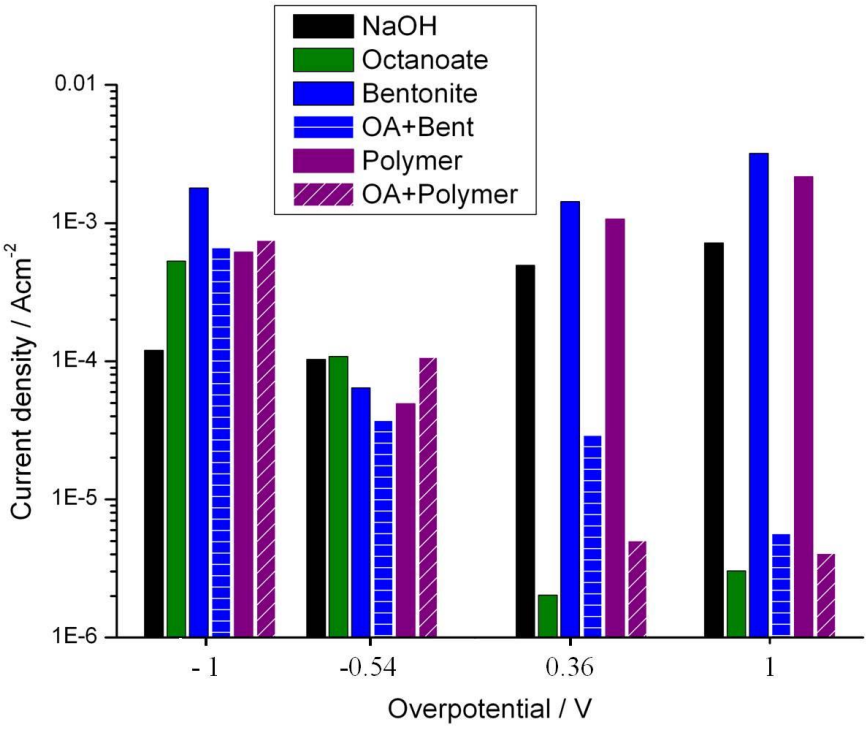

Figure 8.11. The magnitude of the current densities of tests in different solutions using the octanaote additive at –1, –0.54, +0.36 and +1 V overpotentials.

8.5.1.2 Tests Employing the Alternative Additives

The current densities of the alternative additives (oleate, butyrate and CTAB) at –1, –0.54, +0.36 and +1 V overpotentials are shown in Figure 8.12. The oleate had the lowest value of current density among the alternative additives at both –1 and +1 V overpotentials. This was probably due to adsorption of the additive on both the anodic and cathodic sites due to its molecular structure [122]. Furthermore, these values of current density were in agreement with the potentiodynamic polarisation tests (pure electrochemical test in beaker), discussed earlier in this chapter. It is interesting that although there was a marked difference in the current density, *i.e.*, the value at +1 V overpotential was one order of magnitude lower than at –1 V overpotential (10^{-6} A cm^{-2} and 10^{-5} A cm^{-2} respectively), the friction and wear results did not show much difference. This probably suggests that the oleate adsorbed in a different mechanism than the octanoate, which could be caused by the presence of the double bond in the alkyl chain of the molecule. Therefore, this might also suggest that the current density

trend can only be used as a supporting evidence for tribofilm formation, since it is dependant on the type of additive used, and also on other possible electrochemical reactions.

The butyrate at –1 V overpotential showed a maximum current density of 10^{-3} A cm^{-2}, which was similar to the potentiodynamic polarisation tests. However, higher values of current density by around an order of magnitude were seen at the other overpotentials cf. the potentiodynamic polarisation tests. This discrepancy might suggest that the adsorption layer formed by the butyrate additive was not as adherent as were the octanoate or oleate, and can be removed by sliding (thus the higher current density due to the lost inhibition).

The CTAB showed that the current density was slightly lower at –1 V compared with the +1 V overpotential. However, the values were still within the same order of magnitude (10^{-4} A cm^{-2}) which can be considered as a small change. Furthermore, as discussed in Chapter 4, the μ_{mean} was also reduced by a small amount at –1 V overpotential cf. +1 V, *i.e.*, at 0.32 and 0.45 respectively, which might be related to the small reduction in current density. The lower current density at –1 V overpotential might indicate adsorption of CTAB, thus influencing the friction.

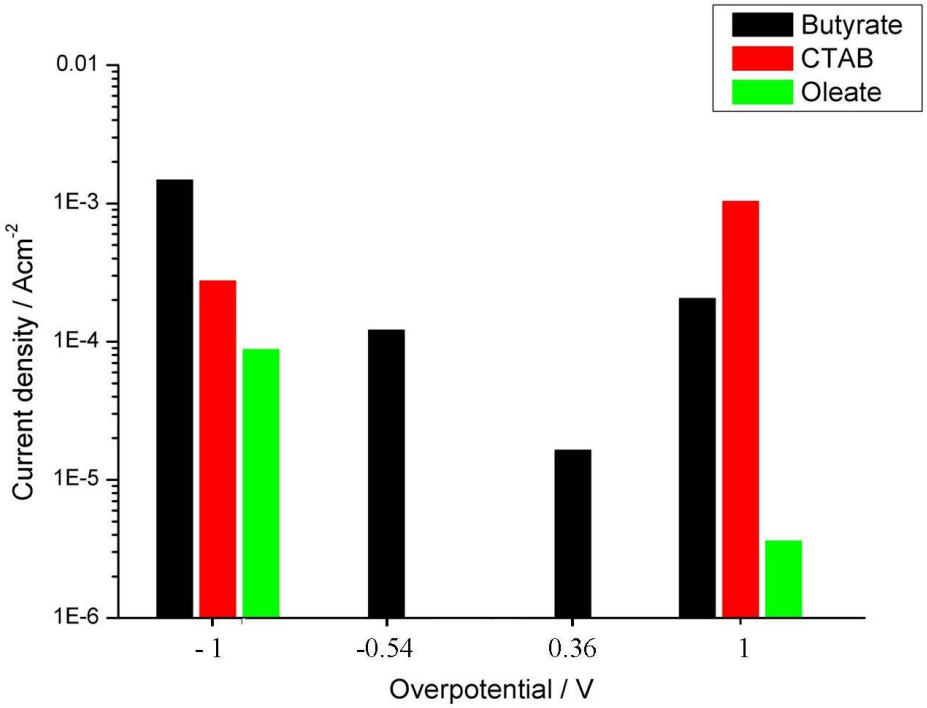

Figure 8.12. The magnitude of the current densities of tests in the solutions using the alternative additives (butyrate, CTAB and oleate), at –1, –0.54, +0.36 and +1 V overpotentials.

8.5.1.3 Active Switching Tests Employing the Octanoate and Butyrate Additives

The current response was also recorded during the active switching tests, which employed the cyclic application of –1 and +1 V overpotential. The results of the active switching, especially incorporating the octanoate additive, showed that friction could be controlled, owing to the adsorption or desorption of the additives (tribofilm). Therefore, analysis of the current density levels in these tests was aimed at explaining the possible tribofilm behaviour.

A summary of the active switching tests are presented in Figure 8.13, showing the graphs of μ *vs.* time and current density *vs.* time, which were both recorded during the tests. Generally, for the octanoate test, the current densities levels were reproducible at each cycle. However, the friction response was relatively less reproducible. Therefore, the discrepancy between current density and friction might suggest that the adsorption was only partially reversible.

In addition, the current densities were high whenever –1 V overpotential were applied, which was at 10^{-3} A cm^{-2}, compared with +1 V overpotentials at 10^{-5} A cm^{-2}. This was in agreement with the results obtained from the potentiostatic tests, *i.e.*, conducted without actively switching the overpotential. The low current densities at +1 V overpotentials were probably indication of adsorption (formation of tribofilm) which could explain the corresponding reduction in friction (see middle graph of Figure 8.13).

On the other hand, for the butyrate, application of –1 V overpotentials showed slightly higher current densities than the octanoate, but were still within the same order of magnitude, *i.e.*, at 10^{-3} A cm^{-2}. This was with the exception on the first switch (around 500 s), where the current density was lower, at 10^{-4} A cm^{-2}, probably due to the additive not having enough time to reach a stable condition. The +1 V overpotentials also showed that the current densities were slightly higher than octanoate at every occasion. Generally, the higher current densities of the butyrate might suggest that the adsorption layer formed was not as robust as octanoate, probably due to the formation of a less closely-packed layer, which was not enough to inhibit electrochemical reactions or produce a low friction contact.

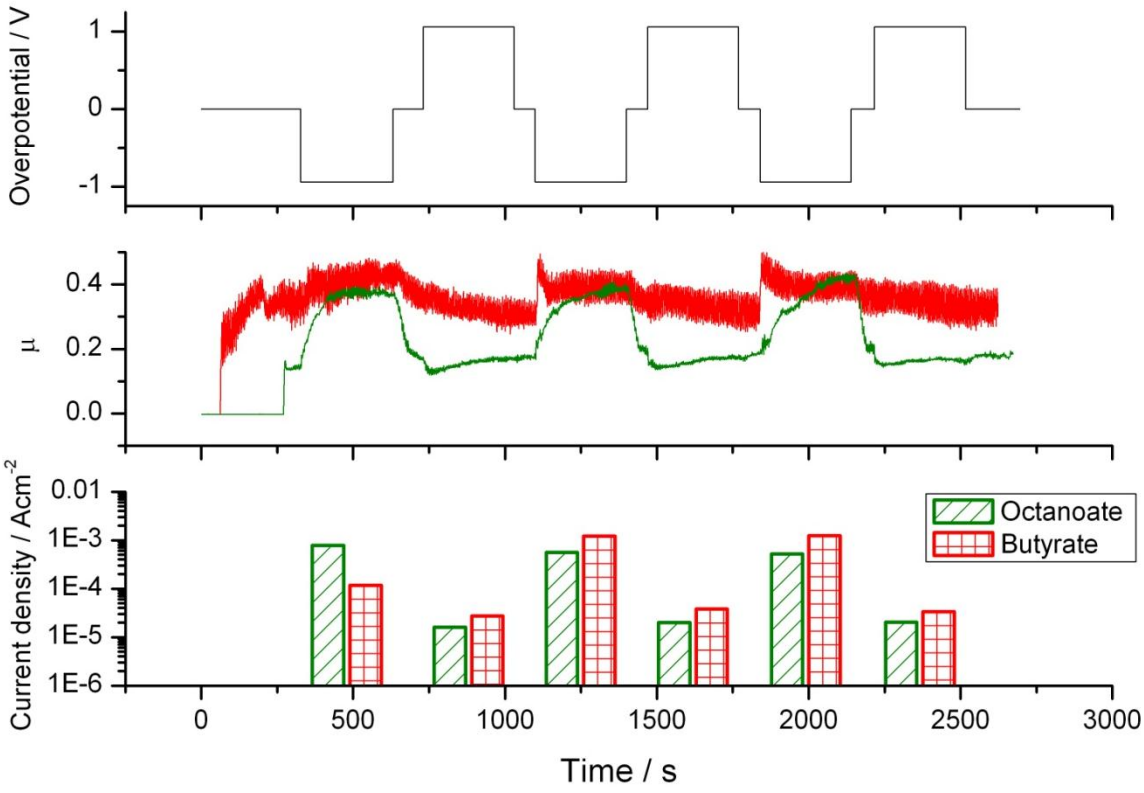

Figure 8.13. A summary of the active switching tests. The top graph shows the applied overpotential over time, between –1 and +1 V. The middle graph is the result of coefficient of friction *vs.* time while the bottom is the average magnitude of current densities during each switch.

8.5.2 Potential Recorded during the Sliding Tests at 0 V Overpotential

The discussions in Section 8.5.1 involved the analysis of the current densities which were recorded during the sliding tests, as a result of the application of overpotentials of –1, –0.54, +0.36 and +1 V. Therefore, this section (Section 8.5.2) will explore the behaviour of the OCP, which represented the potential recorded during the sliding test, at no overpotential application, *i.e.*, at 0 V overpotential. The analysis consisted of investigating the mean values of the OCP and was linked with the friction responses from Chapter 4.

The list of all the average recorded potential drift during sliding (at 0 V overpotential) in the different test solutions is listed in Table 8-1. The information in columns three and four was extracted from Chapter 4 (the μ_{mean} and standard deviation of μ). The table was sorted so that the average potential was in the increasing (negative) order. As a result, it showed that the solution with the oleate additive had the lowest value of average potential and s.d., followed by the octanoate. This was probably due to the oleate forming a good film with a close-packed molecular arrangement, whereas the octanoate formed a relative less close-packed. The difference could be accounted for the tall (oleate) and medium (octanoate) chain lengths of the molecules, *i.e.*, consisting of 18 and 8 carbon atoms respectively.

Despite the butyrate being a fatty acid, which has a similar molecular structure to oleate and octanoate, it had relatively higher values of average potential and μ_{mean}, at –0.45 V *vs.* Ag/AgCl and 0.35 respectively. This could be due to the shorter chain length of the molecules consisting of only 4 carbons, thus might caused a formation of a less effective adsorption film.

The bentonite drilling mud recorded the highest values of average potential, μ_{mean} and standard deviation. This suggested that the bentonite particles had electrochemical interactions with the steel surface and were also entrained in the sliding contacts causing the high friction and two-body abrasion.

Since there is some correlation between the average potential and friction, this could be a useful method to aid analysis. For example, estimating the friction in sliding contacts can possibly be made by monitoring the average potential. However, this requires more testing and further investigation. As far as the author is concerned, there has been no previous work relating the values of the average OCP to the levels of friction or wear.

Test solution	Average potential during sliding / V *vs.* Ag/AgCl	Mean coefficient of friction / μ	Standard deviation of μ
Oleate	–0.22	0.06	0.0119
Octanoate	–0.25	0.16	0.0256
OA+Polymer	–0.28	0.16	0.0106
bentonite+octanoate	–0.28	0.18	0.0245
NaOH	–0.31	0.47	0.0292
Butyrate	–0.45	0.35	0.0273
CTAB	–0.45	0.42	0.0486
Polymer	–0.53	0.32	0.0369
Bentonite	–0.72	0.58	0.0489

Table 8-1. List of the average potential recorded during sliding in the PoD setup, at 0 V overpotential tests. The list was sorted according to the increase in the average potential (second column).

8.6 Analysis of the Electrochemical Performance during the Steel / Sandstone Contacts

This section will report on the performance of the current density and potential which were recorded during the sliding tests employing the steel/sandstone contact pairs. The experimental procedures were generally similar to the previous steel/steel sliding experiments, however, electrical contact to the potentiostat was made via the steel sample in each case, *i.e.*, steel pin or steel disc. Tests were focused on using the bentonite drilling mud as the lubricant due to limitations to the number of sandstone samples available for use.

8.6.1 Assessment of the Magnitude of Current Densities for Evidence of Tribofilm Formation on Steel

The current densities recorded during the tests at –1, –0.54, +0.36 and +1 V overpotentials for the steel/sandstone contact couples are shown in Figure 8.14. At –1 V overpotential, all conditions showed similar values of current density (all were around 10^{-3} A cm^{-2}) which suggested that similar electrochemical reactions occurred, which was the evolution of hydrogen bubbles (gas). The current densities were varied at more anodic potentials due to the promotion of different electrochemical reactions in each condition, especially with the effect of the additive, where present.

In the sandstone pin/steel disc contact couple, the bentonite drilling mud produced a higher current density at +1 V overpotential by one order of magnitude (at 10^{-2} A cm^{-2}) cf. the –1 V overpotential (see grey solid columns in Figure 8.14). Visual observations of the steel disc at

+1 V overpotential after PoD test revealed a formation of mud cake. These suggested that the negatively charged bentonite particles were attracted to the surface and slowly formed agglomerate during the test. This would also support the findings of friction, in which the mean μ was higher at +1 V overpotential, *i.e.* μ_{mean} = 0.85, as opposed to 0.75 at –1 V overpotential. The increased particle agglomeration caused the higher two body-abrasion at more anodic overpotentials, thus increasing the friction. Furthermore, the higher current density could also be due to corrosion of the disc surface which was seen in the form of thin black deposit, revealed when the mud cake was removed.

With the octanoate additive, at +1 V overpotential (grey column with horizontal pattern), the current density was 10^{-5} A cm^{-2}, which was two orders of magnitude lower compared with the absence of additive, *i.e.* the bentonite (grey column). Furthermore, the μ_{mean} was also reduced from 0.85 to 0.17 (by 80%) between the absence and presence of the additive at this overpotential. Therefore, these proved that the low current density supported the evidence of adsorption of the octanoate additive, in agreement with the previous steel/steel contact pair.

When the contact couple was reversed to steel pin/sandstone disc (green column), the trend of current density showed a decrease from –1 V to +1 V overpotential. Therefore, this probably suggest that the adsorption of octanoate additive was also controllable following the reverse. However, the values of current density at the anodic overpotentials, *i.e.*, at +0.36 and +1 V were lower than the case prior to the contact reverse. This was probably because in the case of the steel pin (prior to the reverse), the pin tip was in constant contact with the sandstone disc, which might have resulted in an increased difficulty in tribofilm reformation (readsorption or octanoate additive). This was due to the assumption that the tribofilm was effectively formed only on the steel surface.

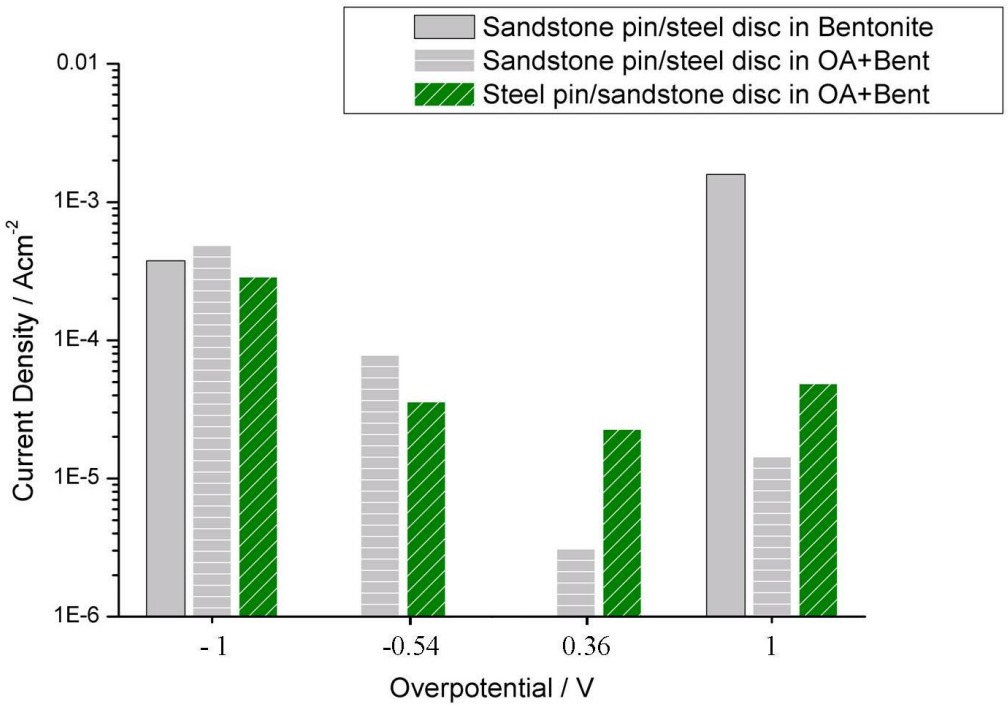

Figure 8.14. The magnitude of the current densities of tests in the steel/sanstone couples in the Bentonite and bentonite+octanoate solutions. The overpotentials used were at –1, –0.54, +0.36 and +1 V.

8.6.2 Potential Recorded during the Sliding Test at 0 V Overpotential

The list of all the recorded average OCP during sliding at 0 V overpotential (no applied potential) in the steel/sandstone contacts is shown in Table 8-2. The table was sorted so that the average potential was in the increasing (negative) order. In the sandstone pin/steel disc contact arrangement, the NaOH recorded the lowest value of average potential at –0.38 V *vs.* Ag/AgCl, and also gave the highest μ_{mean} at 0.90. For the bentonite drilling mud, the average potential was low when the additive was present cf. absence, at –0.50 V and –0.66 V *vs.* Ag/AgCl respectively. The value of μ_{mean} also followed similar trend, *i.e.*, increasing from 0.32 to 0.80 in each case. Therefore, there are two possible conclusions from these results. Firstly, this shows that the potential in the NaOH test solution could not be correlated with the drilling mud, as it produced the lowest average potential but gave the highest friction. Secondly, this might suggest the relationship of higher average potentials giving higher friction was still relevant, but only within the same test solution. However, more work is needed to corroborate this finding.

The reversed contact couple, *i.e.*, steel pin/sandstone disc, showed that the bentonite+octanoate drilling mud produced an average potential of –0.42 V *vs.* Ag/AgCl.

This value was slightly lower than the previous contact prior to the reverse, *i.e.*, sandstone pin/steel disc, which was at –0.50 V. Furthermore, lower values of μ_{mean} and s.d. were also given, at 0.19 and 0.02 respectively. Therefore, this might suggest that the contact arrangement did not affect the relationship between potential and friction (*i.e.*, potential proportional to friction levels), as long as the solution is similar (drilling mud). In addition, this might also indicate that the adsorption was reproducible regardless of the contact arrangement. Similarly, more work is needed to attain a robust conclusion with regards to this hypothesis.

Contact couple type	**Solution**	**Average potential during sliding / V *vs.* Ag/AgCl**	**Mean coefficient of friction / μ**	**Standard deviation of μ**
Sandstone pin / steel disc	NaOH	–0.38	0.90	0.08
	Bentonite+ octanoate	–0.50	0.32	0.09
	Bentonite	–0.66	0.80	0.04
Steel pin / sandstone disc	Bentonite+ octanoate	–0.42	0.19	0.02

Table 8-2. List of the average potential recorded during sliding in the PoD setup, at 0 V overpotential tests. The list was sorted according to the increase in the average potential in the negative direction (third column).

8.7 Summary

The design of the modified rig was assessed in terms of the sturdiness of the electrical connection between the rotating disc and potentiostat. The results of the electrochemical tests conducted in the beaker was reproducible in the rig with minor differences, therefore the rig was concluded to be electrochemically robust. This was important so that the results of the tests incorporating the sliding motion between the pin and disc (triboelectrochemical) would not be susceptible to errors in the potential or current responses.

Open-circuit potential *vs.* time and potentiodynamic polarisation testing have allowed the behaviour of the additives with respect to the different base solution to be studied. Generally, the adsorption of the additive on the surfaces could potentially be detected by the reduction in the magnitude of current density.

The measured currents and potentials during the triboelectrochemical tests correlate well with the static (pure) electrochemical tests, *i.e.*, the OCP *vs.* time and potentiodynamic polarisation. This proved that the static electrochemical tests are a good way of estimating the behaviour prior to the sliding tests. Furthermore, it showed that the mechanical sliding does not have detrimental effects onto the process of recording the in-situ electrochemical reactions. This opens opportunities for further investigation into this field of tribochemistry.

There is a strong relationship between a recorded low current density and low friction and wear. The low current density is due to the adsorption of the additives onto the surfaces which inhibit further electrochemical reaction. In addition, this adsorbed layer could provide a good protection from friction and wear by separating the direct steel/steel contact of the asperities (tribofilm formation). However, this is achievable provided that the molecular structure of the additive is suitable to form a robust tribofilm.

The average values of potential during sliding (tests conducted at 0 V overpotential) can be monitored and potentially could be used to estimate the levels of friction. Particularly, the higher negative potential might suggest a higher friction, *i.e.*, potential is proportional to friction. However, more work is needed to understand the behaviour of the open circuit potential during the sliding test.

9 Summary of the Mechanisms of Contacts

9.1 Introduction

This chapter summarises the mechanisms of contacts and the behaviour of friction obtained from the tests conducted in the different lubricant formulations presented earlier in this thesis. The fundamental findings will be presented to briefly explain the similarities and differences under the various test conditions.

9.2 Mechanisms of Contacts in the Baseline Solutions

The response of friction, related to the different test solutions, can be discussed in terms of the relative (nominal) position on the Stribeck curve (see Figure 9.1). The highest friction was given by the NaOH test solution (μ_{mean} around 0.45) which corresponds to point 1. The friction, although lower than dry sliding ($\mu \approx 1$), was significantly high, particularly when referring to most engineering applications which rely on sliding surfaces, especially for downhole drilling. The high friction was due to the "unprotected" surfaces sliding against each other, *i.e.*, direct steel/steel contacts. Point 2 consists of the level of friction given by the incorporation of butyrate additive, when anodic overpotential is applied. Similarly, the CTAB is also associated with this point, when cathodic overpotential is applied. The reason for both, was due to the adsorption of the molecules on the surfaces, offering "protection" from direct steel/steel contacts, thus reducing the shear strength at the contact. In each case, by leaving the surfaces at OCP, or applying the reverse overpotential, would result in significant increase of the friction levels, approaching point 1, *i.e.*, approaching to the left of the curve. These are due to the repulsion of the additive from the surfaces, impeding the formation of a tribofilm.

The utilisation of octanoate additive results in the friction levels at point 3. The lower friction than butyrate was primarily due to the higher alkyl chain length of the molecules, which render a better boundary lubricating effect. The application of anodic overpotential would result only in a marginal decrease in friction, *i.e.*, small shift to the right of curve, but beneficial in producing a more stable response (smaller perturbation). This is due to the molecules naturally having affinity for the steel surface to produce iron octanoate film (tribofilm). To the contrary, application of cathodic overpotential would result in a rapid increase in friction, shifting close to point 1 on the curve, once more, due to the repulsion of the molecules. Point 4 is the lowest friction, given by the oleate additive, which is unaffected by application of any overpotential due to the different molecular structure. This friction value is probably within the lowest obtainable by steel/steel contacts under similar

conditions ($\mu \approx 0.1$), and further reduction might necessitate the transition into the EHL regime, or utilisation of low friction coatings such as the Diamond Like Coatings (DLC). The former would involve a different system altogether, as this condition is usually possible by using oil based lubricants (such as engine oil, as opposed to aqueous), whilst the latter might not be economically feasible for extensive downhole use and needs substantial investigation.

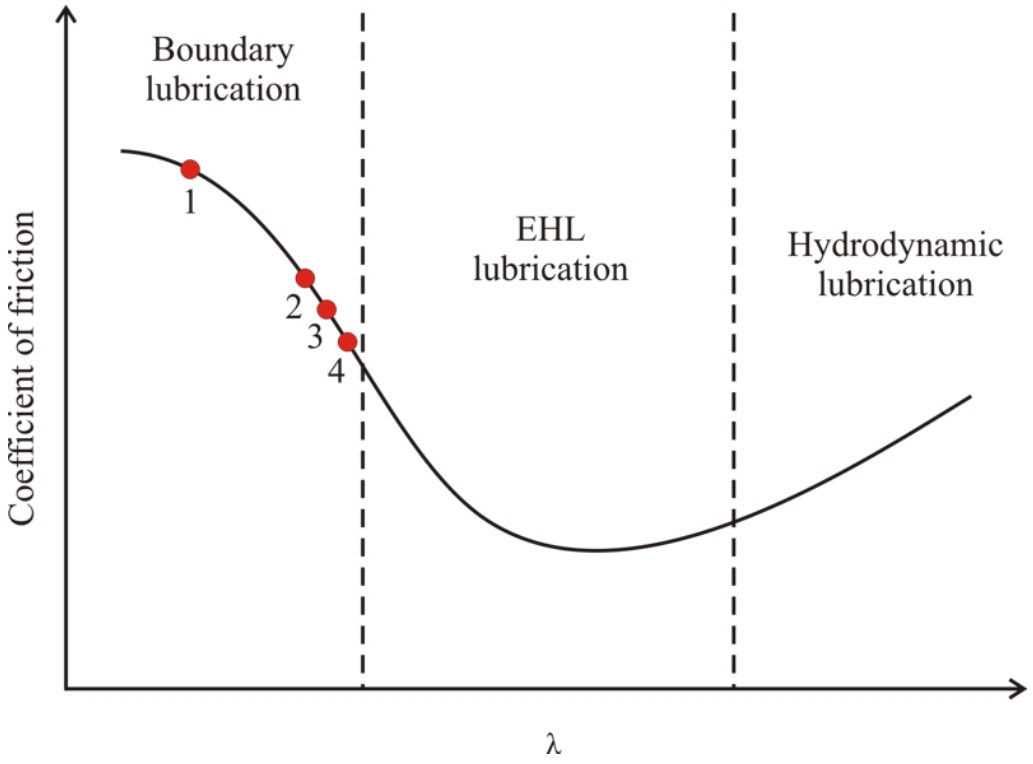

Figure 9.1. The relative position of the frictional behaviour in the test solutions, plotted on the Stribeck curve. λ is the ratio of the separation of the sliding surfaces to the average surface roughness.

The explanation of the mechanisms of contacts in the conditions that gave the high levels of friction are shown in Figure 9.2. These schematics are akin to the low λ values, *i.e.*, at the far left of the Stribeck curve, such as point 1 in the previous Figure 9.1. In the case of which a cathodic overpotential is applied to the steel, the surface will be free from oxide layer (see Figure 9.2 (a)). This includes the NaOH (no additive), butyrate and octanoate test solutions (note that in the latter two, the additive molecules are assumed to be completely repelled owing to the negative charge). In this contact type, direct asperity contacts occur, leading to to adhesion, abrasion and material transfer. Significant adhesion forces are expected due to the sliding of similar materials employed in this project.

In contrast, application of an anodic overpotential would result in the formation of oxide layer (Fe_2O_3 from the Pourbaix diagram) such as shown in Figure 9.2 (b), excluding the conditions where adsorption is possible, *i.e.*, without the butyrate, octanoate or oleate

additives. This oxide layer is not effective in reducing adhesion and abrasion, due to the relatively weak physical property. For example, in comparison with the oxide layer on stainless steel, the chromium oxide layer forms a more complete structure (not porous) and adherent to the steel substrate. Sliding action will cause the production of oxide particles ejected as debris, and probably could cause some dissolution of the steel, evident by the observed dispersion of corrosion particles in the solution and the change in the solution colour (from clear to yellowish), respectively.

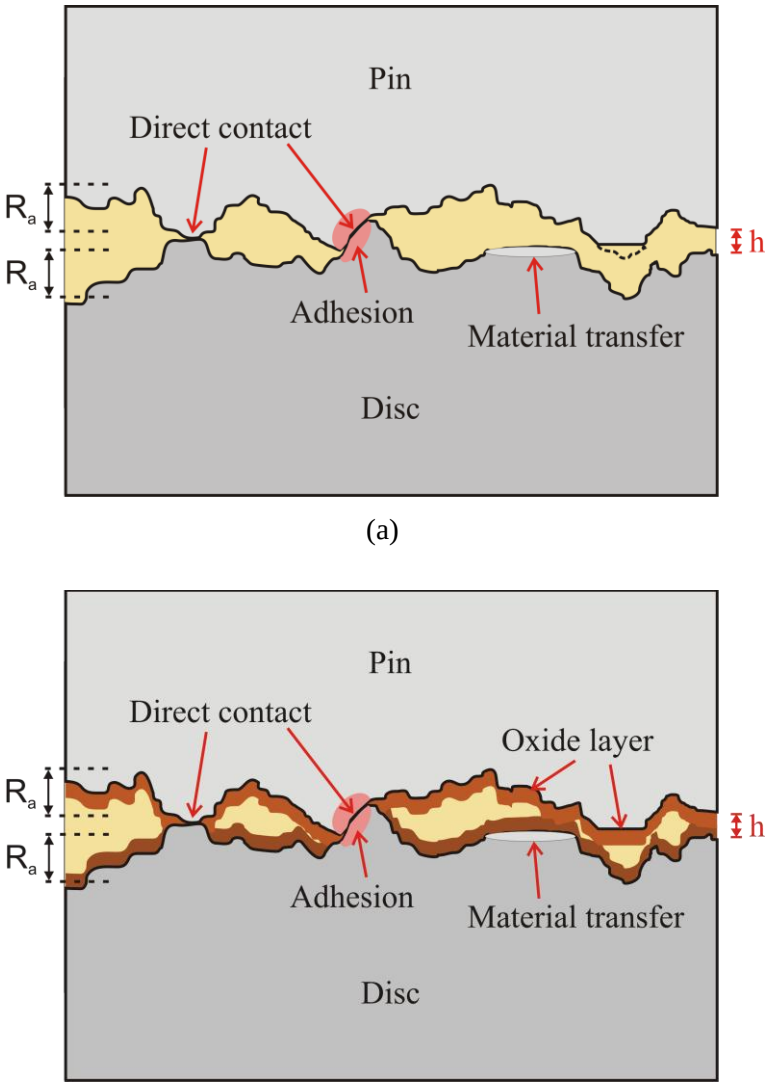

Figure 9.2. Mechanism of contacts which gave the high friction levels in the baseline solutions. Schematics show the severe conditions (a) at application of cathodic overpotentials (excluding CTAB tests), and (b) at application of anodic overpotential in the NaOH test (no additive). Debris not shown for clarity. These contacts are akin to the small λ value in the Stribeck curve.

On the contrary, the schematics showing the mechanisms of contacts pertaining to the conditions giving low friction values are shown in Figure 9.3. Note that these correspond to

the higher λ value, but within the boundary lubrication regime, *i.e.*, towards the right of the Stribeck Curve, such as points 2 and 3 (see previous Figure 9.1). The formation of tribofilm is the key to the reduction in the levels of friction and wear. For molecules with the shorter alkyl chain length (especially proven for octanoate), the formation of tribofilm is expected as islands of disordered molecular arrangement (see Figure 9.3 (a)). Despite these imperfections, the tribofilm is effective in separating the surfaces, reducing adhesion and abrasion levels, which were found in the NaOH tests (additive free). Furthermore, application of an anodic overpotential would probably result in the widening (growing) of these tribofilm islands, thus causing a more stable friction perturbation. However, the overall level of friction can only be marginally reduced, probably because the general separation of the surfaces (*h*) was not affected significantly, and could only be done by employing with longer alkyl chain lengths (such as oleate).

The schematic of the condition utilising a longer alkyl chain length (oleate) additive is shown in Figure 9.3 (b). With regards to the Stribeck curve, this would be close to the far right of the boundary lubrication regime (such as point 4 in previous Figure 9.1). This tribofilm forms a more complete and closely-packed molecular arrangement, resulting in low average friction value and a stable perturbation. This is due to the tribofilm providing a better protection against adhesion and abrasion. However, application of overpotential did not affect the friction response, owing to the additive's affinity for both the cathodic and anodic sites. This could be due to the chemical nature of the oleate additive, thus, testing other types of long chain length additives might give a different result.

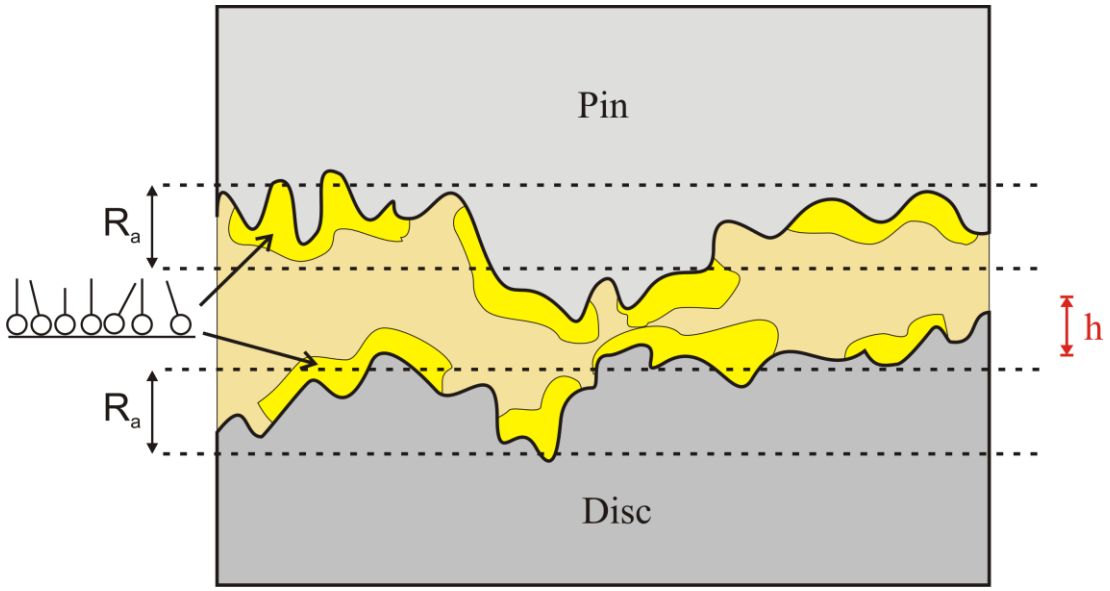

(a)

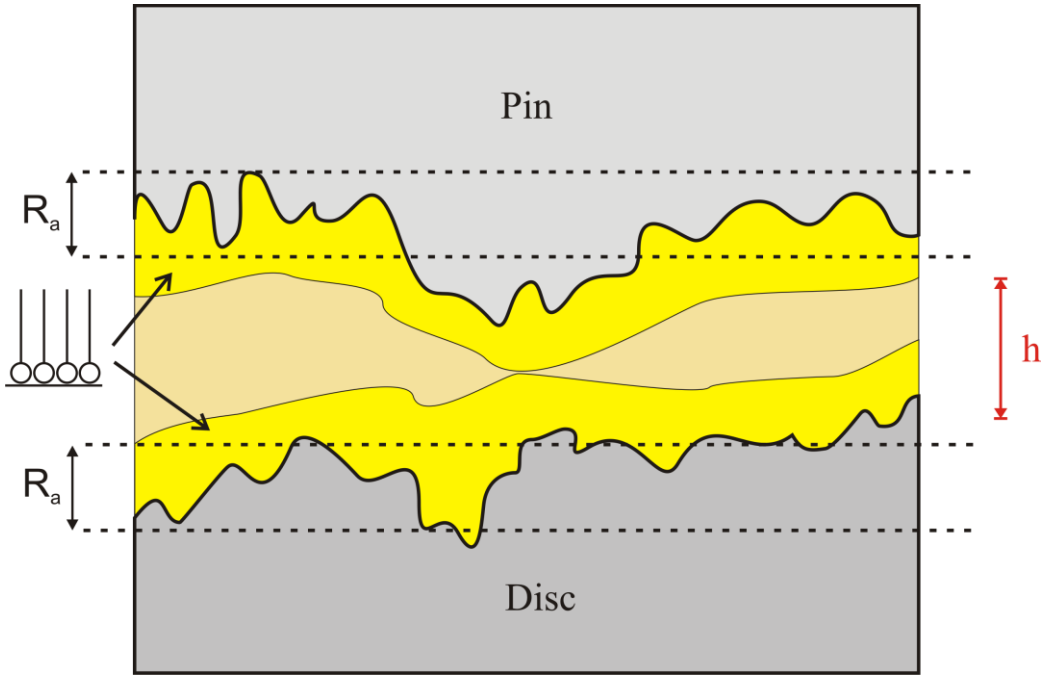

(b)

Figure 9.3. Mechanism of contacts which gave the low friction levels in the baseline solutions. Schematics show the formation of (a) islands of adsorption film (tribofilm), and (b) complete and robust adsorption film. Debris formation is probably negligible. These contacts are akin to the large λ value in the Stribeck curve.

9.3 Mechanisms of Contacts in the Drilling Muds

The investigation of the test conditions employing the drilling muds (bentonite and polymer), aiming at understanding the effects of surface potential on the tribological response are summarised in this section. Furthermore, the discussions of the implications of the octanoate additive in the mud is also included.

9.3.1 Bentonite Drilling Mud

When the bentonite drilling mud is used, high friction is expected due to the direct steel/steel contacts (similar mechanism to the NaOH as discussed previously), combined with the entrainment of the bentonite particles which cause two-body abrasion (see Figure 9.4). At application of a cathodic overpotential, no oxide layer is formed on the steel surface (see Figure 9.4 (a)). Furthermore, most of the bentonite particles will be repelled due to the negative charge, resulting in a slightly lower friction cf. OCP (no potential application). This mechanism also applies to the condition when octanoate additive is present, because similarly, the additive will also be repelled from the surface preventing tribofilm formation.

The result of application of an anodic overpotential is schematically shown in Figure 9.4 (b), which only applies to the condition where the octanoate additive is absent. In this case, production of oxide layer is promoted, which coexist with the increase in the amount of entrained bentonite particles, due to the higher electrostatic attraction between the negative particles and the positive disc. Thus, the result is a slightly higher friction cf. OCP, and a severely abraded surface combined with corrosion.

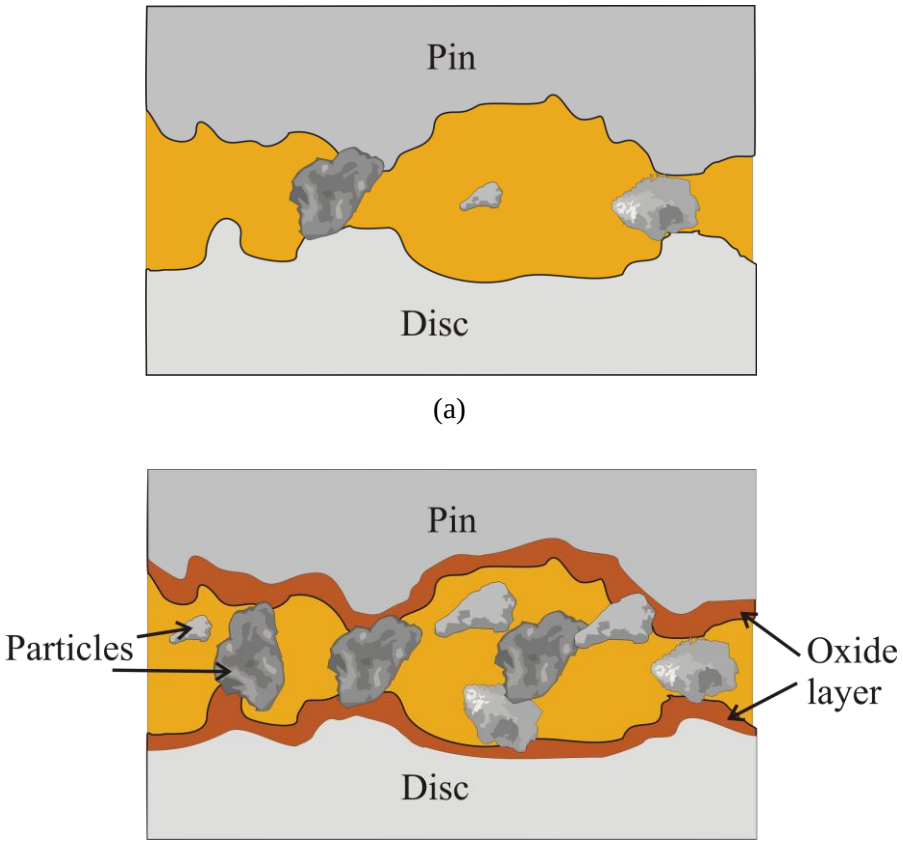

Figure 9.4. Schematic of the mechanisms of contacts in the bentonite drilling mud, showing the entrainment of the bentonite particles, at (a) application of a cathodic overpotential, and (b) application of an anodic overpotential (in the absence of octanoate additive).

The incorporation of octanoate additive showed a transitional behaviour of the tribological response, in which the formation of the tribofilm was effective in reducing friction and two-body abrasion (see in Figure 9.5). Particularly, at OCP, the tribofilm prevents from direct steel/steel contacts, such as found in the previous baseline tests (see previous Section 9.2). However, the direct effect of the tribofilm on the particles is still unclear. For example, it is possible that the tribofilm is effective on its own right, in preventing the ploughing action of the particles, by acting as a relatively strong barrier. Secondly, the tribofilm passivates the steel surface, which causes a lower electrostatic interaction between the particles and the steel surface, therefore resulting in fewer particle entrainment. These possibilities become more evident particularly at the application of anodic overpotential, which would result in the growth of the tribofilm (widening). As such, a reduction in the overall friction level will be seen, along with the reduction in the severity of the ploughing action of the particles (evident by the smaller groove sizes within the wear track, on the steel surface). Furhter work is needed to clarify the mechanism of contact more clearly.

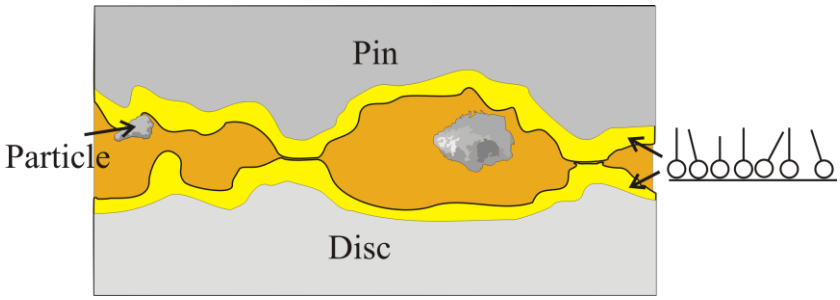

Figure 9.5. Schematic of the mechanisms of contacts in the bentonite drilling mud with octanoate additive, showing the formation of octanoate tribofilm. This incorporates the conditions at OCP and anodic overpotential.

9.3.2 Polymer Drilling Mud

The mechanism of contact in the polymer drilling mud is slightly different to the bentonite, owing to the absence of the particles in the mixture. The polymer mud without the additive showed significant friction reduction at application of cathodic overpotential, probably due to the formation of tribofilm by any of the polymer constituents. Furthermore, it was demonstrated that the incorporation of the octanoate additive will result in further reduction in friction, particularly at the application of anodic overpotential, due to the effective formation of the tribofilm. Although, the exact composition of the polymer is unknown, which makes accurate understanding difficult.

9.4 Steel / Sandstone Contacts in Bentonite Drilling Mud

The sandstone is made from silica grains which could be detached as wear debris during sliding, hence increasing two-body abrasion in the contact. Furthermore, the pores of the sandstone could act as sharp edges, or could trap the debris particles (either bentonite or sandstone), which in either case will cause severe wear to the steel counterface and higher friction in general. The mechanism of contact when using the bentonite drilling mud, and at application of a cathodic overpotential is schematically shown in Figure 9.6 (a). In this condition, no oxide layer will be present, and fewer bentonite particles will be entrained (due to the repulsion from the steel surface). Consequently, a slight reduction in friction and levels of abrasion will be observed cf. the condition at OCP (0 V overpotential). On the other hand, at anodic overpotential, oxide layer is formed, and more bentonite particles will entrain, causing a relatively higher friction and severe wear (see Figure 9.6 (b)). In short, the behaviour similar to the steel/steel contact mode was seen, but generally, the mean values are

significantly higher (*i.e.*, trend shifted upwards in the friction *vs.* overpotential graph), demonstrating the severity of the contacts.

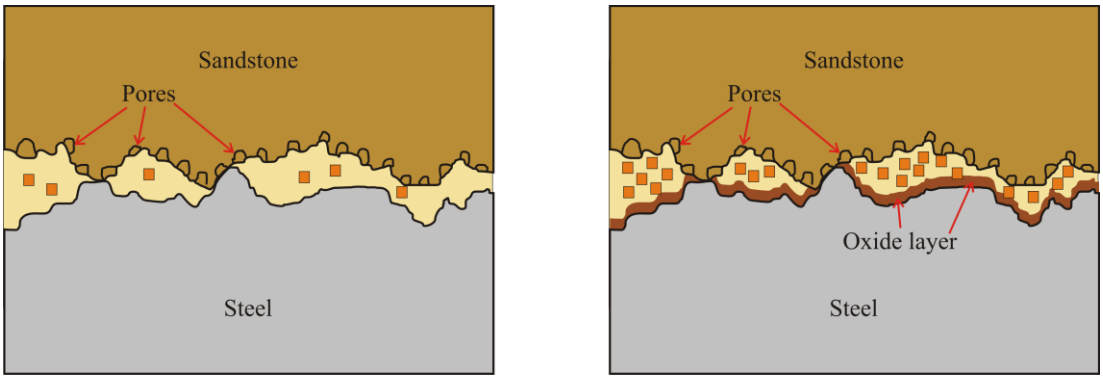

(a) (b)

Figure 9.6. Schematic of the contact between steel/sandstone in the bentonite drilling mud at (a) cathodic overpotential, and (b) anodic overpotential (also applicable to OCP). The debris in the contact represent the bentonite and sandstone particles.

In the case when the octanoate additive is present, the tribofilm is assumed to form only on the steel surface, thus having a sandstone counterface results in a relatively high abrasion and friction levels due to the "semi-protected" state, in comparison with the steel/steel in which the tribofilm forms on both sliding surfaces (see schematics in Figure 9.7). The implication of this steel/sandstone contact mode to the frictional trend, is an upward shift in the friction trend relative to the same test condition in the steel/steel contact mode (*i.e.*, evident from the friction *vs.* overpotential graph). However, there are some differences when the contact arrangement is changed, *i.e.*, between sandstone pin/steel disc, and steel pin/sandstone disc, which will be summarised next.

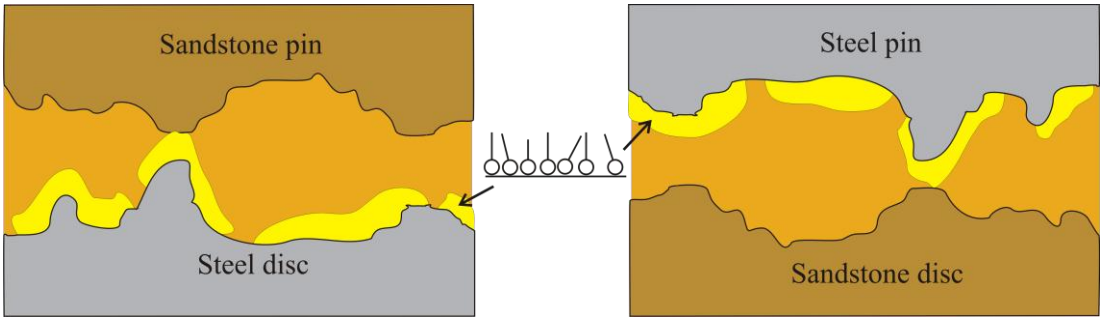

(a) (b)

Figure 9.7. Schematic of the steel/sandstone contact mode, showing the two types of arrangements of (a) sandstone pin/steel disc, and (b) steel pin/sandstone disc. Formation of the octanoate tribofilm is assumed to be on the steel surfaces only. Debris and sandstone porosity not shown for clarity.

In addition to friction shifts, changes to the wear mechanisms include the production of hard debris, due to wear of the sandstone. Particularly for the sandstone pin/steel disc arrangement, the sandstone pin will have a relatively high wear rate, which results in the

production of higher amount of sandstone debris (see Figure 9.8). The contact, therefore, will have a mixture of the particles of the sandstone, bentonite, and steel debris. The formation of tribofilm on the steel disc surface might offer some protection from severe wear and high friction, although not as much as the case of the steel/steel, in which the tribofilm forms on both contacting surfaces. Furthermore the presence of the particles and its interaction with the sandstone pin might cause the tribofilm to be removed, which might explain the increase in friction and wear.

For the other steel/sandstone arrangement, *i.e.*, the steel pin/sandstone disc, there is a slight variation in the wear mechanism. That is, the sandstone material (disc) is more resistant to wear cf. in the previous arrangement (the sandstone pin), probably due to the more effective stress distribution. This would cause less sandstone particles being detached, thus the overall friction levels would also be reduced cf. the previous arrangement (seen in the trend of friction *vs.* overpotential shifting downward, but still higher than the steel/steel). However, the wear resistant sandstone disc might result in a better retention of the trapped particles in the pores. Hence, mixed with the abrasive nature of the sandstone material itself, this might account for the relatively high steel pin wear rate.

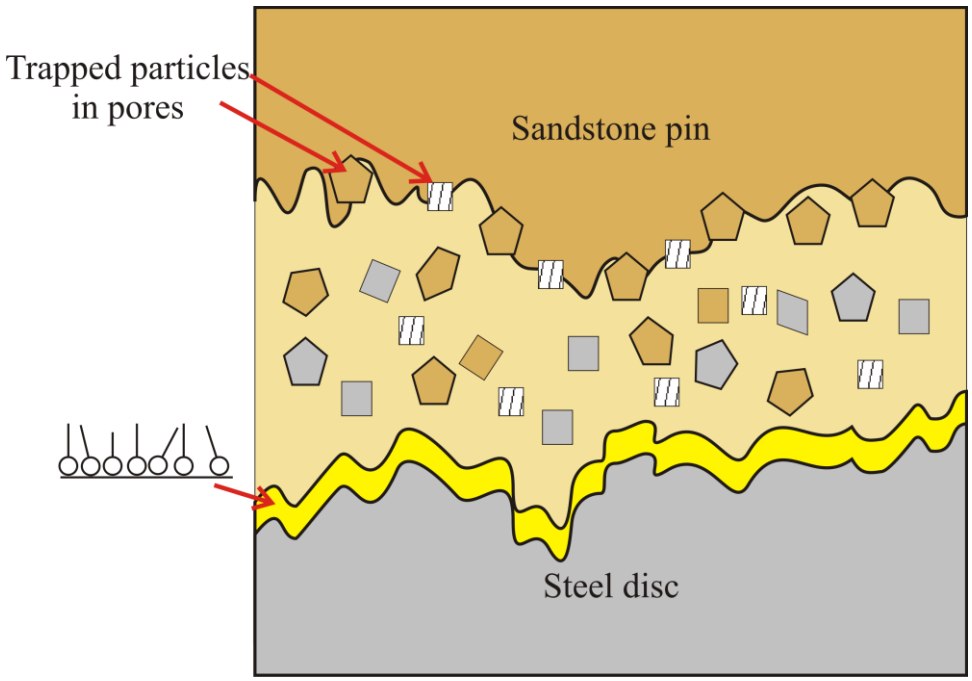

Figure 9.8. Schematic of the mechanism of contact of a sandstone pin/steel disc mode. Legend: brown is sandstone particle, grey is steel debris, and patterned is bentonite particle.

9.5 Summary

An overview of the mechanisms of wear has been presented, which was linked to the behaviour of the friction responses, especially with respect to the variation of cathodic and anodic overpotentials. Furthermore, the interrelationship between the friction and wear results with the tribofilm formation was explained, such as its mechanism of protection from direct steel/steel or steel/sandstone contacts. The influence of particle entrainment has also been clarified in causing abrasion to the steel surface, such as by potentially being trapped in the sandstone pores. Therefore, this project has elucidated a few critical areas related to these conditions, which leaves for future work to expand into realistic engineering applications and increasing the depth of basic understanding.

10 Conclusions

This chapter briefly concludes all the results and discussions, which focuses on the novelty of this project. Particularly, the judgement on the effects of overpotential application on tribological performance is reviewed, and how far the phenomena has been explored and understood by the modus operandi employed. Therefore, this would aid in the future work, directing at expanding the discoveries of this project.

10.1 The Development of Electrochemical and Triboelectrochemical Experiments

The electrochemical tests were useful in obtaining a foundation for the response of the steel samples towards potential application (or polarisation). Particularly, the effect of adsorption could be seen by the reduction in current density values. In the solutions incorporating the friction modifying additives, this suggests that the friction could be reduced when the correct potentials are applied to promote adsorption of the additives. Particularly, the octanoate test solutions showed a low current density in the anodic region, indicating the formation of iron octanoate film.

The triboelectrochemical tribometer (pin-on-disc) was successfully developed and subjected to quality checks. The tribometer was used to test the dependence of friction on potential application. The results from these tests were either mechanical (friction and wear) or electrochemical (current or potential). The electrochemical response could be correlated with the initial tests discussed earlier with good agreement.

10.2 Control of the Tribological Performance

10.2.1 The Baseline Solutions

The systematic programme employed in this project confirms that friction control by electrical potential is achievable in the sliding motion of either steel/steel of stee/sandstone contact type. Assessments were made on the friction-potential relations, by explaining the development of a tenacious tribofilm.

The baseline solutions without additive (NaOH) gave higher friction compared with octanoate tests for the same applied overpotentials. Friction was reduced when the octanoate additive was present at 60 mM concentration. In particular, the static friction was seen to be reduced generally by 33%, *i.e.*, μ static from 0.15 to 0.10, between the NaOH and octanoate solutions. Furthermore changes in the dynamic friction were also seen. For example,

reduction by 66%, *i.e.*, μ_{mean} from 0.47 to 0.16 (at 0 V overpotential) was seen between the NaOH and octanoate tests. In the octanoate test, further reduction by 6% (μ_{mean} from 0.16 to 0.15) was seen when +1 V overpotential was applied, along with a 60% increase in the stablility of friction perturbation. The iron octanoate tribofilm adsorbed onto the steel surfaces which were effective in reducing direct steel/steel contact. Application of anodic overpotentials probably increased the thickness of the tribofilm, or producing a relatively dense layer which was more robust.

Furthermore, the tribofilm has the ability to reduce wear of both pin and disc. A change in the overall wear mechanism was found to have occurred between tests conducted in octanoate and NaOH solutions. Evidence for adhesion and abrasion were less in the octanoate tests, as well as the reduction in the sample wear rates. Apart from mechanical wear, the octanoate additive was also seen to affect levels of corrosion, due to the inhibition of the electrochemical reactions. The steel was prone to corrosion in the NaOH solution and was exacerbated by application of a relatively high anodic overpotential. Whereas in the octanoate solution, no corrosion was seen on the pin or disc samples, even when high anodic overpotential (+1 V) was applied.

Therefore, the results of the octanoate tests show that friction and wear could be reduced by applying anodic overpotentials. This project was aimed at reducing the friction by 10%, thus, the 6% reduction when +1 V overpotential was applied in the octanoate test is encouraging. However, the reduction in the drilling mud was closer to this target, which will be presented in the next section.

For the oleate additive, lowest friction was given among the additives employed in this project (μ_{mean} around 0.09), but to the expense of the sensitivity of friction control with variation of potential application. On the contrary, butyrate additive gave slightly higher friction cf. octanoate, but allows friction reduction by application of a low value of overpotential, *i.e.*, μ_{mean} from 0.35 to 0.25 (by 28%). This is useful because application of a high anodic overpotential (such as +1V) would result in an accelerated corrosion if the tribofilm is stripped off. Therefore, this leaves an opportunity to explore for an additive which has all these good qualities.

For the positively charged additive (CTAB), reduction in friction by 25% was found when cathodic overpotential (–1 V) was applied cf. 0 V, *i.e.*, from 0.42 to 0.32. Application of cathodic overpotential is beneficial due to the absence of corrosion, but the susceptibility to hydrogen embrittlement might increase. This area has not been explored widely and could be incorporated in future work.

The active switching test showed that friction is controllable *in-situ*, *i.e.*, whilst sliding is continued using the octanoate additive. This suggests that this method could be used to actively control friction, hence, would be beneficial in reducing the problems related to stick-slip or vibration. The butyrate showed a less responsive friction with potential switch, which suggests a lower chain length molecule does not necessarily give a good switching behaviour.

10.2.2 The Drilling Mud

The bentonite drilling mud produced the highest levels of friction and wear amogst all the test lubricants in this project. Particularly, the presence of suspended bentonite particles increased the levels of two-body abrasion, when entrained in the contact. Furthermore, due to the negative charge of these particles, larger number of particles were entrained at anodic overpotential, whilst smaller at cathodic. As a result, the levels of friction followed a linear dependence on overpotential, increasing from cathodic, OCP (0 V overpotential) to anodic, *i.e.*, μ_{mean} at 0.52, 0.58, and 0.60 respectively. This seems to contradict the purpose of the drilling mud which should provide lubrication for drilling processes.

However, incorporation of the octanoate additive changed the tribological response altogether. In this system, *i.e.*, bentonite drilling mud with octanoate additive, the negative charged bentonite particles and octanoate molecules coexist, which compete for the positive (anodic) adsorption sites. It was shown that the octanoate molecules adsorbed onto the steel surfaces, forming a tribofilm, which markedly reduced the levels of friction despite the presence of the bentonite particles. For example, at 0 V overpotential, the μ_{mean} was 0.18. This was a reduction by 69% cf. the absence of octanoate (at 0.58). Further friction reduction by 11% was seen at application of +1 V overpotential, *i.e.*, μ_{mean} from 0.18 to 0.16, including a 67% increase in the stability of the friction perturbation. This 11% reduction had reached the aim of this project of 10%. It is interesting that these low friction values were comparable to the baseline solution when the bentonite particles were absent. SEM micrographs indicated a reduction in the width of the grooves from cathodic to anodic overpotentials, which suggested an increase in the protection of the tribofilm from two-body abrasion. The sample wear rates also showed lower values cf. the drilling mud in absence of octanoate additive. Therefore, this encourages future work to test this method in a closer simulation of the downhole drilling (will be discussed in Chapter 10).

Silica sand particles of 5 μm size were added at 3 wt%, to the bentonite drilling mud in order to replicate the cut formation. The levels of friction were not affected cf. the absence of silica in the bentonite drilling mud, *i.e.*, values of μ_{mean} were 0.54, 0.57 and 0.61 at –1, 0 and +1 V overpotentials respectively. The surfaces of pin and disc showed evidence of severe

abrasion and indentation. Corrosion was also seen at anodic overpotentials. In the presence of the octanoate additive, the levels of friction were also comparable to the case of bentonite drilling mud with octanoate (without silica). However, at +1 V overpotential, friction was further reduced by 19% cf. 0 V overpotential, *i.e.*, from 0.24 to 0.17, which is above the targeted reduction of 10%. Furthermore, evidence of adhesion and rough texture were also seen to decrease. Therefore, these suggest the production of a robust tribofilm, imparting lubrication even in the condition of relatively high abrasive concentration.

Generally, with the presence of octanoate additive, it can be seen that application of anodic overpotential (particularly at +1 V) was beneficial in reducing the friction in the descending order of: bentonite+silica+octanoate > bentonite+octanoate > octanoate, *i.e.*, by 19%, 11% and 6% respectively. It is interesting that the level of reduction was obtained proportional to the amount of abrasives, which is counterintuitive. This was probably due to, during sliding, the abrasives interfering with the tribofilm formation at 0 V overpotential (thus increasing friction), but application of +1 V was successful in promoting the adsorption of the octanoate additive to form a robust tribofilm. Furthermore, the μ_{mean} values whenever +1 V overpotential was applied in each case were 0.17, 0.16 and 0.15 respectively. The small difference in these μ_{mean} values indicated the robustness of the tribofilm, which was only slightly affected by the abrasive particles (where present). In this project, the bentonite+silica+octanoate mixture was the closest mud formulation simulating downhole drilling. Therefore, the fact that it gave the most reduction in friction, and above the target of 10%, established the motivation for developing this system in the future work.

The polymer mud generally produced friction lower than the bentonite drilling mud. It showed a reduction in friction at more cathodic overpotentials, *i.e.*, μ_{mean} values of 0.37, 0.32, and 0.21, at +1, 0 and –1 V overpotentials respectively. The addition of the octanoate additive to the polymer mud produced a similar trend to that in the baseline octanoate solution, with a slight reduction in friction over the entire potential range due to the more lubricous nature of the polymer mud. Hence, the lowest μ_{mean} was 0.14 at +1 V overpotential. Wear of the samples were also reduced in the presence of octanoate. All of these suggest the effectiveness of octanoate tribofilm when present in the polymer mud.

The response of friction on overpotential was reproducible in the steel/sandstone contacts, using the bentonite drilling mud with octanoate additive. Similar trends to the steel/steel contacts were seen, *i.e.*, high friction at cathodic overpotentials whilst low friction at anodic. This suggests that the principle of operation was similar regardless of the material and contact type, as long as the formulation of the solution is the same. However, a change in the contact arrangement gave different range of friction reduction, *i.e.*, the sandstone

pin/steel disc gave larger range of μ_{mean} (between 0.90 and 0.20), and the steel pin/sandstone disc gave smaller range (between 0.60 and 0.20). This was probably due to the sandstone pin tip fracturing easily which produced abrasive particles cf. the steel pin counterpart. However, this argument needs to be clarified by conducting more experiments.

10.3 Proof of Formation of the Adsorption Film

The formation of the octanoate tribofilm, which resulted in the low friction contacts, was indicated by the XPS measurement. Thorough analysis of the survey spectra was perfomed using qualitative and quantitative methods, particularly by assessing the trends of carbon, iron, sodium and oxygen. The trends in the carbon atoms distribution (from the high resolution spectra) suggested that a loosely packed and disordered octanoate adsorption was formed at cathodic overpotentials, in contrast to a relatively densely packed and ordered adsorption film at more anodic overpotential (robust tribofilm). Furthermore, the analysis of iron spectra agree with the carbon and oxygen trends and provided an additional indicator of adsorption by suggesting the surface probably being coated by the tribofilm. These XPS results conform to the friction and wear performance found in the sliding tests, and aided in understanding behaviour of the tribofilm formation.

Furthermore, the reduction in the values of currents recorded during the sliding test could indicate the formation of the tribofilm. It was also seen that for the same contact type, lower magnitude of potential could be correlated with low friction obtained from the different test solutions.

10.4 Limitations of the Techniques Employed in this Project

10.4.1 Current Density Calculation

The limitations of the techniques employed in this project included the calculation of the current density values from the test results. This was due to the current density being obtained through dividing the recorded current with the exposed disc surface area. This project has standardised this surface area value to 28 cm^2. Therefore, in certain cases, the effective area in which current is flowing might be smaller than this standard value, thus introducing some errors. For example, in the baseline solution with the octanoate additive, probably the wear track is the only area which contributes to current flow, thus dividing the

current with the whole disc surface will cause an underestimated value of the current density. However, there was no straightforward solution for this, but probably to coat the off wear track with special paint, which has not been tested before. This coat would ensure that the the off wear track is not contributing to any current flow at all (completely passivated), and the calculation of current density will be based on a more accurate surface area by accounting the on wear track only. If this technique is adopted, the implication would probably be an increase in the values of current density, owing to the higher denominator value (the surface area) in the calculation.

10.4.2 Wear Rate Calculation

In addition, another limitation was in the determination of the wear rates of both the pin and disc samples. The pin was fabricated in-house, by machining steel cylinders. This probably had caused some slight variations in the accuracy of the pin geometry, due to the involvement of some manual handling, therefore rendering the wear rate calculation using radii (gemonetrical method) prone to error. Gravimetrical analysis might not be feasible due to crevice corrosion at the sides of the pin, where the counter electrode holder was fixed onto. This could probably be improved in future work, by using ball bearing pins with a more controlled and accurate manufacturing method. Furthermore, the wear track of the disc was relatively large (about 157 cm in circumference), which made investigation of either the cross-sectional profile or wear mechanisms difficult. Particularly, the variation along the wear track was difficult to be monitored, which, if examined thorough enough, could offer more insight into the tribological performance. This might be improved by using a smaller wear track, either by reducing the wear track radius, or changing the contact mode altogether, *i.e.*, from unidirectional to reciprocating which allows for a small and linear wear track.

10.4.3 Temperature Control

The test temperature of this project was not controlled, due to the limitation of the test setup. Obtaining a temperature control would require the installation of a temperature bath, in which the lubricant/solution being constantly fed and recycled. However, if installed, this might enable the testing of higher temperature conditions, mimicking the downhole conditions, which could be looked at in future work.

10.4.4 Sandstone Samples

The sandstone samples were prepared basically by manual methods (machining a sandstone cylinder). Therefore, it was difficult to control the surface finish, *i.e.*, obtaining accurate radii of the sandstone pin, which could have also contributed to the error in the wear rate

calculation. Furthermore, the wear mechanisms of the sandstone samples were more difficult to be determined cf. the steel, due to the incompatibility of the sandstone material for microscopy analysis such as SEM.

10.4.5 Hardware Limitations

The current test setup employs two different hardware being controlled simultaneously, *i.e.*, the rotation of the rig, and the potentiostat. This caused limitations to the test procedures, such . Probably, future development might be directed towards integrating the two types of hardware, which could also benefit in creating a solution for actual engineering applications. Additionally, the potentiostat does not allow the active switching test to be conducted automatically. During test, the changing of potential was done by stopping the potentiostat and restarting, which takes time and limits the rate at which the switching is made.

11 Future Work

11.1 Simulation of Downhole Drilling

The experimental setup in relation to simulating the conditions found during downhole drilling could be improved. This includes the high temperature (up to 150 ºC), and high pressure, which would require the design of a more sophisticated tribometer. This is particularly important in assessing the performance of the friction modifying additives, *i.e.*, to test the feasibility of employing them in harsh conditions. Furthermore, the sliding velocity could also be increased to simulate the rotational motion of the drill bit.

The results of this project could also be used to explore the possibility of solving the problems of wireline or stuck pipe, but would require a dedicated experimental setup to simulate the specific conditions. For example, the mud cake incorporating the octanoate additive would be used to assess the reduction in friction required to "unstick" the steels. Also work will look at active potential switching so that if the operator requires momentary decreases/increases in friction, this can be achieved in a reasonable time.

11.2 Improvements to Wear Rate Calculations

The wear rates found from this study, particularly for the octanoate test solutions, were considered mild. Therefore, future work might be directed towards assessing these findings, such as by comparing the wear rate values when subjected to higher velocities and sliding distance. This might accelerate material loss and could probably show the difference between tests more clearly.

Furthermore, due to constraint on technical capabilities and availability of sandstone samples, the wear mechanism and wear rates of either the pin or disc could not be accurately measured. Therefore, future work might incorporate improvement towards the fabrication method of the sandstone samples. This would allow the exploration of the behaviour of the sandstone material, particularly in assessing if the friction and wear performance could be affected by application of surface potentials, and how this would be related to the steel/steel contacts.

11.3 Formulation of Lubricant

The formulation of the lubricants could also be improved by using more representative constituents of the actual drilling processes. For example, salt could be introduced to test the corrosion reaction and the reproducibility of the friction reduction behaviour. Furthermore, the contents of drilling mud would include many other chemicals which are also polar and

tend to adsorb on surfaces. Therefore, a systematic programme aiming at assessing the mixture of these chemicals with the friction modifiers would be advantageous, especially in examining the feasibility of employing friction control in that condition.

11.4 Lubricant Compositions and Types of Additives

The concentrations of the additives employed in this study have not been rigorously tested to identify the optimum value. Most of the additives were utilised at 60 mM concentrations, but due to insolubility, the oleate additive was only used at 1 mM. Future work could be directed towards discovering the best concentration that could provide friction and wear control, whilst being acceptable for downhole applications.

Other types of friction modifying additives could be tested in the search for the most feasible for use in downhole conditions. It is desirable to get one which fits these criteria:

i. Could provide a sensitive frictional response which is sensitive to the application of potential, probably better than the octanoate molecule

ii. Could reduce as much friction and wear as possible, such as the oleate

iii. Could be preferentially adsorb in conditions where other chemicals are present

iv. Could be controlled by application of low magnitudes of overpotential, *e.g.*, 0.3 V overpotential, as opposed to 1.2 V overpotential.

11.5 Active Switching Experiments

The active switching experiment could be explored in terms of employing a faster potential switch time. It is also desirable to produce a friction response which is stable and more controllable, *i.e.*, by increasing or decreasing in a manner which replicates the switching process closely.

12 References

[1] P. T. F. Allen, G. Conran, B. Lesso, Extended-Reach Drilling: Breaking the 10-km Barrier, in: Oilfield Review.
[2] Schlumberger, in.
[3] I. A. Frigaard, S. Pelipenko, Effective and Ineffective Strategies for Mud Removal and Cement Slurry Design, in: SPE Latin American and Caribbean Petroleum Engineering Conference, Society of Petroleum Engineers, Trinidad and Tobago, 2003.
[4] F. L. Elizabete, R. E. M. Claudia, S. Luciana, G. C. Q. Yure, Pure & Applied Chemistry 81 (2009) 473-494.
[5] R. Caenn, G. V. Chillingar, Journal of Petroleum Science and Engineering 14 (1996) 221-230.
[6] M. C. Sheppard, C. Wick, T. Burgess, SPE Drilling Engineering 2 (1987) 344-350.
[7] T. V. Aarrestad, H. Blikra, Journal of Petroleum Technology 46 (1994) 800-803.
[8] A. Ersoy, M. D. Waller, Wear 188 (1995) 150-165.
[9] C. A. Johancsik, D. B. Friesen, R. Dowson, Journal of Petroleum Technology 36 (1984) 987-992.
[10] Schlumberger, Differential Sticking http://www.glossary.oilfield.slb.com/Display.cfm?Term=differential%20sticking. Accessed in 2010.
[11] H. C. H. Darley, G. R. Gray, Drilling Problems Related to Drilling Fluids, in: Composition and properties of drilling and completion fluids, Gulf Professional Publishing, 1988, pp. 401-415.
[12] H. C. H. Darley, G. R. Gray, Composition and properties of drilling and completion fluids, Gulf professional Publishing.
[13] M. Thakare, Abrasion-Corrosion of Downhole Drill Tool Components, in: School of Engineering Sciences, vol Tribology, Southampton, 2008.
[14] M. Reyes, A. Neville, Wear 255 1143-1156.
[15] Schlumberger, Bit, http://www.glossary.oilfield.slb.com/Display.cfm?Term=bit, in: 2010.
[16] Schlumberger, Bit nozzle, http://www.glossary.oilfield.slb.com/Display.cfm?Term=bit%20nozzle. Accessed in 2010.
[17] J. Truhan, R. Menon, F. LeClaire, J. Wallin, J. Qu, P. Blau, Wear 263 (2007) 234-239.
[18] J. J. Truhan, R. Menon, P. J. Blau, Wear 259 (2005) 1308-1313.
[19] O. A. Falode, O. A. Ehinola, P. C. Nebeife, Applied Clay Science 39 (2008) 19-27.
[20] D. Knox, P. Jiang, Drilling Further With Water-Based Fluids - Selecting the Right Lubricant, in: SPE International Symposium on Oilfield Chemistry, SPE International, Houston, 2005.
[21] MI-Swaco, Starglide, in: 2004.
[22] L. M. Zhang, J. F. Zhou, P. S. Hui, Colloids and Surfaces a-Physicochemical and Engineering Aspects 259 (2005) 189-195.
[23] V. C. Kelessidis, Energy Sources, Part A: Recovery, Utilization, and Environmental Effects 30 (2008) 1729 - 1746.

[24] V. C. Kelessidis, C. Tsamantaki, P. Dalamarinis, Applied Clay Science 38 (2007) 86-96.
[25] H. C. H. Darley, G. R. Gray, Drilling problems related to drilling fluids, in: Composition and properties of drilling and completion fluids, Gulf professional Publishing, pp. 401-491.
[26] H. Zhao, S. Bhattacharjee, R. Chow, D. Wallace, J. H. Masliyah, Z. Xu, Langmuir 24 (2008) 12899-12910.
[27] E. Tombácz, M. Szekeres, Applied Clay Science 27 (2004) 75-94.
[28] P. F. Luckham, S. Rossi, Advances in Colloid and Interface Science 82 (1999) 43-92.
[29] L. Bailey, Schlumberger Progress Meeting, in: Cambridge, 2008.
[30] H. C. H. Darley, G. R. Gray, Clay Mineralogy and the Colloid Chemistry of Drilling Muds, in: Composition and properties of drilling and completion fluids, Gulf Professional Publishing, 1988, pp. 176-180.
[31] I. M. Hutchings, Tribology: Friction and Wear of Engineering Materials, Butterworth-Heinemann, 2003.
[32] J. A. Williams, Engineering Tribology, Oxford University Press, 2000.
[33] R. T. Spurr, T. P. Newcomb, Proceedings of the Physical Society. Section B 70 (1957) 198.
[34] J. D. Gates, Wear 214 (1998) 139-146.
[35] R. J. K. Wood, J. Phys. D: Appl. Phys. 40 (2007) 5502-5521.
[36] J. B. Adams, L. G. H. Jr, D. J. Siegel, H. Yu, J. Zhong, Surface and Interface Analysis 31 (2001) 619-626.
[37] M. Woydt, R. Wäsche, Wear 268 (2010) 1542-1546.
[38] G. Luengo, J. Israelachvili, S. Granick, Wear 200 (1996) 328-335.
[39] A. Gellman, N. Spencer, Proceedings of the Institution of Mechanical Engineers, Part J: Journal of Engineering Tribology 216 (2002) 443-461.
[40] F. P. Bowden, L. Leben, Philosophical Transactions of the Royal Society of London. Series A, Mathematical and Physical Sciences 239 (1940) 1-27.
[41] F. P. Bowden, J. E. Young, Proceedings of the Royal Society of London. Series A, Mathematical and Physical Sciences 208 (1951) 311-325.
[42] M. Ratoi, V. Anghel, C. Bovington, H. A. Spikes, Mechanisms of oiliness additives, in: 5th International Tribology Conference (AUSTRIB 98), Elsevier Sci Ltd, Brisbane, Australia, 1998, pp. 241-247.
[43] W. G. Beare, F. P. Bowden, Phil. Trans. R. Soc. Lond. A 234 (1935) 329-354.
[44] K. V. Shooter, Br. J. Appl. Phys. 2 (1951) 49-51.
[45] K. L. Johnson, Contact Mechanics, Cambridge University Press, 2004.
[46] J. F. Archard, Proceedings of the Royal Society of London. Series A, Mathematical and Physical Sciences 243 (1957) 190-205.
[47] J. A. Greenwood, J. J. Wu, Meccanica 36 (2001) 617-630.
[48] J. A. Greenwood, J. B. P. Williamson, Proceedings of the Royal Society of London. Series A, Mathematical and Physical Sciences 295 (1966) 300-319.
[49] M. G. Gee, M. J. Neale, General Approach and Procedures for Unlubricated Sliding Wear Tests, in: National Physical Laboratory, Neale Consulting Engineers, 1999.
[50] M. Pourbaix, Lectures on Electrochemical Corrosion, Plenum Press, 1973.
[51] L. Young, Anodic Oxide Films, Academic Press, 1961.
[52] K. R. Trethewey, J. Chamberlain, Corrosion for Science and Engineering, Longman, 1995.

[53] T. J. Harvey, Phosphonium Salts as Acid Corrosion Inhibitors, in: Division of Chemistry, Portsmouth University, Portsmouth, 1996.
[54] D. Landolt, Corrosion and Surface Chemistry of Metals, EPFL Press, 2006.
[55] B. Beverskog, I. Puigdomenech, Corrosion Science 38 (1996) 14.
[56] M. M. Stack, B. D. Jana, Wear 256 (2004) 18.
[57] Y. P. Virmani, Corrosion costs and prevention strategies in the United States, in: Federal Highway Administration, Washington DC, 2002.
[58] C. Ren, D. Liu, Z. Bai, T. Li, Materials Chemistry and Physics 93 (2005) 305-309.
[59] E. Abelev, T. A. Ramanarayanan, S. L. Bernasek, Journal of The Electrochemical Society 156 (2009) C331-C339.
[60] D. Landolt, S. Mischler, M. Stemp, Electrochimica Acta 46 (2001) 17.
[61] S. Mischler, Tribology International 41 (2008) 573-583.
[62] A. Neville, M. Reyes, T. Hodgkiess, A. Gledhill, Wear 238 (2000) 138-150.
[63] P. T. Kissinger, W. R. Heineman, Laboratory Techniques in Electroanalytical Chemistry, Marcel Dekker, 1996.
[64] A. J. Bard, L. R. Faulkner, Electrochemical Methods. Fundamentals and Applications, John Wiley &Sons, Inc., 2001.
[65] A. C. Fisher, Electrode Dynamics, Oxford University Press, 2006.
[66] I. Díez-Pérez, C. Vericat, P. Gorostiza, F. Sanz, Electrochemistry Communications 8 (2006) 627-632.
[67] L. Larabi, O. Benali, S. M. Mekelleche, Y. Harek, Applied Surface Science 253 (2006) 1371-1378.
[68] D. H. Everett, Pure Appl. Chem. 31 (1972) 579-638.
[69] G. Attard, C. Barnes, Surfaces, Oxford University Press, 2004.
[70] G. T. Barnes, I. R. Gentle, Interfacial Science, Oxford University Press, 2005.
[71] P. Somasundaran, S. Shrotri, L. Huang, Pure & Appl. Chem 70 (1998).
[72] A. B. G. Stachowiak, Engineering Tribology, Elsevier Butterworth-Heinermann, 2005.
[73] M. Ratoi, C. Bovington, H. Spikes, Tribology Letters 14 (2003) 33-40.
[74] D. C. Duffy, A. Friedmann, S. A. Boggis, D. Klenerman, Langmuir 14 (1998) 6518-6527.
[75] S. M. Hsu, R. S. Gates, Journal of Physics D-Applied Physics 39 (2006) 3128-3137.
[76] Y. Cao, L. Yu, W. Liu, Wear 244 (2000) 126-131.
[77] A. Adhvaryu, G. Biresaw, B. K. Sharma, S. Z. Erhan, Industrial & Engineering Chemistry Research 45 (2006) 3735-3740.
[78] Y. Y. Zhu, G. H. Kelsall, H. A. Spikes, Tribology Transactions 37 (1994) 811-819.
[79] R. W. Carpick, M. Salmeron, Chemical Reviews 97 (1997) 1163-1194.
[80] S. Lee, Y. S. Shon, R. Colorado, R. L. Guenard, T. R. Lee, S. S. Perry, Langmuir 16 (2000) 2220-2224.
[81] O. Berg, D. Klenerman, Journal of the American Chemical Society 125 (2003) 5493-5500.
[82] R. R. Sahoo, S. K. Biswas, Journal of Colloid and Interface Science 333 (2009) 707-718.
[83] T. Edison, Journal of The Telegraph (1877).
[84] V. Guruswamy, J. Bockris, Comprehensive Treatise of Electrochemistry 4 (1981).
[85] R. E. D. Clark, Transactions of Faraday Society 42 (1945) 449-456.

[86] R. E. D. Clark, Transactions of Faraday Society 42 (1945) 456-461.
[87] G. H. Kelsall, Y. Zhu, H. A. Spikes, Journal of Chem. Soc. Faraday Transactions 89 (1993) 5.
[88] D. N. Staicopolus, Journal of The Electrochemical Society 108 (1961) 900-904.
[89] J. O. M. Bockris, S. D. Argade, The Journal of Chemical Physics 50 (1968) 1622-1623.
[90] J. O. M. Bockris, R. K. Sen, Surface Science 30 (1972) 237-241.
[91] Y. Meng, H. Jiang, Q. Chang, P. L. Wong, Science in China, Series A: Mathematics, Physics, Astronomy 45 (2002) 1219-1219.
[92] N. P. Brandon, N. Bonanos, P. O. Fogarty, M. N. Mahmood, J. Electrochem. Soc. 139 (1992) 3489-3492.
[93] N. P. Brandon, N. Bonanos, P. O. Forgaty, M. N. Mahmood, A. J. Moore, R. J. K. Wood, Journal of Applied Electrochemistry 23 (1993) 456-462.
[94] N. P. Brandon, R. J. K. Wood, Wear 170 (1993) 33-38.
[95] Y. Zhu, G. H. Kelsall, H. A. Spikes, Tribology Letters 2 2 (1996) 287-312.
[96] Y. Meng, B. Hu, Q. Chang, Wear 260 (2006) 305-309.
[97] H. Jiang, Y. Meng, S. Z. Wen, P. Wong, Active Control of Frictrion by Applying Electric Fields Across Boundary Films of Stearate, in: Proceedings of the First Asia International Conference on Tribology, vol 1, Tsinghua University Press, 1998, pp. 755-760.
[98] S. He, Y. Meng, Y. Tian, Y. Zuo, Tribology Letters (2010).
[99] Y.-Y. Su, M. Marek, Journal of Materials Engineering and Performance 4 (1995) 154-160.
[100] J. Lahann, S. Mitragotri, T.-N. Tran, H. Kaido, J. Sundaram, I. S. Choi, S. Hoffer, G. A. Somorjai, R. Langer, Science 299 (2003) 371-374.
[101] S. C. Tung, S. S. Wang, Tribology Transactions 34 (1991) 479 - 488.
[102] S. C. Tung, S. S. Wang, Tribology Transactions 34 (1991) 23 - 34.
[103] X. Xu, H. Spikes, Tribology Letters 25 (2007) 141-148.
[104] M. J. Neale (Ed.) The Tribology Handbook, Butterworth Heinemann, 1995, p.
[105] M. A. Quraishi, D. Jamal, Materials Chemistry and Physics 71 (2001) 202-205.
[106] M. Quraishi, D. Jamal, M. Tariq Saeed, Journal of the American Oil Chemists' Society 77 (2000) 265-268.
[107] M. Ashby, Cambridge Engineering Selector v4, in: Granta Design Limited, 2006.
[108] P. Zhang, Q. Xue, Z. Du, Z. Zhang, Wear 242 (2000) 147-151.
[109] J. F. Watts, J. Wolstenholme, An Introduction to Surface Analysis by XPS and AES, John Wiley &Sons Ltd., Chichester, 2003.
[110] A. Mahapatro, D. M. Johnson, D. N. Patel, M. D. Feldman, A. A. Ayon, C. M. Agrawal, Langmuir 22 (2006) 901-905.
[111] E. Jaehne, S. Oberoi, H.-J. P. Adler, Progress in Organic Coatings 61 (2008) 211-223.
[112] E. Johansson, L. Nyborg, Surface and Interface Analysis 35 (2003) 375-381.
[113] M. Przedlacki, C. a. Kajdas, Tribology Transactions 49 (2006) 202 - 214.
[114] G. Shustak, A. J. Domb, D. Mandler, Langmuir 20 (2004) 7499-7506.
[115] F. Gao, A. Erdemir, W. Tysoe, Tribology Letters 20 (2005) 221-227.
[116] C.-W. Cho, Y.-Z. Lee, Surface and Coatings Technology 179 (2004) 1-9.
[117] M. T. Makhlouf, S. A. El-Shatory, A. El-Said, Materials Chemistry and Physics 43 (1996) 76-82.
[118] S. Mischler, A. Spiegel, M. Stemp, D. Landolt, Wear 251 (2001) 1295-1307.

[119] M. Favero, P. Stadelmann, S. Mischler, J. Phys. D: Appl. Phys. 39 (2006) 3175-3183.
[120] M. N. F. Ismail, T. J. Harvey, J. A. Wharton, R. J. K. Wood, A. Humphreys, Wear 267 (2009) 9.
[121] S. Mischler, A.Spiegel, D. Landolt, Wear 225-229 (1999) 1078-1087.
[122] O. Olivares-Xometl, N. V. Likhanova, R. Martínez-Palou, M. A. Domínguez-Aguilar, Materials and Corrosion 60 (2009) 14-21.
[123] S. He, Y. Meng, Y. Tian, Tribology Letters (2010) 1-10.
[124] L. Bailey, Schlumberger Teleconference Meeting, in: 2010.
[125] M. N. F. Ismail, R. J. K. Wood, A. Humphreys, J. A. Wharton, T. Harvey, Electrochemical Friction Control Using Downhole Drilling Lubricants, in: 2010 STLE Annual Meeting & Exhibition, ASME, Las Vegas, 2010, p. 3.
[126] J. O. Bello, R. J. K. Wood, J. A. Wharton, OECD (2005).
[127] S. Akonko, D. Y. Li, M. Ziomek-Moroz, Tribology Letters 18 (2005) 405-410.
[128] D. J. Lacks, A. Levandovsky, Journal of Electrostatics 65 (2007) 107-112.
[129] P. J. Cumpson, Journal of Electron Spectroscopy and Related Phenomena 73 (1995) 25-52.
[130] A. I. Martín-Concepción, F. Yubero, J. P. Espinós, S. Tougaard, Surface and Interface Analysis 36 (2004) 788-792.
[131] T. S. Lassen, S. Tougaard, A. Jablonski, Surface Science 481 (2001) 150-162.
[132] Q.-h. Rao, Z. Wang, H.-f. Xie, Q. Xie, Journal of Central South University of Technology 14 (2007) 478-483.